Institute of Crop Science and Resource Conservation-Soil Science and Soil Ecology

Nutrient elements in micro- to nanosized fractions: occurrence, transport, and plant uptake in agroecosystems

Dissertation

zur Erlangung des Grades

Doktor der Agrawissenschaften (Dr. agr.)

der Landwirtschaftlichen Fakultät

der Rheinischen Friedrich-Wilhelms-Universität Bonn

von

Yunsheng Jia

aus

Anhui, China

Bonn 2023

Vorsitzender:	**Prof. Dr. Mathias Becker**
1. Gutachter:	**Prof. Dr. Wulf Amelung**
2. Gutachter:	**Prof. Dr. Roland Bol**
Fachnahes Mitglied:	**Apl. Prof. Dr. Erwin Klumpp**

Tag der mündlichen Prüfung: 19.01.2023

Angefertigt mit Genehmigung der Landwirtschaftlichen Fakultät der Universität Bonn

Summary

As phosphorus (P) is a non-substitutable nutrient for all organisms and thus pivotal in supporting crop productivity, limited and unevenly distributed phosphate rocks drive research concerns on substituted P fertilizers and management of soil legacy P. My thesis mainly focused on 1) the availability and transformation of P from alternative P fertilizers within soil size fractions; 2) a detailed understanding of colloidal P transport and potential associations with other elements in different arable soil layers; 3) a general exploration of plant uptake preferences of elements from nanoparticles and dissolved salts. As data on nanoparticulate P uptake were rare, I focused on different metallic elements in this third part to achieve a broader understanding of the main factors controlling metal accumulation in crops from metallic nanoparticles (MNPs) applications.

To achieve the above aims, firstly, bone char (BC) and sulfur modified bone char (BC^{plus}), as potential substitutes for mineral P fertilizers, were assessed after 5-year field fertilizations in the P fractions and pools within soil size fractions by wet-sieving, centrifugation, and tangential flow filtration followed by UV-Vis and ICP-OES determinations. Moreover, the colloidal P in different arable soil layers and artificial drainage systems were determined with FFF-OCD-ICP-MS; potential associations between P and other elements were estimated via cluster analysis. To elucidate the uptake of MNPs by crops, data were collected and studied by a meta-analysis, with effect sizes (standardized mean difference) of various factors on metal accumulations in crop tissues calculated for the three most studied non-essential and essential metals, respectively.

Field trial results showed that BC and BC^{plus} fertilization mostly had no detrimental effects on soil macro- and micro-aggregations, nor on different soil P fractions and pools compared to triple superphosphate (TSP) fertilization. Similar to TSP, BC and BC^{plus} increased the mass proportions of large micro-aggregates compared to the no P control.

Detected arable soil colloids consisted of three size fractions including: nanocolloids (0.66-20 nm) enriched in organic carbon (C_{org}) and calcium (Ca); fine and medium-sized colloids (20-170 and 170-450 nm, respectively) rich in C_{org}, iron (Fe), aluminum (Al), and silicon (Si). Colloidal P stocks among three size fractions were 0.6-6.6, 0.2-2.9 and 0.9-7.1 kg ha^{-1} at Ap, Bw, and C horizons, respectively, highlighting that colloidal P contributes only partly to plant fertilizer needs. A cluster analysis revealed high similarity of soil nanocolloids in the C horizon to medium-sized colloids in water, suggesting their potential translocation to water bodies via ditch and tile drainage systems.

The meta-analysis revealed that current studies on crops' uptake of MNPs have focused on worldwide main cereal and vegetable crops (wheat, tomato, bean, maize, rice, and cucumber), and mainly on six main metals: Zn, Ag, Cu, Fe, Ce and Ti. The uptake preference of the elements from nanoparticles or salts were element-specific and varied among tissues. Plants generally accumulated higher concentrations of the three essential metals (Zn, Fe, and Cu) than of the non-essential ones (Ag, Ce, and Ti), and uptake rates were more efficient upon foliar exposure to MNPs than upon supplements to roots. Shoot metal concentrations increased with decreasing particle size diameters and increasing negative zeta potential.

I conclude that alternative sources of P fertilization have potential. The BCs reveal similar effects on P status than TSP, but also nanocolloidal P could contribute to both plant nutrition and ecosystem loss. The mechanisms of nanoparticulate P uptake renders further attention, but studies using MNPs revealed that there are plant uptake preferences depending on both the element and nanoparticle properties, particularly particle size or surface charge.

Zusammenfassung

Da Phosphor (P) ein nicht substituierbarer Nährstoff für alle Organismen und somit entscheidend für die Produktivität von Nutzpflanzen ist, treiben begrenzte und ungleichmäßig verteilte Phosphatgesteine die Forschung zu substituierten P-Düngern und zur Bewirtschaftung von P- im Boden voran. Meine Dissertation konzentrierte sich hauptsächlich auf 1) die Verfügbarkeit und Umwandlung von P aus alternativen P-Düngern in Aggregatgrößenfraktionen; 2) ein detailliertes Verständnis des kolloidalen P-Transports und potenzieller Assoziationen mit anderen Elementen in verschiedenen Ackerbodenhorizonten; 3) eine allgemeine Untersuchung, ob und wie Pflanzen Elemente aus Nanopartikeln gegenüber gelösten Salzen präferieren. Da es nur wenige Daten über die Aufnahme von nanopartikulärem P gibt, habe ich mich in diesem dritten Teil auf verschiedene metallische Elemente konzentriert, um ein umfassenderes Verständnis der wichtigsten Faktoren zu erlangen, die die Anreicherung von Metallen in Nutzpflanzen bei der Anwendung von metallischen Nanopartikeln (MNPs) steuern.

Um die oben genannten Ziele zu erreichen, wurden zunächst Knochenkohle (BC) und schwefelmodifizierte Knochenkohle (BC^{plus}) als potenzieller Ersatz für mineralische P-Dünger nach fünfjähriger Felddüngung in den P-Fraktionen und Pools innerhalb der Bodengrößenfraktionen durch Nasssiebung, Zentrifugation und Tangentialflussfiltration, gefolgt von UV-Vis- und ICP-OES-Bestimmungen, untersucht. Darüber hinaus wurde der kolloidale P-Gehalt in verschiedenen Ackerbodenschichten und künstlichen Entwässerungssystemen mit FFF-OCD-ICP-MS bestimmt; mögliche Zusammenhänge zwischen P und anderen Elementen wurden mittels Clusteranalyse geschätzt. Um die Aufnahme von MNP durch Pflanzen zu klären, wurden Daten gesammelt und in einer Meta-Analyse untersucht, wobei die Effektgrößen (standardisierte mittlere Differenz) verschiedener Faktoren auf die Metallakkumulation in Pflanzengeweben für die drei am meisten untersuchten nicht-essentiellen bzw. essentiellen Metalle berechnet wurden.

Die Ergebnisse der Feldversuche zeigten, dass die BC- und BC^{plus}-Düngung im Vergleich zur Dreifach-Superphosphat-Düngung (TSP) keine nachteiligen Auswirkungen auf die Makro- und Mikroaggregationen im Boden sowie auf die verschiedenen P-Fraktionen und -Pools im Boden hatte. Ähnlich wie bei TSP erhöhten BC und BC^{plus} die Massenanteile großer Mikroaggregate im Vergleich zur Kontrolle ohne P.

Die nachgewiesenen Kolloide im Ackerboden setzten sich aus drei Größenfraktionen zusammen: Nanokolloide (0,66-20 nm), die mit organischem Kohlenstoff (Corg) und Kalzium (Ca) angereichert sind; feine und mittelgroße Kolloide (20-170 bzw. 170-450 nm), die reich an Corg, Eisen (Fe), Aluminium (Al) und Silizium (Si) sind. Die kolloidalen P-Vorräte in den drei Größenfraktionen betrugen 0,6-6,6, 0,2-2,9 bzw. 0,9-7,1 kg ha^{-1} in den Ap-, Bw- und C-Horizonten, was darauf hindeutet, dass kolloidaler P nur teilweise zum Düngebedarf der Pflanzen beiträgt. Eine Clusteranalyse ergab eine hohe Ähnlichkeit der Boden-Nanokolloide im C-Horizont mit mittelgroßen Kolloiden im Wasser, was auf ihre potenzielle Verlagerung in Gewässer über Gräben und Drainagesysteme hindeutet.

Die Meta-Analyse ergab, dass sich aktuelle Studien zur Aufnahme von MNPs durch Nutzpflanzen auf die weltweit wichtigsten Getreide- und Gemüsekulturen (Weizen, Tomaten, Bohnen, Mais, Reis und Gurken) und hauptsächlich auf sechs Hauptmetalle konzentrierten: Zn, Ag, Cu, Fe, Ce und Ti. Die Präferenz für die Aufnahme von Elementen aus Nanopartikeln oder Salzen war elementspezifisch und variierte zwischen den Geweben. Die Pflanzen akkumulierten im Allgemeinen höhere Konzentrationen der drei essenziellen Metalle (Zn, Fe und Cu) als der nicht essenziellen (Ag, Ce und Ti), und die Aufnahmeraten waren effizienter, wenn die Blätter MNPs ausgesetzt waren, als wenn letztere den Wurzeln zugeführt wurden. Die Metallkonzentrationen im Spross nahmen mit abnehmendem Partikeldurchmesser und zunehmendem negativen Zetapotenzial zu.

Aus meinen Untersuchungen folgere ich, dass alternative Quellen für die P-Düngung Potenzial haben. Die BCs zeigen ähnliche Auswirkungen auf den P-Status wie TSP, aber auch nanokolloidaler P könnte sowohl zur Pflanzenernährung als auch zu Ökosystemverlusten beitragen. Die Mechanismen der nanopartikulären P-Aufnahme bedürfen weiterer Aufmerksamkeit, aber Studien unter Verwendung von MNPs haben gezeigt, dass es pflanzliche Aufnahmepräferenzen gibt, die sowohl vom Element als auch von den Eigenschaften der Nanopartikel abhängen, insbesondere von der Partikelgröße oder der Oberflächenladung.

Content

List of figures

LIST OF FIGURES

List of tables

LIST OF TABLES

List of abbreviations

a.s.l	above sea level
ha	hectare
rcf	relative centrifugal force
iSPTC	initial soil P test classes
iSPTC-A	severely deficient initial soil P test class
iSPTC-B	deficient initial soil P test class
iSPTC-C	sufficient initial soil P test class
AF^4	Asymmetric flow field flow fractionation
Ag	Silver
Ag_2S	Silver sulfide
AgCl	Silver chloride
Al	Aluminum
ANOVA	Analysis of variance
BC	Bone char
BC^{plus}	Sulfur modified bone char
BU	Building units
C	Carbon
Ca	Calcium
Cd	Cadmium
Ce	Cerium
CeO_2	Cerium dioxide
C_{org}	Organic carbon
Cu	Copper
CuO	Copper oxide
$Cu(OH)_2$	Copper hydroxide
CI	Confidence interval
DOM	Dissolved organic matter
DP	Dissolved phosphate
DRP	Dissolved reactive phosphate
ENPs	Engineered nanoparticles

LIST OF ABBREVIATIONS

Fe	Iron
Fe_2O_3	Iron(II) oxide
Fe_3O_4	Iron(II,III) oxide
GA	Gum Arabic
H_2S	Hydrogen sulfide
H_2SO_4	Sulfuric acid
ICP-MS	Inductively coupled plasma–mass spectrometry
ICP-OES	Inductively coupled plasma–optical emission spectroscopy
KDa	Kilo Dalton
LMiA	Large microaggregates
Mg	Magnesium
MNPs	Metallic nanoparticles
MWD	Mean weight diameter
N	Nitrogen
$NaHCO_3$	Sodium bicarbonate
NaOH	Sodium hydroxide
No-P	Without phosphate fertilizer application
NPs	Nanoparticles
O	Oxygen
OCD	Organic Carbon Detector
P	Phosphorus
P_i	Inorganic phosphate
P_o	Organic phosphate
P_t	Total phosphate
PEG	Polyethylene glycol thiol
PR	Phosphate rock
PVP	Polyvinylpyrrolidone
S	Sulfur
Si	Silicon
SD	Standard deviation
SE	Standard error
SEL	Size exclusion limit

LIST OF ABBREVIATIONS

SEM-EDX	Scanning electron microscopy-energy dispersive X-ray spectroscopy
SMaA	Small macroaggregates
SMiA	Small microaggregates
SMD	Standard mean difference
SOM	Soil organic matter
Ti	Titanium
TiO_2	Titanium dioxide
TFF	Tangential flow filtration
TP	Total phosphate
TSP	Triple superphosphate
U	Uranium
UV-Vis	Ultraviolet visible spectroscopy
WDCs	Water dispersible colloids
Zn	Zinc
ZnO	Zinc oxide

Chapter 1

General introduction

CHAPTER ONE

1.1 Rationale

Already more than 350 years ago, phosphorus (P) has been recognized as a non-substitutable nutrient element for all organisms in the formations of nucleotides (DNA and RNA), adenosine triphosphate (ATP) and phospholipid bilayers in cell membranes (Jupp et al., 2021). Hence, P plays a crucial role in supporting soil fertility and crop yields. Mineral P fertilization thus enhanced food productivity required by increasingly population, while exhausting limited global phosphate rock (PR) reserves. However, due to unevenly distributed PR reserves and different levels of soil legacy P among countries/areas, farmers may have no access to P fertilizers cost-effectively (Brownlie et al., 2021). Bone char (BC) produced by pyrolyzing wastes of slaughterhouse is promising to be one of the substitutes for mineral P fertilizers or novel P fertilizers (Leinweber et al., 2019; Siebers and Leinweber, 2013; Zimmer et al., 2018) to alleviate the shortage of PR. On the other hand, soil P is hardly soluble, so that particulate P forms (especially in nano- or colloidal forms, which possibly reactive than that of macro- and microaggregates) are likely to become crucial parts of soil legacy P and thus future P bioavailability (Montalvo et al., 2015) and accessibility (Siebers et al., 2018).

In this thesis, the status and fate of BC and modified BC derived P was analysed for the first time within soil aggregates in field long-term (from 2013 to 2018) fertilizations by techniques including wet-sieving, centrifugation and tangential flow filtration and measured with UV-Vis and ICP-OES. The contents of P and other elements in arable soil nanocolloids were determined with AF^4-OCD-ICP-MS and potential binding associations were predicted by cluster analysis. The potential crop uptake of nanoparticles was systematic evaluated with a meta-analysis; as few if any data were available concerning the uptake of nanoparticulate P, this final review concentrated on metallic nanoparticles (MNPs).

With knowledge of alternative fertilizer (such as BC materials) derived P transformation within soil size fractions, and of P binding with other elements in nanocolloids, and also concerning the plant uptake of MNPs, the overarching aim of this thesis was to elucidate substituted and nanoparticulate soil P sources for crops.

1.2 State of the art

1.2.1 Bone char and its potential as P fertilizers

Bone char originates from pyrolyzing defatted animal bones, which normally are wastes in slaughterhouse (Alkurdi et al., 2019; Leinweber et al., 2019). The BC could vary in characteristics due to different pristine materials and pyrolysis parameters. The original light yellow bones becomes brown and black and even turns back to grey and white as the temperature of pyrolysis increases from 300 °C to 900 °C (Reidsma et al., 2016). The specific surface area (42 to 114 $m^2\ g^{-1}$) of BC's mesoporous structure and crystallinity of BC are also related to pyrolysis temperature (Dela Piccolla et al., 2021; Leinweber et al., 2019). After thermochemical conversion in high temperatures, the BC usually enriches in P (11% to 21%) and calcium (Ca) (18% to 39%) mainly in the form of hydroxyapatite (Leinweber et al., 2019). Besides, magnesium (Mg) and carbon (C) are also main elements in BC, while rare in cadmium (Cd) and uranium (U) (Morshedizad and Leinweber, 2017; Siebers and Leinweber, 2013). Due to high contents of Ca and Mg, the pH values of BC are slightly alkaline and range from 7 to 10 (Leinweber et al., 2019; Zimmer et al., 2018). With these properties, BC was also used as adsorbents in the removal contaminants such as heavy metals (Cheung et al., 2001), organic pollutants (Jia et al., 2018; Mendes et al., 2019), and fluoride (Alkurdi et al., 2019).

Being abundant in P and calcium Ca, as well as being free of contaminants such as U and Cd compared to PR, the BC-based materials are promising substitutes for P fertilizers. The BC-contained apatite could be regarded as biologically originated, and poorer in crystallinity than geological apatite, resulting in higher solubility of apatite from BC than from the latter (Zwetsloot et al., 2015). Warren et al. (2008) also suggested that the solubility of BC was between PR and triple superphosphate. Immediate enhancement in soil Olsen-P or labile P after applying BC to soil was detected (Siebers and Leinweber, 2013; Warren et al., 2008). As the materials can be more effectively extracted by formic acid than by water (Zwetsloot et al., 2015), the release of P in slightly alkaline BC could be reduced in alkaline soils, while this inhibition might be alleviated after surface modified with sulfur. As reported by Zimmer et al. (2018), after surface absorption of gaseous H_2S, the pH of the BC materials decreased from ~ 9 to ~ 5 in sulfur modified BC (BC^{plus}). Several studies have evaluated the effects of BC and/or BC^{plus} on plant growth, yet in mostly pot conditions (Azeem et al., 2021a; Leinweber

et al., 2019; Ume et al., 2021). For example, Siebers et al. (2014) reported that compared to no P additions, the BC application increased the dry weights of wheat root and heads in an outdoor pot trial with P deficient soil, while having insignificant effects on lettuce and potato in both P deficient and sufficient soils. Similarly, Azeem et al. (2021b) found that BC produced at both 500 and 800 °C significantly enhanced the length and dry weight of both maize root and shoot at application dosages of 2.5% and 5.0% in pots, while 10% addition accounted for mostly non-significantly effects. The plant availability of BC could be promoted after root inoculation of arbuscular mycorrhizae (Zwetsloot et al., 2016). Microbial activities could also enhance the solubility of BC^{plus} with so-called "in situ digestion", which increase the dissolution of apatite owe to generated H_2SO_4 from microbial sulfoxidation of sulfur in surface of BC^{plus} (Fan et al., 2012). The effects of BC^{plus} on both dry matter yield and P uptake of pot grown rye grass were reported to be larger than those of pure BC additions (Zimmer et al., 2019). However, to our knowledge, only one field trial with BC materials has been performed so far, reporting that after a crop rotation (2013 to 2018), the application of BC materials enhanced crop yields and grain P uptake in initially P deficient soils compared to no P addition (Panten and Leinweber, 2020). **Yet, the different forms of P in this study, e.g., the amount of P bound to particles of different soil size fractions, has not yet been revealed.**

Many previous studies of the fate of fertilizer P in soils focused on mainly bulk soil, and soil macro- or micro-aggregates, but fertilizer P in soil colloids were less clear (Liu et al., 2019a; Menezes-Blackburn et al., 2018; Zhang et al., 2021). However, the colloidal P seems more mobile and critical in soil P loss. This study evaluated residual P in the building units (< 1 μm) or termed as soil colloids as well, which I further worked on in the next section.

1.2.2 Nanocolloids and nanoparticulate P in arable soils

The majority of fertilized P was fixed into soils especially that enriched in aluminum (Al) and iron (hydr)oxides, or Ca and Mg minerals. The different sized soil aggregates contribute to high P retention capacity and thus to soil storage of P. They also support plant growth, while the P remaining can becomes less bioavailable or accessible along time due to physicochemical processes such as precipitation, adsorption and occlusion into macro- or microaggregates (> 250 μm and 20-250 μm, respectively) (Totsche et al., 2018). However, the

captured P could be released again via such as reduction of oxides, desorption, dissolution or disaggregation procedures. As the building units of microaggregates, nanocolloids (1 to 1000 nm) are more labile and have more adsorption sites than larger soil size fractions, which could facilitate the transport of soil P via surface runoff, vertical leaching, or artificial drainage systems for instance (Heathwaite et al., 2005; Hens and Merckx, 2001).

Soil nanocolloids could be extracted by a combination of methods including wet-sieving, centrifugation and tangential flow filtration (Tang et al., 2009). The wet-sieving procedure is usually conducted by shaking a stack of sieves with soil samples immersed in water; with retained fractions on the sieve are collected and the suspensions that passed are further sieved to finer sizes (Elliott et al., 1991; Six et al., 2000). Dry sieving without water is commonly employed to collect soil aggregates and was suggested have larger variations of results than wet-sieving (Robertson et al., 1984). With centrifugation, the fractions that have been less effectively separated by wet-sieving, such as size fractions < 1 μm, can further be isolated into smaller size fractions according to different centrifugation parameters such as speed and duration (Henderson et al., 2012). Filtration could also be used to collect colloids, while lose parts of them may clog pores and/or form a filter cake (Zirkler et al., 2012). The supernatant obtained from centrifugation may contain low concentrations of colloids, and is thus unsuitable for further elemental determinations, especially for P, which usually has poor detection signals such as when using inductively coupled plasma mass spectrometry (ICP-MS).

Tangential flow filtration (also called cross flow filtration) technique could condense soil suspensions containing colloids, as the membrane allows passing through of solvent while rejecting particles larger than its pore size cut-off (Yeats et al., 1990). This technique could also overcome the formation of filter cake but it may face problem of fouling of membrane (Zhao et al., 2000). Other colloidal separation methods are also available such as sedimentation-based techniques (Séquaris and Lewandowski, 2003).

The collected soil colloids could be further isolated into nano-meter sized fractions with the help of asymmetric flow field flow fractionation (AF^4), which has been employed for soil colloids' analysis since the past few decades (Baalousha et al., 2011; Jiang et al., 2015; Li et al., 2021a; Regelink et al., 2013). AF^4 coupled with other detectors such as organic carbon detector

(OCD) and ICP-MS could be applied for measurement of soil colloidal organic C and other elements such as P, respectively (Reszat and Hendry, 2005; Stolpe et al., 2005).

Soil colloids are important carriers of soil P (Bol et al., 2016). Gu et al. (2020) indicated that colloidal P accounted for 45% of total P (passing through 450 nm membrane) in soil waters in a field study. The fate of P in arable soil colloids is much less clear, especially the vertical translocation of colloidal P among various soil depths. Jiang et al. (2015) reported that nanocolloidal P mainly sequestrated by crystalline Fe in top layer of an arable Haplic Luvisol. The vertical transport of colloids could also bring both inorganic- and organic P from surface to subsurface in an agricultural Mollisol (Jiang et al., 2021; Li et al., 2022). It has been indicated that colloidal P could support wheat growth possibly attributed to enhanced diffusion of colloidal P and increased contacting with roots (Montalvo et al., 2015). It is unclear, however, whether plant take up the released P from colloids or whether they internalize intact nanocolloids directly. This knowledge gap also existed in numerous publications on plant uptake of nanoparticles (NPs, in size of 1 to 100 nm for two or more dimensions).

1.2.3 Uptake of nanoparticles by crops

Most of the studies on plant uptake of NPs were conducted with engineered NPs (ENPs), which are usually more uniform, pure and regular in shape than natural NPs (Hochella et al., 2019). ENPs derived from anthropogenic release to the surrounding environment pose potential risks to human health; for example, ENPs could enter food chain after being absorbed by crops (Judy, 2013; Nair et al., 2010; Rico et al., 2011). Generally, there are two main entries of crops' exposure to ENPs: root and foliar uptake. Upon each entry, several physical barriers are in the way of ENPs movement into plant internals. In the surface of both root and leaf cells, there is waxy cuticle, which is usually negatively charged, and that will affect the diffusion of ENPs due to electrical interactions (Onelli et al., 2008). The root-adhered ENPs may undergo dissolution caused by root exudates (Shang et al., 2019), or reduced in the plants and reform NPs inside plant tissues (Wagener et al., 2019). In both cases, dissolved metals can also be taken up and thus contribute to plant metal accumulation. When partially dissolved or stable ENPs may cross the cuticle, they may either enter into the symplastic route after crossing the cell wall or into the apoplastic path without penetrate cell wall and both finally reach the endodermis (Lv et al., 2019). Nevertheless, the Casparian strip

in the endodermis has a smaller size exclusion limit (SEL) than that of cuticle and cell wall, so that it's difficult for ENPs to pass through (Wang et al., 2016b). However, as the Casparian strip is un-completely developed on the root tip meristem, its ability to prevent the internalization of ENPs may decline (Nowack et al., 2006). Also in plant leaf, larger ENPs could enter the plants via the stomata, provided that they are > 20 nm in pore radius (Eichert et al., 2008). It becomes thus understandable that particle size of ENPs plays a pivotal role in its internalization of crops. For ENPs with a size smaller than the SEL of root or leaf barriers, a plant uptake of ENPs is likely; meanwhile, there may also be an enhanced dissolution of ENPs with decreasing particle size (Ma et al., 2012) which can facilitate ionic uptake by plants. To date, many studies indicated that plant can take up ENPs (Dwivedi et al., 2018; Geisler-Lee et al., 2013; Lin and Xing, 2008; Ma et al., 2017; Miralles et al., 2012; Wang et al., 2012; Zhang et al., 2015); however, it is still a challenge to distinguish between uptake of released ions from ENPs and intact core ENPs (Lv et al., 2019; Su et al., 2019).

Plant exposure to metallic NPs (MNPs) have obtained considerable research attentions owe to various specific properties (Huang et al., 2021; Liu et al., 2020; Lv et al., 2019; Sturikova et al., 2018). For example, Ag- and CuO NPs are effective as nanopesticides, Zn- and Fe based NPs are promising for applying as nanofertilizers (Singh et al., 2020). Studies on plant exposure to MNPs usually indicated that plant tissues accumulated metals from MNPs (Ahmed et al., 2021b; Cai et al., 2020; Ma et al., 2017). However, the behaviors of plant uptake of metals from metal salts or MNPs may be different due to factors such as slow release of metals from MNPs or toxic or growth promoting effects on plants and so on. For instance, it was reported that the internalization and translocation of Ag NPs in rice were superior to that of Ag^+ from AgCl solutions (Yang et al., 2020). There are many factors controlling the plant uptake of MNPs, such as particle size and surface charge as mentioned above. Besides, the application concentration, exposure way, growth medium, plant species, etc. can also play their roles in the internalization of MNPs. Therefore, a systematic knowledge of crops uptake of MNPs and its impact factors could be important in optimizing MNPs for agricultural applications. To obtain thus knowledge, a meta-analysis method would be the method of choice to study the effects of various factors on plant uptake and accumulation of MNPs, as it is based on a collected new database according to certain selection criteria.

1.3 Objectives

The overarching aim of this study was to contribute to a better understanding of particle-bound nutrients for plant nutrition. Main focus was lain on the availability of P from alternative fertilizers, and on the fate of colloidal P in soil profiles, while for an understanding of potential nutrient uptake mechanisms from nanoparticulate forms, I performed a meta-analysis on the internalization of metallic nanoparticles by major crops. In detail, I tested the following hypotheses:

1) Alternative P fertilizers could be helpful to alleviate the limitation of PR on global food production. It has been reported that BC and BC^{plus} could provide P for plant growth, but how will these alternative P fertilizers BC and BC^{plus} derived P affect various P fractions or pools within soil size fractions under long-term field conditions?

This study aims to provide essential knowledge of the availability, transformation and storage of P within soil size fractions after continuous BC and BC^{plus} fertilization. For this purpose, I analysed samples from a 5-year field experiment, applied wet-sieving, centrifugation and tangential flow filtration techniques to separate bulk soils into four size fractions, and determined the different P fractions after Hedley sequential extractions.

2) Soil particles have strong fixation of fertilizer P. The residual soil P could be transported facilitating by the movement of soil nanoparticles especially under events. After leaching from topsoil to subsurface soils, how the subsoil nanocolloidal P transport to nearby water flows?

It has been reported that colloidal P could be translocated vertically in forest soil profiles. Here, we have studied an artificially drained lowland catchment (1550 ha) in North-Eastern-Germany. We took daily samples during the winter discharge period 2019/2020 at various spatial scales, i.e., drain outlet, ditch, and brook and analyzed them for total P ($TP_{unfiltered}$), particulate P >750 nm ($TP_{>750\ nm}$), colloidal P ($TP_{colloids}$), and truly dissolved P (truly DP) during baseflow conditions and high flow events. Moreover, I investigated elemental concentrations in soil colloids from both top- and sub-soils. The soil colloids were also fractionated into three size fractions and a cluster analysis was performed to evaluate the transport of soil colloidal P to drainage systems.

3) **Both nanocolloidal P and metallic nanoparticles (MNPs) have been reported could be taken up by plants. Are there crop uptake preferences between MNPs and dissolved metal salts? Which factors are more important in controlling the crop uptake of MNPs?**

Many studies indicated that the plant metal accumulations from metal salts or MNPs are different and have various impact factors. Due to limited data on NP-derived P in plants, I broadened this topic for a meta-analysis, aiming at exploring metal accumulation preferences by crop tissues and outlining the impact factors that control given metal accumulations. I reviewed 173 studies to evaluate the crop accumulation and uptake of metallic nanoparticles (MNPs) and potential critical impact factors.

The three hypotheses were answered in the next three research Chapters and finally answered in the synthesis (Chapter 5) of this thesis.

Chapter 2

Fate and availability of phosphorus from bone char with and without sulfur modification in soil size fractions after five-year field fertilizations

Modified on the basis of the manuscript

Yunsheng Jia, Nina Siebers, Kerstin Panten, Jens Kruse

Submitted to ***Soil and Tillage Research***

CHAPTER TWO

2.1 Introduction

As one of the non-substitutable nutrient elements to all organisms and crops, phosphorus (P) plays a vital role in supporting soil fertility and food production (Holford, 1997; Roberts and Johnston, 2015; Scholz et al., 2013; Vance et al., 2003). However, there are considerable uncertainties on how long the finite rock phosphate (RP) reserves can cover the global needs (Cordell et al., 2009; Obersteiner et al., 2013). Further concerns relate to high contaminations with cadmium (Cd) and uranium (U) and the globally uneven distribution of the remaining P reservoirs (Desmidt et al., 2015; Obersteiner et al., 2013; Scholz et al., 2013) increasingly driving current P research on novel P sources and approaches.

Recent studies have shown that bone char (BC) based materials could be one of the promising recycled P fertilizers (Glaesner et al., 2019; Kruse et al., 2022; Morshedizad and Leinweber, 2017; Morshedizad et al., 2018; Siebers et al., 2014; Siebers et al., 2013; Siebers and Leinweber, 2013; Zimmer et al., 2018; Zwetsloot et al., 2016). Bone char is produced from pyrolysis of animal bone chips, which usually are regarded as wastes in slaughterhouses (Leinweber et al., 2019; Zimmer et al., 2018). It is almost free of soil contaminants such as Cd and U and contains, beside of calcium (Ca) and magnesium (Mg), considerable amounts of P (roughly 130 to 150 g P kg^{-1}), mainly in the form of hydroxyapatite (Leinweber et al., 2019; Siebers and Leinweber, 2013). Furthermore, due to its biological origin and associated lower crystallinity this hydroxyapatite is in fact more soluble than geological apatite (Zwetsloot et al., 2015). Plant availability and P release kinetics of BC were studied mostly in lab or pot experiments (Leinweber et al., 2019; Siebers et al., 2014; Zwetsloot et al., 2016), but recently for the first time also at the field (Panten and Leinweber, 2020). The major factors controlling BC dissolution are soil pH and sinks of soil P and Ca, which are similar with that of RP (Warren et al., 2008). It was shown that P dissolution from BC was generally slower than commercially available highly soluble P fertilizers (Siebers and Leinweber, 2013) and that a higher soil acidity promotes the dissolution of BC (Leinweber et al., 2019; Zimmer et al., 2018; Zimmer et al., 2019). The fertilizing effect for various crops increased compared to no-fertilization (Little et al., 2017; Zwetsloot et al., 2016). Results of these studies suggest that crops such as wheat and grass, with relatively long growth period and developed root system to explore slowly released P from BC-based fertilizers, could have a higher agronomic

efficiency than fast growing vegetables (Leinweber et al., 2019). Moreover, the surface of BC could enrich with up to 20% (w/w) elemental sulfur (S) (BC^{plus}; patent DE102011010525) by absorbing gaseous sulfur from biogas streams, which could increase the P solubility in the soil (Zimmer et al., 2018). A so-called "in situ digestion" process could be involved which fosters apatite dissolution by the release of H_2SO_4 from microbial sulfoxidation (Fan et al., 2012). For example, previous batch and pot experiments indicated a higher solubility of BC^{plus} compared to BC (Morshedizad et al., 2018; Zimmer et al., 2019). This implies that especially BC^{plus} which is recycled from wastes of slaughterhouse and biogas streams could be a suitable alternative for RP fertilizers (Zimmer et al., 2018).

However, in order to be used by organisms and plants, the released P from fertilizer must be both bioavailable (present in a suitable chemical form) and bioaccessible (physically accessible). The bioaccessibility of P and also all other nutrients is largely controlled by soil aggregates, as the incorporation and release of P during aggregate formation and breakdown play a vital role in nutrient storage and cycling (Bronick and Lal, 2005; Six et al., 2004). During the past several decades, extensive works investigated and compared effects of P fertilizations on P speciation and availability in soils (Ajiboye et al., 2008; Alamgir and Marschner, 2013; Baggie et al., 2004; Koch et al., 2018; Siebers et al., 2021). However, little is known about the fate of fertilizer P within soil aggregates, or P fertilization effects on various P pools within soil aggregates (Garland et al., 2018; Wan et al., 2020), and no information is available about the fate of fertilizer P from BC or BC^{plus}. The soil aggregates consist of macro, micro, and nanoscale aggregates composed of inorganic (minerals) and organic (organic matter, microbial biomass/debris) materials resulting from various physical, chemical, and biological processes (Totsche et al., 2018). Soil microaggregates (< 250 µm) possess a relatively high stability and persistence and strongly link with the major biological processes controlling the turnover of nutrients. In literature, it was shown that there is a faster potential P turnover rate in large microaggregates than in small microaggregates (Siebers et al., 2018). However, the functional relation between the soil aggregates and P is still a key to understand the potential of soils to store and supply fertilizer P to plants. Therefore, knowledge of the fate of fertilizer P and its transformation and cycling within the soil aggregates is important for a sustainable fertilizer management.

With differed solubilities and pH, we hypothesize that BC and BC^{plus} introduced P into soil aggregates may perform different and also differ with traditional highly soluble mineral P fertilizer (such as triple superphosphate, TSP) in affecting soil P availability and forms. Hence, the objective of this study was to determine for the first time the fate of fertilizer P from BC, BC^{plus} and TSP in different soil aggregate size fractions under field conditions using samples from the first BC-based long-term P fertilization experiment. We applied Hedley sequential P extraction for soil aggregates under BC and BC^{plus} treatments, and different P forms and availabilities (labile, moderately labile and stable P) were studied. Hence, we provide essential knowledge on the availability, transformation, and storage of P within different soil aggregate size fractions after continuous BC and BC^{plus} fertilizations as needed for an optimum management of these promising fertilizer resources.

2.2 Materials and methods

2.2.1 Study site and experimental design

The study site with 9 °C mean annual temperature and 620 mm mean annual precipitation, is a long-term fertilization arable land located near Braunschweig, Germany (10° 27´ E; 52° 18´ N, elevation 81 m a.s.l.). The soil at the site was described as Haplic Luvisol and Dystric Cambisol (IUSS Working Group WRB, 2015) and were built from sandy fluvial sediments overlaid with sandy loess. Before establishment of this experiment, the site was under continuous long-term P fertilization from 1985 to 2008. Since there were different dosages of fertilizer P for more than two decades and plots were randomly designed (for more details see Vogeler et al. (2009), this left randomly distributed plots with different concentrations of calcium acetate lactate extractable P (P-CAL), which were assigned to initial soil P-test classes (iSPTC) based on their topsoil P-CAL concentrations, i.e., iSPTC-A (severely deficient, < 15 mg P-CAL kg^{-1}), iSPTC-B (deficient, 15 to 30 mg P-CAL kg^{-1}), and iSPTC-C (sufficient, 31 to 60 mg P-CAL kg^{-1}), respectively (Wiesler et al., 2018). Only iSPTC-A and iSPTC-C plots were involved in the present study and analyzed in the following sections. It should be noted that the study site was an extensively managed grassland from 2009 to 2012, and then converted to arable land for the preparation of the current study. Total carbon (C), nitrogen (N) and P contents, and pH for iSPTC-A and -C bulk soils were 13 and 14 g kg^{-1}, 10 and 10 g kg^{-1}, 349

and 520 mg kg^{-1}, and 5.1 and 5.2, respectively. More details on former field characteristics and site management see Panten and Leinweber (2020).

The present study started autumn of 2013 with four different P fertilization treatments on iSPTC-A and iSPTC-C: 1) control, without P addition, termed as No-P; 2) triple superphosphate, TSP; 3) bone char, BC; and 4) bone char enriched with elemental sulfur, BC^{plus}. Each treatment had triplicated plots (5.75 m × 17.5 m), which were arranged in a completely randomized block design. All P treatments (TSP, BC, and BC^{plus}) received an amount of 45 kg P ha^{-1} $year^{-1}$. The plots received a combination of chisel ploughing and conventional ploughing to 25 cm depth before yearly sowing (5-year crop rotation: winter barley, winter oilseed rape, winter wheat, lupin, and winter rye). For details on further fertilizations with other elements see Panten and Leinweber (2020). The crop yields and P uptake of plants in response to the P treatments were published by Panten and Leinweber (2020).

The BC was manufactured by pyrolysis of rendered (de-fatted) crushed bovine bones at around 800 °C. Subsamples of BC were surface-modified by adsorbing H_2S (BC^{plus}) from a biogas stream according to procedure described in patent DE102011010525. The total P contents of the applied P fertilizers are 148 g kg^{-1} (BC), 107 g kg^{-1} (BC^{plus}), and 200 g kg^{-1} (TSP). For more details on properties of both BC based fertilizers see Zimmer et al. (2018).

2.2.2 Soil sampling and soil aggregates separation

In the present study, we investigated soil samples before the start of the trial (21st Aug 2013) and after completion of the first 5-year crop rotation (20th Jul 2018). For soil sampling, eight soil cores were taken per treatment and plot to a depth of 30 cm and combined to a composite bulk sample. The samples were air-dried and sieved through 2 mm (as bulk soil) and stored in plastic bags before soil aggregate separation and other further analyses.

The bulk soil was separated into four soil size fractions slightly adapted from size range defined by Totsche et al. (2018), namely (i) 250 to 2000 µm, small macroaggregates (SMaA); (ii) 53 to 250 µm, large microaggregates (LMiA); (iii) 1 to 53 µm, small microaggregates (SMiA), and (iv) < 1 µm, composite building units (BU). For size fractionation, a combination of wet sieving, centrifugation, and tangential flow filtration (TFF) was applied (Dalwadi and

Sunderland, 2007; Six et al., 2000; Tang et al., 2009). Briefly, bulk soil (< 2 mm) was firstly immersed in deionized water on top of the two-sieves stack (mesh size 250 and 53 μm) and manually shaken up and down. The fraction remaining on the 250 μm and 53 μm sieve were designated as SMaA and LMiA respectively. The wet-sieving procedure took 1 hour for 40.0 g of the studied soil samples by 10 cm diameter sieves. The 1 to 53 μm aggregates were separated by centrifugation at 4000 rcf for 2 min calculated referring to Stork's law (Henderson et al., 2012) and the solids were transferred to a beaker for drying (as SMiA). The supernatant was passed through a TFF system (Minmate™ TFF Capsule (1 KDa m-polyethersulfone membrane, PALL Life Sciences, USA) associated with pressure gauges and a peristaltic pump (Cole-Parmer, Masterflex L/S). The concentrated supernatant was collected and dried (as BU). All of the four soil size fractions were oven dried at 40 °C, weighed, and stored for further analyses.

2.2.3 Soil analyses

The soil aggregates mass distribution proportion was calculated by dividing the weight of each aggregate size fraction by the weight of bulk soil used in the wet sieving procedure. The mean weight diameter (MWD, μm), an evaluation parameter for the changes in soil aggregate stability, was calculated according to the following equation:

$$\text{MWD} = \sum_{x=1}^{n} w_x \times \bar{d}_x \qquad \text{(Eq. 1)}$$

where n is the number of aggregate size fractions, w_x is the ratio of the weight of x^{th} fraction to the weight of bulk soil used in the wet sieving, and $\bar{d}_x$ is the mean diameter of x^{th} fraction (μm). Total elemental contents of Ca, Mg, and iron (Fe) were determined after microwave-assisted digestion of 150 mg soil samples with 0.7 mL HNO_3 and 2 mL HCl using an inductively coupled plasma-optical emission spectroscopy (ICP-OES; Thermo Fisher iCAPTM 7600). The contents of total C, N, and S were analyzed by dry combustion followed by heat conductivity detection of the released trace gases (vario MICRO cube, Elementar, Hanau, Germany).

2.2.4 Sequential P fractionation

For the sequential P fractionation of soil aggregates, a slightly modified Hedley sequential P extraction procedure was applied (Hedley et al., 1982; Negassa et al., 2010; Schmitt et al.,

2017). In short, 0.5 g (0.2 g for BU) of sample were weighed into 50 mL (15 mL for BU) centrifuge tubes and sequentially extracted with 30 mL (12 mL for BU) of: (1) ultrapure deionized water, (2) 0.5 M $NaHCO_3$, (3) 0.1 M NaOH, and (4) 1 M H_2SO_4. Each suspension was shaken at 250 rpm for 18 h followed by centrifugation at 5000 rcf for 20 min. The sequentially extracted P will be named as different P pools hereafter. The concentration of total P (P_t) in the extracts was determined by ICP-OES. Inorganic P (P_i) concentration in the extracts was measured with molybdate blue colorimetric method using a UV-VIS spectrometer at a wavelength of 890 nm (Nagul et al., 2015). Organic P (P_o) concentration in the H_2O, $NaHCO_3$, and NaOH extracts was calculated as the difference between the P_t and P_i of each of these three P pools. The extracted different P pools were further interpreted as follows: (1) H_2O-P + $NaHCO_3$-P = labile P, (2) NaOH-P = moderately labile P, and (3) H_2SO_4-P = stable P. The labile, moderately labile, and stable P will also be noted as P pools hereafter. The total extracted P is the sum of labile, moderately labile and stable P. Also, the proportion of each P pool to the total extracted P for every size fraction was calculated. Meanwhile, the P mass proportion of each size fraction to sum of P of all four soil size fractions was calculated as follows:

$$\text{P proportion of } x^{th} \text{ fraction (\%)} = 100 \times \frac{P_x \times m_x}{\sum_{x=1}^{n} P_x \times m_x} \quad \text{(Eq. 2)}$$

where n is the number of aggregate size fractions, P_x is the P content (g kg^{-1} fraction) of x^{th} fraction, and m_x is the mass (g) of x^{th} fraction.

2.2.5 Statistical analyses

Data analyses and graph plotting were performed with RStudio software version 3.6.3 (R Core Team, 2021). Normality and homogeneity of variances assumptions of data sets were tested by Shapiro-Wilk and Levene's test, respectively (Alboukadel, 2021). If the assumptions were verified, two-way mixed ANOVA was performed to compare means of all treatments (independent factor) and aggregate size fractions (dependent factor) for each soil P class (i.e., iSPTC-A and -C) separately. The assumption of sphericity was tested using the Mauchly's tests, and if the assumption was violated the Greenhouse-Geisser sphericity correction was applied (Alboukadel, 2021). If the assumptions (normality and homogeneity of variances) of the two-way mixed ANOVA were violated, the non-parametric Friedman's ANOVA was

used (Field et al., 2012). It was also tested for significant two-way interactions of the two parameters – treatments and aggregate size fractions – but none were found. Therefore, we performed a multiple paired t-tests for the treatment ignoring size fraction, and vice versa. The p values were adjusted using the Bonferroni multiple testing correction method. Paired t-tests were also applied to compare means of each sample collected in 2013 and 2018 for each treatment in each aggregate size fraction (Alboukadel, 2021; Field et al., 2012). The statistical significance was accepted with $p < 0.05$.

2.3 Results

2.3.1 Mass distribution and MWD of soil size fractions

There was a consistent trend in all treatments at both soil P classes (iSPTC-A and -C) that the aggregate mass proportions declined in the order of SMiA > LMiA ≥ SMaA > BU (Figure 2-1) and were in the range of 32.5±0.1 (mean±sd) to 46.5±1.3%, 25.1±0.4 to 33.0±0.3%, 23.5± 0.1 to 35.4±0.4%, and 0.4±0.2 to 1.9±0.0%, respectively. When comparing the aggregate mass proportions between 2013 and 2018, most treatments (No-P, TSP, and BC) had insignificant effects except for the BC^{plus} treatment in iSPTC-A, which significantly decreased the mass proportion of LMiA from 31.0 (2013) to 27.4% (2018). After five years field applications, only the mass proportion of LMiA in iSPTC-A showed significant increase for all P fertilization treatments (TSP 26.4%, BC 26.7%, BC^{plus} 27.4%) compared to No-P (25.9%). In addition, the TSP treatment (0.90%) significantly decreased the mass proportion of BU in iSPTC-A compared to the BC^{plus} treatment (1.02%), while No-P and BC treatments had insignificant effects on BU mass proportion. The MWD of all treatments ranged between 317 to 449 μm (Figure A-1). In the No-P treatment for iSPTC-C, the SMD significantly decreased (8%) from 2013 (381 μm) to 2018 (352 μm). Similarly, the MWDs of TSP, BC, and BC^{plus} treatments decreased by 8.7%, 2.4%, 8.4% for iSPTC-A, and 3.1%, 5.6%, 13.0% for iSPTC-C after five years, respectively.

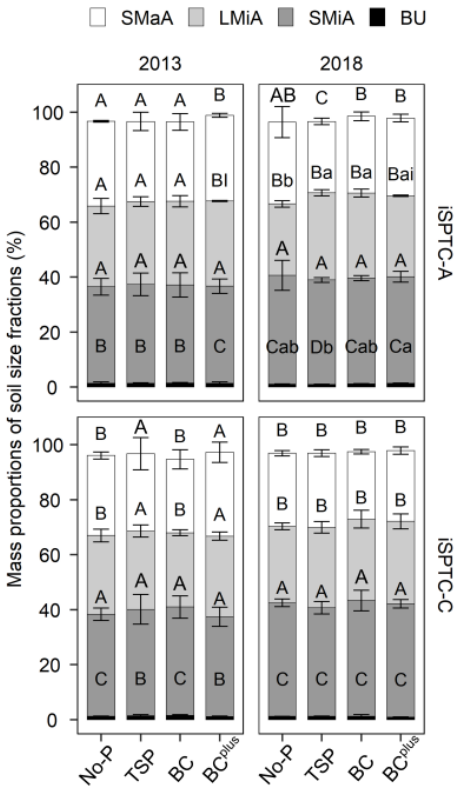

Figure 2-1. Mass proportions of aggregate size fractions (250 to 2000 µm, small macroaggregates, SMaA; 53 to 250 µm, large microaggregates, LMiA; 1 to 53 µm, small microaggregates, SMiA; and < 1 µm, building units, BU) for four treatments (No phosphorus, No-P; triple superphosphate, TSP; bone char, BC; and sulfur modified bone char, BC^{plus}) in severely deficient or sufficient initial soil test P class (iSPTC-A or -C) soil before the start of the field trial (2013) and after 5 years (2018). Significant differences between size fractions within a treatment in a year were labeled with different capital letters; between treatments within a size fraction in a year were labeled with different lowercase letters; between years within a size fraction and a treatment were labeled with i or I, respectively. The value labelled with "I" was tested significantly higher than value labelled with "i". n = 3.

2.3.2 Total elemental contents and P proportions in soil size fractions

The total contents of C, N, S, P, Ca, Fe, and Mg increased with decreasing soil size fractions irrespective of fertilization treatment and soil initial P classes (Table A-1 and A-2). Generally, all total elemental contents in BU were significantly higher (2 to 9 times) than that in SMaA, LMiA, and SMiA, while there were comparable (insignificant) elemental concentrations among the latter three soil size fractions. In each soil size fraction, elemental contents were generally insignificantly affected by different P fertilizer treatments. In line with expectations, the Ca contents and bulk soil pH values increased in all treatments and soil P classes after 5 years. (Table A-1 and A-2).

The P mass proportion for each soil size fraction to the sum of P mass of all soil size fractions was calculated using Eq. 2. In all treatments at both soil P classes, the SMiA size

fraction contained the largest mass proportion of total P (37 to 62%) followed by LMiA (16 to 34%), SMaA (13 to 29%), and BU (3.5 to 8.2%) (Figure 2-2). The P mass proportions of most soil size fractions were not affected by the different fertilizer treatments; however, in the iSPTC-A, TSP application significantly increased the mass proportion of P in LMiA (33%) compared to that of No-P (28%) and of BC (26%) treatments. Furthermore, P mass proportions in LMiA in the iSPTC-C increased significantly (from 21% to 28%) after five years of No-P fertilization.

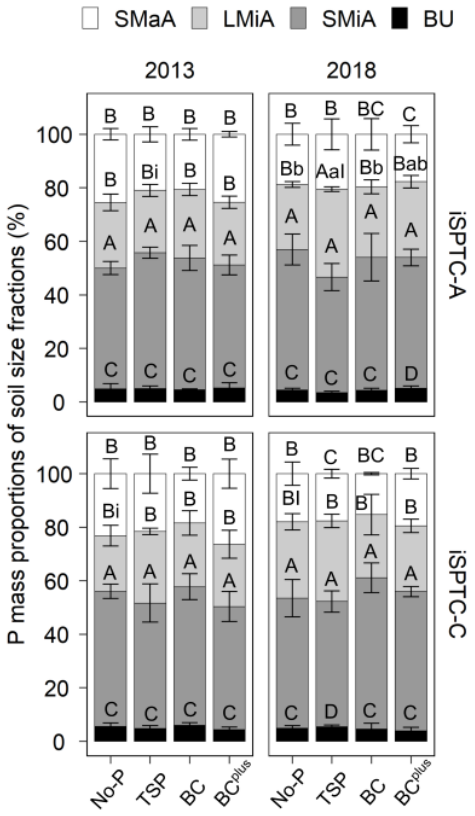

Figure 2-2. Proportions of total Hedley extracted P (mg kg^{-1} bulk soil) in each aggregate size fraction (250 to 2000 µm, small macroaggregates, SMaA; 53 to 250 µm, large microaggregates, LMiA; 1 to 53 µm, small microaggregates, SMiA; and < 1 µm, building units, BU) to sum of total extracted P of four soil size fractions under different treatments (No phosphorus, No-P; triple superphosphate, TSP; bone char, BC; and sulfur modified bone char, BC^{Plus}) in severely deficient or sufficient initial soil test P class (iSPTC-A or -C)soil. Significant differences between size fractions within a treatment in a year were labeled with different capital letters; between treatments within a size fraction in one year were labeled with different lowercase letters; between years within a size fraction and a treatment were labeled with i or I, respectively. The value labelled with "I" was tested significantly higher than value labelled with "i". n = 3.

2.3.3 Sequentially extracted P pools in soil size fractions

When looking at the P concentration in relation to the mass of each size fraction (mg P kg^{-1} size fraction) for different P pools, the P concentrations of each soil size fraction increased in the order of H_2O-P_i < H_2O-P_o < $NaHCO_3$-P_o ≈ $NaHCO_3$-P_i < NaOH-P_i ≈ H_2SO_4-P < NaOH-P_o irrespective of the treatment or iSPTC (Table A-3 and A-4). Within the same treatment, the concentrations of most P pools increased with decreasing aggregate size. Only the H_2O-extractable P pool (H_2O-P_i and H_2O-P_o) showed no clear trend. Most of the extracted P pools exhibited no clear (insignificant) responses to 5-year field BC and BC^{plus} fertilizations in both iSPTCs. The highly soluble TSP only significantly increased concentrations of all P pools except the NaOH-P_o and H_2SO_4-P in iSPTC-A. This was especially visible in the smaller size fractions (SMiA and BU) (Table A-3). For iSPTC-C, such a systematic change in P concentrations was not evident; while concentrations of NaOH-P_o and H_2SO_4-P significantly increased with time in BU under TSP treatment (Table A-4), the concentrations of $NaHCO_3$-P_i in SMaA and SMiA decreased by -30% and -18% after 5-year BC addition, respectively. An even more pronounced decrease was observed for No-P (iSPTC-C) after 5 years: -28% of H_2O-P_i in SMaA, -54% of H_2O-P_o in BU, -33% and -22% of $NaHCO_3$-P_i in SMaA and LMiA, and -9% of NaOH-P_i in BU, respectively.

For iSPTC-A, the TSP, BC, and BC^{plus} treatment increased the total extractable P_i (sum of H_2O-P_i, $NaHCO_3$-P_i, NaOH-P_i, and H_2SO_4-P) from 714 to 853 mg kg^{-1} in BU; in the TSP, from 192 to 235 mg kg^{-1} of SMiA, and 176 to 214 mg kg^{-1} of LMiA, respectively **(**Table A-3). However, a similar increasing trend of total extractable P_i was not detected for iSPTC-C.

2.3.4 Labile, moderately labile, and stable P pools in soil size fractions

The sequentially extracted P pools can be further assigned into three P pools differed in plant availability, i.e., labile P (sum of H_2O-P_i, H_2O-P_o, $NaHCO_3$-P_i, and $NaHCO_3$-P_o), moderately labile P (sum of NaOH-P_i and NaOH-P_o), and stable P (H_2SO_4-P) pools. When relating the P mass of each P pool and size fraction to the total mass of the bulk soil (mg $P_{Pool;\ size\ fraction}$ kg^{-1} soil), the concentrations of the three P pools followed the order of labile P < stable P < moderately labile P pool and increased with decreasing soil size fraction. An exception to this was BU which exhibited the lowest concentrations of each of the three P pools in all treatments and iSPTCs (Figure 2-3**)**. Thus, SMiA accounted for the highest concentrations of all three P pools irrespective of treatments and iSPTCs. Within a treatment

the labile P concentration in SMiA was mostly significantly higher than that in the other soil size fractions, except for TSP and BC^{plus} treatments of iSPTC-A. Moderately labile P was not significantly different between SMaA and LMiA irrespective of treatments except for TSP in iSPTC-A; a general trend for stable P among soil size fractions and iSPTCs were not found. For most cases, there were no significant differences of P pool concentrations between various treatments. Significant variations were only visible for a higher concentration of labile P in LMiA under TSP compared to BC at iSPTC-C (Figure 2-3).

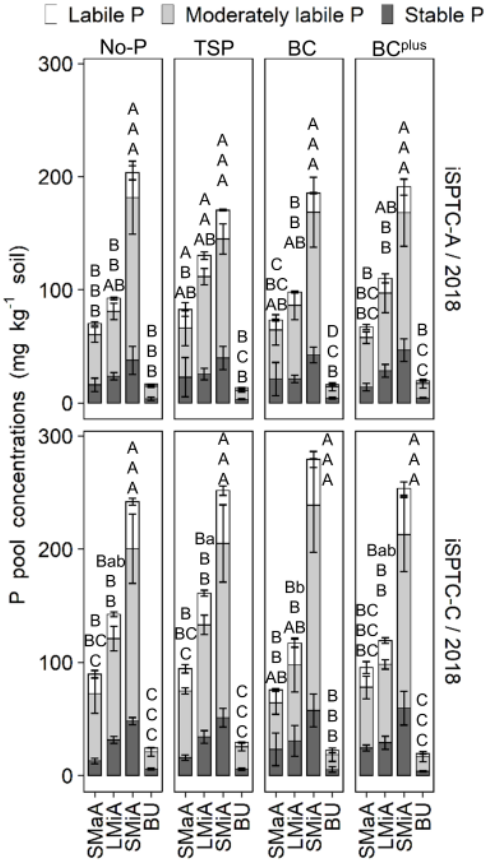

Figure 2-3. Labile (sum of H_2O-P_i, H_2O-P_o, $NaHCO_3$-P_i and $NaHCO_3$-P_o), moderately labile P ($NaOH$-P_i and $NaOH$-P_o) and stable P (H_2SO_4-P) concentrations (mg P kg^{-1} soil) for aggregate size fractions (250 to 2000 µm, small macroaggregates, SMaA; 53 to 250 µm, large microaggregates, LMiA; 1 to 53 µm, small microaggregates, SMiA; and < 1 µm, building units, BU) and treatments (No phosphorus, No-P; triple superphosphate, TSP; bone char, BC; and sulfur modified bone char, BC^{plus}) in severely deficient or sufficient initial soil test P class (iSPTC-A or -C) soil. Significant differences between size fractions within a treatment at each soil P class were labeled with different capital letters; between treatments for a size fraction at each soil P class were labeled with different lowercase letters. n = 3. Significance labels were above each bar of the plot and from top to down were for labile, moderately labile and stable P, respectively.

2.4 Discussion

2.4.1 Size distribution and elemental compositions of soil aggregates

The mass proportion of soil size fractions decreased in the order of SMiA > LMiA ≥ SMaA ≫ BU irrespective of treatments (Figure 2-1), being in line with results described in literature (Fernández-Ugalde et al., 2013; Garland et al., 2018; Krause et al., 2018; Zhang et al., 2020). Before the trial was established in 2013, the field site was used as grassland for four years (from April 2009 to April 2013), and during 2013 and 2018 the site was ploughed annually. Such conversion into cropland results in the breakdown of macroaggregates (Spohn and Giani, 2011). Since macroaggregates are weak associations of biodegradable compounds and microaggregates (Tisdall and Oades, 1982), they easily disintegrate under ploughing (Paul et al., 2013), leading to release of microaggregates.

This release of microaggregates may partially responsible for the significant increase of the LMiA mass proportion after five years of P fertilization compared to No-P. The P fertilization probably stimulated plant or microbe growth, leading to more organic binding agents such as polysaccharides, roots, microbial hyphae or debris, which could have increased soil microaggregation (Tisdall and Oades, 1982). The concomitant decrease of the BU mass in iSPTC-A after highly plant available TSP addition thus could be a result of incorporation of BU into newly formed microaggregates (Jastrow, 1996; Tisdall and Oades, 1982). Furthermore, all three P fertilizers contain significant amount of Ca^{2+} being potentially able to bond clay and organic matter as clay-polyvalent metal-organic matter complexes, which play a critical role in microaggregate formation (Tisdall and Oades, 1982). The P fertilization only resulted in an additional annual Ca input of 21 kg ha^{-1} for BC and BC^{plus}, and ~ 60 kg ha^{-1} for TSP. However, this additional input is most likely negligible when considering the amount of Ca applied by liming twice during the experimental duration (909 + 1441 kg Ca ha^{-1}), which all treatments received. This also explains the significant increase of both Ca concentration and soil pH from 2013 to 2018 (Table A-1 and A-2) (Haynes and Naidu, 1998). Hence, we assume that the significant increase of LMiA in all P fertilized treatments cannot be explained by a Ca^{2+} enhanced microaggregate formation. Therefore, it seems that even under grass to crop land use conversion condition, fertilization with TSP or BC-based materials could enhance soil micro-aggregation. The insignificant change of MWD from 2013 to 2018 could also be combined effects of disaggregation after land use change and P fertilization induced aggregation.

As showed in Table A-1 and A-2, there were higher total elemental concentrations with decreasing aggregate size. Similar results have been reported (Fernández-Ugalde et al., 2013; Luo et al., 2011; Wright, 2009; Zhang et al., 2003) and can be explained by the accumulation of soil organic matter and other elements into small size fractions due to an increase in the specific surface area and a reduced presence of primary mineral particles like sand and silt (Garland et al., 2018; Kahle et al., 2002; Kennedy et al., 2002). In our study, the highest elemental concentrations were found in BU, while the absolute mass of BU was the lowest (0.4 to 1.9%) among all size fractions, the contribution of BU contained P to total plant P uptake could be low. However, we are not sure whether BU contained P will play a role in providing P in micro- or nanoscale rhizosphere (Sinaj et al., 1997). Santner et al. (2012) showed that nanoparticle bound P can buffer P concentration if plant uptake of P is limited by diffusion of free P to the plant roots. BU could also facilitate the movement/transport of soil P as BU is easily transported via soil water flows (Siebers et al., 2023). Moreover, plant roots may internalize BU directly or after partially dissolution with help of root exudates by mechanisms have been reported for engineered nanoparticles (Jia et al., 2022). The contribution of BU to total plant P uptake would be interested for further research.

As reported by Wang et al. (2001), plant uptake of P enhanced with increasing aggregate size which can be attributed to decreased aggregate stability, reduced P fixation, and associated enhanced P release from large aggregates. The observed significant increase of P proportion after TSP addition and P concentration after BC^{plus} addition in LMiA in iSPTC-A (Figure 2-2 and Table A-1) indicated that excessive fertilizer P not used by crops accumulated in this size fraction. Thus, our results suggest that modification with elemental sulfur in BC^{plus} not only increases its solubility, potentially providing more plant available P than untreated BC, but also promotes the accumulation of excess fertilizer P in a bioaccessible form similar to TSP. Meanwhile, SMiA, with the highest mass proportion, exhibited the largest P proportions even its P concentration was only accounted for ~ 30% to that of BU. As SMiA had the highest P mass proportion and BU had the highest P concentration, both particle sizes are < 53 μm, they would contribute to soil P loss especially under events (Heathwaite et al., 2005). Hence, for agricultural managements and controlling of non-point source pollution, we could pay more attention to these two size fractions.

2.4.2 Variations of P pools in soil size fractions

The order of increasing P concentration in the single P pools (i.e., H_2O-P_i ≈ H_2O-P_o < $NaHCO_3$-P_o < $NaHCO_3$-P_i < NaOH-P_i ≈ H_2SO_4-P < NaOH-P_o, Table A-3 and A-4) was in line with literature also stating that more labile P pools were lower than stable P pools (Ranatunga et al., 2013; Siebers et al., 2021). The fact that the concentration of both H_2O-P_i and H_2O-P_o did not follow the general trend of increasing P concentrations with decreasing size can be attributed to methodological artifacts of the wet sieving method we used to fractionate the soil aggregates. Since, during aggregates separation, ultrapure deionized water (about 600 mL) was used, a proportion of the H_2O-P fraction was most likely lost before sequential extraction. We tried to estimate the amount of P been lost during wet-sieving, and the lost P approximately accounted for 1.6 to 29.5% of H_2O-P. Hence, in some cases, the disturbance of wet-sieving to H_2O-P should not be neglected. Meanwhile, there might be other factors contributing to comparable concentrations of H_2O-P among four soil size fractions. Before extraction, the soil size fractions were oven-dried at 40 ℃ to constant weight. As Wang et al. (2020b) reported, air-drying step increased the Hedley extracted labile P pool due to its influences on microbial biomass P and soil organic matter. The oven-drying step we applied here may induce changes in soil H_2O-P and other labile P pools as well. More studies are needed to further elucidate the effects of various drying processes on Hedley extracted P pools.

After five years of P fertilization, most pronounced treatment effects were visible for the TSP treatment, significantly increasing all P pools in iSPTC-A except the NaOH-P_o and H_2SO_4-P pools in most size fractions (Table A-3). The missing effects on the NaOH-P_o and H_2SO_4-P pools were probably a result of the higher stability of P extracted in these P pools. The NaOH-P is representing moderately labile inorganic and organic P most likely sorbed and/or fixed by aluminum- and iron (hydr)oxides (accessory minerals) and P in soil organic matter being only potentially bioavailable (Cross and Schlesinger, 1995; Tisdall and Oades, 1982). The H_2SO_4-P represents mostly insoluble (stable) P associated mainly with Ca and Mg minerals being in occluded or non-occluded forms (Hou et al., 2018). Therefore, turnover times of these two P pools are long and thus five years might not be sufficient to alter these P pools even after application of a highly soluble P fertilizer like TSP as also showed by

Siebers et al. (2021) studying P pools of four long-term trials. On the other hand, the SMiA H_2SO_4-P proportions significantly increased after five years of BC application. However, this effect is likely not a result of P dissolution from BC and then fixation of released P in moderately labile and stable P pools, but rather a sequestration of BC particles being in the size range of the SMiA.

The observed significant reduction of $NaHCO_3$-P_o concentrations (Table A-3) in SMaA and BU in the No-P treatment of iSPTC-A might be a result of the adaption of the microbial community to lower P concentrations and thus higher mineralization rates of $NaHCO_3$-P_o (Grafe et al., 2021). Furthermore, liming and associated increase in soil pH may have affected phosphatase activities, further promoting $NaHCO_3$-P_o mineralization (Acosta-Martinez and Tabatabai, 2000). The $NaHCO_3$-P_o represents labile mineralizable P_o (Hou et al., 2018), which is less stable and more susceptible to microbial mineralization than NaOH-P_o under P limitation (No-P treatment) (Ranatunga et al., 2013). The significant increase of $NaHCO_3$-P_o in the TSP treatment was in line with this concept that the mineralization of P_o is controlled by the supply and need of P (McGill and Cole, 1981). The observed significant increase of $NaHCO_3$-P_i in BU in the TSP treatment of iSPTC-A compared to the No-P treatment (**Table A-3**) was probably a result of the high specific surface area of the large amount of adsorption sites of BU compared to the larger size factions (Wang et al., 2001).

Our findings suggested that five years field fertilization of both highly soluble TSP and slow-release BC and BC^{plus} could not significantly affect the moderately labile and stable P pools, while TSP could contribute to the labile P pool accrual significantly. However, this enrichment in soil labile P may also host high risk of P loss and then eco-problems because of particle facilitated P leaching or runoff, while results of this trial gave no indication on this (Kruse et al., 2022). Under P limitation, moderately labile organic P pool in the loosely aggregated size fraction (SMaA) and the smallest size fraction (BU) which have the highest P content are more prone to be mineralized and replenish soil available P, which needs further demonstration. As reported by Panten and Leinweber (2020), the mean yields during one crop rotation of the present trial showed insignificant differences among treatments, only slight variation (insignificant) of crop yields in the order of BC < BC^{plus} < TSP under P limitation. Thus, we recommend that for the studied P deficient soils, BC and especially

BC^{plus} may be applied combining with TSP, in which way TSP could supply P quickly while BC materials could serve as slow-release fertilizer; for P sufficient soils, BC materials have the potential as substitute for TSP (especially in acidic soils), which will neutralize soil pH and sustain plant labile P in a slow-release and eco-friendly way.

2.5 Conclusions

Previous lab and pot experiments indicated that BC and BC^{plus} are promising recycling substitutes for P fertilizers which, especially in the case of sulfur modified BC, can be alternatives to mineral based P fertilizers such as TSP. The fate of fertilizer P in the soil and thus its agronomic value is largely controlled by the soil aggregates as incorporation and release of P during aggregate formation and breakdown playing a vital role in bioaccessibility, storage, and cycling of soil P. Therefore, this study was the first to compare the short-term effects (5-year) of repeated field P fertilization with TSP, BC, and BC^{plus} on the fate of fertilizer P into soil P pools within different aggregate size fractions. After five years (one crop rotation), the treatment effects were mostly insignificant for concentrations and proportions of P pools. The reported higher solubility of TSP compared to BC were reflected in the significantly higher concentration of labile P in TSP compared to the BC treatments in LMiA of iSPTC-C as well as in SMiA and BU of iSPTC-A. The fact that the differences between TSP and BC^{plus} were not significant, indicates that sulfur modification improve the P availability of BC also at the field scale. As TSP is highly soluble and quick in P supply, for soils sufficient in P, BC and especially BC^{plus} could be alternatives for TSP to maintain soil P pools and decrease particle facilitated P loss. Indeed, longer term field trials with more soil types are needed to fully elucidate the fertilization effects of BC materials on P pools in soil size fractions.

Chapter 3

Loss of subsurface particulate and truly dissolved phosphorus during various flow conditions along a tile drain–ditch–brook continuum

Modified on the basis of

Siebers, N., Kruse, J., **Jia, Y.S.**, Lennartz, B., Koch, S., 2023. Loss of subsurface particulate and truly dissolved phosphorus during various flow conditions along a tile drain-ditch-brook continuum. *Sci. Total Environ*. 866, 161439. https://doi.org/10.1016/j.scitotenv.2023.161439.

CHAPTER THREE

3.1 Introduction

The discharge of phosphorus (P) into the Baltic Sea is a major concern due to eutrophication and ecological damage (HELCOM, 2021). During the last decades, nutrient inputs could be considerably reduced as point sources have mostly been eliminated to a great extent (Nausch, 2011); thus, remaining P inputs originate from diffuse sources, with agriculture contributing to roughly 60% (Nausch et al., 2017). As the major part of soil P is tightly adsorbed to mineral particles or bound within organic matter structures, most crucial P losses from agricultural land to water bodies are linked to particulate P, mobilized by surface runoff and soil erosion by water (Carpenter and Bennett, 2011) but also by subsurface transport in dissolved or colloidal form, which often happens in sudden events (Quinton et al., 2010). Due to the small proportion of dissolved phosphate on soil P losses, dissolved P forms are often only relevant for excessively fertilized soils.

The subsurface transport of dissolved and particulate P from arable land by means of tile drains has been the subject of intensive research, because drains shorten the flow paths of water by bypassing large parts of the soil volume, which reduces the P retention potential of the soil and thus increasing P losses (Nazari et al., 2022). For this reason, a program to monitor element emissions from soil to surface waters in the Zarnow River basin (north-eastern Germany, 49.5 km^2) was initiated in 2001 (Nausch et al., 2017). This program uses a hierarchical approach to estimate the transport of P from the tile drain to a ditch, a brook, and finally a stream (Bitschofsky and Nausch, 2019; Kahle, 2009; Nausch et al., 2017; Tiemeyer et al., 2009, 2006; Zimmer et al., 2016).

Both this monitoring program and recent literature revealed that dissolved P (DP) contributes to total P (TP) losses to a greater extent than previously acknowledged (Hahn et al., 2014; Jordan-Meille and Dorioz, 2004; Kleinman et al., 2007), with a contribution to total losses of between 16 to 69% (Jiang et al., 2021; Nausch et al., 2017; Rodriguez et al., 2020; Ruark et al., 2012). However, there is a considerable methodological uncertainty surrounding the determination of the DP fraction. For example, water samples collected as part of the Zarnow catchment monitoring program are treated with filters with a pore size between 0.4 to 0.8 µm, and P in 0.45 µm filtered samples is considered by definition as dissolved (Greenberg et al., 1985). However, the definition of natural colloids (1 to 1000 nm), as well as

their subset natural nanoparticles (1 to 100 nm), overlaps with the definition of dissolved components (Jarvie et al., 2012). Hence, although DP is intended to be an estimate of the dissolved fraction only, it may in fact still contain large amounts of P bound to nanoparticles and colloids. Losses of P and other nutrients due to particulate transport are a rising concern (Bauke et al., 2022; Gottselig et al., 2017; N. Gottselig et al., 2017; Jiang et al., 2021, 2015). Major parts of soil P are bound within organic matter structures or tightly adsorbed to mineral particles (Alewell et al., 2020). In contrast, apart from soils excessively fertilized with P, only a small part of the soil P is present in dissolved form (Helfenstein et al., 2018). Therefore, P losses from agricultural land to water bodies are mostly linked to particulate P of various size fraction that is mobilized during sudden rain events, either via surface runoff and soil erosion (nm to mm size range) or via subsurface transport by internal soil erosion (nm to µm size range) (Carpenter and Bennett, 2011; Quinton et al., 2010).

Nanocolloids and fine colloids (<450 nm) in particular are more prone to leaching through the soil profile (Fresne et al., 2022); however, larger particles >450 nm can also be transported by means of macropore and preferential flow (McGechan and Lewis, 2002; Wang et al., 2020). Generally, natural colloids are increasingly being recognized as relevant carriers of nutrients in ecosystems due to their composition and high specific surface area (Burger et al., 2021; Gottselig et al., 2017; N. Gottselig et al., 2017; Hens and Merckx, 2002; Jiang et al., 2021, 2015). Fine colloids (<450 nm) are highly mobile in soils and the colloid-facilitated transport of elements is highly dynamic as such transport is closely connected to the water movement in the soil (Koch et al., 2016). Thus, losses of P and other nutrients due to particulate transport are a matter of growing concern (Gottselig et al., 2017; N. Gottselig et al., 2017; Jiang et al., 2021, 2015). It was shown that soil colloids in acidic freshwaters are associated with iron (Fe) and organic carbon (C_{org}) (Andersson et al., 2006; Neubauer et al., 2013) as well as clay minerals in a size range between 100 and 450 nm (Missong et al., 2018; W. Amelung et al., 2017). P preferentially binds to colloids composed of C_{org}, Fe/aluminum (Al) oxides, clays minerals, or calcium carbonates (Domagalski and Johnson, 2011; Gottselig et al., 2017, 2014; N. Gottselig et al., 2017; Gu et al., 2020; Jiang et al., 2021, 2015) mainly forming moderately labile Fe- and Al-associated P and non-labile hydroxyapatite (Liu et al., 2014).

One technique for analyzing both truly dissolved and colloidal elemental exports is asymmetric flow field-flow fractionation (AF^4), which enables the continuous high-resolution size separation of colloids (Baalousha et al., 2011; Qureshi and Kok, 2011). AF^4 is an elution technique in which a narrow sample band or pulse is injected into a stream of liquid and subjected to a field (i.e., crossflow) acting perpendicular to the stream. This leads to different particle retention times and thus to the separation of particles in the flow channel according to particle size. Therefore, particles of different sizes will exit the flow channel at different times, yielding specific elution profiles known as fractograms (Schimpf et al., 2000). The technique allows truly dissolved elements to be determined, as a permeable membrane is located at a site within the channel through which the liquid carrier solution, including all dissolved elements, constantly exits the channel. Therefore, AF^4 is perfectly suited to estimate the potential of subsurface P losses by both colloidal and truly dissolved forms.

Colloidal-bound P may partly explain elevated P concentrations in surface water during baseflow and especially during high flow conditions (Burger et al., 2021; Filella et al., 2006; Fresne et al., 2021; Jiang et al., 2021). As a consequence of climate change, Germany will experience more precipitation events in winter and less frequent, but more intense, precipitation events during the summer (Federal German Government, 2015). In Germany, the average precipitation levels in the winter season have increased by 25% since winter 1881/1882 (German Environment Agency, 2019). Even though precipitation events are of longer duration and lower intensity in winter, winter events are predicted to create high colloidal peak discharges in streams and rivers. It was found that particle-facilitated transport of P dominates P transport in winter, reaching a maximum of 80% of total P loss (Schelde et al., 2002). As not only the quantity varies with flow events but also the P speciation (Bender et al., 2018; Esbroeck et al., 2017), detailed knowledge about the subsurface transport of P in different forms (i.e., dissolved, colloidal, particulate) to adjacent surface waters is essential in order to optimize agricultural practices and reduce P losses. Therefore, the objective of this study was to explore the phosphorus export mechanism from tile-drained agricultural fields by analyzing particle size fractions in the discharge. In doing so, we aim to (i) identify the extent to which precipitation patterns and intensity as well as discharge lead to the mobilization of particles of different sizes, (ii) compare particulate and

dissolved losses, and (iii) determine the origin of particles transported by water in the adjacent field.

3.2 Material and Methods

3.2.1 Study site, sampling, baseflow separation

The study site 'Zarnow catchment' is located about 15 km southeast of the city of Rostock; the brook Zarnow is a tributary of the Warnow River. Further information on the study site as well as the sampling is described in detail in (Nausch et al., 2017; Tiemeyer et al., 2009, 2006; Zimmer et al., 2016). The study period lasted from the beginning of November 2019 until the end of April 2020 and covered the principal discharge period. Water samples at various spatial scales, i.e., drain outlet (4.2 ha catchment area), ditch (179 ha catchment area), and brook (1550 ha catchment area) were taken automatically (Teledyne Isco, Inc., Lincoln, NE) every six hours and mixed into a daily sample. Samples were collected every week. The collected water samples were stored in a cooling box, transported to the laboratory, and immediately processed to avoid alterations of the various P fractions. Water samples were unfiltered or filtered using pre-combusted (6 h, 450 °C) 0.7 µm cellulose acetate membrane filter (Carl Roth). The filtered samples for AF^4 analyses (see below) were stored in PET tubes and shock-frozen immediately after filtration using liquid nitrogen in a cryogenic storage dewar and stored at -20 °C.

The soil samples were collected from an adjacent arable field located in the catchment area of the sampled tile-drainage system. The soil samples were taken from three soil horizons (Ap, Bw, and C) with nine replicates. The disturbed soil samples were collected with an auger (Edelmann-Bohrer, Eijkelkamp) and stored in plastic bags. The collected soil samples were air-dried and passed through a 2 mm sieve before soil colloid extraction.

The water level and volumetric outflow at the collector drain outlet were measured with a Venturi flume (Eijkelkamp Agrisearch Equipment, Giesbeek, Netherlands). The sampling station of the drainage ditch was equipped with an ultrasonic water level measurement device (Teledyne Isco, Inc., Lincoln, NE). At the Zarnow measurement station, the water level was measured with a pressure sensor (UGT GmbH, Müncheberg, Germany). Discharge was measured every 15 min and averaged to a daily mean value using an inductive flowmeter

(Flo-MateTM, Marsh-McBirney, Inc. Frederick, MD) to set up rating curves for the ditch and brook stations.

A simple baseflow separation routine was used to subdivide streamflow data into a fast and slow component. Baseflow was separated from the total daily discharge (Figure 3-1) by using a recursive digital filter as suggested by (Lyne and Hollick, 1979; Nathan and McMahon, 1990):

$$f_k = \propto f_k - 1 + \frac{(1+\propto)}{2}(y_k - y_{k-1}) \quad \text{(Eq. 3)}$$

where f_k is the filtered quick response at the kth sampling point, y_k is the original discharge, and α is the filter parameter.

Flow events were defined when the peak flow exceeded the baseflow by at least a factor of 1.5, resulting in altogether 13 different flow events (Figure 3-1). To represent the baseflow, four points were selected distributed over the entire discharge period where the drain discharge was at or near the modeled baseflow (Figure 3-1).

3.2.2 General analyses and soil colloid extraction

The total phosphorous (TP) of the unfiltered water samples concentrations were determined by alkaline persulphate oxidation (Koroleff, 1983). Briefly, the unfiltered sample was mixed with a solution of $K_2S_2O_8$, H_3BO_3, and NaOH digested in a microwave (Mars 5, CEM). After adding ascorbic acid ($C_6H_8O_6$) and ammonium heptamolybdate, the sample was measured colorimetrically at a wavelength of 885 nm (CFA, AA3 with xy2 autosampler, Seal Analytik).

The P loss rates L (kg ha^{-1} d^{-1}) were calculated as described in (Tiemeyer et al., 2006), by using the P concentration c (mg L^{-1}) and flow rate Q (mm d^{-1}) for the equation

$$L = \frac{cQ}{100} \quad \text{(Eq. 4)}$$

by establishing a linear correlation between measured loss rates and daily discharge, the loss rates could be calculated for days for which only the discharge was available.

The soil colloid (< 450 nm) extraction was performed by combining wet sieving with centrifugation. In brief, 10 g air-dried soil (< 2 mm) was immersed in deionized water on the

top of a sieve stack (20, 53, and 250 µm). The soil particles were separated by manually shaking sieves up and down. The 250 µm mesh-size sieve and soil fractions retained were removed when the water passing through the sieve was clean. The same procedure was repeated for the 53 and 20 µm sieves. The soil suspension which contained the < 20 µm size fraction was collected and centrifuged to soil colloids < 450 nm. The centrifugation parameters (4000 rcf for 5 min) were calculated referring to Stokes law (Henderson et al., 2012). The volume of the resulted soil suspensions was recorded for colloidal elemental concentration calculation.

3.2.3 Asymmetric flow field flow fractionation of water and soil samples

The colloids in the collected water and soil samples and WDCs were size separated using the AF^4 (Postnova Analytics, Landsberg, Germany). The C_{org} contents in different size fractions of colloids were measured by AF^4 coupled to an UV–vis detector with the absorption wavelength at 254 nm (Postnova Analytics) and organic carbon detector (OCD; DOC laboratory Dr. Huber, Germany). The element concentrations of P, Fe, Al, Si, Ca, and Mg in each size fraction were determined by AF^4 coupled to an inductively coupled plasma mass spectrometer (ICP-MS; Agilent 7500, Agilent Technologies, Japan) using post channel calibration with Rh as the internal standard (Nischwitz et al., 2016). Details on the AF^4 separation method and coupling to ICP-MS and OCD detectors can be found in Gottselig et al. (2017) for water samples and in Krause et al. (2020) for the soil samples.

The lowest size limit of 0.66 nm was established by the cutoff of the used membrane (1 kDa). Reference materials (Sulfate Latex Standards 8% w/v 21–630 nm; Postnova Analytics, Landsberg, Germany) were used with the same AF^4 conditions used for the samples to calibrate the particle diameters included in each size fraction. For the water samples the first fraction was estimated through calibration with reference materials to include nanoparticles between 1 kDa (membrane molecular weight cutoff) and 20 nm and the second fraction to include nanoparticles >20 to 60 nm. Furthermore, dynamic light scattering revealed that the third fraction included nanoparticles >60 nm to fine colloids up to the upper size cut-off of the filter (750 nm). For soil colloids, the size fractions were also calibrated according to Latex standards; the 1st size fraction ranged from 0.66 to 20 nm, the 2nd size fraction was 20 to 100 nm, and the 3rd size fraction from 100 to 450 nm, which was the size cutoff set for

centrifugation. Because the AF4 technique does not recover dissolved species, total element recovery of aqueous water phases was not assessed in the same run. However, by measuring without AF4 fractionation (zero crossflow) total elemental concentrations can be determined as well using the AF4 system. In the filtered and unfractionated samples, total elemental concentrations of P, Fe, Al, Si, Ca, and Mg were determined by ICP–MS (Agilent 7500, Agilent Technologies) as described above.

3.2.4 Statistical analyses

Statistical analyses were performed in Excel, including XLSTAT 2021.5 (Excel 2016, Microsoft Corporation, Washington, USA), Origin(Pro) 2022 (OriginLab Corporation, Northampton, MA, USA), and RStudio 3.6.3. In the water samples, we tested proportions of particulate elemental concentrations of colloids <750 nm in relation to total elemental concentrations of colloids <750 nm for normal distribution using the Shapiro–Wilk test ($P<0.05$) and for homogeneity of variances using the Brown–Forsythe test ($\alpha=0.05$). The differences between sampling locations within one elemental proportion were tested by a one-way ANOVA ($\alpha=0.05$). If significant differences occurred, we used the Tukey HSD test for post-hoc separation of means ($\alpha=0.05$). The similarity or dissimilarity between the time series data of the three sampling sites was evaluated based on Euclidean distance. The P stocks from colloids extracted from soil samples were tested using multilevel model as both variables (horizons and size fractions) violated the data independence assumption. The modelling work was done with *lme()* function from R package "*nlme*". Both variables (horizons and fractions) and their interactions (horizons × fractions) were added into the baseline model successively. The method maximum likelihood (ML) was chosen for the model. The *post hoc* tests were performed for significant effects ($p < 0.05$). The *pairwise.t.test()* function from R package "*stats*", with p values adjusting method "bonferroni" and paired parameter as "FALSE" were applied for multiple comparisons. Hierarchical tree cluster analysis with 1 − Pearson's r as the distance measure, complete linkage rule, and without normalization as described in Gottselig et al. (2017) was applied to the element concentrations obtained for the AF4 separated particle size fractions from water and soil colloids identifying fraction-specific preferential binding of P.

3.3 Results

3.3.1 Discharge and total P losses

The total precipitation of 197 mm in the discharge period 2019/2020 was equal to that record in the discharge period 2013/2014 (Nausch et al., 2017). However, it amounted to only 74 % and 69 % of that recorded in the discharge periods 2003/2004 and 2005/2006, respectively (Tiemeyer et al., 2009), or only 29% of the long-term annual average of 689 mm. Rainfall of ≥6.0 mm day^{-1} took place in the first week of November and between 31.01.2020 and 13.03.2020 (Figure B-1). These rainfall events generated discharge peaks in the tile drain, ditch, and brook, while the later rain events in particular led to an increase in discharge (Figure 3-1). For the tile drain, ditch, and brook, the proportion of modeled baseflow to total flow amounted to 15, 17, and 42%, respectively, which confirms expectations that the brook is groundwater driven. The mean TP concentrations in the unfiltered samples ($TP_{unfiltered}$) were comparable for each sampling station (tile drain: 0.046 mg L^{-1}, ditch: 0.027 mg L^{-1}, brook: 0.030 mg L^{-1}). Over the complete sampling period 2019/2020, the lowest area-normalized $TP_{unfiltered}$ losses (g ha^{-1}) were found for the brook and the highest were found for the ditch (Table 3-1).

3.3.2 Truly DP, $TP_{colloids}$, and $TP_{>750nm}$ in water samples

To characterize the total P composition of the unfiltered water samples in more detail, the samples were split into three fractions: truly DP, particulate P < 750 nm ($TP_{colloids}$), and particulate P >750 nm ($TP_{>750\ nm}$). The TP concentrations, as well as their proportions of $TP_{unflitered}$, were determined separately (Table 3-2). Taking all events into account, it was found that at all three sampling stations, the mean shares of the three P fractions in the overall P loss were similar. The majority of $TP_{unflitered}$ was formed by $TP_{>750\ nm}$ (54% ± 28; 55% ± 21; 59% ± 24), followed by truly DP (37% ± 21; 38% ± 19; 34% ± 32), and by a rather small contribution of $TP_{colloids}$ (5% ± 2; 6% ± 4; 6% ± 2) (tile drain, ditch, brook, respectively; Table 3-2). Thus, during flow events, 63 to 66% of $TP_{unfiltered}$ was

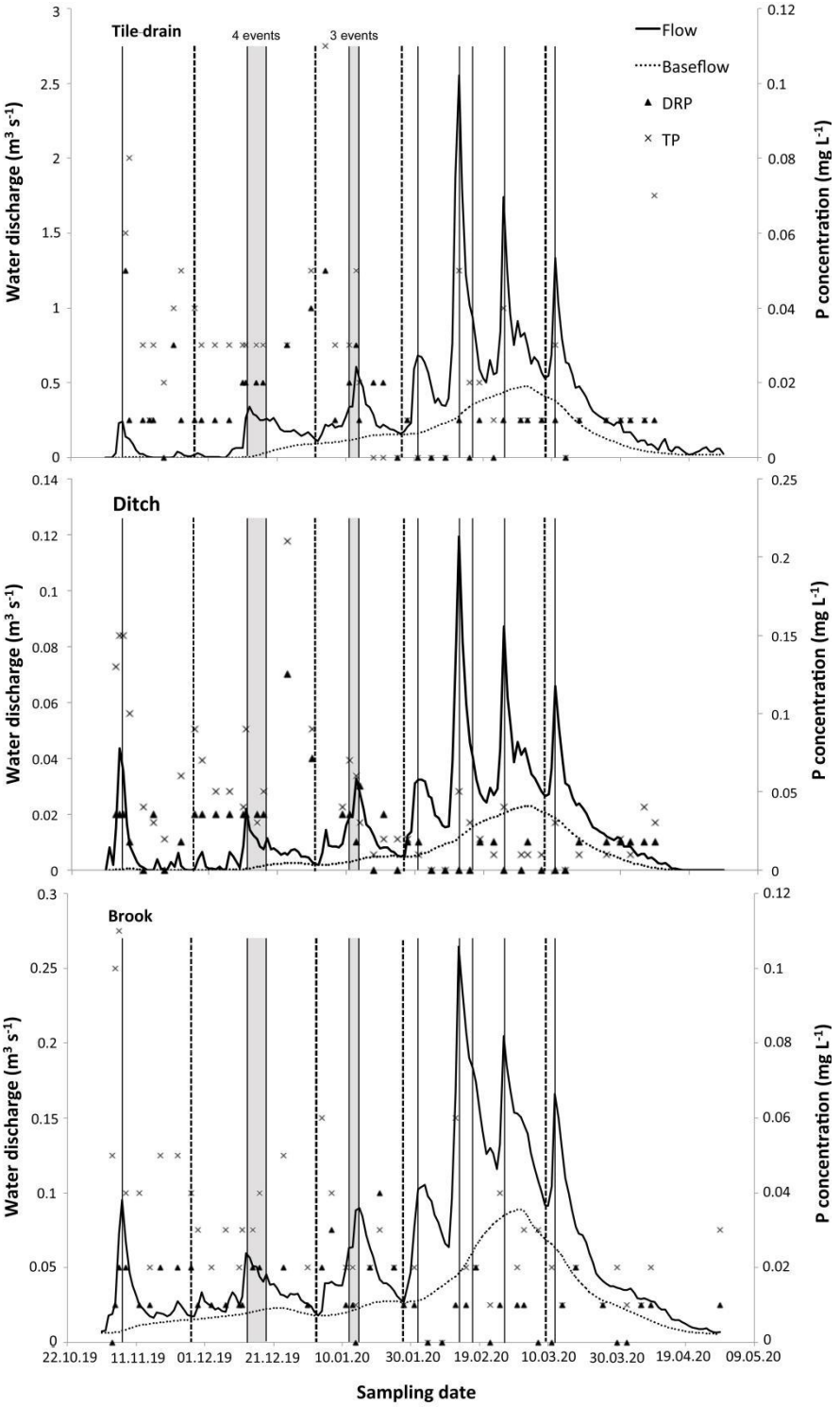

Figure 3-1. Measured flow, fitted baseflow, dissolved reactive P (DRP), and total P (TP) during the study period (2019/2020) at the three sampling stations tile-drain, ditch, and brook. Vertical broken lines mark the sampling points of the baseflow while vertical bold lines mark the sampling points of the specific flow events (1 to 13) for subsequent measurements. Several sampled events are located in the gray highlighted areas.

Table 3-1. Water discharge, drainage area, P loss rates of total P ($TP_{unfiltered}$), particulate P >750 nm ($TP_{>750\ nm}$), colloidal P ($TP_{colloids}$), and truly dissolved P (truly DP), and coefficients of determination of the discharge (mm d^{-1}) versus the P loss rates (kg ha^{-1} d^{-1}).

	$TP_{unfiltered}$			$TP_{>750\ nm}$			$TP_{colloids}$			**Truly DP**		
	Tile-drain	Ditch	Brook	Tile-drain	Ditch	Brook	Tile-drain	Ditch	Brook	Tile-drain	Ditch	Brook
Discharge (mm period^{-1})	120	137	60	120	137	60	120	137	60	120	137	60
Drainage area (ha)	4.2	179	1550	4.2	179	1550	4.2	179	1550	4.2	179	1550
Area normalized loss rate (g ha^{-1} period^{-1})	48	55	18	36	41	12	2	3	1	11	1	5
Loss rate (g period^{-1})	**202**	**9774**	**27677**	**151**	**7330**	**18451**	**10**	**489**	**1845**	**45**	**244**	**7380**
R^2	0.835	0.806	0.575	0.851	0.823	0.655	0.939	0.978	0.747	0.830	0.926	0.585

present as particulate P ($TP_{>750\ nm}$ + $TP_{colloids}$), whereas during baseflow this figure amounted to 97 to 99%. This was reflected in an even more pronounced dominance of $TP_{>750\ nm}$ during baseflow conditions (82 to 92% of $TP_{unflitered}$), while truly DP during baseflow was almost negligible (1 to 3% of $TP_{unflitered}$). The mean proportions of $TP_{colloids}$ in the ditch and brook during baseflow (7%±6; 7%±4) were comparable to those recorded during flow events. In contrast, for the tile drain, the mean proportions of $TP_{colloids}$ at baseflow (15%±17 of $TP_{unfiltered}$) were higher compared to both the flow events and to the other sampling stations. This, however, was not significant, since this higher proportion was mostly due to the high initial peak in the proportion of $TP_{colloids}$ (41% of $TP_{unflitered}$) during the early stages of baseflow formation at the onset of the discharge period, while $TP_{>\ 750\ nm}$ peaked during the very first flow event. After the occurrence of these peak concentrations and proportions of $TP_{colloids}$ (baseflow) and $TP_{>\ 750\ nm}$ (flow events), the values dropped and remained at a similar level (Table 3-2).

Considering the change in the proportions of $TP_{>750\ nm}$, $TP_{colloids}$, and truly DP during the runoff period, it is obvious that the proportions remained relatively constant during baseflow, but were subject to partly strong fluctuations during event flow. For the latter, the observed variations in the composition of $TP_{unflitered}$ were mainly caused by $TP_{>750\ nm}$ and truly DP, while the proportions of $TP_{colloids}$ remained at a relatively constant level.

3.3.3 Elemental loads in water samples

Taking into account all sampling stations, flow regimes, and colloidal size fractions obtained by AF^4 measurements, the particulate elemental loads in the <750 nm filtrate (water colloids$_{0.66–750\ nm}$) followed the order Al ≤ P < Fe ≤ Si < Mg < C_{org} < Ca (Table B-1). The proportion of the respective particulate elemental load in relation to the total elemental load in the <750 filtrate (colloidal + truly dissolved load) was similar between flow events (13 to 27%). However, during baseflow, the mean proportion of colloidal P and Al differed significantly at 85 and 100%, respectively, while the other elements were in the range of 9 to 30% (Table 3-3). There were also no significant changes in the proportions of colloidal loads between the three sampling stations, with the exception of C_{org}, which showed significantly higher proportions within the ditch compared to the tile drain and the brook during flow events (Table 3-3).

Table 3-2. Concentrations of total P ($TP_{unfiltered}$), total P in particles >750 nm ($TP_{>750\ nm}$, calculated by subtracting $TP_{colloid}$ and truly DP from $TP_{unfiltered}$), total P in colloids <750 nm ($TP_{colloids}$), and truly dissolved P (truly DP), and proportions of $TP_{>750\ nm}$, $TP_{colloids}$, and truly DP to $TP_{unfiltered}$ (%) for the baseflow and the flow events for the three sampling stations: tile-drain, ditch, and brook. n.d. = not detected.

Time of sampling	Tile-drain				Ditch				Brook			
	$TP_{unfiltered}$ mg L^{-1}	$TP_{>750\ nm}$ µg L^{-1}	$TP_{colloids}$ µg L^{-1}	truly DP µg L^{-1}	$TP_{unfiltered}$ mg L^{-1}	$TP_{>750\ nm}$ µg L^{-1}	$TP_{colloids}$ µg L^{-1}	truly DP µg L^{-1}	$TP_{unfiltered}$ mg L^{-1}	$TP_{>750\ nm}$ µg L^{-1}	$TP_{colloids}$ µg L^{-1}	truly DP µg L^{-1}
Baseflow 1	0.03	15.55	12.15	2.29	0.07	67.06	2.67	0.27	0.03	25.46	3.89	0.65
		(52)	(41)	(8)		(96)	(4)	(0)		(85)	(13)	(2)
Baseflow 2	0.05	48.91	0.95	0.13	0.09	88.55	1.34	0.11	0.02	18.84	0.88	0.28
		(98)	(2)	(0)		(98)	(1)	(0)		(94)	(4)	(1)
Baseflow 3	0.01	8.92	0.84	0.24	0.02	18.53	1.34	0.13	0.01	9.19	0.71	0.10
		(89)	(8)	(2)		(93)	(7)	(1)		(92)	(7)	(1)
Baseflow 4	0.01	9.11	0.78	0.11	0.01	8.47	1.44	0.09	0.02	19.16	0.76	0.09
		(91)	(8)	(1)		(85)	(14)	(1)		(96)	(4)	(0)
Event 1	0.08	69.29	1.99	8.72	0.10	80.59	2.42	16.99	0.04	36.34	1.47	2.19
		(87)	(2)	(11)		(81)	(2)	(17)		(91)	(4)	(5)
Event 2	0.03	17.25	1.47	11.27	0.04	22.14	1.94	15.91	0.02	9.44	1.18	9.39
		(58)	(5)	(38)		(55)	(5)	(40)		(47)	(6)	(47)
Event 3	0.03	19.77	1.79	8.45	0.09	74.13	1.79	14.07	0.03	17.54	1.62	10.85
		(66)	(6)	(28)		(82)	(2)	(16)		(58)	(5)	(36)
Event 4	0.03	4.82	3.01	22.17	0.03	4.66	2.66	22.68	0.03	10.80	2.39	16.81
		(16)	(10)	(74)		(16)	(9)	(76)		(36)	(8)	(56)
Event 5	0.03	16.72	1.23	12.06	0.05	29.99	1.98	18.03	0.04	30.03	1.43	8.54
		(56)	(4)	(40)		(60)	(4)	(36)		(75)	(4)	(21)

Table 3-2. (Continued)

Time of sampling	Tile-drain				Ditch				Brook			
	$TP_{unfiltered}$ mg L^{-1}	$TP_{>750\ nm}$ µg L^{-1}	$TP_{colloids}$ µg L^{-1}	truly DP µg L^{-1}	$TP_{unfiltered}$ mg L^{-1}	$TP_{>750\ nm}$ µg L^{-1}	$TP_{colloids}$ µg L^{-1}	truly DP µg L^{-1}	$TP_{unfiltered}$ mg L^{-1}	$TP_{>750\ nm}$ µg L^{-1}	$TP_{colloids}$ µg L^{-1}	truly DP µg L^{-1}
Event 6	0.03	18.12	1.60	10.28	0.07	51.78	2.43	15.79	0.02	8.34	1.64	10.02
		(60)	(5)	(34)		(74)	(3)	(23)		(42)	(8)	(50)
Event 7	0.05	37.41	1.70	10.89	0.06	40.12	2.18	17.70	0.02	12.45	1.57	5.98
		(75)	(3)	(22)		(67)	(4)	(29)		(62)	(8)	(30)
Event 8	0.02	2.83	1.71	15.46	0.03	6.00	2.15	21.85	0.01		1.81	16.72
		(14)	(9)	(77)		(20)	(7)	(73)			(18)	(167)
Event 9	n.d.		1.44	1.26	0.01	4.39	1.90	3.71	0.02	17.20	1.54	1.26
						(44)	(19)	(37)		(86)	(8)	(6)
Event 10	0.05	37.42	2.08	10.50	0.05	32.97	2.45	14.57	0.06	49.20	2.32	8.48
		(75)	(4)	(21)		(66)	(5)	(29)		(82)	(4)	(14)
Event 11	0.02	8.29	1.44	10.27	0.03	13.04	2.29	14.66	0.02	11.28	1.41	7.31
		(41)	(7)	(51)		(43)	(8)	(49)		(56)	(7)	(37)
Event 12	0.04	30.76	1.65	7.59	0.04	24.58	2.30	13.12	0.04	30.98	2.06	6.96
		(77)	(4)	(19)		(61)	(6)	(33)		(77)	(5)	(17)
Event 13	0.03	23.14	1.68	5.18	0.03	15.22	2.24	12.55	0.02	11.40	1.61	6.98
		(77)	(6)	(17)		(51)	(7)	(42)		(57)	(8)	(35)
Mean proportion (%)												
Baseflow		82 ± 21	15 ± 17	3 ± 3		93 ± 6	7 ± 6	1 ± 0		92 ± 5	7 ± 4	1 ± 1
Event		54 ± 28	5 ± 2	37 ± 21		55 ± 21	6 ± 4	38 ± 19		59 ± 25	6 ± 2	34 ± 23

Table 3-3. Proportions of particulate loads of colloids <750 nm in relation to total elemental loads in the filtrate$_{750nm}$ (dissolved + particulate, filtered to <750 nm) for the different flow regimes for the three sampling stations: tile-drain, ditch, and brook and the mean of all sampling stations (all stations).

	C_{org}	P	Fe	Al	Si	Ca	Mg
	% particulate						
Baseflow							
Tile-drain	10[a]	84[a]	11[a]	64[a]	28[a]	9[a]	7[a]
Ditch	13[a]	92[a]	17[a]	100[b]	25[a]	11[a]	9[a]
Brook	6[a]	85[a]	18[a]	71[a]	37[a]	14[a]	11[a]
All stations	**10**	**87**	**15**	**79**	**30**	**11**	**9**
Flow events							
Tile-drain	12[a]	17[b]	22[b]	15[c]	31[a]	15[a]	14[a]
Ditch	21[b]	14[b]	20[a]	14[c]	26[a]	13[a]	12[a]
Brook	9[a]	21[b]	23[b]	21[c]	23[a]	15[a]	13[a]
All stations	**14**	**17**	**22**	**17**	**27**	**14**	**13**

3.3.4 Distribution pattern of P within water colloids$_{0.66-750nm}$

The colloidal size fraction studied here (water colloids$_{0.66\ nm-750nm}$) was mainly present in three size fractions (Table B-1). During flow events, the main proportions of $TP_{colloids}$ (67 to 73%) were found in water colloids$_{60-750nm}$, followed by water colloids$_{20-60nm}$ (26 to 32%), with minor contributions (<1%) in water colloids$_{0.66-20nm}$. However, during baseflow, the mean proportions of water colloids$_{20-60nm}$ increased to 42 to 47%, whereas the portions of water colloids$_{60-750nm}$ decreased to 51 to 58% (data not shown). In terms of the sampling stations, significantly higher mean proportions of $TP_{colloids}$ were found in water colloids$_{20-60nm}$ (lower in water colloids$_{60-750nm}$) from the ditch compared to the tile drain and brook during flow events, while at baseflow this difference was only significant between the ditch and tile drain. Based on the calculation of Euclidean distance, the time course of the proportions of all size fractions was most similar between the tile drain and brook, regardless of the flow regime. However, the absolute difference between sampling stations was generally larger for events than for baseflow conditions. There was no visible trend in the time course of the distribution pattern of P within the three size fractions during flow events, while a trend of decreasing proportions of water colloids$_{0.66–20nm}$ and water colloids$_{20–60nm}$ with time, as well as increasing proportions of water colloids$_{60–750nm}$ with time, was indicated during baseflow.

3.3.5 Associations of P with other elements

Hierarchical tree cluster analysis generally revealed three clusters for all size fractions (Table 3-4). When all stations under event flow conditions were included in the cluster analysis, P clustered mainly with Al, Fe, Mg, and Si in water colloids$_{0.66–20nm}$, with Al and Si in water colloids$_{20–60nm}$, and with Al, Fe, and Si in water colloids$_{60–750nm}$. When the results of the cluster analysis were considered separately for the individual stations and flow regimes, the tile drain showed a noticeably different cluster composition, with P sharing a cluster with Al, Fe, and Si; for the ditch and brook, however, P clustered with Al, Fe, and Mg. For water colloids$_{20–60nm}$, all P clusters exhibited a different composition between sampling stations, with Si once again only being present in the tile drain cluster. In water colloids$_{60–750nm}$, P clustered exclusively with C_{org} in the tile drain and in the ditch, while it clustered with Si in the brook (Table 3-4).

Table 3-4. Hierarchical tree cluster analysis with 1 – Pearson's r as the distance measure and complete linkage; for water colloids analysis was done for all sampling stations, size fractions (1st: 0.66 to 20 nm; 2nd: > 20 to 60 nm; 3rd: 60 to 750 nm), and for the flow event and for stocks of soil colloids analysis was done for all soil horizons. Numbers in parentheses are the 1 - Pearson's r distance. A low value of the linkage distance indicates stronger potential binding.

Sampling station & horizon	Number of cluster and elements			Number of cluster and elements			Number of cluster and elements		
	1	2	3	1	2	3	1	2	3
	First size fraction			Second size fraction			Third size fraction		
Tile-drain	C_{org}/Mg	P/Al/Fe/Si	Ca	P/Al/Si	Fe/Ca/Mg	C_{org}	Mg/Ca	Fe/Al/Si	C_{org}/P
	(0.42)	(0.574)	(1.94)	(0.17)	(0.25)	(0.57)	(0.13)	(0.28)	(0.64)
Ditch	Si/Ca	P/Al/Fe/Mg	C_{org}	P/Al/Fe/Mg	Al/Si	C_{org}	Mg/Ca	Fe/Al/Si	C_{org}/P
	(0.00)	(0.24)	(0.93)	(0.17)	(0.22)	(1.37)	(0.15)	(0.50)	(1.08)
Brook	P/Al/Fe/Mg	C_{org}/Ca	Si	P/Al/Mg	Fe/Ca/Si	C_{org}	P/Si	Fe/Ca/Al/Mg	C_{org}
	(0.28)	(0.62)	(1.10)	(0.32)	(0.72)	(1.38)	(0.44)	(0.67)	(1.36)
All stations	P/Al/Fe/Mg/Si	C_{org}/Ca		Fe/Ca/Mg	P/Al/Si	C_{org}	Mg/Ca	P/Al/Fe/Si	C_{org}
	(0.38)	(0.48)		(0.34)	(0.58)	(1.01)	(0.22)	(0.65)	(1.23)
Ap	Al/Fe/Si	P/Mg/Ca/C_{org}		P/Mg/Ca/Al/Fe/Si	C_{org}		P/Mg/Ca/Al/Fe/Si	C_{org}	
	(0.008)	(0.791)		(0.454)	(1.106)		(0.762)	(1.640)	
Bw	Al/Fe/Si	P/Mg/Ca/C_{org}		P/Mg/Ca/Al/Fe/Si	C_{org}		Mg/Ca/Al/Fe/Si/C_{org}	P	
	(0.021)	(0.784)		(0.299)	(1.822)		(0.453)	(1.165)	
C	P/C_{org}	Mg/Ca/Al/Fe/Si		P/Mg/Ca/Al/Fe/Si	C_{org}		Mg/Ca/Al/Fe/Si/C_{org}	P	
	(0.693)	(0.693)		(0.139)	(0.604)		(0.509)	(1.239)	
All horizons	Mg/Ca/Al/Fe/Si	P/C_{org}		P/Mg/Ca/Al/Fe/Si	C_{org}		Mg/Ca/Al/Fe/Si/C_{org}	P	
	(0.306)	(0.441)		(0.072)	(0.336)		(0.068)	(0.368)	

Hierarchical tree cluster analysis revealed no connection between water colloids$_{0.66–20nm}$, water colloids$_{20–60nm}$, and water colloids$_{60–750nm}$, as each size fraction formed a separate cluster (Figure 3-2). Within the three size fraction clusters, there is a clear separation between the ditch, tile drain, and brook, with the ditch forming a separate cluster while the tile drain and brook are grouped within a single cluster, irrespective of events. This is different for water colloids$_{20–60nm}$, where the brook and tile drain form a cluster under baseflow conditions, while the ditch (during both baseflow and flow events) clusters with the tile drain and brook under flow event conditions. For water colloids$_{60–750nm}$, all three sampling stations form a cluster under flow event conditions; under baseflow conditions, meanwhile, the ditch and the brook cluster, and the tile drain forms a separate cluster (Figure 3-2).

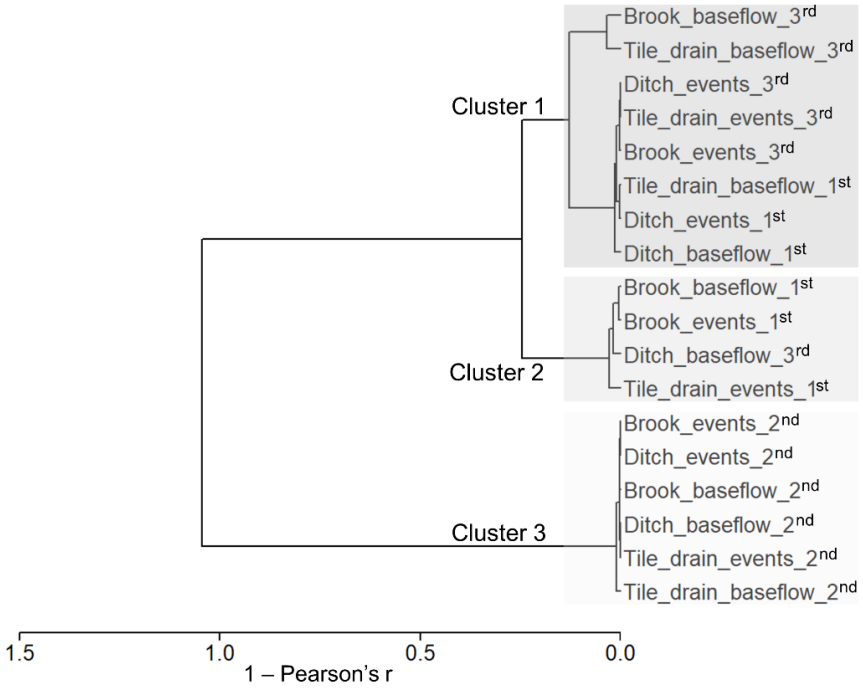

Figure 3-2. Dendrogram of a hierarchical tree cluster analysis based on elemental colloidal composition in three size fractions (1st: 0.66 to 20 nm; 2nd: > 20 to 60 nm; 3rd: 60 to 750 nm) in water samples determined by AF4 of samples obtained from the three different sampling stations for baseflow and flow events.

3.3.6 Composition of soil colloids and fate in water

Generally, as for the water colloids, three size fractions were identified for the soil colloids, namely soil colloids0.66–20nm, soil colloids20–100nm, and soil colloids100–450nm (Table B-1, B-5). The colloidal P stocks for the three size fractions were 1.3 to 4.4, 0.6 to 1.7, and 3.6 to 5.1 kg ha^{-1} for the Ap, Bw, and C horizon, respectively (Figure 3-3 and Table B-5). The highest

P concentrations were found in soil colloids$_{0.66-20nm}$ from the Ap horizon, while the C horizon exhibited the highest P stocks in soil colloids$_{20-100nm}$ and soil colloids$_{100-450nm}$. Between the size fractions, colloidal P stocks in soil colloids$_{20-100nm}$ were significantly lower than those in soil colloids$_{0.66-20nm}$ and soil colloids$_{100-450nm}$ for both the Ap and Bw horizons, while these were not significant for the C horizon (Figure 3-3).

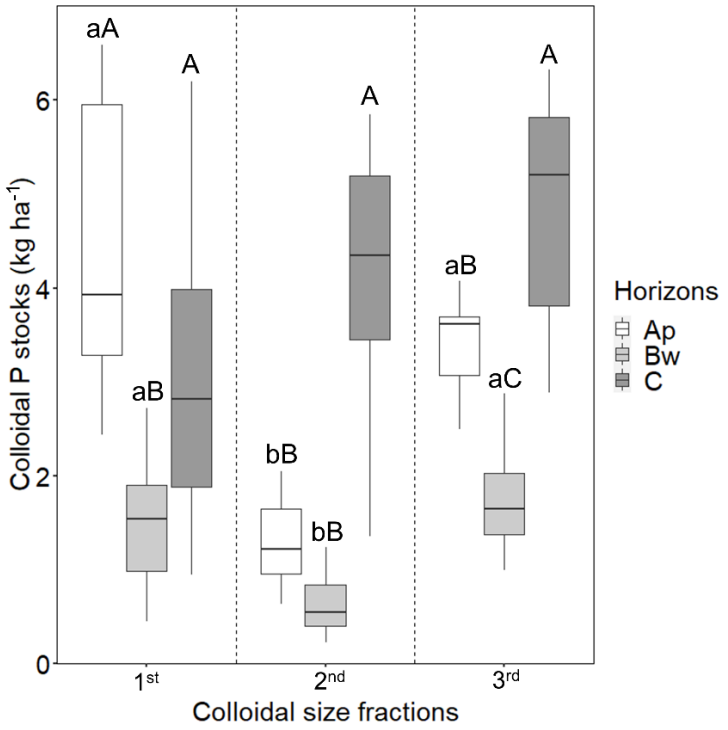

Figure 3-3. Colloidal P stocks (kg ha^{-1}) of three size fractions (1st: 0.66 to 20 nm; 2nd: 20 to 100 nm; 3rd: 100 to 450 nm) in different soil horizons. Significant differences (p < 0.05) between size fractions but within the same soil horizon were labeled with lowercase letters, and between horizons but within the same size fraction with uppercase letters.

Hierarchical tree cluster analysis of soil colloids generally revealed two clusters for all three size fractions (Table 3-4). When all three horizons (Ap, Bw, C) were grouped in a cluster analysis (All), P mainly clustered with C_{org} in soil colloids$_{0.66-20nm}$ and with all elements except C_{org} in soil colloids$_{20-100nm}$, and formed a separate cluster in soil colloids$_{100-450nm}$. Results of the cluster analysis conducted on soil horizon samples revealed that in soil colloids$_{0.66-20nm}$, P mainly clustered with C_{org}, while in the Ap and Bw horizons, Mg and Ca were also part of the P cluster. For soil colloids$_{20-100nm}$, the results were identical for all soil horizons with P and Mg/Ca/Al/Fe/Si clustering together, while C_{org} formed a separate cluster. In soil colloids$_{100-450nm}$, the results differed between Ap and the other horizons, with

P clustering with all elements except C_{org} in the Ap horizon and forming a separate cluster in the Bw and C horizons (Table 3-4). In order to estimate the origin of water colloids within the adjacent soil, we conducted a hierarchical tree cluster analysis of both water and soil colloid concentrations (both in µg L^{-1}). This analysis revealed three main clusters, with soil colloids$_{20–100nm}$ and soil colloids$_{100–450nm}$ from all soil horizons—i.e., Ap, Bw, C—clustering together in cluster 1. Cluster 2 included water colloids$_{20–60nm}$ for all sampling stations, i.e., tile drain, ditch, and brook, as well as soil colloids$_{0.66–20nm}$ from the C horizon. In cluster 3, soil colloids$_{0.66–20nm}$ from the Ap and Bw horizons clustered with water colloids$_{0.66–20nm}$ and water colloids$_{60–750nm}$. The distance measure of soil colloids from the C horizon to the water colloids was smaller than for the Ap and Bw horizons, indicating that there were more similarities between soil colloids$_{0.66–20nm}$ from the C horizon and water colloids$_{20–60nm}$ (Figure B-3).

3.4 Discussion

3.4.1 Precipitation, discharge, and P transport at the monitoring stations

The initial peak of particulate P loss at all sampling stations during the first rain event at the beginning of the discharge period (Table 3-2) was also observed for other hydrological discharge periods at the same site (Nausch et al., 2017) and was reported by others from irrigation experiments (de Jonge et al., 2004; Kjaergaard et al., 2004; Schelde et al., 2002; Zhuang et al., 2007). This can be explained by a re-mobilization of particulate P, especially of particles >750 nm, which settled in the drain and ditch during dry fall outside of the discharge season and were subsequently transported further downstream. After the first event in the subsequently sampled baseflow, the load of $TP_{>750\ nm}$ in tile drain was lower, whereas for particles <750 nm it remained the same level. This suggests that the re-mobilization potential was exhausted faster for particles >750 nm than for colloids <750 nm that were continuously mobilized at the same rate. Event flow particularly affected the transport of $TP_{>750\ nm}$, leading mainly to an effect of varying discharge intensity and thus straining and attachment at the solid-water interface (Wang et al., 2020a). This effect is greater for larger particles, as these particles are more prone to get stuck when the pore space is too small to admit them.

A colloidal export of around 5 to 6% of $TP_{unfiltered}$ is in line with the finding of Burger et al. (2021) for exports from a forested headwater catchment after winter precipitation events with a mean precipitation of 3 mm d^{-1} for the event under study. A dominance of colloidal P losses over dissolved losses during flow events, as reported by Schelde et al. (2002), was not observed in this study for $TP_{colloids}$ <750 nm. However, when the $TP_{>750\ nm}$ fraction was considered, which by size definition also contains colloids < 1000 nm, particulate P loss dominated at ~ 2 times higher than the dissolved loss. Although it is widely accepted that P is mainly transported in a particulate form during storm events and high discharge periods, studies estimating the losses from catchments via truly DP (<1 nm) are still rare. However, there is a rising awareness that even during storm flow, proportions of truly DP can be high and can make up the dominant P fraction, accounting for up to 61% of total P losses (Gu, 2017). In our study, although on average the majority of P (~50%) during storm events at all stations was still lost via particles >750 nm, losses via truly DP accounted for more than one third of total P losses (Figure B-4).

When total P losses rates per hectare of this study are compared to those from previous hydrological discharge periods (Tiemeyer et al., 2009), it becomes obvious that P losses not only result from differences in the intensity and amount of precipitation, but also from differences in temporal or spatial precipitation was comparable to that recorded in other hydrological discharge periods, the strength of events differed, leading to differences in the P discharge at single stations and thus also to differing P exports.

3.4.2 Composition of water $colloids_{0.66–750nm}$

The size ranges of the three dominant size fractions of water colloids identified in our study were in agreement with other studies analyzing natural colloids in watershed samples (Burger et al., 2021; Gottselig et al., 2017a; Gottselig et al., 2014; Gottselig et al., 2017b). The cluster analysis of elements regarding the size fractions separately but the sampling stations collectively (all stations combined) revealed that in water colloids0.66–20nm, P mainly clustered with Al, Fe, Si, and Mg (Table 3-4), which hints at the presence of both of Fe/Al (hydr)oxides (Gottselig et al., 2017a; Hassellov and von der Kammer, 2008; Jiang et al., 2015) and clay minerals with P adsorbed to them. In terms of the latter, the mineral composition of transported particles in the Zarnow catchment is, besides illite and illite-mixed layer minerals,

known to be dominated by chlorites (Nausch et al., 2017), which are characterized by the presence of Fe/Mg silicates with a small amount of Al in the crystal structures (Hamer et al., 2003). The water colloids20–60nm were characterized by high concentrations of Fe, Al, Ca, and Mg, hinting at a mixed composition of clay minerals and Fe/Al (hydr)oxides. However, the clustering of P with Al and Si only indicates that P was adsorbed to the surfaces of clay minerals (most likely illite, given the missing Mg in the cluster) by means of ligand exchange with a metal hydroxide (Yaghi and Hartikainen, 2013), which is also corroborated by the soil pH of >7. The clustering of P with Al, Fe, and Si in water colloids$_{60–750nm}$ indicates associations with both Fe/Al (hydr)oxides and clay minerals like illite, which is due to the fact that the third peak, also called the release peak, can also contain smaller particles from water colloids$_{0.66–20nm}$ and water colloids$_{20–60nm}$ that were retained by the membrane during crossflow.

The influence of the sampling location factor (tile drain, ditch, or brook) on the composition of the clusters was strongest for water colloids$_{0.66–20nm}$ and water colloids$_{20–60nm}$. In the tile drain, P was mainly associated with both clay minerals and hydroxides, while in the ditch and brook, the composition of the clusters hints at Fe/Al (hydr)oxides and Mg compounds that are not clay-associated, given the missing Si in the clusters. This fits with the results of suspended particulate matter (>800 nm) SEM-EDX analyses performed by Nausch et al. (2017) at the same sampling stations, which suggested that samples from the ditch and brook waters were enriched in Fe phosphates and that, for the brook in particular, clay minerals were underrepresented in the suspended matter, presumably due to sedimentation at times of low flow velocity. This indicates that, to some extent, the elemental composition of colloids at different sampling stations reflects the elemental composition of suspended particulate matter >800 nm, as colloids act as building units for larger size fractions (Totsche et al., 2018).

The composition of the P cluster of the ditch was consistently different for water colloids$_{0.66–20nm}$ and water colloids$_{20–60nm}$ compared to the tile drain and brook, irrespective of flow events. Cluster separation by sampling location and event (Figure 3-2) revealed that especially in water colloids$_{0.66–20nm}$, the colloidal composition of the ditch was different to those of the tile drain and brook, presumably as a result of different forms and amounts of

soil organic matter (SOM) due to an increased input of organic detritus into the ditch. The fact that nano-sized C_{org} clustered with Mg (tile drain) and Ca (brook) (Table 3-4) suggests that C=O groups of the SOM (e.g., carboxyl[ate] groups) can be assumed to be complexed and stabilized with divalent Ca^{2+} in the brook (Rowley et al., 2018) and divalent Mg^{2+} in the tile drain (Ellerbrock and Gerke, 2021). However, nano-sized C_{org} formed a separate cluster in the ditch, indicating that the majority of nano-sized C_{org} in the ditch may be fresh and not complexed. In general, the data obtained in our study confirms that the particulate but also the dissolved subsurface output of elements, particularly P, from the soil into the watershed is high, and is expected to dramatically increase during seasons with higher precipitation and a greater number of flow events.

3.4.3 Composition of water-extractable soil colloids

To identify the possible origin of colloids transported to the tile drain, ditch, and brook, we investigated water-extractable colloids from soils at various depths within the tile drain catchment. The higher stocks of colloidal P in the Ap horizon than in the Bw horizon (Figure 3-3, Table B-5) were caused by the enrichment of fertilizer P applied to the topsoil. Excess colloidal P could be transported from the topsoil to the subsoil via water-extractable colloids in intensively managed agricultural soils, especially in areas with surplus P fertilization (Chen and Arai, 2020; Rubaek et al., 2013).

When we examined the general composition of soil colloids as revealed by AF^4 analyses, the dominance of C_{org} in soil $colloids_{0.66–20nm}$ was in agreement with the results reported by others (Jiang et al., 2015; Krause et al., 2020). In this size fraction, P mainly clustered with either C_{org} or C_{org}/Ca/Mg, hinting at either organic P compounds or P-Ca/Mg-C_{org} complexes (Audette et al., 2016; Ellerbrock and Gerke, 2021; Rowley et al., 2018). Cluster analysis of soil $colloids_{20–100nm}$ hints at an association of P with clay minerals and/or Fe/Al (hydr)oxides. A closer examination of the molar ratio between Si and Al revealed values between 1.7 and 2.3 (Table B-6), indicating that 2:1 clay minerals such as illite were dominant. There was a slight (not significant) increase of this ratio from the Ap (1.7 to 1.9) to the Bw (1.9 to 2.1) and C (2.2 to 2.3) horizons for all three size fractions (Table B-6), suggesting increasing proportions of 1:1 clay minerals or Fe/Al (hydr)oxides in the Ap horizon and colloidal silica or quartz in the C horizon. Soil $colloids_{100–450nm}$ seemed to be mainly composed of 2:1 clay

minerals due to a molar ratio of around 2.2 (Table B-6). The differing associations of P with other elements with respect to the soil horizon followed no clear trend and was partly a combination of clusters from soil colloids$_{0.66–20nm}$ and soil colloids$_{20–100nm}$, indicating the presence of particles from soil colloids$_{0.66–20nm}$ and soil colloids$_{20–100nm}$ in the release peak (soil colloids$_{100–450nm}$).

The clustering between soil colloids$_{0.66–20nm}$ from the C horizon and water colloids$_{20–60nm}$ (Figure B-3) suggests that a large proportion of colloids transported in the water samples may have their origin in the water-extractable nanocolloids within the C horizon. Since the pipes of the tile-drainage system are located in this soil horizon, it is plausible that there is an increased loss of nanocolloids from this horizon. This also agrees with literature attesting that, for the most part, colloids <200 nm are transported below ground (Fresne et al., 2022). Cluster analysis suggested that mainly clay minerals such as illite were transported from the soil into the water through the tile drain, as both soil (soil colloids$_{0.66–20nm}$) and water (water colloids$_{20–60nm}$) exhibited a cluster composed of Al/Fe (soil colloids) or Al (water colloids) and Si. When soil water enters the tile-drain pipes, the redox status and ionic strength of the water are altered (Zimmer et al., 2016). This can not only foster the aggregation of nanocolloidal particles into larger colloids—explaining the larger size of clay particles in the water samples—but can also facilitate the formation of new, e.g., colloidal iron (III) (hydr)oxides and larger particles within the tile drain (i.e., ochre floc formation (Zimmer et al., 2016). Due to the high P sorption capacity of these particles (Gottselig et al., 2017b), leached truly DP is easily adsorbed to their surface. This is indicated by the clustering of Fe with P in water colloids$_{0.66–20nm}$ from the tile drain, which was not observed in the corresponding size fraction of the soil samples. The fact that Fe and P also clustered in water colloids$_{0.66–20nm}$ and water colloids$_{20–60nm}$ from the ditch implies that this formation and agglomeration of P-bearing colloids proceeded along the flow path with an increasing importance of iron(III) (hydr)oxides over clay particles.

The clustering of soil colloids$_{20–100nm}$ and soil colloids$_{100–450nm}$ from all horizons suggests that colloids are transported within the soil profile. In this context, sorption and desorption processes of colloids during transport and associated aggregation and disintegration processes can influence the size of the colloids and thus their distribution among the size

fractions within the horizons. However, in the Ap and Bw horizons, only soil colloids$_{0.66\text{-}20nm}$ clustered with colloids in the water samples, which suggests that smaller nanocolloids from the soil are more prone to leaching through the soil profile than fine- and medium-sized soil colloids, as was also found by Fresne et al. (2022). Macropore and preferential flow are the main processes of colloid and particle transport (McGechan and Lewis, 2002; Wang et al., 2020a). For instance, Koch et al. (2016) showed that at the present study site, event-based colloidal transport primarily takes place in singular macropores of biogenetic nature, while dissolved forms also pass through the soil matrix, the secondary pore system, or the interaggregate pore space. As a result, the transport of nano-sized colloids to the tile drain via such preferential pathways can be particularly fast, as large parts of the soil matrix get bypassed without substantially affecting the particle size. It is important to note that the results of this study apply only to the period from winter to spring, when vegetation cover is limited and evapotranspiration is minor. As plant water demand and evapotranspiration losses increase during the summer, water flux and P transport will likely vary.

3.5 Conclusions

In conclusion, our study showed that (i) under baseflow conditions, mainly nano-sized clay-dominated colloids were transported from the soil horizon in which the tile drain was located (C horizon) into adjacent water bodies, while (ii) event flow also enabled the mobilization of larger particles. The fact that the colloidal (<750 nm) fraction was comparable between baseflow and flow events indicates that (iii) the discharge prevailing during the runoff period did not exhaust colloid mobilization and that even under baseflow conditions, colloidal P was exported from the soil through the tile-drainage system. Furthermore, (iv) higher and varying flows during discharge events facilitated the transport of even larger particles (>750 nm) through the soil matrix. The results of this study highlight the role of larger particles and colloids in P export. The impact of rainfall intensity and pattern on particulate P discharge must be considered more closely so that drainage management can be adjusted to achieve reduced P export from agricultural land.

Chapter 4

Uptake of metallic nanoparticles containing essential (Cu, Zn and Fe) and non-essential (Ag, Ce and Ti) elements by crops: A meta-analysis

Modified on the basis of

Jia, Y.S., Klumpp, E., Bol, R., Amelung, W. 2022. Uptake of metallic nanoparticles containing essential (Cu, Zn and Fe) and non-essential (Ag, Ce and Ti) elements by crops: A meta-analysis. *Crit. Rev. Environ. Sci. Technol.*, 1-22. https://doi.org/10.1080/10643389.2022.2156225.

CHAPTER FOUR

4.1 Introduction

Nanotechnology has been predicted to great potential to enhance global agricultural productivity and food security in a sustainable manner (Kah et al., 2018; Lowry et al., 2019; Marchiol et al., 2020). Nanoparticles (NPs) have unique properties, such as a large specific surface area, specific optical and electrical properties, tuneable functionalities, and high adsorption capacities (Colvin, 2003; Khan et al., 2019; Marchiol et al., 2020; Rai et al., 2018). Engineered nanoparticles (ENPs) have been used in applications such as optics, electronics, paints, pigments, coatings, cosmetics and personal care products as well as in products for agriculture such as agrochemicals (fertilizers, pesticides and herbicides), delivery carriers of bioactive molecules, nano-sensors for pathogen and pesticide detection, and even agents for soil conservation and remediation (for a review of commercial nano products in various applications, see Figure C-1) (Ahmed et al., 2021a; Ghormade et al., 2011; Sharma et al., 2020; Wang et al., 2016b). In addition to these ENPs with high purity and defined shapes (Hochella et al., 2019; Hochella et al., 2015), NPs like clay minerals and metal (hydr)oxides are also formed by natural processes and have proven to be significant carriers of many essential plant elements, such as phosphorus (P), aluminium (Al), and iron (Fe), in both aquatic environments (Gottselig et al., 2017b; River and Richardson, 2018) and soils (Hens and Merckx, 2002; Jiang et al., 2015; Li et al., 2021a). Nowadays, due to their ubiquity in the environment, plants have significant contact with both ENPs and naturally formed NPs.

Plants can be exposed to ubiquitous natural NPs, or ENPs that have been applied in agriculture as either pesticides or fertilizers (Ghormade et al., 2011). Several studies have reported that NPs may be taken up by plants, which can result in potential toxic or promoting effects on plant growth (Ahmed et al., 2022; Dietz and Herth, 2011; Huang et al., 2022; Khan et al., 2019; Liu et al., 2020; Ma et al., 2010; Miralles et al., 2012). From the published data, however, it has become clear that plant exposure to metal or metallic NPs (MNPs, e.g., Ag (silver), TiO_2 (Ti, titanium), CuO (Cu, copper), ZnO (Zn, zinc), $Fe/Fe_2O_3/Fe_3O_4$, hydroxyapatite) leads to metal accumulation or the presence of intact MNPs in plant tissues (Avellan et al., 2019; Larue et al., 2012; Li et al., 2021b; Marchiol et al., 2019; Wang et al., 2018; Wang et al., 2012; Zhao et al., 2012). An overall assessment of the accumulation of different MNPs in crops, however, is still lacking and the reported beneficial or harmful impacts on

plants due to MNPs' applications are not consistent (Dodds et al., 2021; Landa, 2021; Liu et al., 2021). This indicates the need for a systematic data analysis of potential factors in plant uptake of MNPs. Moreover, it is unclear whether the plant uptake of MNPs differs for essential and non-essential elements.

The uptake of metals from MNPs can involve either direct internalization of MNPs, or entry of dissolved MNPs, or uptake of both nanoparticulate and ionic metals simultaneously. Although studies have addressed plant uptake of MNPs (Avellan et al., 2019; Lin and Xing, 2008; Ma et al., 2017; Su et al., 2020; Wagener et al., 2019; Zhu et al., 2008), the uptake mechanisms involved are less understood, with only some basic mechanisms having been reported. The MNPs from the air, water and soil can be internalized via both the roots and the leaves (Lv et al., 2019; Su et al., 2019).

In root entry pathway, the uptake of MNPs first pass the mucilage layer and then the cuticle: a layer of waxy lipid polymers which inhibits the passage of particles larger than a few nm (Wang et al., 2016b). The cuticle is underdeveloped in developing root tips allowing MNPs to reach the epidermis directly (Nowack et al., 2006). After reaching the root epidermis MNPs have two pathways to reach the xylem, the apoplastic and symplastic pathways (Liu et al., 2020). In the apoplastic pathway, the Casparian strip acts as another physical barrier, with size exclusion limits (SEL) even smaller than SEL of the cuticle, and prevents large particles from passing through. In the symplastic pathway, there is no need to overcome the Casparian strip barrier but MNPs do have to cross the cell wall (with SEL ≤ 10 nm) and plasmodesmata (with SEL from 1 to 100 nm) (Wang et al., 2016b). Endocytosis is another possible mechanism for MNPs to enter cells, and is believed to be dependent on clathrin on the plasma membrane (Miralles et al., 2012). Once in the xylem vessels, MNPs could be transported upward to shoot and leaf tissues (Ma et al., 2017). For foliar exposure, the uptake mechanism is similar to that found in roots. The leaf surface is also covered with waxy cuticle, and MNPs can be internalized via the symplastic or apoplastic pathway once they penetrate it (Avellan et al., 2021). Apart from crossing the cuticle, an additional pathway for foliar exposure is via the leaf stomata. This pathway has a SEL > 20 nm, and it is therefore theoretically more favorable for larger MNPs to approach the endodermis and then enter the

leaf apoplast towards the phloem (Eichert et al., 2008). The MNPs in the leaf phloem vessels can then be transported down to the shoots and roots (Avellan et al., 2019).

As discussed above, particle size may be one of the most important factors in plant uptake of MNPs, regardless of whether plant uptake of MNPs is via endocytosis or through cell wall pores (Carpita et al., 1979; Miralles et al., 2012). The SEL of plant cells allowing MNPs to penetrate is still unclear and depends upon factors such as plant species and growth stages (Hu et al., 2020; Lv et al., 2019). Theoretically, MNPs with a size (especially the hydrodynamic diameter) smaller than the SEL are more able to be internalized by the plant than larger sized particles. However, even if the size of MNPs is less than the SEL, it does not mean that NPs can easily enter the plants, other factors such as surface charge of MNPs can have an effect, e.g., the negatively charged root surface attracts positive charged MNPs but repels negatively charged ones (Lv et al., 2019; Onelli et al., 2008). Another potential factor controlling metal uptake is which part of the plant is exposed to MNPs, i.e., root or leaf. Wang et al. (2016b) recently summarized a list of possible internalization sites for MNPs, spanning a SEL range from < 1 nm to hundreds of nanometers for different physiological and chemical barriers in root and leaf tissues. The uptake of MNPs can also be affected by other plant related factors, such as plant transpiration rates (Zhang et al., 2019b), and root exudation patterns (Shang et al., 2019). Meanwhile, microbial activities could affect the uptake of MNPs by plants. For example, bean roots colonized by *Pseudomonas chlororaphis* O6 (a beneficial root-associated bacterium) showed reduced uptake of Zn when exposed to toxic levels of ZnO NPs (Dimkpa et al., 2015). The formation of mutualistic symbioses between arbuscular mycorrhizal fungi and maize plants also reduced the accumulation of Zn after application of ZnO NPs to the roots (Wang et al., 2016a).

MNPs can undergo physical (aggregation, agglomeration, and deposition), chemical (dissolution, sulfidation, and redox reactions), and biological alterations within the soil-plant system (Ahmed et al., 2021a; Guasch et al., 2017). These transformation processes are affected by many intrinsic and environmental factors. For example, the dissolution of Ag NPs can be influenced by the method of synthesis, particle size, surface coating, zeta potential, concentration, pH, temperature, light, dissolved organic matter (DOM), dissolved O_2, root exudates, accompanying ions, and ionic strength (Azimzada et al., 2017; del Real et al., 2016;

Kittler et al., 2010; Su et al., 2020; Zhang et al., 2011). Before or upon exposure to plants, MNPs can be transformed by the above processes. This can result in changes to the properties of the MNPs, such as increasing size (e.g., enhanced aggregation of TiO_2 NPs with DOM in the environment (Zehlike et al., 2019)), or surface modification (e.g., Ag NPs in the surface of spheric Ag NPs be sulfidated to Ag_2S NPs (Wang et al., 2018)).

We are not aware of any study that has fully explored the uptake of MNPs by different crops as a function of element, size, and exposure pathway. Moreover, there is a lack of systematic knowledge of the differences between the uptake of essential and non-essential elements by plants and the preferences for nanoparticulate and dissolved forms of elements by crops remains unclear. Here, we performed a meta-analysis to examine the metal accumulations within plant tissues after MNPs applications for crops in agroecosystems. Our main focus was to explore: 1) accumulation behaviors of essential and non-essential elements in various plant tissues, 2) the factors that affect metal accumulation in various plant tissues, and 3) the degree to which metal accumulation from MNPs in plants is affected by the method of exposure, also compared to the pure application of the metals in dissolved forms.

4.2 Materials and methods

4.2.1 Data collection

We constructed our database in multiple steps as recommended by Moher et al. (2009). First, we searched for articles at the Web of Science Core Collection Database on 25 Feb 2021 with "plant and nanoparticles" as title; the publication year was left un-restricted. Since we focused on studies of the uptake of MNPs in crop plants, the resulting records were screened according to the following criteria:

(1) empty records and reviews without their own data were excluded, only original research articles were considered;

(2) studies on aquatic plants and flowers were excluded (only vegetables were further included);

(3) studies on nanowires or nanosheets were excluded, while articles dealing with NPs or nanopowders were retained;

(4) all studies related to metal-, metal (hydr)oxide-, multi-metal (hydr)oxide-based MNPs were included.

After these steps, the references of the included publications were double-checked by the criteria from (1) to (4) in the same manner, making sure there were no duplicates and that all publications fulfilled the criteria. Ultimately, 173 publications were assembled in the database.

Based on the data available in the collected literature, we focused on the six elements (three essential elements for plants: Cu, Zn and Fe; and three non-essential elements: Ag, Ce (Cerium) and Ti) that appeared most abundantly in MNPs-crop studies. Essential and non-essential element groups were sorted according to decreasing solubilities of corresponding MNPs (Table C-1). Procedures in extracting data and grouping factors were described as follows:

The data from texts and tables were extracted directly, while data from figures were extracted using WebPlotDigitizer (https://automeris.io/WebPlotDigitizer/) software. Subsequently we calculated means, standard deviations (SD) or standard errors (SE) and recorded the number of replicates for metal concentrations in plant tissues (root, shoot and leaf) for each MNPs treatment and control group. As very few studies reported metal accumulation in edible tissues, like fruit, we didn't include these data as they might cause bias when calculating the magnitude of effects. Missing SD values were estimated with Rubin and Schenker's approach based on studies having similar means (Terrer et al., 2021). When extracting data, different units among studies were made uniform for further analysis: the applied concentrations of MNPs were transformed to ppm (mg kg^{-1} or mg L^{-1}); the metal concentrations in plants were displayed as mg kg^{-1} dry weight; reported concentration data based on the weight of wet biomass were excluded; the particle size was displayed in nm; and zeta potential as mV. Nine potential impact factors were isolated and grouped into the following classes:

(1) MNPs' "Particle size" in the size ranges of 1 ~ 10, 10 ~ 30, 30 ~ 60, 60 ~ 100, and > 100 nm. As only very few studies reported on the hydrodynamic diameter of MNPs in solutions, the TEM/SEM size of MNPs was used to include more studies. However, it should be noted that the hydrodynamic diameter is a more suitable parameter than TEM/SEM size when assessing the plant internalization of MNPs on the basis of the SEL of respective physical barriers.

(2) The "Zeta potential" (ζ) was considered in the ranges of ζ < -20, -20 < ζ < 0 (abbreviated as "> -20"), 0 < ζ < 20 ("< 20"), and ζ > 20 mV, and "Unsure" for MNPs of un-specified charge. It is suggested that zeta potentials between -20 and 20 mV promote the agglomeration of NPs (Schwabe et al., 2013). Based on this and combined with the distribution of zeta potentials in our database, we partitioned this factor into the above groups.

(3) "Surface coating" was classified as polyvinylpyrrolidone (PVP), citrate, polyethylene glycol-thiol (PEG) and polyoxyethylene (20) Sorbitan mono-Laurat (PEG+Tween20), PEG, and gum Arabic (GA). "Others" was used when the identity of the coating material was unspecified and "Bare" indicated the absence of any surface coating.

(4) The "Applied concentrations" were grouped into the ranges of < 1, 1 ~ 100, 100 ~ 1000 to > 1000 ppm (mg kg^{-1} or mg L^{-1}).

(5) "Crop plant" was divided into cereals (maize (Zea mays), rice (Oryza sativa), wheat (Triticum aestivum), barley (Hordeum vulgare), sorghum (Sorghum bicolor), oat (Avena sativa), sunflower (Helianthus annuus) and canola (Brassica napus)), vegetables & fruits (bean (Phaseolus vulgaris), peanut (Arachis hypogaea), potato (Solanum tuberosum), tomato (Solanum lycopersicum), cucumber (Cucumis sativus), muskmelon (Cucumis melo), pumpkin (Cucurbita maxima), zucchini (Cucurbita pepo), carrot (Daucus carota), pepper (Capsicum), eggplant (Solanum melongena), lettuce (Lactuca sativa), cilantro (Coriander), mustard (Brassica), cress (Lepidium sativum), onion (Allium cepa), cauliflower (Brassica oleracea) and citrus), and grasses (tobacco (Nicotiana tabacum), alfalfa, grass); "others" comprised crops withfewer than two observations.

(6) "Growth medium" included "Soil", "Hydroponics" and "Other media".

(7) The "Exposure period" was classified into "< 1 day", "1 day ~ 1 week", "1 week ~ 1 month" and "> 1 month".

(8) The "MNPs type" was divided according to the dominant metal.

(9) The "Exposure way" was described as "Root", "Foliar", and "Seed + Foliar" which denoted that seeds were germinated with exposure to MNPs followed by foliar exposure (spraying) to MNPs.

4.2.2 Statistical analysis

All statistical analyses were performed in R 4.0.5 (R Core Team, 2021). The standardized mean difference (SMD) estimator of the magnitude of effect was calculated using the following equation:

$$SMD = (m_t - m_c)/SD \quad \text{(Eq. 5)}$$

where *SMD* is the magnitude of effect of metal accumulations in plants; m_t and m_c are the mean concentrations of the treatment group and the control group in each experiment, respectively. Metal concentrations following different exposure regimes were compared for root, shoot and leaf tissues for three essential and three non-essential elements for plants. The differences between root and foliar exposure for both essential and non-essential elements were tested using the multilevel mixed-effect model with the "lme" function in the "nlme" package; posthoc tests were performed using the "glht" function in the "multcomp" package. A multilevel mixed-effect model was applied as a way to fit data lacking independence, and did not need to consider sphericity (Andy et al., 2012).

When calculating SMD values, the SD (standard deviation) was calculated as follows:

$$SD = \sqrt{\left[\left((n_t - 1){S_t}^2\right) + (n_c - 1){S_c}^2\right]/(n_t + n_c - 2)} \quad \text{(Eq. 6)}$$

where nt and nc represent the sample sizes of the treatment and control groups, and St and Sc denote the standard deviations of the treatment and control groups. 95% confidence intervals (CIs) were also calculated for each SMD. The random effect model was chosen to calculate SMD since there were heterogeneities between studies based on results of the Q test and the I^2 test (results of heterogeneity tests were shown in Table C-2.1 to C-7.3) (Gardea-Torresdey et al., 2000; Higgins and Thompson, 2002; Higgins et al., 2003). As studies with different crop species, various particle sizes and zeta potentials etc., were included, we both expected and detected a moderate to high heterogeneity between studies. Consequently, both the magnitude of overall and subgroup effects for each combination of element and plant tissue were estimated using a random effect model with the "metacont" function in the R package "meta" (Balduzzi et al., 2019). Publication bias tests were conducted with the "metabias" function in "meta" package. The Pustejovsky method was chosen for the

"method.bias" parameter used for the magnitude of effect was SMD in our study (results of publication bias tests are shown in Table C-2.1 to C-7.3) (Egger et al., 1997; Pustejovsky and Rodgers, 2019; Sterne et al., 2000). The results indicated that publication biases were detected maily insignificant, except for factors with number of datasets ⩽ 10 which were not tested. The package "ggplot2" was used for plotting figures.

4.3 Results

4.3.1 Dominance of specific MNPs in plant uptake studies

Collecting information for crop plant uptake of MNPs showed that there were 35 types of MNPs included, and that most studies focused on Ag- (Ag and Ag_2S), Zn- (Zn and ZnO), CeO_2, Fe- (Fe, Fe_2O_3, Fe_3O_4 and $FePO_4$), Cu- (Cu and CuO) and TiO_2-based MNPs (Figure 4-1). Some precious metal (Au and Pt) NPs, and plant essential elements containing NPs such as apatite and MgO were moderately studied. Other MNPs, such as Mn, PbS, Pd, Cu/Se, and $CuFe_2O_4$ were less studied, contributing only one study each to our database. In contrast, NPs consisting of Ag, CeO_2, ZnO, CuO and TiO_2 were the top five MNPs in all studies found, with each type having been included in > 15 studies.

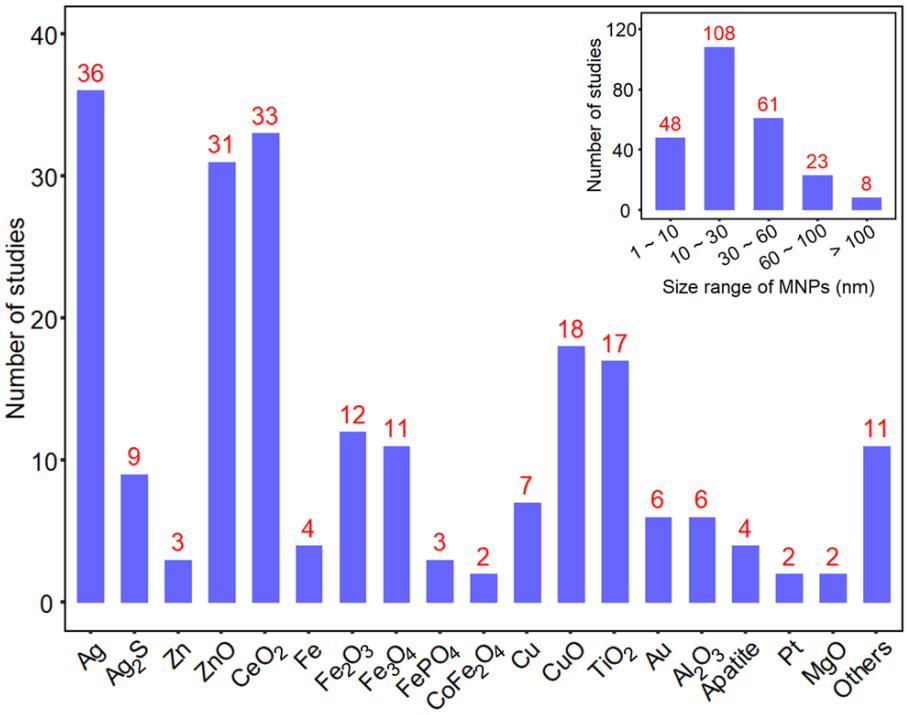

Figure 4-1. The most frequently studied types of metallic nanoparticles (MNPs). The subfigure at the top right is the distribution of size ranges (nm) of MNPs. Data was collected for this meta-analysis on 25 Feb of 2021, more recent publications are not included.

Data collection revealed that most MNPs studied had a size range between 10 and 30 nm. The size of MNPs used in this study indicates the primary TEM/SEM size, except for additional notes. The majority (63%) of all studied MNPs were smaller than 30 nm, while 19% studies were performed with MNPs < 10 nm (subfigure in Figure 4-1). More than 30 different crops have been studied (with no discrimination between varieties), with wheat (31), tomato (24), bean (21), maize (20), rice (19) and cucumber (17) being the most abundant (Figure C-2). About 58% of all studies were conducted in hydroponics while not with soil medium, particularly when the trial plants were cucumber and rice. The vast majority of all studies (84%) examined root exposure to MNPs rather than exposure of leaves or stems. MNPs concentrations that plants were exposed to range from 1 to 1000 ppm (Figure C-3).

4.3.2 Uptake of metal elements by crops

To evaluate the uptake of MNPs by crops, we concentrated on MNPs that had been frequently studied, categorized these as elements that are either not essential elements (Ag, Ce, and Ti) to plants or are additionally essential for plants (Cu, Zn and Fe), and then recorded their accumulation in various plant tissues (Figure 4-2). For all studies, we observed that median metal concentrations in tissues decreased by as many as two orders of magnitude from root through the shoot to the leaf (Figure 4-2). Note, that Figure 4-2 has an exponential scale for y-axis. For instance, the ratios of median Ag concentrations of root to shoot and root to leaf were 41:1 and 152:1, respectively. For Ce, concentrations in roots exceeded those of the shoots by 2 orders of magnitude; relative differences for the other elements were one magnitude lower (Figure 4-2). The only exception was Zn, where the median Zn concentrations among root, shoot and leaf were relatively similar. A closer look at the data revealed that foliar exposure to MNPs enhanced accumulation of metals in leaf. This helps to explain the high Zn median concentration in leaf as there were more observations via foliar exposure. The statistical tests confirmed that the metal concentrations in root were significantly higher than those of shoot and leaf following root exposure (Figure C-4.1), while foliar exposure led to significantly higher metal concentrations in leaf than

shoot and root (Ce and Zn, Figure C-4.2). The one exception to this is Ti, where there was less data and the distribution was more skewed. Moreover,

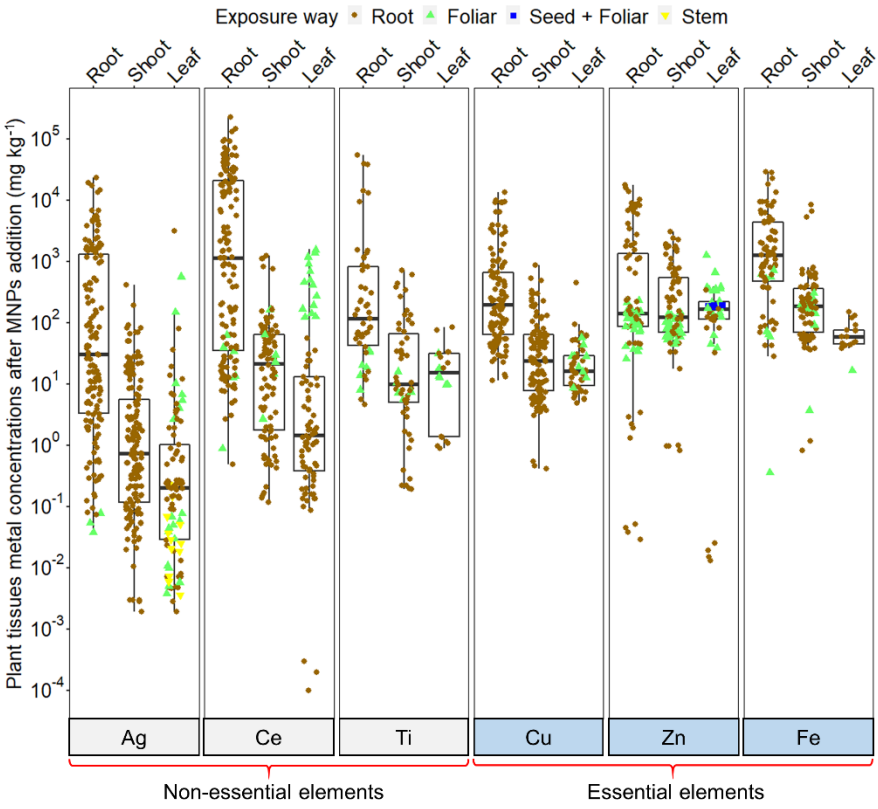

Figure 4-2. The metal concentrations (mg kg^{-1} dry weight) (exponential-scaled y-axis) in different plant tissues after exposure to metallic nanoparticles (MNPs). In order from left to right in each column, it shows metal concentration in root, shoot and leaf tissue. There are four types of plant exposure to MNPs: root exposure (brown rounded dot), foliar exposure (green triangle), seed and foliar application (blue square), and stem injection (yellow upside-down triangle). The left three columns are Ag, Ce and Ti which are non-essential elements for plants and the right three are Cu, Zn and Fe which are plant essential elements.

plant essential metals like Zn and Fe were mainly accumulated in higher concentrations (especially in shoot and leaf) than observed for non-essential metals like Ag and Ce, when comparing data from similar exposure concentration ranges (Figure C-4.3 and C-4.4). Intriguingly, comparable levels of Cu and Ti were accumulated in plant tissues (Figure 4-2).

As some MNPs can be dissolved prior to metal uptake, we also evaluated the differences between metal concentrations in plants after exposure to both MNPs and dissolved metal salts. The differences in element uptake among these treatments are displayed in Figure 4-3. We subtracted the metal concentrations from tissues receiving MNPs treatments from the concentrations in tissues exposed to dissolved metal salts. In this figure, a negative value in

Figure 4-3 indicates the preferred uptake of dissolved metals, while a positive one indicates a preferred uptake of MNPs. The results showed that in each plant tissue, the preferred uptake of a given metal form was generally element-specific. A rough trend could be concluded that non-essential elements (Ag and Ce) containing MNPs are more prone to be taken up as dissolved form especially in root and leaf, while essential elements (Cu and Zn) as nano forms in root and shoot, and Fe as nano forms in root and leaf. It should be noted that there were no data points in Figure 4-3 for Ti as TiO_2 NPs essentially do not dissolve. In detail, Ag was primarily accumulated from in dissolved metal salts, while Zn and Fe were primarily acquired as MNPs. Variations were large and the differences were not significantly different from zero, likely indicating that both uptake mechanisms are possible, especially for Zn. The pattern slightly changed in the shoots, which were more prone to take up Ag and Zn as MNPs, while Fe in dissolved metal salts. No apparent uptake preferences on MNPs or dissolved metal salts were found for Ce and Cu in the shoots. Differences in the preferred form of metal uptake was most pronounced in the leaves, which exhibited a preferred uptake of dissolved forms of Ag, Ce and Cu, but of MNPs for Zn and Fe (Figure 4-3). In addition, we subtracted the metal concentrations in plant tissues under MNPs treatments from the metal concentrations of dissolved metal treatments based on soil and hydroponic conditions separately, there were more evident uptake preferences of non-essential metals under hydroponics than soil culture (Figure C-5). The overall uptake preferences (based on data of soil and hydroponic cultures together) on dissolved Ag and nano Fe for root, dissolved Fe for shoot, dissolved Ag and Ce and nano Fe for leaf, are similar to that in hydroponic growth medium, while uptake preferences were obscure in both root and shoot under soil culture, except for Cu which showed slightly preferred uptake of nano forms.

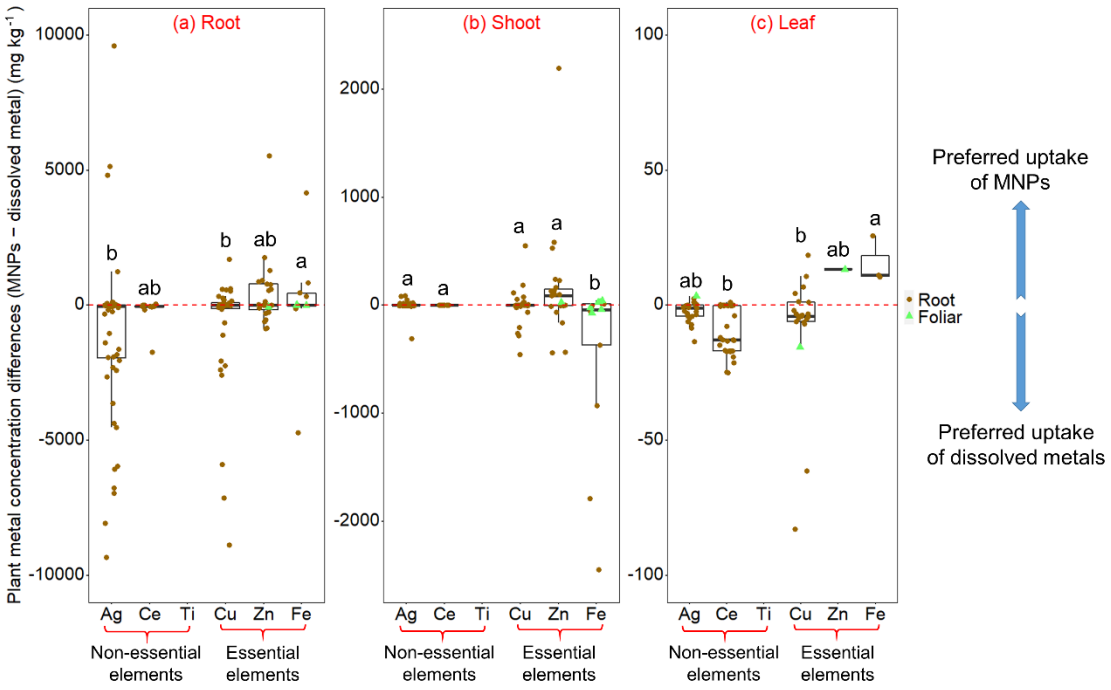

Figure 4-3. Metal concentration differences (mg kg^{-1} dry weight) in various plant tissues treated with either metallic nanoparticles (MNPs) or dissolved metal salts. No data for Ti as TiO_2 NPs do not "dissolve". The three big columns from left to right indicate metal concentration differences in root, shoot and leaf, respectively. Note that the scales of y-axis for three tissues are different. The brown round dot represents root exposure and the green triangle represent foliar exposure. Within each column, the left three metals (Ag, Ce, Ti) and the right three (Cu, Zn, Fe) are plant non-essential and essential elements, respectively. When mainly data points above the zero line (red dashed horizontal line), there is preferred uptake of MNPs by plant tissues; otherwise, the preference is for dissolved metals. Within each column, lower case letters indicate significant concentration differences between the six elements. $P < 0.05$.

4.3.3 Magnitude of effects

To evaluate potential factors affecting the plant uptake of MNPs, we related the element accumulations in root, shoot and leaf to the properties of the MNPs (particle size, zeta potential, surface coating, and MNPs type) and growth conditions (applied concentration, crop plant, growth medium, exposure-period, and method of exposure) (Figure 4-1 and 4-2, and Figure C-6.1 to C-6.4). The magnitude of effects relative to controls without metal additions as MNPs or dissolved metal salts were calculated as SMD. The results showed that the overall SMD for the accumulations of Ag declined in the order of root (5.5) > shoot (2.1) > leaf (1.7) (Figure 4-1), all indicating increased plant

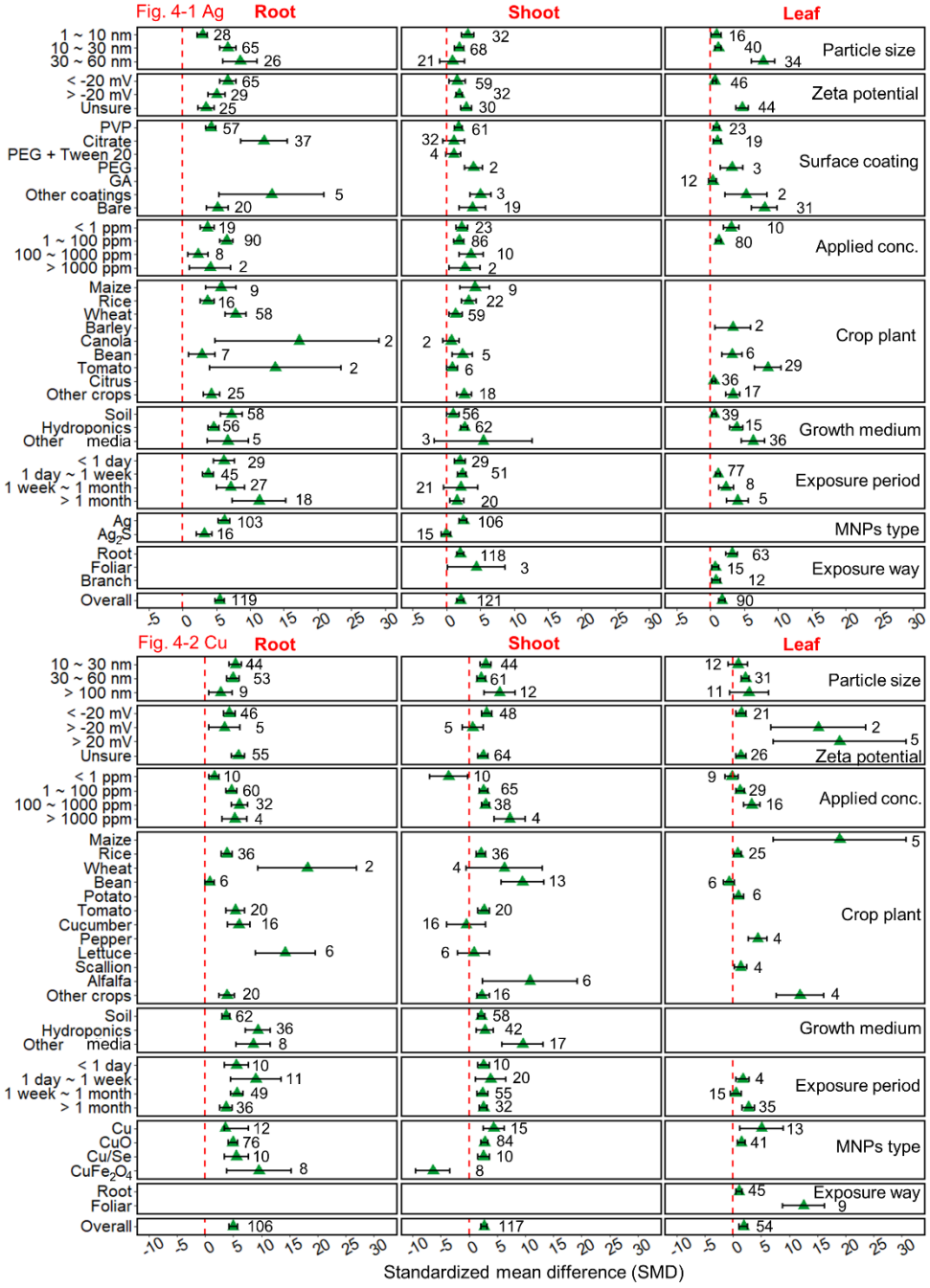

Figure 4-1 and 4-2. The magnitude of effects (standardized mean difference, SMD) of Ag and Cu concentrations in root, shoot and leaf (from left to right), respectively. The factors were grouped into several groups: particle size (nm), zeta potential (mV), surface coating (for Ag only), application concentration (ppm), crop plant, growth medium, exposure period, MNPs type and exposure way. The error bars represent 95 % confidence intervals. There is insignificant effect if the error bar crosses the vertical red dashed line (SMD = 0). The number beside each error bar indicates number of observations. When there is a significant positive (error bar to the right side of red line) or negative effect (error bar to the left side of red line) the observation number is found to be the right of the bar, while the observation number is found to the left of the bar for insignificant effects. Acronyms used for surface coating are: PVP (polyvinylpyrrolidone), PEG + Tween 20 (polyethylene glycol-thiol and polyoxyethylene (20) Sorbitan mono-Laurat), GA (gum Arabic), and "Bare" indicates no surface coating.

uptake of Ag after exposure to Ag-based NPs. In roots, the SMD and its 95% confidence intervals (CIs) were always above zero, demonstrating that all factors under consideration facilitated the accumulation of Ag in the roots. In contrast, there were SMD values in shoot with their 95% CIs overlapping with zero, which indicated insignificant positive or negative effects on plant uptake of MNPs affected by factors such as the particle-size range of "30 ~ 60 nm", surface coating with "citrate" and "PEG + Tween 20", growth media other than soil and hydroponics ("other media"), exposure period between "1 week ~ 1 month" or a modification in Ag speciation (e.g., Ag_2S NPs rather than Ag NPs) (Figure 4-1). It can be concluded that plants all tended to accumulate Ag from exposure to MNPs, while varying the MNPs properties showed little if any effect on Ag accumulation in plant tissues. Only a modification of Ag NPs to Ag_2S NPs seems to hinder Ag uptake, as deduced from the lower SMD (-0.03, CIs (-0.75, 0.68)) of Ag_2S NPs (Figure 4-1).

The results for Ce and Ti are displayed in the Figure S6-1 and S6-2; Supplementary Materials. Similar to Ag, the Ce and Ti based MNPs exhibited the same overall decrease in SMD from roots through shoots to leaves. Cereals seem to accumulate Ce more than some other crops. In general, much like Ag, varying the properties of Ce or Ti MNPs hardly affected the degree of both Ce and Ti accruals in root and shoot (Figure C-6.1 and C-6.2). There were more insignificant effects on Ce accumulation in leaf than that in root and shoot, while for Ti accumulation in leaf, all factors showed insignificant effects. Exceptions included where large particle size, "60 ~ 100 nm", for Ce based MNPs resulted in a significant decrease in Ce concentration in leaf and where intermediate zeta potentials between 0 and 20 mV seemed to hinder Ti uptake by root of barley (Figure C-6.2). It is worth noting that the magnitude of effect in shoot decreased with increasing particle size for MNPs containing non-essential elements (Ag, Ce and Ti), and shoots accumulated metals with smaller MNPs. In contrast, MNPs with elements essential for plants (Cu, Zn and Fe) showed an initial decline followed by an escalating trend of shoot SMD with increasing MNP size.

The metal uptake of MNPs containing Cu also mostly showed positive effects by most of the factors (Figure 4-2). In general, the SMD values for Cu-based MNPs increased with higher applied concentrations in all three plant tissues. Similar trends were also found for Zn- and Fe-based MNPs (Figure C-6.3 and C-6.4), with the exception that in shoot there was reduced

enrichment with increasing concentration of Fe-based MNPs. We also found that the SMD for all three essential elements Cu, Zn and Fe increased in roots and shoots as the zeta potential became more negative, i.e., when the absolute value of the negative surface charge of MNPs increased. In contrast to the non-essential elements especially Ce and Ti, mainly factors showed significant positive effects on leaf SMD for essential elements Cu and Zn. It also appeared that Zn was more easily taken up than Fe from MNPs with all factors promoting leaf accumulation of Zn. The accumulation of Fe in leaf, however, declined for specific factors such as in "muskmelon" plant, a soil growth medium, and exposure periods exceeding one month. Zero valent Fe generally exhibited larger SMD values than other Fe MNPs, such as Fe_2O_3, Fe_3O_4 and $FePO_4$ (Figure C-6.4). Plants grown in hydroponics, usually showed larger metal enrichment (more positive SMD) than soil cultures.

To compare the accumulation of different metals by each crop, we concentrated on the top five crops (three cereals and two vegetables) studied in soil cultures and calculated the SMD (Figure C-7.1 to C-7.5). The SMD for non-essential elements in shoot was less than that detected in root, which was observed with Ag and Ti in wheat (Figure C-7.3), and Ce in tomato (Figure C-7.4). For essential elements, the variations of SMD were generally minor. Meanwhile, after exposure to MNPs, the metal accumulations in shoot were different among crops. Since metal concentrations after both root and foliar application of MNPs were used in Figure C-7.1 to C-7.5, we assessed differences of metal accumulations in each crop primarily based on metal concentrations in shoot. This could minimize the influences of unrinsed root or leaf surface adhered MNPs to the results. Maize took up significantly higher concentrations of both essential (Zn and Fe) and non-essential (Ag and Ce) elements from the MNPs treatments than no metal addition (positive SMD), and tomato and cucumber showed similar results. Wheat had a positive SMD for essential elements (Zn and Fe), but a negative SMD for non-essential elements (Ag and Ti), while rice exhibited uptake preference of Cu relative to Zn. (Figure 4-1, 4-2 and C-7.1 to C-7.5).

4.4 Discussion

4.4.1 Main MNPs in plant uptake studies

It is well accepted that plants acquire nutrients as dissolved or ionic elements. Over the last two decades, however, there has been increasing evidence that plants can also take up NPs (Khodakovskaya et al., 2009; Lin and Xing, 2008; Onelli et al., 2008), even if it remains challenging to distinguish between the internalization of elements in intact NPs and from those dissolved NPs (Avellan et al., 2019; Ma et al., 2017; Su et al., 2020). Our meta-analysis studied metal accumulation in commonly studied crops (wheat, tomato, bean, maize, rice and cucumber) that usually have high economic yields and/or involve large harvesting areas worldwide. It should be noted that only studies where the concentrations of applied MNPs were recorded in the units of mg kg^{-1} or mg L^{-1} were included in this study. Ag-, Zn-, Ce-, Fe-, Cu-, and Ti-based MNPs (Figure 4-1) were the most commonly studied for their specific MNPs properties and their potential applications in precision and sustainable agriculture (Kah et al., 2018; Raliya et al., 2018). Ag NPs have received intense research due to their broad spectrum of antimicrobial properties (Nair et al., 2010), however, the high cost of Ag has limited its use in agriculture compared to its other applications such as textiles, cosmetics and food packaging (Huang et al., 2021). Cu based MNPs, such as Cu^0, CuO, and especially $Cu(OH)_2$), are promising nanopesticides (Adisa et al., 2019), which can be effective even at concentrations lower than traditional soluble Cu salts (Borgatta et al., 2018; Zhao et al., 2016). Apart from acting as nanopesticides, some MNPs are commonly applied as nanofertilizers. Seed coatings with Cu and Zn based MNPs generally increased seed germination by efficiently providing essential micronutrients (Gilbertson et al., 2020; Sturikova et al., 2018). Nanoparticulate Fe-based (Fe^0, Fe_2O_3 and Fe_3O_4) fertilizers could alleviate impaired plant photosynthesis and respiration induced by Fe deficiency (Li et al., 2020; Yuan et al., 2018). ZnO NPs helped to improve grain Zn content thus promoting crop growth in Zn deficient soils (Yusefi-Tanha et al., 2020) at lower dosages than dissolved Zn salts sprayings (Elhaj Baddar and Unrine, 2021). Even TiO_2 NPs have been suggested as a nanofertilizer to improve CO_2 assimilation and photosynthesis due to the enhanced activity of a key photosynthetic enzyme ribulose-1,5-bisphosphate carboxylase/oxygenase (Gao et al., 2008; Raliya et al., 2018), although Ti is no an essential element for plants. Hence, the elements most studied are also those most commonly in use; even though the use of commercial agricultural products containing MNPs is still in its infancy (Figure C-1).

4.4.2 Plant uptake and translocation of MNPs

The entry tissues of MNPs generally accumulated higher metal concentrations than other plant organs: i.e., when roots were exposed to MNPs first, the metal concentrations in roots were 1-2 orders of magnitude higher than those in shoots and leaves, whereas foliar exposure to MNPs, such as of Ce and Zn based MNPs, led to elevated metal accumulations in the leaves (Figure 4-2 and Figure C-4.1 to C-4.2). Examination of the magnitude of effects confirmed that root exposure resulted in higher root SMD than foliar exposure, while leaf SMD by foliar exposure exceeded that when the exposure occurred in the root. Exceptions to this pattern were observed with Ag accumulation in leaf and Zn accumulation in root (Figure 4-1 and 4-2 and Figure C-6.1 to C-6.4). The overall result was in line with studies on the uptake of CeO_2 NPs by hydroponic cucumber (Ma et al., 2015), the exposure of rice to CuO NPs in soil (Peng et al., 2017), and outdoor lysimeter experiments where wheat and canola had been exposed to sewage sludge containing Ag NPs (Schlich et al., 2017). Some of these differences can be induced by methodological challenges. In principle, MNPs could adhere to root surfaces or the outer epidermis and risk not be rinsed out efficiently by deionized water (Zhang et al., 2012). However, there are reported methods which could rinse root adhered MNPs efficiently. For example, rinsing with $CaCl_2$ solution reduced > 92% of iron that had accumulated on or in cucumber roots (from zero valent iron NPs) in comparison to the unwashed control (Dwivedi et al., 2018). The Na_4EDTA elution combined with 45 Hz and 300 W ultrasonication for 30 min method removed root adsorbed CuO NPs completely (Almendros et al., 2022; Zhou et al., 2011). The authors also suggested that it was root surface coordinated or mechanically adhered CuO NPs which were hard to be rinsed, rather than electrostatically attracted ones as the positive or negative zeta potentials didn't affect the desorption of CuO NPs (Zhou et al., 2011). Even if MNPs adsorbed onto the mucilage layer or waxy cuticle of the root surface could be washed out to some degree; however, this is no longer possible once the MNPs have crossed the root surface and entered into epidermis (Geisler-Lee et al., 2013; Lv et al., 2019). Physical barriers with SELs of a few nm would prevent root cells from internalizing of larger MNPs, which in turn can promote the aggregation of MNPs and thus concentrate the metal contents on the root (Wang et al., 2016b).

The foliar application of MNPs seems to be more efficient than root exposure. In our study, foliar applications always resulted in higher shoot SMD values than for root applications, suggesting that metal accumulations in shoot were more efficient when applying MNPs on

the leaf (Figure 4-1 and 4-2 and Figure C-6.1 to C-6.4). This trend was also suggested by other studies. In case of CeO_2 NPs, leaf spraying of 100 mg L^{-1} CeO_2 NPs led to 13, 163 and 915 mg Ce kg^{-1} in root, shoot and leaf of spinach grown in soil, respectively (Zhang et al., 2019a); while root exposure to 1.0 g kg^{-1} soil CeO_2 NPs accumulated 210.7 and 0.1 mg Ce kg^{-1} in soybean root and shoot (Priester et al., 2012). The latter has much larger differences of Ce concentrations between root and shoot than the former, which indicates low shoot uptake of CeO_2 NPs via root exposure. Note, MNPs applied to the leaf can adhere to and be retained by the leaf in a similar manner as occurs in root (Keller et al., 2018). The SEL of leaf stomata has been estimated to exceed 20 nm (Eichert et al., 2008), which is larger than that of the cell wall. This enables much larger MNPs to enter the plant via the stomata into the leaf apoplast (He et al., 2022). Once trapped in the concave structure of stomata, it also becomes difficult to wash the MNPs out, which increases the possibility of internalization (Zhu et al., 2021). Effective uptake via leaf exposure with subsequent internalization and translocation was especially supported by the data for Zn and Fe, which revealed fairly high concentrations in shoot and root tissues after foliar exposure to MNPs (Figure C-4.2).

The higher concentrations of MNPs-derived metals in entry tissues compared to those in other tissues (Figure 4-2) demonstrated that plant translocated a proportion the metals via the vascular system (Su et al., 2020). Apart from when the root of plants was exposed to MNPs, plant tissues (except for entry tissues) accumulated significantly higher essential metals (Cu, Zn and Fe) from MNPs than non-essential metals (Ag, Ce, and Ti) (Figure C-4.3 and C-4.4). Generally, crops do not favor the uptake and accumulation of non-essential or toxic elements, with plants using common mechanisms such as transporter discrimination between non-essential and essential elements; hence, there is usually a restrained translocation of non-essential elements to upward tissues (Khan et al., 2014). An efficient translocation to the aboveground tissues of soybean was reported for Zn from ZnO NPs, while CeO_2 NPs enriched only roots (Priester et al., 2012). Foliar application of ZnO NPs to tomato leaves accumulated more Zn than shoots and roots, whereas applying TiO_2 NPs in the same manner led to higher Ti concentrations in roots rather than in shoots and leaves (Raliya et al., 2015).

4.4.3 Factors of the uptake of MNPs by crops

4.4.3.1 Particle Size

Particle size has been generally assumed to be important in governing plant uptake of MNPs (Huang et al., 2021; Liu et al., 2020; Lv et al., 2019). Our collected data indicated that only 19% of all studies used MNPs < 10 nm (Figure 4-1), which are more prone to be taken up by roots directly as the SEL of cell wall pores is ≤ 10 nm (Carpita et al., 1979; Miralles et al., 2012). It is challenging to link the primary size (TEM/SEM size) of applied MNPs to the SEL of plant barriers, because the MNPs' hydrodynamic sizes are normally larger than their TEM/SEM size (Table C-1) (Gao et al., 2021; Ma et al., 2012; Zhang et al., 2019a). Moreover, the hydrodynamic sizes of MNPs are influenced by factors such as ionic strength, dissolved organic carbon and root exudates (Su et al., 2020; Yang et al., 2019). Accordingly, uptake of elements from MNPs ≥ 10 nm can still occur if they partially dissolve, which can take place following the release of root exudates (Peng et al., 2015). Huang et al. (2017) reported that malic and citric acids could be more efficient in dissolving nano Cu than oxalic and succinic acids. Crops with different compositions of root exudates may, therefore, differ in their uptake of MNPs. Moreover, the effects of soybean root exudates were reported to vary depending on the MNPs concerned, i.e., aggregation of nano $Cu(OH)_2$, but dissolution of nano CeO_2 (Cervantes-Aviles et al., 2021). Further research is needed to expand our knowledge of the effect of root exudates on plant uptake of MNPs, as well as transformations of MNPs at the root-soil interface. Both are critical if the uptake of MNPs by root is to be understood.

Our analysis confirmed a systematic increase in shoot SMD with decreasing particle size diameter for all six elements. The one exception was shoot SMD of Fe in the size range of 30 ~ 60 nm (Figure C-6.4). Since both root and leaf were the main entry tissues for MNPs, the metal accumulations in these tissues can partially be attributed to MNPs that adhere to the surface and are difficult to remove by surface washing of the tissue as discussed above. Metal concentrations in shoot should mainly be due to the transport of MNPs within the plant via vascular system. Cell wall pores, which were not permeable for > 20 nm, exhibited a size-exclusion effect for MNPs that contained Fe (Kulikova et al., 2017). Smaller particles can overcome the SEL of entry tissues and exhibit facilitated transport of MNPs to other tissue parts (Larue et al., 2012). Another contributor to size dependent internalization and transport

of metals in the plant is that MNPs of smaller particle size have a larger surface to volume ratio and, as a result, can likely be more easily dissolved (Schwabe et al., 2015).

4.4.3.2 Zeta potential

In addition to size, it is likely that the zeta potential affects the internalization and transport of MNPs (Avellan et al., 2019; Liu et al., 2019b; Zhu et al., 2012). Root and leaf have negatively charged surfaces (Lv et al., 2019), meaning that MNPs with zeta potentials < 0 mV will be electrostatically repelled. This interaction will reduce the adhesion of MNPs, but can also facilitate its transport (Avellan et al., 2019). Interestingly, NPs with absolute values of zeta potential higher than 20 or 30 mV are more prone to be internalized by plants (Hu et al., 2020), while electrostatic forces with zeta potentials between -30 to +30 mV could be negligible (Zhou et al., 2011). Our results confirmed enhanced metal accumulations in shoot (higher SMD) for Zn and Cu and for the other metals in roots when the zeta potential became more negative, i.e., from -20 mV < ζ < 0 mV to ζ < -20 mV (Figure 4-2 and Figure C-6.3). As mentioned above, electrostatic forces between MNPs and root surface are much weaker than mechanical adhesion (Zhou, et al., 2011). Therefore, negatively charged MNPs could be adhered onto root surface and thus may be internalized into root cells rather than be repelled by root surface. Once inside root cells, MNPs could flow into xylem or phloem vessels (or saps). More negative zeta potential would prevent MNPs from being adhered to negatively charged xylem or phloem surface and facilitate the transport of MNPs (Su et al., 2019). On the other hand, more negative zeta potential (i.e., ζ < -20 mV) would resist formation of large aggregates of MNPs which favors the transport of MNPs inside plants.

4.4.3.3 Other factors

Other factors assessed in this meta-analysis that may affect plant uptake of MNPs are surface coatings, the type of MNPs, the concentration of applied MNPs, the crop species, the growth medium and period, as well as the type of exposure (Huang et al., 2021; Miralles et al., 2012). There are even more potential factors that can affect plant uptake of MNPs, such as microbial activities or community, or MNPs' dissolution, but available information was scarce for quantitative data evaluation. The dissolution of Ag NPs may be negligible within hours or few days, and TiO_2 NPs do not dissolve (Hedberg et al., 2019), however, large amounts of our collected studies were conducted more than one week (see "Exposure period"

in Figure 4-1 and 4-2, and Figure C-6.1 to C-6.4) and the contribution of dissolved MNPs to plant metal uptake could be considerable, such as CuO and ZnO NPs which have relatively high solubilities (Table C-1). Moreover, the MNPs inside plant roots may undergo dissolution due to oxidation by like reactive oxygen species (Huang et al., 2021) and then the released metal could be transported to other plant tissues, while CeO_2 NPs may not dissolve once entered into roots (Wojcieszek et al., 2019). Thus, dissolution of MNPs adds uncertainties in evaluating the plant uptake of MNPs. Many factors such as size, shape, DOM, chloride, pH, and crystallinity could play a role in the dissolution of MNPs (see Hedberg et al. (2019) and references therein), which were not the main focus of this study and will not be discussed here.

In our analysis, a PVP coating on Ag NPs enhanced the accumulation of Ag in shoot compared to a citrate coating, while Ag NPs coated with citrate exhibited higher SMD of root than those coated with PVP. This could be because PVP coated Ag NPs have stronger steric repulsion than citrate coated Ag NPs, which resists aggregation and therefore facilitates translocation (Su et al., 2020). CeO_2 NPs had a positive surface charge when coated with chitosan, but were negatively charged after coating with polyacrylic acid. While the application of CeO_2 NPs with different surface charges had varying effects upon uptake of Ce in both cucumber root and shoot (Liu et al., 2019b), the coating material itself may have had minimal effects on uptake of Ce in leaf if the zeta potential was not affected (Schwabe et al., 2015). However, as plant leaf surfaces are covered with cuticular waxes and / or trichomes (as in wheat), coating with surfactants could still promote the delivery of MNPs to leaf surfaces after foliar exposure (Huang and Keller, 2021). Therefore, different surface coatings would not decrease the uptake of MNPs as all coating materials showed positive to significantly positive SMD for all tissues (Figure 4-1, and Figure C-6.1).

Increasing the dose of MNPs could also contribute to elevated accumulation of metals in the plants. Our analysis showed larger SMD for higher dosages, particularly for Cu and Zn (Figure 4-2 and Figure C-6.3), which was in line with other studies (Rizwan et al., 2019; Rui et al., 2018). Note, an accumulation threshold could be reached if the transport vascular systems or porous membrane structures are blocked due to aggregates of MNPs resulting from too high dosages (Su et al., 2020). Moreover, excess dosage of MNPs could induce toxic

effects on plant growth, for example, 500 mg L^{-1} Fe_2O_3 NPs inhibited root growth of hydroponic rice which may due to accumulation of reactive oxygen species (Li et al., 2021b).

The uptake of MNPs was crop species dependent but also interacted with other factor such as phosphate, as Zhang et al. (2019b) reported that phosphate has more efficient effects on the translocation of CeO2 NPs derived Ce in monocots (maize and wheat) than dicots (cabbage and soybean). The authors also suggested that root exudate components and plant xylems could mainly contribute to the different uptake performances between crop species. When exposed to equivalent concentrations of Ag NPs, there was a larger accumulation of Ag in wheat than in cowpea (Wang et al., 2015). In our study, the wheat roots were more prone to accumulate Ag from MNPs than shoot, while there were comparable effects for these two tissues of maize (Figure C-7.1, C-7.2 and C-7.3).

When evaluating the data in Figure 4-1, it appears that the various factors also interact. The largest magnitude of effects was paired with the largest effect variations for certain surface coatings and crop species in root and leaf but not in shoot, i.e., not for the translocation in the plant. This could allow optimization of the efficacy of MNPs (such as nanopesticides) at tissue surfaces if no further translocation is desired. Due to the presence of these interactions, no specific ranking can be made among the different factors. All factors seem to affect the efficiency of MNPs internalization and transport, and create different and likely also synergistic options to manipulate the MNPs uptake by plants.

4.4.4 Uptake preferences upon exposure to MNPs and dissolved metals by plants

Many publications on plant uptake of MNPs cannot distinguish metal uptake by direct internalization of MNPs from that of metal ions that can be released from MNPs (Cocozza et al., 2019; Dimkpa et al., 2013; Zhang et al., 2015). However, such a differentiation can be assessed using an exposure to dissolved metals as control. The analyses of available data indicated that there are element specific uptake preferences among various tissues (Figure 4-3). For elements which are essential for plant growth, i.e., for Cu, Zn and Fe, the preferred uptake of both nanoparticulate and dissolved forms was observed, with a slight bias towards particulate forms (Figure 4-3). This is presumably due to the specific needs of the plants to internalize these elements and reflecting the specific applications of the MNPs as nano-pesticide or nano-fertilizer. In addition, the concentration or speciation of the metals could

also contribute to these differences. Lin and Xing (2008) reported that the uptake of ZnO NPs was preferred over elevated concentration of Zn salts in ryegrass roots. Hydroponic exposure to zero valent iron NPs by cucumber roots resulted in significantly higher Fe accumulation than exposure with Fe-EDTA (Dwivedi et al., 2018). In the case of Cu, exposure to nano forms elicited higher metal uptake of soil grown cucumber roots than exposure to dissolved metals (Ahmed et al., 2021b). The growth medium may play an important role in uptake preferences of MNPs. In soil matrices, there were no obvious root and shoot uptake preferences of non-essential metals (Ag and Ce), while the preferences of dissolved ions became apparent in hydroponics (Figure C-5). Both MNPs and dissolved metals being applied into soils could be partially absorbed to soil particles and their availabilities are decreased (Dwivedi et al., 2018). Hence, hydroponic application would be more efficient than soil culture and this was confirmed by above results. While root surface may be blocked under high application rates of MNPs with low solubility, there could be preferred uptake of dissolved metals. However, this may not be true under deficient application dosages with less blockage of root cell wall pores, as reported by Ahmed et al. (2022) that there was a preferred uptake of nano Al_2O_3 NPs by maize shoot at medium application concentrations but higher uptake of dissolved Al^{3+} salts at elevated dosage under hydroponics.

The uptake of non-essential metals Ag and Ce showed a clearer preference to dissolved forms than non-essential elements (Cu, Zn and Fe) (Figure 4-3). The roots exhibited a slight preference for ionic Ag and strong preference for Ce, which was not apparent in the shoots. Saleeb et al. (2019) pointed out that uptake preferences of Ag NPs or of Ag ions are plant-specific. In particular, *Arabidopsis* and poplar have been found to facilitate faster uptake of ionic Ag than of Ag NPs in hydroponics (Wang et al., 2013), while no respective significant differences were observed for soil fescue root uptake of $AgNO_3$ compared to Ag NPs (Layet et al., 2019). In contrast, Ag NPs contributed to higher Ag accumulation in hydroponic rice root than that did $AgNO_3$ (Yang et al., 2019), while modifying the Ag NPs to Ag_2S NPs resulted in lower accumulations (del Real et al., 2017). Moreover, it is also possible that dissolved Ag^+ can be reduced to nano Ag^0 (Guo et al., 2019), or, vice versa, nanoparticulate Ag can release Ag^+ with help of root exudates (Stegemeier et al., 2015). With this variability, a final definitive evaluation of preferred uptake of specific Ag forms is difficult. The preference for ionic forms of Ce in root may be due to reduced bioavailability of CeO_2 NPs

when applied to soils and their subsequent interactions with soil organic matter and mineral particles (Ma et al., 2020). When grown in hydroponics, plant roots acquired more Ce from CeO_2 NPs than from Ce salts (Zhang et al., 2015). As both forms of Ce can be taken up by plants, differences in the solubility between nano CeO_2 and Ce salts might not be a limiting factor for uptake (Barrios et al., 2016).

Figure 4-3 also reveals that uptake preferences of different metals in dissolved or nanoparticulate forms varied among plant tissues. Compared with roots, plant shoots did not exhibit any preference for the uptake of non-essential metals in dissolved or nanoparticulate form, while essential elements exhibited some bias towards nanoparticulate Zn and dissolved Fe. Layet et al. (2019) also reported that there were insignificant differences in the uptake of Ag between Ag NPs and $AgNO_3$ in plant shoot at environmentally equivalent concentrations. However, when treated with high concentrations, wheat shoots accumulated more Ag from Ag NPs than from exposure to $AgNO_3$ (del Real et al., 2017). Similarly, Yang et al. (2020) reported that there might be higher translocation of nano Ag into rice shoot than $AgNO_3$, as shown in the variations of the Box-Whisker plot (Figure 4-3). After being grown in soil for more than 200 days, tomato shoots accumulated low but similar Ce contents from nano CeO_2 and Ce salt treatments (Barrios et al., 2016).

The clearest uptake preferences were found in leaves which preferred to take up Ag, Ce and Cu in ionic forms but Zn and Fe in nanoparticulate form. In part, these data indicate a concentration effect. The accumulation of Ag after hydroponic exposure in poplar leaves was higher after the addition of Ag salts than when Ag NPs were added at low concentration (0.1 mg L^{-1}). This difference vanished when the exposure concentrations rose to 1 mg Ag L^{-1} (Wang et al., 2013). The leaves of fescue accumulated similar amounts of Ag from ionic and nanoparticulate Ag at low soil exposure concentrations (0.0015 and 0.15 mg kg^{-1}) (Layet et al., 2019). For Ce, the effects were opposite: a slightly higher concentration of Ce in tomato leaf was observed when treated with CeO_2 NPs than with the application of low concentrations of ionic Ce (62.5 and 125 ppm) (Barrios et al., 2016). In wheat, the uptake of Ce in leaf from ionic forms exceeded that from nanoparticulate forms at a similar concentration (100 ppm), and the effects were more pronounced than for pumpkin and sunflower (Schwabe et al., 2015). Clearly, the uptake preferences depend on exposure concentration, crop-species, and

element. Although not yet investigated, factors such as growth duration, particle size, and zeta potential are also likely to affect uptake preferences.

4.5 Conclusion

The uptake of Ag-, Zn-, Ce-, Fe-, Cu- and Ti-based MNPs by wheat, maize, rice, tomato, bean and cucumber were most frequently reported in the literature. Our meta-analysis showed that metal concentrations generally declined from root through shoot to leaf under root exposure to MNPs, and foliar exposure showed more efficient metal accumulations in plant shoot than root application of MNPs. The presence of the metals in shoot indicates internal vascular transport of metals or even MNPs. As expected, the plant uptake of MNPs was higher for essential (Cu, Zn and Fe) than non-essential elements (Ag, Ce, and Ti). Metal accumulations in shoot decreased with increasing MNPs size for non-essential elements. There is a decline followed by rising trend of shoot accumulation of essential elements with increasing size of MNPs. The metal accumulation of essential elements in both root and shoot was enhanced as the zeta potential became more negative. Both element specific and tissues variable uptake preferences of MNPs were reported. Non-essential elements (Ag and Ce) were acquired preferably as dissolved ions particularly under hydroponics, whereas uptake as nanoparticulate forms occurred more frequently for the essential elements (Cu, Zn and Fe), although true tracing studies in this context are rare. The conclusion obtained in this study should be interpreted carefully, as they are mainly based on overall results of the studies. Precise determination of the dissolution of MNPs upon exposing to plants or after internalization is still a critical challenge for future research. Advanced techniques are needed to pinpoint and trace the fate of MNPs inside the plant and determine the metal form in which it is translocated within and between tissues. Natural NPs are ubiquitous and important carriers for both essential and non-essential elements and plant uptake of those NPs are interesting hint for future investigations.

Chapter 5

Final discussion

CHAPTER FIVE

5.1 Summary of the research objectives

Alternative phosphorus (P) sources could alleviate limitations especially in agricultural productions owe to shortage and heterogeneous distribution of worldwide mineral phosphate rock (PR) reserves. Recycling of P from waste streams from agricultural or industrial production, or remobilization/reutilization of soil inherent P are promising clues for sustainable P management. Mineral P fertilizer substitutes such as bone char (BC) and surface modified BC (BC^{plus}) have been demonstrated capable of supplying P for plant growth (Leinweber et al., 2019; Panten and Leinweber, 2020). However, **it is unclear to what degree will P derived from BC materials influence the pools and fractions of soil P under long-term field conditions.** Meanwhile, soil P from geogenic or anthropogenic sources is usually hardly soluble and bioavailable, so that its fate in colloidal form largely determines transport and potential plant uptake (Montalvo et al., 2015). Yet, **the transport of soil colloidal P from arable topsoil via subsurface to nearby streams through, e.g., artificial drainage system is less documented.** Even less is known on the uptake of P in nanoparticulate form, and I am not aware of studies that analyzed this explicitly, also due to the difficulty that plants might not merely take up nutrients in nanoparticulate phases but dissolve them during all stages of nutrient acquisition. Yet, many studies indicated that metallic nanoparticles could contribute to metal enrichments in plant tissues (Liu et al., 2020; Su et al., 2020). The knowledge of plant uptake of MNPs might be also helpful in understanding or management of soil nanoparticulate P or other bound mineral nutrients, which might at least partly compensate for the lack of respective direct studies. Nevertheless, **a comprehensive understanding of controlling factors on plant uptake of MNPs and possible uptake preferences of MNPs by plant tissues is also not yet available.**

The present thesis focused on elucidating above three issues. I firstly evaluated the effects of a potential alternative P fertilizer that relies on BC based materials and studied P pools and P fractions within soil size fractions after 5-year field fertilization experiment. The transport of colloidal P in arable soil - stream water system was deduced by measuring different sized colloidal P in top- and subsurface soils, and in tile-drain, ditch and brook waters, then assessing potential P binding associations via cluster analysis. Furthermore, I performed a meta-analysis by collecting 173 studies on crops uptake of MNPs in order to

uncover potential uptake preferences of MNPs by different plant tissues, as well as the main controlling factors of plant internalization of MNPs.

In doing so, I got basic results for the following questions.

1) **It has been reported that BC and BC^{plus} could provide P for plant growth, but how will the P from these alternative P fertilizers affect various P fractions or pools within soil size fractions under long-term field conditions?**

By sampling soil samples from a 5-year field fertilization experiment, with treatments including: bone char (BC), sulfur modified bone char (BC^{plus}), triple superphosphate (TSP, as conventional P fertilizer control), and no P fertilization control (No-P), I firstly fractionated bulk soil into four size fractions: small macroaggregates (250 to 2000 μm, SMaA), large microaggregates (53 to 250 μm, LMiA), small microaggregates (1 to 53 μm, SMiA) and composite building units (< 1 μm, BU); and then assessed soil P status after Hedley sequential extraction. I found mostly no significant effects after BC and BC^{plus} additions compared to No-P on soil P pools. However, sulfur modification of BC tended to result in higher portions of labile P, comparable to TSP. Therefore, I conclude that especially BC^{plus} behaves in a similar manner as TSP, without any positive but also without any detrimental effects on soil P status; thus, supporting earlier indications that bone char waste streams may become a useful substitute for traditional TSP additions towards a more sustainable agriculture with more closed P cycles.

2) **Soil particles have strong fixation of fertilizer P. The residual soil P could be transported facilitating by the movement of soil nanoparticles especially under rainfall events. After leaching from topsoil to subsurface soils, how is the subsoil nanocolloidal P transported to nearby water flows?**

To gain deeper knowledge about particulate subsurface P transport from inland sources to the brook, we have studied an artificially drained lowland catchment (1550 ha) in North-Eastern-Germany. We took daily samples during the winter discharge period 2019/2020 at various spatial scales, i.e., drain outlet, ditch, and brook and analyzed them for total P ($TP_{unfiltered}$), particulate P >750 nm ($TP_{>750\ nm}$), colloidal P ($TP_{colloids}$), and truly dissolved P (truly DP) during baseflow conditions and high flow events. The majority of $TP_{unflitered}$ was

formed by $TP_{>750\ nm}$ (54 to 59%), followed by truly DP (34 to 38%), and small contribution of $TP_{colloids}$ (5 to 6%) in the tile drain, ditch, and brook. During flow events 63 to 66% of $TP_{unfiltered}$ was present as particulate P ($TP_{>750\ nm}$ + $TP_{colloids}$), whereas it was 97 to 99% during baseflow; thus, truly DP was almost negligible (1 to 3% of $TP_{unflitered}$) during baseflow. We also found that colloids transported in the water samples have their origin in the water extractable nano-colloids (0.66 to 20 nm) within the C horizon, which are mainly composed of clay minerals. Along the flow path there is agglomeration of the P-bearing nano-colloids from the soil with increasing importance of iron (III) (hydr)oxides over clay particles. Event flow was able to transport larger particles (>750 nm) through the soil matrix. However, the discharge did not exhaust colloid mobilization and there was an export of colloidal-P through the tile-drainage system during the complete runoff period, even under baseflow conditions. Therefore, is it essential to consider more closely the impact of rainfall intensity and pattern on particulate P discharge to adjust drainage management for a reduced P export from agricultural lands.

3) **Both nanocolloidal P and metallic nanoparticles (MNPs) could be taken up by plants. Are there crop uptake preferences between MNPs and dissolved metal salts? Which factors are more important in controlling the crop uptake of MNPs?**

We reviewed 173 studies to evaluate the crop accumulation and uptake of metallic nanoparticles (MNPs). Those studies focused on the main global cereal and vegetable crops (wheat, tomato, bean, maize, rice and cucumber), specifically their uptake of six MNPs (containing mainly Zn, Ag, Cu, Fe, Ce and Ti). Our study showed that the plant uptake preference of MNPs or metal salts was element-specific and varied among tissues. Plants generally accumulated higher concentrations of the three essential elements (Zn, Cu and Fe) than of the non-essential ones (Ag, Ce and Ti). Plant uptake rates were more efficient when MNPs were exposed to leaves than to roots. Shoot metal concentrations increased with decreasing particle size of the exposed MNPs, i.e., from 30 ~ 60 nm < 10 ~ 30 nm < 1 ~ 10 nm diameter. The uptake of MNPs increased with a higher negative zeta potential (especially Zn and Cu), as it can induce repulsion at tissue surfaces and facilitate internal translocation. Yet, plants may not only acquire the intact MNPs but also dissolve the metals prior to internalization and distinguishing among these processes is still challenging. Our analysis indicates efficient MNPs uptake particularly for the plant-essential elements while dissolved

metals dominate uptake for the non-essential elements. We conclude that for plant nanofertilizers, application of smaller MNPs of essential nutrients would be more efficient for crop uptake, but by the same having also the greatest toxicity risk. Nevertheless, the uptake efficiency might be higher if applied with smaller particle size, then the dosage could be reduced and respective risks should decline correspondingly.

5.2 Synthesis and outlook

5.2.1 The fate of P derived from P fertilizers in soil size fractions

Alternative P fertilizers are promising alleviations of exhausting global PR reserves and reliance on PR import for areas like Europe. There are several types of recycled materials, which could be potential mineral P fertilizers substitutes. According to different treatment techniques, these recycled materials could be assigned into three groups (Huygens and Saveyn, 2018): 1) precipitated phosphate salts, such as struvite recycled from municipal wastewater treatment plants via precipitation (recycling P from aqueous phase); 2) pyrolysis and gasification materials, such as bone char produced from pyrolysing animal bone chips, which derived from slaughter house wastes, or biochar produced from crop residues or straws in a similar manner (recycling P from solid phase); 3) thermal oxidation materials and derivates, e.g. poultry litter ash. Among studied mineral P fertilizer substitutes, bone char enriches in P, Ca and C (carbon, 6-38%) (Table 5-1) (Leinweber et al., 2019), while almost free of soil pollutants like U and Cd, and therefore cleaner than mineral PR (Siebers and Leinweber, 2013).

Conventional P fertilizers (such as superphosphates and ammonium phosphates) derived from PR are usually high in solubility, while bone char (3-20% and 92-95% of total P could be extracted in water and formic acid, respectively) is less water-soluble but citric/formic acid soluble (Hertzberger et al., 2020; Leinweber et al., 2019). It was reported that after incubation of 34 days, no more than 3.7% P of added bone char was extracted (by each of the three extractants: $NaHCO_3$, NH_4NO_3, H_2O) (Morshedizad et al., 2016). Besides studying bone char, bone ash has been evaluated on their fertilization effects by researchers as well. Bone ash was reported with low soluble calcium phosphates, and lower P utilization efficiency than compost (Browaldh, 1992). It was suggested that the slow release of P from pyrolyzed

BC materials enables them as controlled release P fertilizers with low risk of P losses. Meanwhile, these materials perform better in acidic soils owe to their alkaline pH values, which differed from conventional P fertilizers as well. With different properties between conventional and alternative P fertilizers, the fate of introduced P with soil profile could be varied between conventional and alternative P fertilizers, especially for between bone char and triple superphosphate, when looking at their big differences in solubility and pH values.

Table 5-1. Properties of example conventional and alternative P fertilizers.

	Materials	Formula / Main component	Solubility/pK_{sp}	pH	P (%)	Ca (%)	N (%)
Conventional P fertilizers	Triple superphosphate	$Ca(H_2PO_4)_2 \cdot H_2O$	> 90% water soluble	1-3	24.6	15	/
	Diammonium phosphate	$(NH_4)_2HPO_4$	> 90% water soluble	7-8	23.5	/	18
Alternative P fertilizers	Bone char	$Ca_5(PO_4)_3OH$	54.45	7-10	11-21	18-39	/

After studying the fate of P from bone char materials (BC and BC^{plus}) via 5-year field fertilizations, I found that in four soil size fractions, there were mostly insignificant differences of labile, moderately labile and stable P pools among TSP (triple superphosphate), BC and BC^{plus}. The dominant mineral constituent of BC materials is biological hydroxyapatite, which is more soluble than geological or synthesized hydroxyapatite but much less than TSP, and could release inorganic phosphate (P_i) slowly compared to that of TSP. Moreover, the mesoporous structure of BC (specific surface area: 42 to 114 $m^2\ g^{-1}$) also contributes to higher solubility (Leinweber et al., 2019). Our results that in few cases total P_i was increased after 5-year TSP, BC and BC^{plus} applications, also confirmed the slightly accrual of soil P_i by the studied fertilizers (Table A-3), which demonstrated the similar effects of BC and BC^{plus} with TSP on soil P pool. Nonetheless, in most cases there were no significant increases of various P fractions during this 5 years crop rotation even under TSP treatment. Hence, we speculated that with longer durations, there could be more apparent effects as indicated by other studies (Table 5-2).

Table 5-2. Fertilization effects on soil P fractions.

Fertilizers	Soil group (WRB)	P dosage (kg ha^{-1} $year^{-1}$)	Field trial duration (year)	Effects on soil P pool	Reference
TSP	Cambisol	45	5	Significant increases of bicarbonate P_i, and total P_i in BU	This study
BC	Cambisol	45	5	Significant increases of bicarbonate P_i in BU, and total P_i in SMiA	This study
BC^{plus}	Cambisol	45	5	Significant increases of H_2SO_4-P_i, and total P_i in LMiA	This study
MAP	Chernozem	4~10	24	Significant increases of resin P_i, microbial P, bicarbonate and NaOH P_i.	Selles et al., 1995
TSP	Gleysol	20	10	Significant increase of resin-P and bicarbonate P_i.	Zheng et al., 2003
TSP	Regosol	20~80	21	Significant increase of bicarbonate P_i.	Wang et al., 2010

TSP = triple superphosphate; BC = bone char; BC^{plus} = sulphur modified bone char; MAP = monoammonium phosphate; P_i = inorganic phosphate; BU = building units; SMiA = small microaggregates; LMiA = large microaggregates.

The P from soluble fertilizer such as TSP would undergo reactions including precipitation or adsorption within soils. It is believed that precipitation of P will be dominant under high P concentration while adsorption prevalent on low P conditions. The soluble fertilizer granules dissolve rapidly even under low soil moisture (for example below field capacity) and release P, which may be precipitated by soil cations (i.e. Fe^{3+}, Al^{2+}, Ca^{2+}, Mg^{2+}) as less soluble precipitates, and deposit near the application sites; however, part of the fertilizer P could diffuse away and the P concentration declines and then at certain stage adsorption (onto hydrous oxides, alumino-silicates, carbonates, or organic matter) overwhelm precipitation (Sample et al., 1980). After either precipitation or adsorption onto soil particles, the fertilizer P shall be most probably and firstly involved into building units (BU) of soil aggregates after application. When it comes to BC materials, which were applied as submicro- to few millimeter particles and mainly in more stable biological hydroxyapatite form, the particles could be mixed with soil aggregates after plowing and undergoes dissolution slowly. There might be no hotspots of P due to slow dissolution of BC materials (no precipitation process), since the released P will be adsorbed or diffused after dissolution. Hence, P from BC materials could contribute more to P pool in larger aggregates, as even slowly released P be adsorbed by BU, this part will become more stable along time and be

integrated into larger aggregates. This speculation was relatively supported by our results that TSP significantly increased the P_i in BU, while BC and BC^{plus} significantly enhanced P_i in SMiA and LMiA, respectively (Table A-3).

5.2.2 Transport of arable soil colloidal P

Arable soils received excess fertilizer P, which reacted with building units as descried above, and then the residual P (or legacy P) could be transported horizontally or vertically along with the movement of soil colloids in soil profiles to adjacent water bodies. As fertilizations occur normally in or above the plowing layer, the topsoil usually contains higher colloidal P content than subsoils (Li et al., 2022). I found in the study arable soil (Cambisol), the Ap horizon also has the highest colloidal P concentrations (2.5 ± 0.6 mg kg^{-1} soil, sum of three size fractions), followed with comparable colloidal P concentrations between Bw and C horizons (1.1 ± 0.4 and 1.2 ± 0.4 mg kg^{-1} soil, respectively). Leaching of colloidal P from soil C horizon to water flow in drainage system was indicated by results of cluster analysis (Figure B-3), especially the nano-sized colloids, while it may become larger in size as its high similarity with the fine-sized colloids in water samples.

Compared with legacy P in larger soil aggregates (micro- or macro-aggregates), the colloidal P would be more prone to move with water flow inside soils, and have higher probability to reach root surfaces. Even the absolute mass of soil colloids is much less than soil micro- or macro-aggregates, the release of P from colloids might be easier than micro- or macro-aggregates when affecting by roots, as the P concentrations in soil colloids (or BU) were 3-4 times higher than that in micro- or macro-aggregates (based on results in chapter 2) and with less organic matter coatings than larger aggregates. Once the soil colloids move into the rhizosphere, they could be dissolved due to root exudates (Lv et al., 2019), and the released P could replenish soil available P pool. I determined the rhizosphere and non-rhizosphere soil colloidal P (< 450 nm) concentrations with samples collected from the Selhausen rhizotron facility, and found that the rhizosphere colloidal P concentrations (6.3 and 23.4 mg kg^{-1} soil for Cambisol and Luvisol, respectively) were higher than that in non-rhizosphere colloids (3.0 and 6.6 mg kg^{-1} soil, respectively; own unpublished data). As the soils were collected two weeks before winter wheat harvesting, the higher rhizosphere

colloidal P concentrations could be due to rhizodeposition or root/microbe debris, which contain organic P and can be involved in the formation of soil colloidal size fractions.

5.2.3 Direct uptake of metallic nanoparticles or absorb of ionic metals in nature

Nanomaterials are not only receiving additional concerns but they also exhibit great potentials in enhancing global agricultural productivity (Marchiol et al., 2020). Crops may be exposed to both engineered and natural nanomaterials in the environment, and metallic nanoparticles (MNPs) may be internalized directly or dissolved before being taken up.

5.2.3.1 Metals take up from MNPs and dissolved metal salts

Based on meta-analysis of 173 research articles on crop uptake of MNPs, I found that crop tissues accumulated higher concentrations of essential elements (Zn, Fe and Cu) than of non-essential one (Ag, Ce and Ti). It is believed that crops generally do not favor the uptake of non-essential elements, including mechanisms such as transporter discrimination between essential and no-essential elements, and limited translocation of non-essential elements to aboveground edible tissues (Khan et al., 2014). My analysis confirmed that this discrimination occurred even if the non-essential elements were (initially) applied as MNPs. Moreover, the translocation factors of non-essential elements (Ag and Ce) were higher when applied as MNP treatments compared with application as dissolved metal salts (Figure 5-1), showing that translocation of non-essential elements to above-ground tissues was facilitated when applied as MNPs, while there were no such translocation preferences for essential elements (Zn, Cu and Fe). Higher translocation factors for Ag applied as Ag NPs than $AgNO_3$ has also been reported but no explanations were offered (Wang et al., 2015).

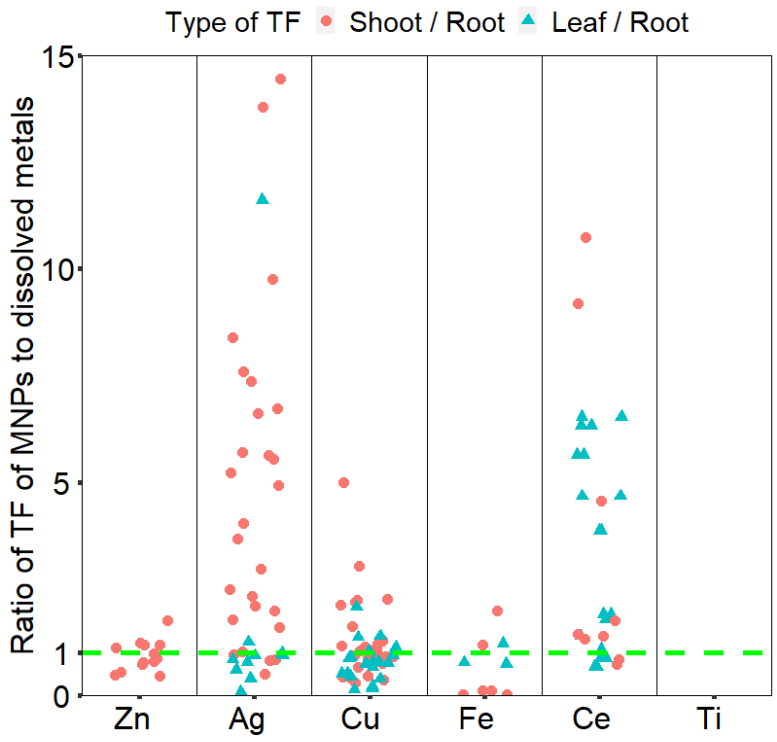

Figure 5-1. Ratios of translocation factors (TF) of MNPs to dissolved metal salts. The translocation factor was calculated as (metal concentration in shoot or leaf / metal concentration in root) for both MNPs and dissolved metal salts treatments. As no dissolved Ti salts, no data shown here for Ti. Metals were ordered according to dissolution rates of MNPs. The green horizontal line (y = 1) means no translocation preference between MNPs and dissolved metal salts.

5.2.3.2 Direct uptake of MNPs

One of the most challenging and critical unsolved issues regarding plant uptake of MNPs is how to distinguish between direct uptake of intact MNPs and uptake of metals after dissolution of MNPs? Theoretically, only MNPs in size (as hydrodynamic diameter to be more scientifically) lower than the SEL (size exclusion limit) of plant physical barriers are allowed to enter into plant tissues. Hence, the particle size could be one of the most important factors on plant direct uptake of MNPs. The meta-analysis results also demonstrated this as I found that the shoot metal concentrations generally increased with declining particle size. However, since most of the studied MNPs are partially or less soluble (enhanced dissolution due to root exudates) except for TiO_2 NPs, which not dissolve, even when the initial particle size is larger than the SEL, the core MNPs might be smaller than the SEL and internalization of MNPS is possible. While the above process was difficult to track, I cannot discount the possibility that nanoparticles detected inside plant tissues could be in situ phyto-synthesized

as well (Khan et al., 2019). Such processes pose uncertainties in evaluation of plant direct uptake of MNPs. Based on the present analysis, the uptake of MNPs would be more efficient via foliar exposure, and direct uptake of MNPs could be more viable in this pathway as it is less affected from interactions with soil solutions or root exudates; due to similar reasons, hydroponic cultures likely promote a direct uptake of MNP compared to the uptake from soil medium.

5.3 Conclusion

My work emphasizes the importance of soil nanocolloids/nanoparticles in P management. It is important to study mineral P fertilizer substitutes (such as bone char) especially in areas that currently depend on high import of mined P, such as Europe. Meanwhile, owe to decades of excess P fertilizations, many arable soils in Europe store high amounts of residual P, and the colloidal (especially nanocolloidal) P could flow into streams and other water bodies, frequently followed with eco-problems. In contrary, colloidal P could support plant growth as well, even it is unclear whether it has been taken up directly or after dissolution; this issue also fits for other elements as crops expose to engineered and natural nanoparticles in the environment.

My thesis firstly evaluated the fate of P from one promising mined P fertilizer alternative—bone char and sulfur modified bone char—within soil aggregates based on a 5-year field experiment. I demonstrated generally no both positive and negative effects of BC materials compared to a conventional mineral P fertilizer (triple superphosphate). Besides, I confirmed the colloidal building units highly enrich P, even if their absolute mass is relatively small. As soil colloids are important in the transport of soil residual P, I further analyzed the colloidal P and also other elements in top- and sub-soil layers, and nearby water flows in order to get knowledge of the transport of colloidal P from subsurface soil to drainage system. The nano-sized colloids in subsoils could contribute to the soil colloidal P loss to nearby waters, especially under strong rainfall events. The nanocolloidal P could be mobile and release P when moves into rhizosphere. I finally reviewed the crop uptake of metallic nanoparticles (MNPs) and especially focused on direct uptake or ionic uptake. Even if many studies didn't distinguish these two ways, there were element-specific uptake preferences

between essential and non-essential elements, and the translocation factors were higher for non-essential metals when exposed as MNPs form.

References

REFERENCES

Acosta-Martinez, V., Tabatabai, M.A., 2000. Enzyme activities in a limed agricultural soil. Biol. Fertil. Soils 31, 85-91.

Adisa, I.O., Pullagurala, V.L.R., Peralta-Videa, J.R., Dimkpa, C.O., Elmer, W.H., Gardea-Torresdey, J.L., White, J.C., 2019. Recent advances in nano-enabled fertilizers and pesticides: a critical review of mechanisms of action. Environ. Sci. Nano 6(7), 2002-2030.

Ahmed, B., Rizvi, A., Ali, K., Lee, J., Zaidi, A., Khan, M.S., Musarrat, J., 2021a. Nanoparticles in the soil–plant system: A review. Environ. Chem. Lett. 19, 1545-1609.

Ahmed, B., Rizvi, A., Syed, A., Jailani, A., Elgorban, A.M., Khan, M.S., Al-Shwaiman, H.A., Lee, J., 2021b. Differential bioaccumulations and ecotoxicological impacts of metal-oxide nanoparticles, bulk materials, and metal-ions in cucumbers grown in sandy clay loam soil. Environ. Pollt. 289, 117854.

Ahmed, B., Rizvi, A., Syed, A., Rajput, V.D., Elgorban, A.M., Al-Rejaie, S.S., Minkina, T., Khan, M.S., Lee, J., 2022. Understanding the phytotoxic impact of Al(3+), nano-size, and bulk Al_2O_3 on growth and physiology of maize (Zea mays L.) in aqueous and soil media. Chemosphere 300, 134555.

Ajiboye, B., Akinremi, O.O., Hu, Y.F., Jürgensen, A., 2008. XANES speciation of phosphorus in organically amended and fertilized vertisol and mollisol. Soil Sci. Soc. Am. J. 72(5), 1256-1262.

Alamgir, M., Marschner, P., 2013. Short-term effects of application of different rates of inorganic P and residue P on soil P pools and wheat growth. J. Soil Sci. Plant Nutr. 176(5), 696-702.

Alboukadel, K., 2021. rstatix: Pipe-friendly framework for basic statistical tests, Online.

Alkurdi, S.S.A., Al-Juboori, R.A., Bundschuh, J., Hamawand, I., 2019. Bone char as a green sorbent for removing health threatening fluoride from drinking water. Environ. Int. 127, 704-719.

Almendros, P., Gonzalez, D., Fernandez, M.D., Garcia-Gomez, C., Obrador, A., 2022. Both Zn biofortification and nutrient distribution pattern in cherry tomato plants are influenced by the application of ZnO nanofertilizer. Heliyon 8(3), e09130.

Andy, F., Jeremy, M., Zoe, F., 2012. Discovering statistics using R. Ashford Colour Press Ltd, Great Britain.

Audette, Y., O'Halloran, I.P., Voroney, R.P., 2016. Kinetics of phosphorus forms applied as inorganic and organic amendments to a calcareous soil. Geoderma 262, 119-124.

Avellan, A., Yun, J., Morais, B.P., Clement, E.T., Rodrigues, S.M., Lowry, G.V., 2021. Critical review: Role of inorganic nanoparticle properties on their foliar uptake and in planta translocation. Environ. Sci. Technol. 55(20), 13417-13431.

Avellan, A., Yun, J., Zhang, Y.L., Spielman-Sun, E., Unrine, J.M., Thieme, J., Li, J.R., Lombi, E., Bland, G., Lowry, G.V., 2019. Nanoparticle size and coating chemistry control foliar uptake pathways, translocation, and leaf-to-rhizosphere transport in wheat. ACS nano 13(5), 5291-5305.

Azeem, M., Ali, A., Arockiam Jeyasundar, P.G.S., Bashir, S., Hussain, Q., Wahid, F., Ali, E.F., Abdelrahman, H., Li, R., Antoniadis, V., Rinklebe, J., Shaheen, S.M., Li, G., Zhang, Z., 2021a. Effects of sheep bone biochar on soil quality, maize growth, and fractionation and phytoavailability of Cd and Zn in a mining-contaminated soil. Chemosphere 282, 131016.

Azeem, M., Ali, A., Arockiam Jeyasundar, P.G.S., Li, Y., Abdelrahman, H., Latif, A., Li, R., Basta, N., Li, G., Shaheen, S.M., Rinklebe, J., Zhang, Z., 2021b. Bone-derived biochar improved soil quality and reduced Cd and Zn phytoavailability in a multi-metal contaminated mining soil. Environ. Pollut. 277, 116800.

Azimzada, A., Tufenkji, N., Wilkinson, K.J., 2017. Transformations of silver nanoparticles in wastewater effluents: Links to Ag bioavailability. Environ. Sci. Nano 4(6), 1339-1349.

Baalousha, M., Stolpe, B., Lead, J.R., 2011. Flow field-flow fractionation for the analysis and characterization of natural colloids and manufactured nanoparticles in environmental systems: A critical review. J. Chromatogr. A. 1218(27), 4078-4103.

Baggie, I., Rowell, D.L., Warren, G.P., Robinson, J.S., 2004. Utilisation by upland rice of plant residue- and fertiliser-phosphorus in two tropical acid soils. Nutr. Cycl. Agroecosys. 69(1), 73-84.

REFERENCES

Balduzzi, S., Rücker, G., Schwarzer, G., 2019. How to perform a meta-analysis with R: A practical tutorial. Evid. Based Ment. Health 22, 153-160.

Barrios, A.C., Rico, C.M., Trujillo-Reyes, J., Medina-Velo, I.A., Peralta-Videa, J.R., Gardea-Torresdey, J.L., 2016. Effects of uncoated and citric acid coated cerium oxide nanoparticles, bulk cerium oxide, cerium acetate, and citric acid on tomato plants. Sci. Total Environ. 563-564, 956-964.

Bol, R., Julich, D., Brödlin, D., Siemens, J., Kaiser, K., Dippold, M.A., Spielvogel, S., Zilla, T., Mewes, D., von Blanckenburg, F., Puhlmann, H., Holzmann, S., Weiler, M., Amelung, W., Lang, F., Kuzyakov, Y., Feger, K.H., Gottselig, N., Klumpp, E., Missong, A., Winkelmann, C., Uhlig, D., Sohrt, J., von Wilpert, K., Wu, B., Hagedorn, F., 2016. Dissolved and colloidal phosphorus fluxes in forest ecosystems—an almost blind spot in ecosystem research. J. Plant. Nutr. Soil Sci. 179(4), 425-438.

Borgatta, J., Ma, C.X., Hudson-Smith, N., Elmer, W., Plaza Pérez, C.D., Torre-Roche, D.L.R., Zuverza-Mena, N., Haynes, C.L., White, J.C., Hamers, R.J., 2018. Copper based nanomaterials suppress root fungal disease in watermelon (Citrullus lanatus): Role of particle morphology, composition and dissolution behavior. ACS Sustain. Chem. Eng. 6(11), 14847-14856.

Bronick, C.J., Lal, R., 2005. Soil structure and management: A review. Geoderma 124(1-2), 3-22.

Browaldh, M., 1992. Influence of organic and inorganic fertilizers on common bean (Phaseolus vulgarisL.) grown in a P-fixing Mollic Andosol. Biol. Agric. Hortic. 9(1), 87-104.

Brownlie, W.J., Sutton, M.A., Reay, D.S., Heal, K.V., Hermann, L., Kabbe, C., Spears, B.M., 2021. Global actions for a sustainable phosphorus future. Nat. Food 2(2), 71-74.

Burger, D.J., Vogel, J., Kooijman, A.M., Bol, R., de Rijke, E., Schoorl, J., LΓjcke, A., Gottselig, N., 2021. Colloidal catchment response to snowmelt and precipitation events differs in a forested headwater catchment. Vadose Zone J. 20(3), e20126.

Cai, L., Cai, L., Jia, H., Liu, C., Wang, D., Sun, X., 2020. Foliar exposure of Fe3O4 nanoparticles on Nicotiana benthamiana: Evidence for nanoparticles uptake, plant growth promoter and defense response elicitor against plant virus. J. Hazard. Mater. 393, 122415.

Carpenter, S.R., Bennett, E.M., 2011. Reconsideration of the planetary boundary for phosphorus. Environ. Res. Lett. 6(1), 014009.

Carpita, N., Sabularse, D., Montezinos, D., Delmer, D.P., 1979. Determination of the pore size of cell walls of living plant cells. Science 205(4411), 1144-1147.

Cervantes-Aviles, P., Huang, X., Keller, A.A., 2021. Dissolution and aggregation of metal oxide nanoparticles in root exudates and soil leachate: Implications for nanoagrochemical application. Environ. Sci. Technol. 55(20), 13443-13451.

Chen, A., Arai, Y., 2020. Current uncertainties in assessing the colloidal phosphorus loss from soil. Adv. Agron., pp. 117-151.

Cheung, C.W., Chan, C.K., Porter, J.F., Mckay, G., 2001. Combined diffusion model for the sorption of cadmium, copper, and zinc ions onto bone char. Environ. Sci. Technol. 35, 1511-1522.

Cocozza, C., Perone, A., Giordano, C., Salvatici, M.C., Pignattelli, S., Raio, A., Schaub, M., Sever, K., Innes, J.L., Tognetti, R., Cherubini, P., 2019. Silver nanoparticles enter the tree stem faster through leaves than through roots. Tree Physiol. 39(7), 1251-1261.

Colvin, V.L., 2003. The potential environmental impact of engineered nanomaterials. Nat. Biotechnol. 21(10), 1166-1170.

Cordell, D., Drangert, J.-O., White, S., 2009. The story of phosphorus: Global food security and food for thought. Glob. Environ. Change 19(2), 292-305.

Cross, A.F., Schlesinger, W.H., 1995. A literature review and evaluation of the Hedley fractionation: Applications to the biogeochemical cycle of soil phosphorus in natural ecosystems. Geoderma 64, 197-214.

Dalwadi, G., Sunderland, V.B., 2007. Purification of PEGylated nanoparticles using tangential flow filtration (TFF). Drug Dev. Ind. Pharm. 33(9), 1030-1039.

de Jonge, L.W., Moldrup, P., Rubaek, G.H., Schelde, K., Djurhuus, J., 2004. Particle leaching and particle-facilitated transport of phosphorus at field scale. Vadose Zone J. 3, 462-470.

REFERENCES

del Real, A.E.P., Castillo-Michel, H., Kaegi, R., Sinnet, B., Magnin, V., Findling, N., Villanova, J., Carriere, M., Santaella, C., Fernandez-Martinez, A., Levard, C., Sarret, G., 2016. Fate of Ag-NPs in sewage sludge after application on agricultural soils. Environ. Sci Technol. 50(4), 1759-1768.

del Real, A.E.P., Vidal, V., Carriere, M., Castillo-Michel, H., Levard, C., Chaurand, P., Sarret, G., 2017. Silver nanoparticles and wheat roots: A complex interplay. Environ. Sci. Technol. 51(10), 5774-5782.

Dela Piccolla, C., Hesterberg, D., Muraoka, T., Novotny, E.H., 2021. Optimizing pyrolysis conditions for recycling pig bones into phosphate fertilizer. Waste Manage. 131, 249-257.

Desmidt, E., Ghyselbrecht, K., Zhang, Y., Pinoy, L., Van der Bruggen, B., Verstraete, W., Rabaey, K., Meesschaert, B., 2015. Global phosphorus scarcity and full-scale P-recovery techniques: A review. Crit. Rev. Environ. Sci. Technol. 45(4), 336-384.

Dietz, K.J., Herth, S., 2011. Plant nanotoxicology. Trends Plant Sci. 16(11), 582-589.

Dimkpa, C.O., Hansen, T., Stewart, J., McLean, J.E., Britt, D.W., Anderson, A.J., 2015. ZnO nanoparticles and root colonization by a beneficial pseudomonad influence essential metal responses in bean (Phaseolus vulgaris). Nanotoxicology 9(3), 271-278.

Dimkpa, C.O., McLean, J.E., Martineau, N., Britt, D.W., Haverkamp, R., Anderson, A.J., 2013. Silver nanoparticles disrupt wheat (Triticum aestivum L.) growth in a sand matrix. Environ. Sci. Technol. 47(2), 1082-1090.

Dodds, W.K., Guinnip, J.P., Schechner, A.E., Pfaff, P.J., Smith, E.B., 2021. Fate and toxicity of engineered nanomaterials in the environment: A meta-analysis. Sci. Total Environ. 796, 148843.

Dwivedi, A.D., Yoon, H., Singh, J.P., Chae, K.H., Rho, S.C., Hwang, D.S., Chang, Y.S., 2018. Uptake, distribution, and transformation of zerovalent iron nanoparticles in the edible plant Cucumis sativus. Environ. Sci. Technol. 52(17), 10057-10066.

Egger, M., Smith, G.D., Schneider, M., Minder, C., 1997. Bias in meta-analysis detected by a simple, graphical test. BMJ-Brit. Med. J. 315(7109), 629-634.

Eichert, T., Kurtz, A., Steiner, U., Goldbach, H.E., 2008. Size exclusion limits and lateral heterogeneity of the stomatal foliar uptake pathway for aqueous solutes and water-suspended nanoparticles. Physiol. Plant. 134(1), 151-160.

Elhaj Baddar, Z., Unrine, J.M., 2021. Effects of soil pH and coatings on the efficacy of polymer coated ZnO nanoparticulate fertilizers in wheat (Triticum aestivum). Environ. Sci. Technol. 55(20), 13532-13540.

Ellerbrock, R.H., Gerke, H.H., 2021. FTIR spectral band shifts explained by OM-cation interactions. J. Plant. Nutr. Soil Sci. 184(3), 388-397.

Elliott, E.T., Palm, C.A., Reuss, D.E., Monz, C.A., 1991. Organic matter contained in soil aggregates from a tropical chronosequence correction for sand and light fraction. Agric. Ecosyst. Environ. 34(1-4), 443-451.

Fan, X.H., Schnug, E., Haneklaus, S., Li, Y.C., 2012. In situ digestion of rock phosphates to mobilize plant-available phosphate for organic farming. Commun. Soil Sci. Plant Anal. 43(17), 2191-2201.

Fernández-Ugalde, O., Barré, P., Hubert, F., Virto, I., Girardin, C., Ferrage, E., Caner, L., Chenu, C., 2013. Clay mineralogy differs qualitatively in aggregate-size classes: Clay-mineral-based evidence for aggregate hierarchy in temperate soils. Eur. J. Soil Sci. 64(4), 410-422.

Field, A., Miles, J., Field, Z., 2012. Discovering statistics using R. SAGE Publications Ltd.

Fresne, M., Jordan, P., Daly, K., Fenton, O., Mellander, P.E., 2022. The role of colloids and other fractions in the below-ground delivery of phosphorus from agricultural hillslopes to streams. Catena 208.

Gao, F., Liu, C., Qu, C., Zheng, L., Yang, F., Su, M., Hong, F., 2008. Was improvement of spinach growth by nano-TiO_2 treatment related to the changes of Rubisco activase? Biometals 21(2), 211-217.

REFERENCES

Gao, X.Y., Kundu, A., Bueno, V., Rahim, A.A., Ghoshal, S., 2021. Uptake and translocation of mesoporous SiO_2-coated ZnO nanoparticles to Solanum lycopersicum following foliar application. Environ. Sci. Technol. 55(20), 13551-13560.

Gardea-Torresdey, J.L., Tiemann, K.J., Gamez, G., Dokken, K., Cano-Aguilera, I., Furenlid, L.R., Renner, M.W., 2000. Reduction and accumulation of gold(III) by Medicago sativa alfalfa biomass: X-ray absorption spectroscopy, pH, and temperature dependence. Environ. Sci. Technol. 34(20), 4392-4396.

Garland, G., Bünemann, E.K., Oberson, A., Frossard, E., Snapp, S., Chikowo, R., Six, J., 2018. Phosphorus cycling within soil aggregate fractions of a highly weathered tropical soil: A conceptual model. Soil Biol. Biochem. 116, 91-98.

Geisler-Lee, J., Wang, Q., Yao, Y., Zhang, W., Geisler, M., Li, K.G., Huang, Y., Chen, Y.S., Kolmakov, A., Ma, X.M., 2013. Phytotoxicity, accumulation and transport of silver nanoparticles by Arabidopsis thaliana. Nanotoxicology 7(3), 323-337.

Ghormade, V., Deshpande, M.V., Paknikar, K.M., 2011. Perspectives for nano-biotechnology enabled protection and nutrition of plants. Biotechnol. Adv. 29(6), 792-803.

Gilbertson, L.M., Pourzahedi, L., Laughton, S., Gao, X., Zimmerman, J.B., Theis, T.L., Westerhoff, P., Lowry, G.V., 2020. Guiding the design space for nanotechnology to advance sustainable crop production. Nat. Nanotechnol. 15(9), 801-810.

Glaesner, N., Hansen, H.C.B., Hu, Y.F., Bekiaris, G., Bruun, S., 2019. Low crystalline apatite in bone char produced at low temperature ameliorates phosphorus-deficient soils. Chemosphere 223, 723-730.

Gottselig, N., Amelung, W., Kirchner, J.W., Bol, R., Eugster, W., Granger, S.J., Hernandez-Crespo, C., Herrmann, F., Keizer, J.J., Korkiakoski, M., Laudon, H., Lehner, I., Lofgren, S., Lohila, A., Macleod, C.J.A., Molder, M., Muller, C., Nasta, P., Nischwitz, V., Paul-Limoges, E., Pierret, M.C., Pilegaard, K., Romano, N., Sebastia, M.T., Stahli, M., Voltz, M., Vereecken, H., Siemens, J., Klumpp, E., 2017a. Elemental composition of natural nanoparticles and fine colloids in European forest stream waters and their role as phosphorus carriers. Glob. Biogeochem. Cycles 31(10), 1592-1607.

Gottselig, N., Bol, R., Nischwitz, V., Vereecken, H., Amelung, W., Klumpp, E., 2014. Distribution of phosphorus-containing fine colloids and nanoparticles in stream water of a forest catchment. Vadose Zone J. 13(7), 1-11.

Gottselig, N., Nischwitz, V., Meyn, T., Amelung, W., Bol, R., Halle, C., Vereecken, H., Siemens, J., Klumpp, E., 2017b. Phosphorus binding to nanoparticles and colloids in forest stream waters. Vadose Zone J. 16(3), 1-12.

Grafe, M., Kurth, J.K., Panten, K., Raj, A.D., Baum, C., Zimmer, D., Leinweber, P., Schloter, M., Schulz, S., 2021. Effects of different innovative bone char based P fertilizers on microbiota catalyzing P turnover in agricultural soils. Agr. Ecosyst. Environ. 314, 107419.

Gu, S., 2017. Release of dissolved and colloidal phosphorus from riparian wetlands: A field and laboratory assessment of the mechanisms and controlling factors, University Rennes 1.

Gu, S., Gruau, G., Dupas, R., Jeanneau, L., 2020. Evidence of colloids as important phosphorus carriers in natural soil and stream waters in an agricultural catchment. J. Environ. Qual. 49(4), 921-932.

Guasch, H., Bonet, B., Bonnineau, C., Barral, L., 2017. Engineered nanoparticles in the environments: Interactions with microbial systems and microbial activity, Microbial Ecotoxicology, pp. 251-281.

Guo, H.Y., Ma, C.X., Thistle, L., Huynh, M., Yu, C.H., Clasby, D., Chefetz, B., Polubesova, T., White, J.C., He, L.L., Xing, B.S., 2019. Transformation of Ag ions into Ag nanoparticle-loaded AgCl microcubes in the plant root zone. Environ. Sci. Nano 6(4), 1099-1110.

Hamer, M., Graham, R.C., Amrheim, C., Bozhilov, K.N., 2003. Dissolution of ripidolite (Mg, Fe-chlorite) in organic and inorganic acid solutions. Soil Sci. Soc. Am. J. 67(2), 654-661.

Hassellov, M., von der Kammer, F., 2008. Iron oxides as geochemical nanovectors for metal transport in soil-river systems. Elements 4(6), 401-406.

REFERENCES

Haynes, R.J., Naidu, R., 1998. Influence of lime, fertilizer and manure applications on soil organic matter content and soil physical conditions: A review. Nutr. Cycl. Agroecosyst. 51(2), 123-137.

He, J.Z., Zhang, L., He, S.Y., Ryser, E.T., Li, H., Zhang, W., 2022. Stomata facilitate foliar sorption of silver nanoparticles by Arabidopsis thaliana. Environ. Pollt. 292, 118448.

Heathwaite, L., Haygarth, P., Matthews, R., Preedy, N., Butler, P., 2005. Evaluating colloidal phosphorus delivery to surface waters from diffuse agricultural sources. J. Environ. Qual. 34, 287-298.

Hedberg, J., Blomberg, E., Odnevall Wallinder, I., 2019. In the search for nanospecific effects of dissolution of metallic nanoparticles at freshwater-like conditions: A critical review. Environ. Sci. Technol. 53(8), 4030-4044.

Hedley, M.J., Stewart, J.W.B., Chauhan, B.S., 1982. Changes in inorganic and organic soil phosphorus fractions induced by cultivation practices and by laboratory incubations. Soil Sci. Soc. Am. J. 46(5), 970-976.

HELCOM, 2021. Inputs of nutrients (nitrogen and phosphorus) to the subbasins (2019), Online.

Henderson, R., Kabengi, N., Mantripragada, N., Cabrera, M., Hassan, S., Thompson, A., 2012. Anoxia-induced release of colloid- and nanoparticle-bound phosphorus in grassland soils. Environ. Sci. Technol. 46(21), 11727-11734.

Hens, M., Merckx, R., 2001. Functional characterization of colloidal phosphorus species in the soil solution of sandy soils. Environ. Sci. Technol. 35, 493-500.

Hens, M., Merckx, R., 2002. The role of colloidal particles in the speciation and analysis of "dissolved" phosphorus. Water Res. 36(6), 1483-1492.

Hertzberger, A.J., Cusick, R.D., Margenot, A.J., 2020. A review and meta-analysis of the agricultural potential of struvite as a phosphorus fertilizer. Soil Sci. Soc. Am. J. 84(3), 653-671.

Higgins, J.P.T., Thompson, S.G., 2002. Quantifying heterogeneity in a meta-analysis. Stat. Med. 21(11), 1539-1558.

Higgins, J.P.T., Thompson, S.G., Deeks, J.J., Altman, D.G., 2003. Measuring inconsistency in meta-analyses. BMJ-Brit. Med. J. 327(7414), 557-560.

Hochella, M.F., Mogk, D.W., Ranville, J., Allen, I.C., Luther, G.W., Marr, L.C., McGrail, B.P., Murayama, M., Qafoku, N.P., Rosso, K.M., Sahai, N., Schroeder, P.A., Vikesland, P., Westerhoff, P., Yang, Y., 2019. Natural, incidental, and engineered nanomaterials and their impacts on the Earth system. Science 363(6434), eaau8299.

Hochella, M.F., Spencer, M.G., Jones, K.L., 2015. Nanotechnology: Nature's gift or scientists' brainchild? Environ. Sci. Nano 2(2), 114-119.

Holford, I.C.R., 1997. Soil phosphorus: Its measurement, and its uptake by plants. Aust. J. Soil Res. 35(2), 227-240.

Hou, E.Q., Tan, X., Heenan, M., Wen, D.Z., 2018. A global dataset of plant available and unavailable phosphorus in natural soils derived by Hedley method. Sci. Data 5, 180166.

Hu, P.G., An, J., Faulkner, M.M., Wu, H.H., Li, Z.H., Tian, X.L., Giraldo, J.P., 2020. Nanoparticle charge and size control foliar delivery efficiency to plant cells and organelles. ACS Nano 14(7), 7970-7986.

Huang, D.Y., Dang, F., Huang, Y.N., Chen, N., Zhou, D.M., 2021. Uptake, translocation, and transformation of silver nanoparticles in plants. Environ. Sci. Nano 9(1), 12-39.

Huang, G., Zuverza-Mena, N., White, J.C., Hu, H., Xing, B., Dhankher, O.P., 2022. Simultaneous exposure of wheat (Triticum aestivum L.) to CuO and S nanoparticles alleviates toxicity by reducing Cu accumulation and modulating antioxidant response. Sci. Total Environ. 839, 156285.

Huang, X., Keller, A.A., 2021. Metabolomic response of early-stage wheat (Triticum aestivum) to surfactant-aided foliar application of copper hydroxide and molybdenum trioxide nanoparticles. Nanomaterials 11(11).

REFERENCES

Huang, Y., Zhao, L., Keller, A.A., 2017. Interactions, transformations, and bioavailability of nano-copper exposed to root exudates. Environ. Sci. Technol. 51(17), 9774-9783.

Huygens, D., Saveyn, H.G.M., 2018. Agronomic efficiency of selected phosphorus fertilisers derived from secondary raw materials for European agriculture. A meta-analysis. Agron. Sustain. Dev. 38(5).

IUSS Working Group WRB, 2015. World Reference Base for Soil Resources 2014, FAO, Rome, Italy.

Jastrow, J.D., 1996. Soil aggregate formation and the accrual of particulate and mineral associated organic matter. Soil Biol. Biochem. 28(4-5), 665-676.

Jia, P.Q., Tan, H.W., Liu, K.R., Gao, W., 2018. Removal of methylene blue from aqueous solution by bone char. Appl. Sci. 8(10), 1903.

Jia, Y.S., Klumpp, E., Bol, R., Amelung, W., 2022. Uptake of metallic nanoparticles containing essential (Cu, Zn and Fe) and non-essential (Ag, Ce and Ti) elements by crops: A meta-analysis. Crit. Rev. Environ. Sci. Technol., 1-22.

Jiang, X., Livi, K.J.T., Arenberg, M.R., Chen, A., Chen, K.Y., Gentry, L., Li, Z., Xu, S., Arai, Y., 2021. High flow event induced the subsurface transport of particulate phosphorus and its speciation in agricultural tile drainage system. Chemosphere 263, 128147.

Jiang, X.Q., Bol, R., Nischwitz, V., Siebers, N., Willbold, S., Vereecken, H., Amelung, W., Klumpp, E., 2015. Phosphorus containing water dispersible nanoparticles in arable soil. J. Environ. Qual. 44(6), 1772-1781.

Judy, J.D., 2013. Bioavailability of manufactured nanomaterials in terrestrial ecosystems. PhD Thesis, University of Kentucky, 1-140 pp.

Jupp, A.R., Beijer, S., Narain, G.C., Schipper, W., Slootweg, J.C., 2021. Phosphorus recovery and recycling-closing the loop. Chem. Soc. Rev. 50(1), 87-101.

Kah, M., Kookana, R.S., Gogos, A., Bucheli, T.D., 2018. A critical evaluation of nanopesticides and nanofertilizers against their conventional analogues. Nat. Nanotechnol. 13(8), 677-684.

Kahle, M., Kleber, M., Jahn, R., 2002. Carbon storage in loess derived surface soils from central Germany influence of mineral phase variables. J. Plant Nutr. Soil Sci. 165(2), 141-149.

Keller, A.A., Huang, Y.X., Nelson, J., 2018. Detection of nanoparticles in edible plant tissues exposed to nano-copper using single-particle ICP-MS. J. Nanopart. Res. 20(4), 101.

Kennedy, M.J., Pevear, D.R., Hill, R.J., 2002. Mineral surface control of organic carbon in black shale. Science 295(5555), 657-660.

Khan, M.A., Castro-Guerrero, N., Mendoza-Cozatl, D.G., 2014. Moving toward a precise nutrition: preferential loading of seeds with essential nutrients over non-essential toxic elements. Front. Plant Sci. 5, 51.

Khan, M.R., Adam, V., Rizvi, T.F., Zhang, B.H., Ahamad, F., Josko, I., Zhu, Y., Yang, M.Y., Mao, C.B., 2019. Nanoparticle-plant interactions: Two-way traffic. Small 15(37), e1901794.

Khodakovskaya, M., Dervishi, E., Mahmood, M., Xu, Y., Li, Z.R., Watanabe, F., Biris, A.S., 2009. Carbon nanotubes are able to penetrate plant seed coat and dramatically affect seed germination and plant growth. ACS Nano 3(10), 3221-3227.

Kittler, S., Greulich, C., Diendorf, J., Ko¨ller, M., Epple, M., 2010. Toxicity of silver nanoparticles increases during storage because of slow dissolution under release of silver Ions. Chem. Mater. 22(16), 4548-4554.

Kjaergaard, C., Moldrup, P., de Jonge, L.W., Jacobsen, O.H., 2004. Colloid mobilization and transport in undisturbed soil columns. II. the role of colloid dispersibility and preferential flow. Vadose Zone J. 3(2), 424-433.

Koch, M., Kruse, J., Eichler-Löbermann, B., Zimmer, D., Willbold, S., Leinweber, P., Siebers, N., 2018. Phosphorus stocks and speciation in soil profiles of a long term fertilizer experiment evidence from sequential fractionation P K edge XANES and 31P NMR spectroscopy. Geoderma 316, 115-126.

Koch, S., Kahle, P., Lennartz, B., 2016. Visualization of colloid transport pathways in mineral soils using titanium(IV) oxide as a tracer. J. Environ. Qual. 45(6), 2053-2059.

REFERENCES

Krause, L., Klumpp, E., Nofz, I., Missong, A., Amelung, W., Siebers, N., 2020. Colloidal iron and organic carbon control soil aggregate formation and stability in arable Luvisols. Geoderma 374.

Krause, L., Rodionov, A., Schweizer, S.A., Siebers, N., Lehndorff, E., Klumpp, E., Amelung, W., 2018. Microaggregates stability and storage of organic carbon is affected by clay content in arable Luvisols. Soil Tillage Res. 182, 123-129.

Kruse, J., Panten, K., Siebers, N., 2022. The fate of phosphorus from bone char-based fertilizers in soil pools in a 5-year crop rotation. Nutr. Cycl. Agroecosystems 124(2), 263-277.

Kulikova, N.A., Polyakov, A.Y., Lebedev, V.A., Abroskin, D.P., Volkov, D.S., Pankratov, D.A., Klein, O.I., Senik, S.V., Sorkina, T.A., Garshev, A.V., Veligzhanin, A.A., Garcia Mina, J.M., Perminova, I.V., 2017. Key roles of size and crystallinity of nanosized iron hydr(oxides) stabilized by humic substances in iron bioavailability to plants. J. Agric. Food Chem. 65(51), 11157-11169.

Landa, P., 2021. Positive effects of metallic nanoparticles on plants: Overview of involved mechanisms. Plant Physiol. Biochem. 161, 12-24.

Larue, C., Laurette, J., Herlin-Boime, N., Khodja, H., Fayard, B., Flank, A.M., Brisset, F., Carriere, M., 2012. Accumulation, translocation and impact of TiO2 nanoparticles in wheat (Triticum aestivum spp.): Influence of diameter and crystal phase. Sci. Total Environ. 431, 197-208.

Layet, C., Santaella, C., Auffan, M., Chevassus-Rosset, C., Montes, M., Levard, C., Ortet, P., Barakat, M., Doelsch, E., 2019. Phytoavailability of silver at predicted environmental concentrations: Does the initial ionic or nanoparticulate form matter? Environ. Sci. Nano 6(1), 127-135.

Leinweber, P., Hagemann, P., Kebelmann, L., Kebelmann, K., Morshedizad, M., 2019. Bone char as a novel phosphorus fertilizer, Phosphorus recovery and recycling. Springer, Singapore, pp. 419-432.

Li, F., Zhang, Q., Klumpp, E., Bol, R., Nischwitz, V., Ge, Z., Liang, X., 2021a. Organic carbon linkage with soil colloidal phosphorus at regional and field scales: Insights from size fractionation of fine particles. Environ. Sci. Technol. 55(9), 5815-5825.

Li, M.S., Zhang, P., Adeel, M., Guo, Z.L., Chetwynd, A.J., Ma, C.X., Bai, T.H., Hao, Y., Rui, Y.K., 2021b. Physiological impacts of zero valent iron, Fe_3O_4 and Fe_2O_3 nanoparticles in rice plants and their potential as Fe fertilizers. Environ. Pollut. 269, 116134.

Li, P.Y., Wang, A.D., Du, W.C., Mao, L., Wei, Z.B., Wang, S.F., Yuan, H.Y., Ji, R., Zhao, L.J., 2020. Insight into the interaction between Fe-based nanomaterials and maize (Zea mays) plants at metabolic level. Sci. Total Environ. 738, 139795.

Li, Y., Livi, K.J.T., Arenberg, M.R., Xu, S., Arai, Y., 2022. Depth sequence distribution of water extractable colloidal phosphorus and its phosphorus speciation in intensively managed agricultural soils. Chemosphere 286(1), 131665.

Lin, D.H., Xing, B.S., 2008. Root uptake and phytotoxicity of ZnO nanoparticles. Environ. Sci. Technol. 42(15), 5580-5585.

Little, N.G., Mohler, C.L., Ketterings, Q.M., DiTommaso, A., 2017. Effects of organic nutrient amendments on weed and crop growth. Weed Sci. 63(3), 710-722.

Liu, J., Sui, P., Cade, B., Hu, Y.F., Yang, J.J., Huang, S.M., Ma, Y.B., 2019a. Molecular-level understanding of phosphorus transformation with long-term phosphorus addition and depletion in an alkaline soil. Geoderma 353, 116-124.

Liu, M.Y., Feng, S., Ma, Y.H., Xie, C.J., He, X., Ding, Y.Y., Zhang, J.Z., Luo, W.H., Zheng, L.R., Chen, D.L., Yang, F., Chai, Z.F., Zhao, Y.L., Zhang, Z.Y., 2019b. Influence of surface charge on the phytotoxicity, transformation, and translocation of CeO_2 nanoparticles in cucumber plants. ACS Appl. Mater. Interfaces 11(18), 16905-16913.

Liu, W.T., Zeb, A.R., Lian, J.P., Wu, J.N., Xiong, H.X., Tang, J.C., Zheng, S.N., 2020. Interactions of metal-based nanoparticles (MBNPs) and metal-oxide nanoparticles (MONPs) with crop plants: A critical review of research progress and prospects. Environ. Rev. 28(3), 294-310.

REFERENCES

Liu, Y.L., Xiao, Z.G., Chen, F.R., Yue, L., Zou, H., Lyu, J.Z., Wang, Z.Y., 2021. Metallic oxide nanomaterials act as antioxidant nanozymes in higher plants: Trends, meta-analysis, and prospect. Sci. Total Environ. 780, 146578.

Lowry, G.V., Avellan, A., Gilbertson, L.M., 2019. Opportunities and challenges for nanotechnology in the agri-tech revolution. Nat. Nanotechnol. 14(6), 517-522.

Luo, X.S., Yu, S., Li, X.D., 2011. Distribution, availability, and sources of trace metals in different particle size fractions of urban soils in Hong Kong: Implications for assessing the risk to human health. Environ. Pollut. 159(5), 1317-1326.

Lv, J.T., Christie, P., Zhang, S.Z., 2019. Uptake, translocation, and transformation of metal-based nanoparticles in plants: Recent advances and methodological challenges. Environ. Sci. Nano 6(1), 41-59.

Ma, R., Levard, C., Marinakos, S.M., Cheng, Y., Liu, J., Michel, F.M., Brown, G.E., Lowry, G.V., 2012. Size-controlled dissolution of organic-coated silver nanoparticles. Environ. Sci. Technol. 46(2), 752-759.

Ma, X.M., Geiser-Lee, J., Deng, Y., Kolmakov, A., 2010. Interactions between engineered nanoparticles (ENPs) and plants: Phytotoxicity, uptake and accumulation. Sci. Total Environ. 408(16), 3053-3061.

Ma, Y.H., He, X., Zhang, P., Zhang, Z.Y., Ding, Y.Y., Zhang, J.Z., Wang, G.H., Xie, C.J., Luo, W.H., Zhang, J., Zheng, L.R., Chai, Z.F., Yang, K., 2017. Xylem and phloem based transport of CeO_2 nanoparticles in hydroponic cucumber plants. Environ. Sci. Technol. 51(9), 5215-5221.

Ma, Y.H., Xie, C.J., He, X., Zhang, B.X., Yang, J., Sun, M.H., Luo, W.H., Feng, S., Zhang, J.Z., Wang, G.H., Zhang, Z.Y., 2020. Effects of ceria nanoparticles and $CeCl_3$ on plant growth, biological and physiological parameters, and nutritional value of soil grown common bean (Phaseolus vulgaris). Small 16(21), e1907435.

Ma, Y.H., Zhang, P., Zhang, Z.Y., He, X., Zhang, J.Z., Ding, Y.Y., Zhang, J., Zheng, L.R., Guo, Z., Zhang, L.J., Chai, Z.F., Zhao, Y.L., 2015. Where does the transformation of precipitated ceria nanoparticles in hydroponic plants take place? Environ. Sci. Technol. 49(17), 10667-10674.

Marchiol, L., Filippi, A., Adamiano, A., Degli Esposti, L., Iafisco, M., Mattiello, A., Petrussa, E., Braidot, E., 2019. Influence of hydroxyapatite nanoparticles on germination and plant metabolism of tomato (Solanum lycopersicum L.): Preliminary evidence. Agronomy 9(4), 161.

Marchiol, L., Iafisco, M., Fellet, G., Adamiano, A., 2020. Nanotechnology support the next agricultural revolution: Perspectives to enhancement of nutrient use efficiency. Adv. Agron. 161, 27-116.

McGechan, M.B., Lewis, D.R., 2002. Transport of particulate and colloid-sorbed contaminants through soil, part 1: General principles. Biosyst. Eng. 83(3), 255-273.

McGill, W.B., Cole, C.V., 1981. Comparative aspects of cycling of organic C, N, S and P through soil organic matter. Geoderma 26(4), 267-286.

Mendes, K.F., de Sousa, R.N., Takeshita, V., Alonso, F.G., Régo, A.P.J., Tornisielo, V.L., 2019. Cow bone char as a sorbent to increase sorption and decrease mobility of hexazinone, metribuzin, and quinclorac in soil. Geoderma 343, 40-49.

Menezes-Blackburn, D., Giles, C., Darch, T., George, T.S., Blackwell, M., Stutter, M., Shand, C., Lumsdon, D., Cooper, P., Wendler, R., Brown, L., Almeida, D.S., Wearing, C., Zhang, H., Haygarth, P.M., 2018. Opportunities for mobilizing recalcitrant phosphorus from agricultural soils: A review. Plant Soil 427(1-2), 5-16.

Miralles, P., Church, T.L., Harris, A.T., 2012. Toxicity, uptake, and translocation of engineered nanomaterials in vascular plants. Environ. Sci. Technol. 46(17), 9224-9239.

Moher, D., Liberati, A., Tetzlaff, J., Altman, D.G., Group, P., 2009. Preferred reporting items for systematic reviews and meta-analyses: The PRISMA statement. PLoS Med. 6(7), e1000097.

Montalvo, D., Degryse, F., McLaughlin, M.J., 2015. Natural colloidal P and its contribution to plant P uptake. Environ. Sci. Technol. 49(6), 3427-3434.

Morshedizad, M., Leinweber, P., 2017. Leaching of phosphorus and cadmium in soils amended with different bone chars. Clean (Weinh) 45(8), 1-7.

REFERENCES

Morshedizad, M., Panten, K., Klysubun, W., Leinweber, P., 2018. Bone char effects on soil: Sequential fractionations and XANES spectroscopy. Soil 4(1), 23-35.

Morshedizad, M., Zimmer, D., Leinweber, P., 2016. Effect of bone chars on phosphorus-cadmiuminteractions evaluated by three extraction procedures. J. Plant. Nutr. Soil Sci. 179, 388-398.

Nagul, E.A., McKelvie, I.D., Worsfold, P., Kolev, S.D., 2015. The molybdenum blue reaction for the determination of orthophosphate revisited: Opening the black box. Anal. Chim. Acta. 890, 60-82.

Nair, R., Varghese, S.H., Nair, B.G., Maekawa, T., Yoshida, Y., Kumar, D.S., 2010. Nanoparticulate material delivery to plants. Plant Sci. 179(3), 154-163.

Nausch, G., 2011. Eutrophierung der Ostsee. Meeresverschmutzung und Meeresschutz. Chemie in unserer Zeit 45(3), 164-170.

Nausch, M., Woelk, J., Kahle, P., Nausch, G., Leipe, T., Lennartz, B., 2017. Phosphorus fractions in discharges from artificially drained lowland catchments (Warnow River, Baltic Sea). Agric. Water Manag. 187, 77-87.

Negassa, W., Kruse, J., Michalik, D., Appathurai, N., Zuin, L., Leinweber, P., 2010. Phosphorus speciation in agro-industrial byproducts: Sequential fractionation, solution (31)P NMR, and P K- and L(2,3)-edge XANES spectroscopy. Environ. Sci. Technol. 44(6), 2092-2097.

Nowack, B., Schulin, R., Robinson, B.H., 2006. Critical assessment of chelant-enhanced metal phytoextraction. Environ. Sci. Technol. 40(17), 5225-5232.

Obersteiner, M., Peñuelas, J., Ciais, P., van der Velde, M., Janssens, I.A., 2013. The phosphorus trilemma. Nat. Geosci. 6(11), 897-898.

Onelli, E., Prescianotto-Baschong, C., Caccianiga, M., Moscatelli, A., 2008. Clathrin-dependent and independent endocytic pathways in tobacco protoplasts revealed by labelling with charged nanogold. J. Exp. Bot. 59(11), 3051-3068.

Panten, K., Leinweber, P., 2020. Agronomic evaluation of bone char as phosphorus fertiliser after five years of consecutive application. J. Cultivated Plants 72(12), 561-576.

Paul, B.K., Vanlauwe, B., Ayuke, F., Gassner, A., Hoogmoed, M., Hurisso, T.T., Koala, S., Lelei, D., Ndabamenye, T., Six, J., Pulleman, M.M., 2013. Medium-term impact of tillage and residue management on soil aggregate stability, soil carbon and crop productivity. Agric. Ecosyst. Environ. 164, 14-22.

Peng, C., Duan, D.C., Xu, C., Chen, Y.S., Sun, L.J., Zhang, H., Yuan, X.F., Zheng, L.R., Yang, Y.Q., Yang, J.J., Zhen, X.J., Chen, Y.X., Shi, J.Y., 2015. Translocation and biotransformation of CuO nanoparticles in rice (Oryza sativa L.) plants. Environ. Pollut. 197, 99-107.

Peng, C., Xu, C., Liu, Q.L., Sun, L.J., Luo, Y.M., Shi, J.Y., 2017. Fate and transformation of CuO nanoparticles in the soil-rice system during the life cycle of rice plants. Environ. Sci. Technol. 51(9), 4907-4917.

Priester, J.H., Ge, Y., Mielke, R.E., Horst, A.M., Moritz, S.C., Espinosa, K., Gelb, J., Walker, S.L., Nisbet, R.M., An, Y.J., Schimel, J.P., Palmer, R.G., Hernandez-Viezcas, J.A., Zhao, L., Gardea-Torresdey, J.L., Holden, P.A., 2012. Soybean susceptibility to manufactured nanomaterials with evidence for food quality and soil fertility interruption. Proc. Natl. Acad. Sci. U. S. A. 109(37), E2451-E2456.

Pustejovsky, J.E., Rodgers, M.A., 2019. Testing for funnel plot asymmetry of standardized mean differences. Res. Synth. Methods 10(1), 57-71.

Quinton, J.N., Govers, G., Van Oost, K., Bardgett, R.D., 2010. The impact of agricultural soil erosion on biogeochemical cycling. Nat. Geosci. 3(5), 311-314.

R Core Team, 2021. R: A language and environment for statistical computing, Vienna, Austria.

Rai, P.K., Kumar, V., Lee, S., Raza, N., Kim, K.H., Ok, Y.S., Tsang, D.C.W., 2018. Nanoparticle-plant interaction: Implications in energy, environment, and agriculture. Environ. Int. 119, 1-19.

Raliya, R., Nair, R., Chavalmane, S., Wang, W.N., Biswas, P., 2015. Mechanistic evaluation of translocation and physiological impact of titanium dioxide and zinc oxide nanoparticles on

the tomato (Solanum lycopersicum L.) plant. Metallomics : integrated biometal science 7(12), 1584-1594.

Raliya, R., Saharan, V., Dimkpa, C., Biswas, P., 2018. Nanofertilizer for precision and sustainable agriculture: Current state and future perspectives. J. Agric. Food Chem. 66(26), 6487-6503.

Ranatunga, T.D., Reddy, S.S., Taylor, R.W., 2013. Phosphorus distribution in soil aggregate size fractions in a poultry litter applied soil and potential environmental impacts. Geoderma 192, 446-452.

Regelink, I.C., Weng, L., Koopmans, G.F., van Riemsdijk, W.H., 2013. Asymmetric flow field-flow fractionation as a new approach to analyse iron-(hydr)oxide nanoparticles in soil extracts. Geoderma 202-203, 134-141.

Reidsma, F.H., van Hoesel, A., van Os, B.J.H., Megens, L., Braadbaart, F., 2016. Charred bone: Physical and chemical changes during laboratory simulated heating under reducing conditions and its relevance for the study of fire use in archaeology. J. Archaeol. Sci. Rep. 10, 282-292.

Reszat, T.N., Hendry, M.J., 2005. Characterizing dissolved organic carbon using asymmetrical flow field-flow fractionation with on-line UV and DOC detection. Anal. Chem. 77(13), 4194-4200.

Rico, C.M., Majumdar, S., Duarte-Gardea, M., Peralta-Videa, J.R., Gardea-Torresdey, J.L., 2011. Interaction of nanoparticles with edible plants and their possible implications in the food chain. J. Agric. Food Chem. 59(8), 3485-3498.

River, M., Richardson, C.J., 2018. Stream transport of iron and phosphorus by authigenic nanoparticles in the Southern Piedmont of the U.S. Water Res. 130, 312-321.

Rizwan, M., Ali, S., Ali, B., Adrees, M., Arshad, M., Hussain, A., Ur Rehman, M.Z., Waris, A.A., 2019. Zinc and iron oxide nanoparticles improved the plant growth and reduced the oxidative stress and cadmium concentration in wheat. Chemosphere 214, 269-277.

Roberts, T.L., Johnston, A.E., 2015. Phosphorus use efficiency and management in agriculture. Resour. Conserv. Recycl. 105, 275-281.

Robertson, J., Thomas, C.J., Caddy, B., Lewis, A.J.M., 1984. Particle size analysis of soils — A comparison of dry and wet sieving techniques. Forensic Sci. Int. 24(3), 209-217.

Rowley, M.C., Grand, S., Verrecchia, E.P., 2018. Calcium-mediated stabilisation of soil organic carbon. Biogeochemistry 137(1-2), 27-49.

Rubaek, G.H., Kristensen, K., Olesen, S.E., Ostergaard, H.S., Heckrath, G., 2013. Phosphorus accumulation and spatial distribution in agricultural soils in Denmark. Geoderma 209, 241-250.

Rui, M.M., Ma, C.X., White, J.C., Hao, Y., Wang, Y.Y., Tang, X.L., Yang, J., Jiang, F.P., Ali, A., Rui, Y.K., Cao, W.D., Chen, G.C., Xing, B.S., 2018. Metal oxide nanoparticles alter peanut (Arachis hypogaea L.) physiological response and reduce nutritional quality: A life cycle study. Environ. Sci. Nano 5(9), 2088-2102.

Saleeb, N., Gooneratne, R., Cavanagh, J., Bunt, C., Hossain, A.K.M.M., Gaw, S., Robinson, B., 2019. The mobility of silver nanoparticles and silver ions in the soil-plant system. J. Environ. Qual. 48(6), 1835-1841.

Sample, E.C., Soper, R.J., Racz, G.J., 1980. Reactions of phosphate fertilizers in soils. In: F.E. Khasawneh, E.C. Smaple, E.J. Kamprath (Eds.), The role of phosphorus in agriculture. American Society of Agronomy, Crop Science Society of America, Soil Science Society of America, Madison, Wisconsin USA, pp. 263-310.

Santner, J., Smolders, E., Wenzel, W.W., Degryse, F., 2012. First observation of diffusion-limited plant root phosphorus uptake from nutrient solution. Plant Cell Environ. 35(9), 1558-1566.

Schelde, K., Moldrup, P., Jacobsen, O.H., de Jonge, H., de Jonge, L.W., Komatsu, T., 2002. Diffusion-limited mobilization and transport of natural colloids in macroporous soil. Vadose Zone J. 1(1), 125-136.

Schlich, K., Hoppe, M., Kraas, M., Fries, E., Hund-Rinke, K., 2017. Ecotoxicity and fate of a silver nanomaterial in an outdoor lysimeter study. Ecotoxicology 26(6), 738-751.

REFERENCES

Schmitt, D., Pagliari, P.H., do Nascimento, C.A.C., 2017. Chemical distribution of phosphorus in soils used during the development of sorption isotherms. Soil Sci. Soc. Am. J. 81(1), 84-93.

Scholz, R.W., Ulrich, A.E., Eilitta, M., Roy, A., 2013. Sustainable use of phosphorus: A finite resource. Sci. Total Environ. 461, 799-803.

Schwabe, F., Schulin, R., Limbach, L.K., Stark, W., Burge, D., Nowack, B., 2013. Influence of two types of organic matter on interaction of CeO_2 nanoparticles with plants in hydroponic culture. Chemosphere 91(4), 512-520.

Schwabe, F., Tanner, S., Schulin, R., Rotzetter, A., Stark, W., von Quadt, A., Nowack, B., 2015. Dissolved cerium contributes to uptake of Ce in the presence of differently sized CeO_2-nanoparticles by three crop plants. Metallomics 7(3), 466-477.

Séquaris, J.M., Lewandowski, H., 2003. Physicochemical characterization of potential colloids from agricultural topsoils. Colloids Surf. A Physicochem. Eng. Asp. 217(1-3), 93-99.

Shang, H.P., Guo, H.Y., Ma, C.X., Li, C.Y., Chefetz, B., Polubesova, T., Xing, B.S., 2019. Maize (Zea mays L.) root exudates modify the surface chemistry of CuO nanoparticles: Altered aggregation, dissolution and toxicity. Sci. Total Environ. 690, 502-510.

Sharma, S., Rana, V.S., Pawar, R., Lakra, J., Racchapannavar, V., 2020. Nanofertilizers for sustainable fruit production: A review. Environ. Chem. Lett. 19(2), 1693-1714.

Siebers, N., Bauke, S.L., Tamburini, F., Amelung, W., 2018. Short-term impacts of forest clear-cut on P accessibility in soil microaggregates: An oxygen isotope study. Geoderma 315, 59-64.

Siebers, N., Godlinski, F., Leinweber, P., 2014. Bone char as phosphorus fertilizer involved in cadmium immobilization in lettuce, wheat, and potato cropping. J. Plant. Nutr. Soil Sci. 177(1), 75-83.

Siebers, N., Kruse, J., Jia, Y., Lennartz, B., Koch, S., 2023. Loss of subsurface particulate and truly dissolved phosphorus during various flow conditions along a tile drain-ditch-brook continuum. Sci Total Environ. 866, 161439.

Siebers, N., Kruse, J., Leinweber, P., 2013. Speciation of phosphorus and cadmium in a contaminated soil amended with bone char: Sequential fractionations and XANES spectroscopy. Water Air Soil Pollut. 224(5).

Siebers, N., Leinweber, P., 2013. Bone char: A clean and renewable phosphorus fertilizer with cadmium immobilization capability. J. Environ. Qual. 42(2), 405-411.

Siebers, N., Wang, L., Funk, T., von Tucher, S., Merbach, I., Schweitzer, K., Kruse, J., 2021. Subsoils—a sink for excess fertilizer P but a minor contribution to P plant nutrition: evidence from long-term fertilization trials. Environ. Sci. Eur. 33, 60.

Sinaj, S., Frossard, E., Fardeau, J.C., 1997. Isotopically exchangeable phosphate in size fractionated and unfractionated soils. Soil Sci. Soc. Am. J. 61(5), 1413-1417.

Singh, R.P., Handa, R., Manchanda, G., 2020. Nanoparticles in sustainable agriculture: An emerging opportunity. J. Control. Release 329, 1234-1248.

Six, J., Bossuyt, H., Degryze, S., Denef, K., 2004. A history of research on the link between (micro)aggregates, soil biota, and soil organic matter dynamics. Soil Tillage Res. 79(1), 7-31.

Six, J., Paustian, K., Elliott, E.T., Combrink, C., 2000. Soil structure and organic matter: I. distribution of aggregate-size classes and aggregate-associated carbon. Soil Sci. Soc. Am. J. 64(2), 681-689.

Spohn, M., Giani, L., 2011. Impacts of land use change on soil aggregation and aggregate stabilizing compounds as dependent on time. Soil Biol. Biochem. 43(5), 1081-1088.

Stegemeier, J.P., Schwab, F., Colman, B.P., Webb, S.M., Newville, M., Lanzirotti, A., Winkler, C., Wiesner, M.R., Lowry, G.V., 2015. Speciation matters: bioavailability of silver and silver sulfide nanoparticles to alfalfa (Medicago sativa). Environ. Sci. Technol. 49(14), 8451-8460.

Sterne, J.A.C., Gavaghan, D., Egger, M., 2000. Publication and related bias in meta-analysis: Power of statistical tests and prevalence in the literature. J. Clin. Epidemiol. 53(11), 1119-1129.

Stolpe, B., Hassellöv, M., Andersson, K., Turner, D.R., 2005. High resolution ICPMS as an on-line detector for flow field-flow fractionation; multi-element determination of colloidal size distributions in a natural water sample. Anal. Chim. Acta 535(1-2), 109-121.

REFERENCES

Sturikova, H., Krystofova, O., Huska, D., Adam, V., 2018. Zinc, zinc nanoparticles and plants. J. Hazard. Mater. 349, 101-110.

Su, Y.M., Ashworth, V., Geitner, N.K., Wiesner, M.R., Ginnan, N., Rolshausen, P., Roper, C., Jassby, D., 2020. Delivery, fate, and mobility of silver nanoparticles in citrus trees. ACS Nano 14(3), 2966-2981.

Su, Y.M., Ashworth, V., Kim, C., Adeleye, A.S., Rolshausen, P., Roper, C., White, J., Jassby, D., 2019. Delivery, uptake, fate, and transport of engineered nanoparticles in plants: A critical review and data analysis. Environ. Sci. Nano 6(8), 2311-2331.

Tang, Z.Y., Wu, L.H., Luo, Y.M., Christie, P., 2009. Size fractionation and characterization of nanocolloidal particles in soils. Environ. Geochem. Health 31(1), 1-10.

Terrer, C., Phillips, R.P., Hungate, B.A., Rosende, J., Pett-Ridge, J., Craig, M.E., van Groenigen, K.J., Keenan, T.F., Sulman, B.N., Stocker, B.D., Reich, P.B., Pellegrini, A.F.A., Pendall, E., Zhang, H., Evans, R.D., Carrillo, Y., Fisher, J.B., Van Sundert, K., Vicca, S., Jackson, R.B., 2021. A trade-off between plant and soil carbon storage under elevated CO2. Nature 591(7851), 599-603.

Tiemeyer, B., Kahle, P., Lennartz, B., 2009. Phosphorus losses from an artificially drained rural lowland catchment in North-Eastern Germany. Agric. Water Manag. 96(4), 677-690.

Tisdall, J.M., Oades, J.M., 1982. Organic matter and water-stable aggregates in soils. J. Soil Sci. 33(2), 141-163.

Totsche, K.U., Amelung, W., Gerzabek, M.H., Guggenberger, G., Klumpp, E., Knief, C., Lehndorff, E., Mikutta, R., Peth, S., Prechtel, A., Ray, N., Kogel-Knabner, I., 2018. Microaggregates in soils. J. Plant Nutr. Soil Sci. 181(1), 104-136.

Ume, L., Hussain, A., Nazir, A., Shafiq, M., Firdaus e, B., 2021. Potential application of biochar composite derived from rice straw and animal bones to improve plant growth. Sustainability 13(19), 11104.

Vance, C.P., Uhde-Stone, C., Allan, D.L., 2003. Phosphorus acquisition and use: Critical adaptations by plants for securing a nonrenewable resource. New Phytol. 157(3), 423-447.

Vogeler, I., Rogasik, J., Funder, U., Panten, K., Schnug, E., 2009. Effect of tillage systems and P-fertilization on soil physical and chemical properties, crop yield and nutrient uptake. Soil Tillage Res. 103, 137-143.

Wagener, S., Jungnickel, H., Dommershausen, N., Fischer, T., Laux, P., Luch, A., 2019. Determination of nanoparticle uptake, distribution, and characterization in plant root tissue after realistic long-term exposure to sewage sludge using information from Mass Spectrometry. Environ. Sci. Technol. 53(9), 5416-5426.

Wan, W.J., Li, X., Han, S., Wang, L., Luo, X.S., Chen, W.L., Huang, Q.Y., 2020. Soil aggregate fractionation and phosphorus fraction driven by long-term fertilization regimes affect the abundance and composition of P-cycling-related bacteria. Soil Tillage Res. 196.

Wang, C.Z., Wang, R.Y., Huo, Z.L., Xie, E., Dahlke, H.E., 2020a. Colloid transport through soil and other porous media under transient flow conditions—A review. WIREs Water 7(4), e1439.

Wang, F., Liu, X., Shi, Z., Tong, R., Adams, C.A., Shi, X., 2016a. Arbuscular mycorrhizae alleviate negative effects of zinc oxide nanoparticle and zinc accumulation in maize plants--A soil microcosm experiment. Chemosphere 147, 88-97.

Wang, J., Koo, Y., Alexander, A., Yang, Y., Westerhof, S., Zhang, Q., Schnoor, J.L., Colvin, V.L., Braam, J., Alvarez, P.J., 2013. Phytostimulation of poplars and Arabidopsis exposed to silver nanoparticles and Ag(+) at sublethal concentrations. Environ. Sci. Technol. 47(10), 5442-5449.

Wang, J., Wu, Y., Zhou, J., Bing, H., Sun, H., Luo, J., Pu, S., 2020b. Air-drying changes the distribution of Hedley phosphorus pools in forest soils. Pedosphere 30(2), 272-284.

Wang, P., Lombi, E., Menzies, N.W., Zhao, F.J., Kopittke, P.M., 2018. Engineered silver nanoparticles in terrestrial environments: A meta-analysis shows that the overall environmental risk is small. Environ. Sci. Nano 5(11), 2531-2544.

Wang, P., Lombi, E., Zhao, F.J., Kopittke, P.M., 2016b. Nanotechnology: A new opportunity in plant sciences. Trends Plant Sci. 21(8), 699-712.

REFERENCES

Wang, P., Menzies, N.W., Lombi, E., Sekine, R., Blamey, F.P., Hernandez-Soriano, M.C., Cheng, M., Kappen, P., Peijnenburg, W.J., Tang, C., Kopittke, P.M., 2015. Silver sulfide nanoparticles (Ag_2S-NPs) are taken up by plants and are phytotoxic. Nanotoxicology 9(8), 1041-1049.

Wang, X., Yost, R.S., Linquist, B.A., 2001. Soil aggregate size affects phosphorus desorption from highly weathered soils and plant growth. Soil Sci. Soc. Am. J. 65(1), 139-146.

Wang, Z.Y., Xie, X.Y., Zhao, J., Liu, X.Y., Feng, W.Q., White, J.C., Xing, B.S., 2012. Xylem- and phloem-based transport of CuO nanoparticles in maize (Zea mays L.). Environ. Sci. Technol. 46(8), 4434-4441.

Warren, G.P., Robinson, J.S., Someus, E., 2008. Dissolution of phosphorus from animal bone char in 12 soils. Nutr. Cycl. Agroecosys. 84(2), 167-178.

Wiesler, F., Appel, T., Dittert, K., Ebertseder, T., Müller, T., Nätscher, L., Olfs, H.W., Rex, M., Schweitzer, K., Steffens, D., Taube, F., Zorn, W., 2018. Phosphordungung nach Bodenuntersuchung und Pflanzenbedarf: VDLUFA-Standpunkt.

Wojcieszek, J., Jimenez-Lamana, J., Bierla, K., Ruzik, L., Asztemborska, M., Jarosz, M., Szpunar, J., 2019. Uptake, translocation, size characterization and localization of cerium oxide nanoparticles in radish (Raphanus sativus L.). Sci. Total Environ. 683, 284-292.

Wright, A.L., 2009. Phosphorus sequestration in soil aggregates after long-term tillage and cropping. Soil Tillage Res. 103(2), 406-411.

Yaghi, N., Hartikainen, H., 2013. Enhancement of phosphorus sorption onto light expanded clay aggregates by means of aluminum and iron oxide coatings. Chemosphere 93(9), 1879-1886.

Yang, Q.Q., Shan, W.Y., Hu, L.G., Zhao, Y., Hou, Y.Z., Yin, Y.G., Liang, Y., Wang, F.Y., Cai, Y., Liu, J.F., Jiang, G.B., 2019. Uptake and transformation of silver nanoparticles and ions by rice plants revealed by dual stable isotope tracing. Environ. Sci. Technol. 53(2), 625-633.

Yang, Q.Q., Xu, W., Liu, G.L., Song, M.Y., Tan, Z.Q., Mao, Y.X., Yin, Y.G., Cai, Y., Liu, J.F., Jiang, G.B., 2020. Transformation and uptake of silver nanoparticles and silver ions in rice plant (Oryza sativa L.): The effect of iron plaque and dissolved iron. Environ. Sci. Nano 7(2), 599-609.

Yeats, P.A., Strain, P.M., Whitehouse, B.G., 1990. Cross-flow filtration of colloids from aquatic environments. Limnol. Oceanogr. 35(6), 1368-1375.

Yuan, J.X., Chen, Y., Li, H.S., Lu, J.Y., Zhao, H., Liu, M., Nechitaylo, G.S., Glushchenko, N.N., 2018. New insights into the cellular responses to iron nanoparticles in Capsicum annuum. Sci. Rep. 8(1), 3228.

Yusefi-Tanha, E., Fallah, S., Rostamnejadi, A., Pokhrel, L.R., 2020. Zinc oxide nanoparticles (ZnONPs) as a novel nanofertilizer: Influence on seed yield and antioxidant defense system in soil grown soybean (Glycine max cv. Kowsar). Sci. Total Environ. 738, 140240.

Zehlike, L., Peters, A., Ellerbrock, R.H., Degenkolb, L., Klitzke, S., 2019. Aggregation of TiO_2 and Ag nanoparticles in soil solution - Effects of primary nanoparticle size and dissolved organic matter characteristics. Sci. Total Environ. 688, 288-298.

Zhang, H.L., Lu, L., Zhao, X.P., Zhao, S., Gu, X.Y., Du, W.C., Wei, H., Ji, R., Zhao, L.J., 2019a. Metabolomics reveals the "invisible" responses of spinach plants exposed to CeO_2 nanoparticles. Environ. Sci. Technol. 53(10), 6007-6017.

Zhang, M.K., He, Z.L., Calvert, D.V., Stoffella, P.J., Yang, X.E., Li, Y.C., 2003. Phosphorus and heavy metal attachment and release in sandy soil aggregate fractions. Soil Sci. Soc. Am. J. 67(4), 1158-1167.

Zhang, P., Ma, Y.H., Xie, C.J., Guo, Z.L., He, X., Valsami-Jones, E., Lynch, I., Luo, W.H., Zheng, L.R., Zhang, Z.Y., 2019b. Plant species-dependent transformation and translocation of ceria nanoparticles. Environ. Sci. Nano 6(1), 60-67.

Zhang, P., Ma, Y.H., Zhang, Z.Y., He, X., Zhang, J., Guo, Z., Tai, R.Z., Zhao, Y.L., Chai, Z.F., 2012. Biotransformation of ceria nanoparticles in cucumber plants. ACS Nano 6(11), 9943-9950.

Zhang, Q.Q., Song, Y.f., Wu, Z., Yan, X.Y., Gunina, A., Kuzyakov, Y., Xiong, Z.Q., 2020. Effects of six-year biochar amendment on soil aggregation, crop growth, and nitrogen and phosphorus use efficiencies in a rice-wheat rotation. J. Clean. Prod. 242, 118435.

REFERENCES

Zhang, W., Yao, Y., Sullivan, N., Chen, Y.S., 2011. Modeling the primary size effects of citrate-coated silver nanoparticles on their ion release kinetics. Environ. Sci. Technol. 45(10), 4422-4428.

Zhang, W.L., Ebbs, S.D., Musante, C., White, J.C., Gao, C.M., Ma, X.M., 2015. Uptake and accumulation of bulk and nanosized cerium oxide particles and ionic cerium by radish (Raphanus sativus L.). J. Agric. Food Chem. 63(2), 382-390.

Zhang, Y.Q., Dalal, R.C., Bhattacharyya, R., Meyer, G., Wang, P., Menzies, N.W., Kopittke, P.M., 2021. Effect of long-term no-tillage and nitrogen fertilization on phosphorus distribution in bulk soil and aggregates of a Vertisol. Soil Tillage Res. 205.

Zhao, L.J., Ortiz, C., Adeleye, A.S., Hu, Q.R., Zhou, H.J., Huang, Y.X., Keller, A.A., 2016. Metabolomics to detect response of lettuce (Lactuca sativa) to $Cu(OH)_2$ nanopesticides: Oxidative stress response and detoxification mechanisms. Environ. Sci. Technol. 50(17), 9697-9707.

Zhao, L.J., Peralta-Videa, J.R., Ren, M.H., Varela-Ramirez, A., Li, C.Q., Hernandez-Viezcas, J.A., Aguilera, R.J., Gardea-Torresdey, J.L., 2012. Transport of Zn in a sandy loam soil treated with ZnO NPs and uptake by corn plants: Electron microprobe and confocal microscopy studies. Chem. Eng. J. 184, 1-8.

Zhao, Y.J., Wu, K.F., Wang, Z.J., ZHao, L., Li, S.S., 2000. Fouling and cleaning of membrane a literature review. J. Environ. Sci. 12(2), 241-251.

Zhou, D., Jin, S., Li, L., Wang, Y., Weng, N., 2011. Quantifying the adsorption and uptake of CuO nanoparticles by wheat root based on chemical extractions. J. Environ. Sci. 23(11), 1852-1857.

Zhu, H., Han, J., Xiao, J.Q., Jin, Y., 2008. Uptake, translocation, and accumulation of manufactured iron oxide nanoparticles by pumpkin plants. J. Environ. Monit. 10(6), 713-717.

Zhu, J.H., Wang, J., Zhan, X.H., Li, A., White, J.C., Gardea-Torresdey, J.L., Xing, B.S., 2021. Role of charge and size in the translocation and distribution of zinc oxide particles in wheat Cells. ACS Sustain. Chem. Eng. 9(34), 11556-11564.

Zhu, Z.J., Wang, H.H., Yan, B., Zheng, H., Jiang, Y., Miranda, O.R., Rotello, V.M., Xing, B.S., Vachet, R.W., 2012. Effect of surface charge on the uptake and distribution of gold nanoparticles in four plant species. Environ. Sci. Technol. 46(22), 12391-12398.

Zhuang, J., McCarthy, J.F., Tyner, J.S., Perfect, E., Flury, M., 2007. In situ colloid mobilization in Hanford sediments under unsaturated transient flow conditions: Effect of irrigation pattern. Environ. Sci. Technol. 41, 3199-3024.

Zimmer, D., Kahle, P., Baum, C., 2016. Loss of soil phosphorus by tile drains during storm events. Agric. Water Manag. 167, 21-28.

Zimmer, D., Kruse, J., Siebers, N., Panten, K., Oelschlager, C., Warkentin, M., Hu, Y.F., Zuin, L., Leinweber, P., 2018. Bone char vs. S-enriched bone char: Multi-method characterization of bone chars and their transformation in soil. Sci. Total Environ. 643, 145-156.

Zimmer, D., Panten, K., Frank, M., Springer, A., Leinweber, P., 2019. Sulfur-enriched bone char as alternative P fertilizer: Spectroscopic, wet chemical, and yield response evaluation. Agriculture 9(1), 21.

Zirkler, D., Lang, F., Kaupenjohann, M., 2012. "Lost in filtration" — The separation of soil colloids from larger particles. Colloids Surf. A Physicochem. Eng. Asp. 399, 35-40.

Zwetsloot, M.J., Lehmann, J., Bauerle, T., Vanek, S., Hestrin, R., Nigussie, A., 2016. Phosphorus availability from bone char in a P-fixing soil influenced by root-mycorrhizae-biochar interactions. Plant Soil 408(1-2), 95-105.

Zwetsloot, M.J., Lehmann, J., Solomon, D., 2015. Recycling slaughterhouse waste into fertilizer: How do pyrolysis temperature and biomass additions affect phosphorus availability and chemistry? J. Sci. Food. Agric. 95(2), 281-288.

Appendix A

Supplementary materials for chapter 2

Fate and availability of phosphorus from bone char with and without sulfur modification in soil size fractions after five-year field fertilizations

APPENDIX A

Table A-1. Elemental concentrations of soil size fractions (SMaA, LMiA, SMiA and BU) and bulk soil pH of treatments (No-P, TSP, BC and BC^{plus}) at year 2013 and year 2018 in iSPTC-A soil.

Treatment	Size fraction	Bulk soil pH ($CaCl_2$)		C (g kg^{-1} fraction)		N (g kg^{-1} fraction)		S (mg kg^{-1} fraction)	
		Before start (2013)	2018	Before start (2013)	2018	Before start (2013)	2018	Before start (2013)	2018
No-P	SMaA	5.1±0.1	5.9±0.3	10.2±1.4^{C}	10.0±1.3^{C}	0.53±0.05^{C}	0.56±0.05^{C}	120±10^{B}	117±28^{B}
	LMiA			11.8±0.5^{BC}	12.4±1.3^{BC}	0.74±0.02^{BC}	0.78±0.07^{B}	137±22^{B}	145±12^{B}
	SMiA			13.8±0.8^{B}	14.0±0.4^{B}	0.97±0.05^{B}	0.95±0.03^{B}	168±24^{B}	178±4^{B}
	BU			47.9±1.7^{A}	46.4±0.4^{A}	3.75±0.21^{A}	3.61±0.08^{A}	673±59^{A}	772±44^{A}
TSP	SMaA	5.2±0.1^{i}	6.0±0.3^{I}	10.4±1.0^{B}	10.1±1.9^{B}	0.58±0.05^{B}	0.56±0.10^{B}	124±11^{B}	144±14^{B}
	LMiA			11.3±1.1^{B}	12.6±1.4^{B}	0.71±0.07^{B}	0.83±0.11^{B}	138±10^{B}	169±14^{B}
	SMiA			13.0±0.9^{B}	13.6±1.0^{B}	0.90±0.09^{B}	0.93±0.10^{B}	169±6^{B}	183±7^{B}
	BU			48.1±10.1^{A}	48.9±3.9^{A}	3.72±0.77^{A}	3.85±0.33^{A}	700±251^{A}	846±149^{A}
BC	SMaA	5.1±0.1^{i}	6.0±0.1^{I}	9.5±0.9^{B}	8.6±1.4^{B}	0.53±0.05^{B}	0.55±0.09^{B}	116±8^{B}	131±11^{B}
	LMiA			11.3±1.1^{B}	11.8±0.7^{B}	0.72±0.06^{B}	0.79±0.05^{B}	134±14^{B}	152±6^{B}
	SMiA			12.7±0.5^{B}	14.1±0.6^{B}	0.89±0.06^{B}	0.99±0.06^{B}	164±12^{B}	193±15^{B}
	BU			44.1±4.0^{A}	57.4±6.8^{A}	3.44±0.34^{A}	4.20±0.84^{A}	597±119^{A}	1205±253^{A}
BC^{plus}	SMaA	5.2±0.1^{i}	6.0±0.2^{I}	11.1±0.4^{B}	8.6±1.6^{B}	0.58±0.04^{B}	0.49±0.08^{B}	128±7^{B}	134±17^{B}
	LMiA			11.7±0.6^{B}	11.6±0.7^{B}	0.74±0.03^{B}	0.73±0.05^{B}	141±19^{B}	151±6^{B}
	SMiA			14.0±0.7^{B}	13.5±0.5^{B}	0.99±0.05^{B}	0.90±0.04^{B}	173±20^{B}	186±10^{B}
	BU			52.0±6.4^{A}	48.8±11.9^{A}	4.02±0.51^{A}	3.68±1.03^{A}	777±168^{A}	889±137^{A}

Table A-1. (Continued)

Treatment	Size fraction	P		Ca		Fe		Mg	
		g kg^{-1} fraction							
		Before start (2013)	2018	Before start (2013)	2018	Before start (2013)	2018	Before start (2013)	2018
No-P	SMaA	0.33±0.07^{B}	0.24±0.04^{C}	0.72±0.14^{B}	1.07±0.34^{C}	5.6±0.8^{C}	6.2±0.7^{B}	0.41±0.05^{C}	0.48±0.03^{C}
	LMiA	0.33±0.03^{B}	0.36±0.05^{C}	0.96±0.16^{B}	1.33±0.23^{BC}	7.0±0.3^{C}	7.7±0.4^{B}	0.62±0.02^{C}	0.68±0.04^{C}
	SMiA	0.52±0.13^{B}	0.51±0.07^{B}	1.32±0.20^{Bi}	2.06±0.23^{BI}	9.6±0.5^{BC}	11.8±1.1^{B}	0.95±0.08^{B}	1.20±0.09^{B}
	BU	1.36±0.19^{A}	1.56±0.03^{A}	3.81±0.48^{A}	4.72±0.49^{A}	28.9±2.5^{A}	25.3±3.8^{A}	3.07±0.15^{A}	3.02±0.14^{A}
TSP	SMaA	0.26±0.02^{B}	0.32±0.10^{B}	0.80±0.15^{C}	1.12±0.26^{C}	6.2±0.2^{B}	5.6±0.6^{C}	0.49±0.06^{C}	0.50±0.07^{C}
	LMiA	0.28±0.05^{B}	0.41±0.03^{B}	0.89±0.02^{BCi}	1.45±0.09^{BCI}	6.6±0.2^{B}	7.5±0.5^{BC}	0.61±0.01^{BC}	0.69±0.02^{BC}
	SMiA	0.52±0.06^{B}	0.45±0.02^{B}	1.32±0.11^{Bi}	1.88±0.16^{BI}	9.4±0.4^{B}	9.8±0.1^{B}	0.96±0.04^{B}	0.99±0.06^{B}
	BU	1.38±0.43^{A}	1.47±0.07^{A}	3.75±0.27^{Ai}	5.18±0.23^{AI}	26.9±5.5^{A}	25.3±2.9^{A}	3.13±0.26^{A}	2.98±0.21^{A}
BC	SMaA	0.26±0.02^{C}	0.26±0.08^{B}	0.66±0.09^{Ci}	1.02±0.04^{BI}	5.8±0.8^{B}	7.1±1.1^{B}	0.43±0.04^{C}	0.54±0.16^{B}
	LMiA	0.31±0.03^{C}	0.32±0.06^{B}	0.86±0.07^{C}	1.40±0.30^{B}	6.8±0.0^{B}	7.6±0.8^{B}	0.60±0.01^{C}	0.70±0.08^{B}
	SMiA	0.51±0.06^{B}	0.48±0.09^{B}	1.24±0.15^{B}	1.74±0.50^{B}	9.4±0.4^{B}	9.7±1.8^{B}	0.94±0.05^{B}	0.94±0.22^{B}
	BU	1.12±0.11^{A}	1.35±0.28^{A}	3.51±0.18^{A}	5.18±0.61^{A}	26.1±4.3^{A}	35.4±0.4^{A}	3.04±0.13^{A}	3.37±0.33^{A}
BC^{plus}	SMaA	0.33±0.07^{B}	0.24±0.01^{B}	0.86±0.10^{C}	0.87±0.26^{B}	6.0±0.4^{B}	4.7±1.3^{B}	0.47±0.09^{C}	0.38±0.13^{B}
	LMiA	0.31±0.07^{Bi}	0.37±0.08^{BI}	0.99±0.10^{C}	1.40±0.32^{B}	6.9±0.5^{B}	7.2±1.3^{B}	0.62±0.02^{BC}	0.66±0.11^{B}
	SMiA	0.53±0.13^{B}	0.49±0.11^{B}	1.40±0.11^{B}	1.89±0.30^{B}	9.6±0.6^{B}	10.0±0.7^{B}	0.97±0.07^{B}	0.98±0.08^{B}
	BU	1.59±0.27^{A}	1.49±0.47^{A}	4.05±0.22^{A}	4.38±1.12^{A}	29.6±3.6^{A}	25.5±7.6^{A}	3.16±0.26^{A}	2.89±0.49^{A}

SMaA = small macroaggregate. LMiA = large microaggregate. SMiA = small microaggregate. BU = building units. TSP = triple superphosphate. BC = bone char. BC^{plus} = sulfur modified bone char. The pH values were measured with bulk soil samples of each treatment.
Significant differences between size fractions within a treatment in the same year were labeled with different capital letters; between four treatments within an aggregate size fraction in the same year were labeled with different lowercase letters; between years within a size fraction and a treatment were labeled with i or I, respectively. The value labelled with "I" was tested significantly higher than value labelled with "i". Values were mean ± standard deviation (n = 3).

APPENDIX A

Table A-2. Elemental concentrations of soil size fractions (SMaA, LMiA, SMiA and BU) and bulk soil pH of treatments (No-P, TSP, BC and BC^{plus}) at year 2013 and year 2018 in iSPTC-C soil.

Treatment	Size fraction	Bulk soil pH ($CaCl_2$)		C (g kg^{-1} fraction)		N (g kg^{-1} fraction)		S (mg kg^{-1} fraction)	
		Before start (2013)	2018	Before start (2013)	2018	Before start (2013)	2018	Before start (2013)	2018
No-P	SMaA	5.2±0.1^{i}	5.9±0.2^{I}	10.8±1.0^{B}	10.4±0.3^{B}	0.58±0.05^{C}	0.59±0.03^{B}	123±10^{B}	113±26^{B}
	LMiA			12.0±0.6^{B}	12.6±0.0^{B}	0.75±0.06^{BC}	0.80±0.00^{B}	141±11^{B}	136±20^{B}
	SMiA			13.8±0.6^{B}	14.1±1.2^{B}	0.94±0.05^{B}	1.00±0.08^{B}	169±12^{B}	175±12^{Bab}
	BU			54.2±2.0^{A}	49.6±4.2^{A}	4.20±0.23^{A}	3.76±0.28^{A}	753±80^{A}	779±47^{A}
TSP	SMaA	5.2±0.0^{i}	6.1±0.2^{I}	10.5±1.2^{B}	11.1±1.1^{C}	0.57±0.04^{B}	0.61±0.05^{C}	127±18^{B}	148±9^{BC}
	LMiA			12.7±0.4^{B}	13.1±0.5^{BC}	0.81±0.03^{B}	0.85±0.01^{B}	150±19^{B}	122±8^{C}
	SMiA			13.8±0.8^{B}	14.7±0.8^{B}	0.97±0.09^{B}	1.01±0.03^{B}	169±12^{B}	167±21^{Bb}
	BU			47.9±5.8^{A}	47.3±0.7^{A}	3.58±0.49^{A}	3.69±0.11^{A}	807±215^{A}	717±11^{A}
BC	SMaA	5.2±0.0^{i}	6.0±0.3^{I}	10.0±0.5^{B}	9.0±1.9^{B}	0.54±0.01^{B}	0.49±0.08^{B}	121±9^{B}	127±20^{B}
	LMiA			12.1±0.8^{B}	11.6±2.4^{B}	0.75±0.07^{B}	0.76±0.14^{B}	142±21^{B}	148±31^{B}
	SMiA			13.4±0.6^{B}	15.0±1.2^{B}	0.93±0.08^{Bi}	1.04±0.08^{BI}	161±10^{Bi}	205±5^{BaI}
	BU			48.3±6.6^{A}	59.5±15.8^{A}	3.60±0.53^{A}	4.75±0.93^{A}	790±217^{Ai}	1124±250^{AI}
BC^{plus}	SMaA	5.2±0.1	5.8±0.4	11.3±0.9^{C}	10.6±1.0^{C}	0.61±0.04^{C}	0.56±0.06^{C}	129±17^{Bi}	145±11^{BI}
	LMiA			12.6±0.3^{BC}	10.6±0.7^{C}	0.81±0.03^{BCI}	0.66±0.06^{Ci}	150±7^{B}	172±42^{B}
	SMiA			14.2±0.1^{B}	14.7±0.3^{B}	0.99±0.03^{B}	0.97±0.04^{B}	176±5^{Bi}	199±3^{BabI}
	BU			53.7±1.6^{A}	54.2±0.5^{A}	4.17±0.23^{A}	4.21±0.08^{A}	770±87^{A}	983±188^{A}

Table A-2. (Continued)

Treatment	Size fraction	P		Ca		Fe		Mg	
		g kg^{-1} fraction							
		Before start (2013)	2018	Before start (2013)	2018	Before start (2013)	2018	Before start (2013)	2018
No-P	SMaA	0.45±0.13^{B}	0.33±0.07^{B}	0.78±0.02^{B}	1.21±0.30^{B}	5.3±0.9^{B}	5.8±0.7^{B}	0.40±0.03^{C}	0.55±0.15^{C}
	LMiA	0.40±0.06^{Bi}	0.51±0.04^{BI}	1.02±0.10^{B}	1.34±0.19^{B}	6.5±0.5^{B}	7.0±0.1^{B}	0.59±0.03^{C}	0.65±0.02^{C}
	SMiA	0.76±0.07^{B}	0.58±0.07^{B}	1.40±0.07^{B}	1.66±0.22^{B}	9.2±0.1^{B}	9.1±0.3^{B}	0.90±0.03^{B}	0.92±0.04^{B}
	BU	2.58±0.56^{AI}	2.11±0.52^{Ai}	4.71±0.50^{A}	5.12±0.59^{A}	33.9±2.1^{AI}	25.2±3.1^{Ai}	3.28±0.17^{A}	2.89±0.09^{Aab}
TSP	SMaA	0.40±0.04^{C}	0.35±0.00^{C}	0.84±0.09^{B}	1.26±0.36^{B}	6.0±0.6^{B}	6.4±0.7^{C}	0.44±0.08^{C}	0.46±0.07^{D}
	LMiA	0.51±0.05^{BC}	0.55±0.03^{B}	1.15±0.06^{B}	1.69±0.29^{B}	7.1±0.3^{B}	7.5±0.1^{C}	0.62±0.03^{C}	0.67±0.01^{C}
	SMiA	0.65±0.06^{B}	0.64±0.06^{B}	1.51±0.04^{B}	2.19±0.25^{B}	9.7±0.4^{B}	10.2±0.3^{B}	0.93±0.01^{B}	1.02±0.04^{B}
	BU	1.91±0.13^{Ai}	2.43±0.09^{AI}	4.51±0.60^{A}	5.15±0.66^{A}	27.6±4.4^{A}	23.0±0.4^{A}	2.93±0.16^{A}	2.81±0.03^{Ab}
BC	SMaA	0.37±0.03^{B}	0.31±0.01^{B}	0.79±0.03^{C}	1.56±0.61^{B}	5.6±0.6^{B}	5.6±0.1^{B}	0.40±0.04^{C}	0.54±0.22^{B}
	LMiA	0.47±0.08^{B}	0.39±0.12^{B}	1.07±0.01^{BCi}	1.72±0.05^{BI}	6.6±0.9^{B}	8.1±0.4^{B}	0.60±0.04^{Ci}	0.76±0.02^{BI}
	SMiA	0.71±0.11^{B}	0.67±0.11^{B}	1.48±0.04^{Bi}	2.25±0.12^{BI}	9.4±0.4^{B}	10.6±1.4^{B}	0.91±0.04^{B}	1.06±0.12^{B}
	BU	2.30±0.76^{A}	2.05±0.38^{A}	4.37±0.38^{A}	6.78±1.37^{A}	28.4±5.1^{A}	30.8±7.1^{A}	2.99±0.19^{A}	3.42±0.33^{Aa}
BC^{plus}	SMaA	0.48±0.10^{B}	0.37±0.05^{B}	0.83±0.09^{B}	1.51±0.19^{B}	5.7±1.1^{B}	6.7±1.2^{B}	0.44±0.07^{C}	0.42±0.05^{C}
	LMiA	0.43±0.08^{B}	0.40±0.01^{B}	1.10±0.10^{B}	1.36±0.48^{B}	7.0±0.4^{B}	6.9±1.5^{B}	0.62±0.02^{BC}	0.62±0.15^{BC}
	SMiA	0.70±0.07^{B}	0.61±0.06^{B}	1.44±0.12^{B}	1.79±0.23^{B}	9.5±0.4^{B}	9.8±0.3^{B}	0.92±0.01^{B}	0.95±0.04^{B}
	BU	2.19±0.30^{A}	2.26±0.18^{A}	4.85±0.56^{A}	5.31±0.60^{A}	33.1±3.5^{A}	27.4±4.1^{A}	3.22±0.25^{A}	2.93±0.21^{Aab}

SMaA = small macroaggregate. LMiA = large microaggregate. SMiA = small microaggregate. BU = building units. TSP = triple superphosphate. BC = bone char. BC^{plus} = sulfur modified bone char. The pH values were measured with bulk soil samples of each treatment.

Significant differences between size fractions within a treatment in the same year were labeled with different capital letters; between four treatments within an aggregate size fraction in the same year were labeled with different lowercase letters; between years within a size fraction and a treatment were labeled with i or I, respectively. The value labelled with "I" was tested significantly higher than value labelled with "i". Values were mean ± standard deviation (n = 3).

APPENDIX A

Table A-3. Phosphorus concentrations (mg kg^{-1} fraction) of P fractions in soil size fractions (SMaA, LMiA, SMiA and BU) of treatments (No-P, TSP, BC and BC^{plus}) at year 2013 and year 2018 in iSPTC-A soil.

Treatment	Size fraction	H_2O-P_i		H_2O-P_o		$NaHCO_3$-P_i		$NaHCO_3$-P_o
		mg kg^{-1} fraction (%)						
		Before start (2013)	2018	Before start (2013)	2018	Before start (2013)	2018	Before start (2013)
No-P	SMaA	6.8 ± 5.8^{AB} (1.9)	3.7±0.4 (1.6)	24±26 (6)	7 ± 3^{B} (3^{A})	13 ± 3^{C} (4)	13 ± 5^{C} (5)	15 ± 3^{BI} (5^{B})
	LMiA	6.4 ± 2.8^{AB} (1.9)	4.4±3.3 (1.2)	3±1 (1)	7 ± 2^{B} (2^{AB})	27 ± 8^{B} (8)	19 ± 5^{C} (5)	10 ± 3^{B} (3^{B})
	SMiA	5.0 ± 2.8^{B} (1.0)	5.5±1.4 (1.1^{ab})	4 ± 2^{I} (1)	2 ± 1^{Ci} (0^{Bb})	31 ± 8^{B} (6)	31 ± 7^{B} (6)	16 ± 2^{B} (3^{B})
	BU	13.4 ± 5.9^{A} (1.0)	7.4±6.4 (0.5)	7±14 (0)	13 ± 2^{A} (1^{AB})	71 ± 20^{A} (4)	63 ± 13^{Ab} (4)	110 ± 18^{AI} (8^{A})
TSP	SMaA	10.0±8.9 (3.7)	8.9 ± 2.3 (3.0^{A})	29 ± 24^{A} (11)	24±25 (8)	10 ± 1^{C} (4)	18 ± 5^{C} (6)	12 ± 1^{B} (5^{AB})
	LMiA	4.8±1.7 (1.7)	8.5 ± 2.0 (2.1^{AB})	3 ± 4^{B} (1)	9±8 (2)	13 ± 4^{Ci} (5^{i})	29 ± 7^{BI} (7^{I})	14 ± 3^{B} (5^{AB})
	SMiA	2.9 ± 1.2^{i} (0.6^{i})	8.8 ± 0.4^{I} (2.0^{ABaI})	2 ± 1^{Bi} (0^{i})	6 ± 1^{I} (1^{aI})	23 ± 3^{Bi} (4^{i})	37 ± 2^{BI} (8^{I})	13 ± 2^{B} (2^{B})
	BU	7.9±3.9 (0.6)	10.2 ± 1.8 (0.7^{B})	14 ± 6^{AB} (1)	12±3 (1)	50 ± 10^{Ai} (3)	98 ± 9^{AaI} (5)	78 ± 16^{Ai} (6^{A})
BC	SMaA	8.5±10.1 (3.1)	2.8 ± 2.0 (1.0^{AB})	22±27 (8)	7 ± 2^{A} (3)	10 ± 1^{C} (4^{AB})	11 ± 5^{C} (4)	12 ± 0^{B} (5^{AB})
	LMiA	4.3±1.9 (1.4)	4.5 ± 0.9 (1.5^{A})	4±3 (1)	3 ± 1^{B} (1)	17 ± 2^{BC} (5^{A})	23 ± 6^{B} (8)	12 ± 0^{B} (4^{AB})
	SMiA	2.2±0.6 (0.4)	2.5 ± 0.9 (0.5^{ABb})	4±2 (1)	2 ± 1^{B} (1^{b})	22 ± 1^{B} (4^{AB})	24 ± 1^{B} (5)	14 ± 3^{B} (3^{B})
	BU	10.9±8.3 (0.9)	3.2 ± 2.4 (0.2^{B})	4±10 (0)	7 ± 1^{A} (0)	50 ± 10^{Ai} (4^{B})	65 ± 6^{AabI} (4)	85 ± 28^{A} (7^{A})
BC^{plus}	SMaA	8.3 ± 4.4^{AB} (2.4^{A})	4.9±1.2 (2.1)	31 ± 22^{A} (9^{A})	6 ± 3^{B} (2^{A})	13 ± 4^{C} (4)	13 ± 3^{B} (6)	16 ± 2^{BI} (5)
	LMiA	6.8 ± 2.1^{AB} (2.2^{A})	6.1±3.7 (1.6)	2 ± 1^{B} (1^{B})	2 ± 1^{B} (1^{B})	24 ± 13^{BC} (7)	25 ± 13^{B} (7)	11 ± 5^{B} (4)
	SMiA	5.7 ± 1.7^{B} (1.1^{AB})	6.8 ± 3.7 (1.3^{ab})	2 ± 2^{B} (0^{B})	3 ± 1^{B} (1^{Bab})	32 ± 6^{B} (6)	33 ± 10^{B} (7)	15 ± 3^{B} (3)
	BU	10.4 ± 1.9^{A} (0.7^{B})	5.7±4.5 (0.3)	17 ± 7^{AB} (1^{B})	12 ± 5^{A} (1^{B})	71 ± 20^{A} (4)	85 ± 35^{Aab} (5)	103 ± 18^{A} (7)

Table A-3. (Continued)

Treatment	Size fraction	$NaHCO_3$-P_o		NaOH-P_i		NaOH-P_o		H_2SO_4-P	
		mg kg^{-1} fraction (%)							
		2018	Before start (2013)	2018	Before start (2013)	2018	Before start (2013)	2018	
No-P	SMaA	10 ± 3^{Bi} (4)	56 ± 14^{C} (17)	52 ± 14^{D} (21^{AB})	143 ± 23^{C} (45)	99 ± 11^{B} (42)	72 ± 55^{B} (20)	58 ± 32^{B} (23)	
	LMiA	14 ± 4^{B} (4)	80 ± 14^{BC} (24)	75 ± 16^{C} (21^{AB})	137 ± 28^{C} (42)	146 ± 20^{B} (41)	67 ± 13^{B} (20^{i})	92 ± 16^{B} (26^{abI})	
	SMiA	16 ± 1^{B} (3)	109 ± 26^{B} (22)	126 ± 19^{B} (25^{A})	241 ± 88^{B} (46)	235 ± 24^{B} (46)	114 ± 50^{B} (22)	94 ± 21^{B} (18)	
	BU	82 ± 9^{Ai} (5)	383 ± 51^{Aa} (23)	318 ± 20^{A} (18^{B})	430 ± 22^{A} (27)	735 ± 162^{A} (41)	349 ± 137^{A} (21)	337 ± 105^{A} (19)	
TSP	SMaA	12 ± 0^{B} (4^{B})	50 ± 9^{C} (19)	58 ± 14^{C} (19^{B})	111 ± 12^{B} (43^{ABI})	107 ± 41^{B} (34^{ABi})	40 ± 10^{B} (15)	88 ± 63^{B} (26)	
	LMiA	13 ± 3^{B} (3^{B})	66 ± 7^{BC} (24)	90 ± 10^{C} (22^{B})	118 ± 25^{B} (41^{AB})	181 ± 18^{B} (44^{A})	64 ± 28^{B} (22)	81 ± 17^{B} (19^{b})	
	SMiA	15 ± 1^{B} (3^{B})	90 ± 12^{B} (17^{i})	127 ± 10^{B} (28^{AI})	297 ± 49^{AB} (57^{A})	150 ± 42^{B} (33^{AB})	90 ± 3^{B} (17)	104 ± 25^{B} (23)	
	BU	127 ± 15^{AI} (7^{A})	305 ± 40^{Abi} (20)	387 ± 32^{AI} (21^{B})	576 ± 402^{A} (34^{B})	480 ± 102^{A} (26^{B})	351 ± 55^{A} (24)	359 ± 49^{A} (20)	
BC	SMaA	10 ± 3^{B} (4^{B})	46 ± 9^{C} (18)	47 ± 13^{D} (18)	120 ± 25^{C} (46^{A})	110 ± 40^{B} (42)	42 ± 7^{B} (16)	74 ± 47^{B} (27)	
	LMiA	7 ± 6^{B} (2^{B})	65 ± 6^{BC} (21)	72 ± 1^{C} (23)	138 ± 19^{C} (45^{AB})	138 ± 47^{B} (43)	67 ± 25^{B} (22)	69 ± 13^{B} (22^{ab})	
	SMiA	15 ± 1^{B} (3^{B})	83 ± 6^{Bi} (16)	98 ± 2^{BI} (21)	296 ± 50^{B} (58^{A})	230 ± 79^{B} (47)	86 ± 10^{B} (17^{i})	110 ± 19^{B} (23^{I})	
	BU	76 ± 16^{A} (6^{A})	299 ± 34^{Ab} (22)	317 ± 30^{A} (21)	373 ± 58^{A} (27^{B})	519 ± 220^{A} (32)	336 ± 74^{A} (25)	361 ± 48^{A} (23)	
BC^{plus}	SMaA	9 ± 2^{Bi} (4^{AB})	59 ± 9^{C} (18)	57 ± 6^{B} (24)	135 ± 25^{B} (42)	98 ± 26^{B} (41)	70 ± 57^{B} (20)	50 ± 11^{B} (21)	
	LMiA	11 ± 5^{B} (3^{B})	82 ± 11^{C} (27)	85 ± 25^{B} (23)	118 ± 32^{B} (38)	148 ± 60^{B} (39)	64 ± 19^{Bi} (20)	97 ± 15^{BI} (26^{a})	
	SMiA	16 ± 3^{B} (3^{B})	117 ± 13^{B} (23)	124 ± 29^{B} (25)	242 ± 89^{B} (45)	190 ± 73^{B} (38)	119 ± 45^{B} (22)	120 ± 23^{B} (25)	
	BU	87 ± 27^{A} (6^{A})	389 ± 41^{Aa} (21)	351 ± 95^{A} (20)	634 ± 352^{A} (33)	615 ± 276^{A} (34)	364 ± 126^{A} (20)	337 ± 38^{A} (20)	

Table A-3. (Continued)

Treatment	Size fraction	P_i		P_o		P_i / P_o	
		mg kg^{-1} fraction (%)					
		Before start (2013)	2018	Before start (2013)	2018	Before start (2013)	2018
No-P	SMaA	148 ± 65^{B} (43)	126 ± 51^{C} (51)	183 ± 13^{CI} (57)	115 ± 13^{Ci} (49)	0.8±0.3	1.1 ± 0.5^{A}
	LMiA	181 ± 36^{B} (55)	190 ± 37^{BC} (53)	150 ± 29^{C} (45)	167 ± 18^{BC} (47)	1.3±0.4	1.1 ± 0.1^{A}
	SMiA	260 ± 82^{B} (50)	257 ± 48^{B} (50)	261 ± 92^{B} (50)	253 ± 24^{B} (50)	1.1±0.5	1.0 ± 0.1^{AB}
	BU	817 ± 181^{A} (49)	727 ± 135^{A} (41)	820 ± 40^{A} (51)	1048 ± 129^{A} (59)	1.0±0.2	0.7 ± 0.2^{B}
TSP	SMaA	109 ± 10^{C} (42)	173 ± 77^{C} (54)	153 ± 19^{B} (58)	143 ± 48^{B} (46)	0.7 ± 0.1^{B}	1.3 ± 0.6^{AB}
	LMiA	148 ± 24^{BC} (52)	208 ± 32^{BC} (50)	136 ± 26^{B} (48)	203 ± 11^{B} (50)	1.1 ± 0.0^{A}	1.0 ± 0.2^{B}
	SMiA	206 ± 14^{B} (40)	277 ± 31^{B} (62)	312 ± 51^{B} (60)	171 ± 41^{B} (38)	0.7 ± 0.1^{B}	1.7 ± 0.5^{A}
	BU	714 ± 81^{Ai} (47)	853 ± 67^{AI} (47)	860 ± 443^{A} (53)	956 ± 6^{A} (53)	1.0 ± 0.4^{AB}	0.9 ± 0.1^{B}
BC	SMaA	107 ± 14^{C} (41^{AB})	135 ± 61^{C} (50)	154 ± 20^{C} (59^{AB})	127 ± 40^{B} (50)	0.7 ± 0.1^{B}	1.1±0.6
	LMiA	153 ± 18^{BC} (50^{AB})	169 ± 7^{C} (54)	155 ± 21^{C} (50^{AB})	149 ± 54^{B} (46)	1.0 ± 0.1^{A}	1.2±0.4
	SMiA	192 ± 15^{Bi} (38^{B})	235 ± 19^{BI} (50)	313 ± 50^{B} (62^{A})	247 ± 77^{B} (50)	0.6 ± 0.1^{B}	1.0±0.3
	BU	696 ± 87^{A} (51^{A})	747 ± 62^{A} (48)	666 ± 110^{A} (49^{B})	814 ± 236^{A} (52)	1.1 ± 0.2^{A}	0.9±0.2
BC^{plus}	SMaA	151 ± 62^{C} (44)	125 ± 20^{C} (53)	182 ± 15^{B} (56)	113 ± 22^{B} (47)	0.8 ± 0.3^{B}	1.2±0.4
	LMiA	176 ± 44^{BCi} (57)	214 ± 51^{BCI} (57)	131 ± 29^{B} (43)	161 ± 64^{B} (43)	1.4 ± 0.3^{A}	1.5±0.8
	SMiA	273 ± 63^{B} (52)	284 ± 65^{B} (58)	259 ± 91^{B} (48)	209 ± 74^{B} (42)	1.1 ± 0.5^{AB}	1.4±0.5
	BU	834 ± 159^{A} (46)	778 ± 165^{A} (45)	1014 ± 310^{A} (54)	973 ± 391^{A} (55)	0.9 ± 0.3^{B}	0.8±0.2

SMaA = small macroaggregate. LMiA = large microaggregate. SMiA = small microaggregate. BU = building units. TSP = triple superphosphate. BC = bone char. BC^{plus} = sulfur modified bone char. P_t = total P. P_i = total inorganic P. P_o = total organic P.

Significant differences between size fractions within a treatment in the same year were labeled with different capital letters; between four treatments within an aggregate size fraction in the same year were labeled with different lowercase letters; between years within a size fraction and a treatment were labeled with i or I, respectively. The value labelled with "I" was tested significantly higher than value labelled with "i". Values were mean ± standard deviation (n = 3). Values in brackets were proportions of each P fraction to total P in each soil size fraction.

APPENDIX A

Table A-4. Phosphorus concentrations (mg kg^{-1} fraction) of P fractions in size fractions (SMaA, LMiA, SMiA and BU) of treatments (No-P, TSP, BC and BC^{plus}) at year 2013 and year 2018 in iSPTC-C soil.

Treatment	Size fraction	H_2O-P_i		H_2O-P_o		$NaHCO_3$-P_i		$NaHCO_3$-P_o	
		mg kg^{-1} fraction (%)							
		Before start (2013)	2018	Before start (2013)	2018	Before start (2013)	2018	Before start (2013)	2018
No-P	SMaA	$14±1^{BI}$ (3^{AB})	$10±2^{Ci}$ (3^{A})	$11±4^{B}$ (2^{A})	16±9 (5)	$36±2^{BI}$ (8^{AB})	$24±5^{Di}$ (7^{AB})	$21±6^{B}$ (5)	$16±2^{B}$ (5)
	LMiA	$16±0^{B}$ (4^{AI})	$9±4^{Cb}$ (2^{ABi})	$5±2^{C}$ (1^{AB})	7±5 (1)	$51±5^{BI}$ (13^{AI})	$40±3^{Ci}$ (8^{ABi})	$22±4^{B}$ (6)	$20±2^{B}$ (4)
	SMiA	$18±3^{B}$ (2^{AB})	$14±2^{Bb}$ (2^{AB})	$8±2^{BC}$ (1^{B})	9±3 (1)	$72±9^{B}$ (9^{AB})	$55±3^{B}$ (10^{A})	$24±6^{B}$ (3)	$22±1^{B}$ (4)
	BU	$49±21^{A}$ (2^{B})	$20±2^{A}$ (1^{B})	$26±2^{AI}$ (1^{BI})	$12±2^{i}$ (1^{i})	$229±47^{A}$ (7^{B})	$153±13^{A}$ (6^{B})	$135±19^{A}$ (5)	$101±14^{A}$ (5)
TSP	SMaA	$18±4^{B}$ (4^{A})	$11±2^{B}$ (3^{A})	$29±18^{A}$ (8)	14±7 (4^{A})	$33±5^{D}$ (8)	$30±1^{C}$ (9^{A})	$17±5^{B}$ (4^{B})	$17±2^{B}$ (5)
	LMiA	$15±1^{Bi}$ (3^{AB})	$16±1^{ABaI}$ (3^{A})	$10±5^{B}$ (2)	8±4 (1^{AB})	$53±5^{C}$ (11)	$52±9^{B}$ (9^{A})	$16±6^{B}$ (3^{B})	$19±10^{B}$ (3)
	SMiA	$18±2^{B}$ (3^{AB})	$20±1^{Aa}$ (3^{A})	$7±4^{B}$ (1)	9±4 (1^{AB})	$70±2^{B}$ (11)	$66±4^{B}$ (10^{A})	$23±4^{B}$ (4^{B})	$22±4^{B}$ (4)
	BU	$31±4^{A}$ (2^{B})	$24±10^{A}$ (1^{B})	$18±7^{AB}$ (1)	15±3 (1^{B})	$189±12^{A}$ (8^{I})	$166±24^{A}$ (6^{Bi})	$168±48^{A}$ (8^{A})	$128±36^{A}$ (5)
BC	SMaA	$16±4^{B}$ (4^{A})	$6±0^{D}$ (2^{AB})	$23±22^{A}$ (6)	$6±3^{AB}$ (2^{A})	$33±5^{BI}$ (9^{I})	$23±2^{Ci}$ (7^{i})	$20±8^{B}$ (5)	$11±6^{B}$ (3^{AB})
	LMiA	$15±1^{B}$ (3^{AB})	$11±3^{Cab}$ (3^{A})	$7±3^{A}$ (1)	$5±1^{AB}$ (1^{AB})	$53±6^{B}$ (11)	$40±12^{BC}$ (10)	$17±6^{B}$ (4)	$10±8^{B}$ (2^{B})
	SMiA	$18±2^{B}$ (3^{AB})	$16±1^{Bab}$ (2^{AB})	$9±3^{A}$ (1)	$4±1^{B}$ (1^{AB})	$71±3^{BI}$ (10)	$58±2^{Bi}$ (9)	$25±6^{B}$ (4)	$18±9^{B}$ (3^{AB})
	BU	$41±14^{A}$ (2^{B})	$19±2^{A}$ (1^{B})	$18±6^{A}$ (1)	$13±9^{A}$ (1^{B})	$208±45^{A}$ (7)	$179±24^{A}$ (7)	$145±46^{A}$ (7)	$132±20^{A}$ (6^{A})
BC^{plus}	SMaA	$16±3^{B}$ (4)	$12±5^{AB}$ (3^{A})	$17±11^{B}$ (4)	14±11 (4)	$36±2^{C}$ (8)	$29±9^{C}$ (8^{AB})	$18±3^{B}$ (4)	$12±1^{B}$ (3)
	LMiA	$15±1^{B}$ (4)	$12±1^{Bab}$ (3^{A})	$8±6^{BC}$ (2)	6±3 (1)	$51±5^{BC}$ (12)	$37±3^{C}$ (9^{A})	$21±5^{B}$ (5)	$15±7^{B}$ (4)
	SMiA	$17±2^{B}$ (2)	$14±2^{ABb}$ (2^{AB})	$6±1^{C}$ (1)	7±2 (1)	$71±8^{B}$ (10)	$55±11^{B}$ (9^{A})	$23±3^{B}$ (3)	$22±3^{B}$ (4)
	BU	$40±22^{A}$ (2)	$17±4^{A}$ (1^{B})	$27±1^{A}$ (1)	14±7 (1)	$210±40^{A}$ (8)	$164±16^{A}$ (6^{B})	$148±29^{A}$ (7)	$117±40^{A}$ (5)

Table A-4. (Continued)

Treatment	Size fraction	NaOH-P_i		NaOH-P_o		H_2SO_4-P	
		mg kg^{-1} fraction (%)					
		Before start (2013)	2018	Before start (2013)	2018	Before start (2013)	2018
No-P	SMaA	107 ± 26^{C} (24^{AB})	79 ± 14^{Dab} (24^{AB})	202 ± 96^{B} (44)	143 ± 47^{B} (42)	55 ± 12^{B} (13)	48 ± 7^{B} (14^{B})
	LMiA	120 ± 33^{C} (29^{A})	132 ± 16^{Cab} (26^{AB})	95 ± 47^{Bi} (23^{i})	190 ± 27^{BI} (37^{I})	93 ± 14^{B} (24)	113 ± 9^{B} (22^{A})
	SMiA	196 ± 21^{B} (26^{AB})	178 ± 6^{B} (31^{A})	330 ± 72^{B} (43)	190 ± 68^{B} (32)	111 ± 10^{B} (15^{i})	116 ± 5^{B} (20^{AI})
	BU	534 ± 15^{AI} (17^{Bi})	484 ± 23^{Ai} (20^{BI})	1160 ± 520^{A} (36)	844 ± 383^{A} (33)	442 ± 45^{A} (15)	498 ± 101^{A} (20^{Aa})
TSP	SMaA	100 ± 25^{D} (25^{AB})	95 ± 4^{Da} (27^{B})	148 ± 28^{B} (36)	123 ± 17^{B} (35)	56 ± 3^{C} (14^{B})	59 ± 7^{C} (17)
	LMiA	150 ± 6^{C} (30^{A})	147 ± 10^{Ca} (27^{B})	153 ± 33^{B} (30)	191 ± 30^{B} (35)	108 ± 13^{B} (21^{A})	118 ± 26^{B} (21)
	SMiA	210 ± 8^{B} (32^{A})	208 ± 10^{B} (33^{A})	200 ± 75^{B} (30)	181 ± 63^{B} (28)	123 ± 19^{B} (19^{AB})	129 ± 17^{B} (20)
	BU	514 ± 24^{A} (21^{BI})	498 ± 5^{A} (17^{Ci})	648 ± 67^{Ai} (27^{i})	1132 ± 152^{AI} (39^{I})	349 ± 20^{Ai} (14^{AB})	468 ± 47^{AI} (16^{b})
BC	SMaA	97 ± 25^{D} (26^{AB})	64 ± 10^{Db} (21)	131 ± 15^{B} (35)	104 ± 36^{B} (34)	51 ± 8^{C} (14^{B})	93 ± 56^{B} (30)
	LMiA	146 ± 8^{C} (31^{A})	115 ± 24^{Cab} (30)	128 ± 53^{B} (26)	111 ± 55^{B} (27)	106 ± 15^{BC} (22^{A})	103 ± 40^{B} (26)
	SMiA	208 ± 7^{B} (29^{AB})	189 ± 21^{B} (28)	263 ± 103^{B} (36)	248 ± 110^{B} (36)	116 ± 14^{B} (17^{AB})	135 ± 22^{B} (21)
	BU	518 ± 30^{A} (19^{B})	516 ± 34^{A} (21)	999 ± 635^{A} (33)	704 ± 209^{A} (28)	368 ± 38^{A} (13^{B})	486 ± 95^{A} (19^{ab})
BC^{plus}	SMaA	110 ± 24^{C} (23)	78 ± 11^{Cab} (21^{B})	219 ± 79^{B} (45)	130 ± 27^{B} (35)	61 ± 5^{B} (13^{i})	95 ± 14^{B} (26^{I})
	LMiA	123 ± 37^{C} (28)	105 ± 5^{Cb} (26^{A})	120 ± 54^{B} (27)	126 ± 11^{B} (32)	96 ± 15^{B} (23)	97 ± 15^{B} (24)
	SMiA	198 ± 23^{B} (29)	181 ± 23^{B} (29^{A})	267 ± 114^{B} (37)	191 ± 58^{B} (31)	117 ± 19^{B} (17)	144 ± 36^{B} (24)
	BU	530 ± 9^{A} (20)	495 ± 31^{A} (18^{B})	809 ± 204^{A} (29)	1003 ± 260^{A} (37)	424 ± 71^{A} (15)	447 ± 4^{A} (17^{b})

Table A-4. (Continued)

Treatment	Size fraction	P_i		P_o		P_i / P_o	
		mg kg^{-1} fraction (%)					
		Before start (2013)	2018	Before start (2013)	2018	Before start (2013)	2018
No-P	SMaA	212±35^{C} (49^{B})	160±25^{C} (48^{AB})	234±94^{B} (51^{A})	175±53^{B} (52^{AB})	1.0±0.2^{B}	0.9±0.2^{B}
	LMiA	280±26^{C} (70^{AI})	294±23^{B} (58^{ABi})	122±43^{Bi} (30^{Bi})	217±31^{BI} (42^{ABI})	2.4±0.7^{A}	1.4±0.2^{AB}
	SMiA	396±31^{B} (53^{AB})	364±5^{Bb} (63^{A})	362±76^{B} (47^{AB})	220±66^{B} (37^{B})	1.1±0.3^{B}	1.7±0.4^{A}
	BU	1255±97^{A} (41^{Bi})	1156±128^{A} (47^{BI})	1869±562^{AI} (59^{AI})	1339±420^{Ai} (53^{Ai})	0.7±0.2^{Bi}	0.9±0.2^{BI}
TSP	SMaA	208±29^{D} (52^{AB})	195±10^{D} (56^{A})	195±25^{B} (48^{AB})	154±8^{B} (44^{B})	1.1±0.2^{B}	1.3±0.1^{B}
	LMiA	326±13^{C} (65^{A})	334±40^{C} (60^{A})	180±42^{B} (35^{B})	218±31^{B} (40^{B})	1.9±0.4^{A}	1.6±0.3^{B}
	SMiA	420±20^{B} (65^{A})	424±14^{Ba} (67^{A})	230±75^{B} (35^{B})	212±56^{B} (33^{B})	1.9±0.6^{A}	2.1±0.5^{A}
	BU	1084±31^{A} (45^{B})	1156±33^{A} (40^{B})	1345±198^{A} (55^{A})	1717±95^{A} (60^{A})	0.8±0.1^{B}	0.7±0.0^{C}
BC	SMaA	197±29^{C} (53^{AB})	186±49^{C} (60)	175±10^{B} (47^{AB})	121±43^{B} (40)	1.1±0.1^{B}	1.8±1.1^{AB}
	LMiA	320±21^{B} (68^{A})	268±65^{BC} (69)	152±59^{B} (32^{B})	127±63^{B} (31)	2.3±0.7^{A}	2.3±0.6^{A}
	SMiA	414±12^{B} (59^{AB})	398±16^{Ba} (61)	297±107^{B} (41^{AB})	270±109^{B} (39)	1.5±0.7^{AB}	1.7±0.8^{AB}
	BU	1135±119^{A} (42^{B})	1201±147^{A} (48)	1692±708^{A} (58^{A})	1317±298^{A} (52)	0.7±0.2^{B}	0.9±0.1^{B}
BC^{plus}	SMaA	223±26^{C} (47^{ABi})	214±24^{C} (58^{AI})	254±76^{B} (53^{ABI})	156±24^{B} (42^{Bi})	0.9±0.1^{Bi}	1.4±0.1^{BI}
	LMiA	286±34^{C} (66^{A})	251±22^{C} (63^{A})	149±51^{B} (34^{B})	147±20^{B} (37^{B})	2.0±0.6^{A}	1.7±0.4^{AB}
	SMiA	402±39^{B} (58^{AB})	394±9^{Bab} (64^{A})	296±114^{B} (42^{AB})	220±59^{B} (36^{B})	1.5±0.7^{AB}	1.9±0.4^{A}
	BU	1204±120^{A} (44^{B})	1124±47^{A} (42^{B})	1521±193^{A} (56^{A})	1555±147^{A} (58^{A})	0.8±0.0^{B}	0.7±0.1^{C}

SMaA = small macroaggregate. LMiA = large microaggregate. SMiA = small microaggregate. BU = building units. TSP = triple superphosphate. BC = bone char. BC^{plus} = sulfur modified bone char. P_t = total P. P_i = total inorganic P. P_o = total organic P.
Significant differences between size fractions within a treatment in the same year were labeled with different capital letters; between four treatments within an aggregate size fraction in the same year were labeled with different lowercase letters; between years within a size fraction and a treatment were labeled with i or I, respectively. The value labelled with "I" was tested significantly higher than value labelled with "i". Values were mean ± standard deviation (n = 3). Values in brackets were proportions of each P fraction to total P in each soil size fraction.

APPENDIX A

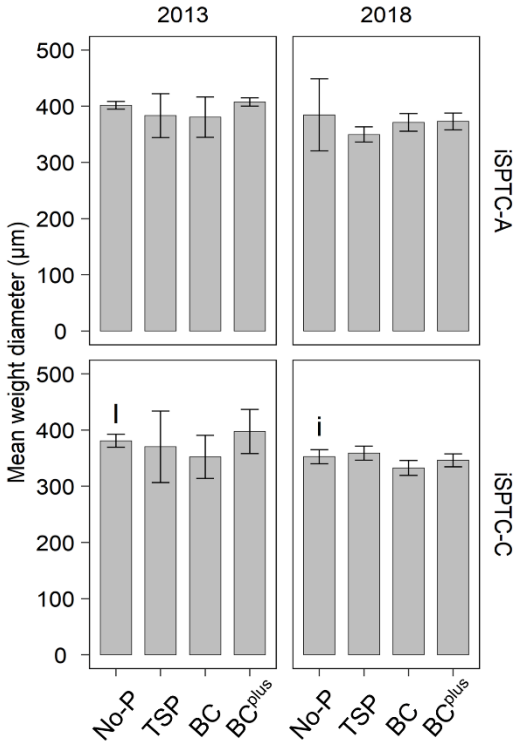

Figure A-1. Effects of treatments (No phosphorus, No-P; triple superphosphate, TSP; bone char, BC; and sulfur modified bone char, BC^{plus}) on mean weight diameter (MWD, µm) in iSPTC-A and iSPTC-C soils. Significant differences between years within a size fraction and a treatment were labeled with i or I, respectively. The value labelled with "I" was tested significantly higher than value labelled with "i". n = 3.

Appendix B

Supplementary materials for chapter 3

Loss of subsurface particulate and truly dissolved phosphorus during various flow conditions along a tile drain–ditch–brook continuum

APPENDIX B

Table B-1. Elemental loads of the three identified size fractions during the different baseflow and the flow events for every sampling station.

Baseflow	C_{org}			P			Fe			Al			Si			Ca			Mg		
	1st	2nd	3rd	1st	2nd	3rd	1st	2nd	3rd	1st	2nd	3rd	1st	2nd	3rd	1st	2nd	3rd	1st	2nd	3rd
	mg h^{-1}																				
Tile-drain 1	2	1	10	0	0	0	0	1	0	0	0	0	0	12	16	0	15	2	0	2	0
Tile-drain 2	30	22	48	0	0	0	0	6	1	0	0	0	0	1	5	9	178	16	1	19	2
Tile-drain 3	91	0	71	0	0	0	0	8	2	0	0	0	0	4	7	14	250	21	1	23	2
Tile-drain 4	121	2	287	0	1	1	2	37	8	0	1	1	1	10	31	53	1166	123	5	99	10
Ditch 1	719	493	2306	2	33	28	23	344	72	6	15	5	15	668	675	372	9808	1151	54	1094	109
Ditch 2	1893	0	787	0	7	7	13	164	37	2	8	2	17	102	148	198	4951	598	21	421	44
Ditch 3	2514	713	9085	1	26	32	48	698	187	7	28	13	25	220	481	833	19337	2119	77	1547	153
Ditch 4	1986	1861	12640	2	91	121	218	2682	826	32	110	67	51	722	2058	3137	65502	7159	262	5163	526
Brook 1	6979	0	9257	7	188	140	49	620	131	4	16	7	369	7232	4128	1299	17226	789	215	2589	137
Brook 2	5393	0	7483	2	34	47	105	1156	222	26	79	20	288	334	1429	1638	33750	3159	173	3145	276
Brook 3	1957	979	4816	0	26	45	61	1025	183	6	29	9	22	232	904	1741	31117	2325	159	2825	219
Brook 4	44133	0	41788	1	161	256	331	6955	1419	20	180	187	10	2484	5836	9983	214378	20997	824	18083	1678
Mean																					
Tile-drain	61	6	104	0	0	1	1	13	3	0	0	0	0	7	15	19	402	19	2	36	3
Ditch	1778	767	6205	1	39	47	75	972	281	12	40	22	27	428	841	1135	24900	1135	104	2056	208
Brook	14616	245	15836	2	102	122	136	2439	489	14	76	56	172	2570	3074	3665	74118	3665	343	6660	577

Table B-1. (Continued)

Flow events / Tile-drain	C_{org}			P			Fe			Al			Si			Ca			Mg		
	1st	2nd	3rd	1st	2nd	3rd	1st	2nd	3rd	1st	2nd	3rd	1st	2nd	3rd	1st	2nd	3rd	1st	2nd	3rd
	mg h^{-1}																				
1	18	9	137	0	0	1	0	8	2	0	0	0	0	3	7	12	214	27	1	26	3
2	7	0	33	0	0	0	0	3	1	0	0	0	0	1	3	7	91	9	1	10	1
3	29	10	178	0	0	1	1	14	4	0	0	0	0	6	16	28	370	38	3	39	4
4	36	0	131	0	2	1	1	12	5	1	2	1	1	32	37	16	227	47	3	33	6
5	34	9	122	0	0	1	1	14	4	0	1	0	0	9	18	23	355	34	3	36	3
6	36	25	165	0	0	2	1	20	5	0	0	1	0	6	26	36	531	58	3	47	5
7	54	0	309	0	1	3	2	41	10	0	2	2	0	26	56	54	1064	127	6	96	11
8	60	0	241	0	1	3	2	35	9	0	1	1	0	18	48	50	858	90	5	76	8
9	55	0	288	0	1	3	3	37	8	0	1	0	0	20	40	70	932	78	6	92	9
10	503	184	1175	0	7	12	7	185	46	1	5	3	0	67	164	228	5082	627	28	583	69
11	231	0	399	0	1	4	3	55	13	0	1	1	0	25	54	107	1465	157	11	176	18
12	239	0	922	0	2	8	5	94	28	0	2	3	0	58	143	160	2460	237	15	238	23
13	140	48	651	0	2	6	4	64	16	0	1	1	0	24	67	130	1709	127	12	164	15

Table B-1. (Continued)

Flow events / Ditch	C_{org}			P			Fe			Al			Si			Ca			Mg		
	1st	2nd	3rd	1st	2nd	3rd	1st	2nd	3rd	1st	2nd	3rd	1st	2nd	3rd	1st	2nd	3rd	1st	2nd	3rd
	mg h^{-1}																				
1	4758	389	8437	0	25	52	32	635	208	4	24	16	0	202	606	1003	15702	2022	104	1567	180
2	3041	1076	7412	0	16	46	29	553	163	3	16	15	0	180	641	962	14626	1708	95	1416	152
3	12339	3411	18194	0	34	106	73	1313	364	5	33	27	0	165	1229	2508	35231	3619	202	2998	310
4	3388	1534	6599	2	46	57	78	926	254	34	84	42	0	545	1156	1196	21386	3014	155	2181	261
5	3520	969	4912	1	20	33	44	552	146	14	39	19	0	189	505	796	13713	1725	87	1255	138
6	5570	2783	10668	0	42	127	63	1283	434	5	51	47	0	388	1357	2206	32382	3695	182	2781	302
7	9951	2782	20874	1	90	165	163	2585	683	33	156	78	0	1542	2407	3393	63080	7833	348	5511	615
8	10894	396	15011	1	72	138	137	2220	608	22	86	46	0	749	1892	3038	55138	6651	294	4661	519
9	17785	2028	25188	1	71	149	125	2268	500	16	87	52	0	900	1883	3359	59940	7103	359	5934	655
10	49171	20434	77042	9	441	605	494	9017	2390	64	349	189	0	4012	8261	11499	236261	29315	1357	25175	3000
11	16967	4489	27998	0	119	258	202	3031	836	30	132	66	0	1560	3072	5039	72144	7747	504	7589	790
12	43040	7891	62903	0	194	527	342	5693	1793	50	268	227	0	2386	6628	8825	136302	15015	823	12538	1302
13	23496	286	32335	0	181	350	280	5293	1541	43	217	137	0	1551	4212	6715	123757	14782	674	11441	1271

Table B-1. (Continued)

Flow events / Brook	C_{org}			P			Fe			Al			Si			Ca			Mg		
	1st	2nd	3rd	1st	2nd	3rd	1st	2nd	3rd	1st	2nd	3rd	1st	2nd	3rd	1st	2nd	3rd	1st	2nd	3rd
	mg h^{-1}																				
1	11348	42476	150692	0	74	281	186	3405	864	10	61	50	0	821	3562	6849	94963	9515	733	10379	1050
2	4007	344	11853	0	14	91	56	1148	283	2	13	12	0	368	1183	2387	32371	2583	248	3537	308
3	3316	1717	17634	0	42	135	49	2352	577	8	48	25	0	869	2077	2036	66435	8085	218	4785	489
4	829	0	19112	26	216	198	433	3970	924	378	649	200	0	1010	2622	4471	90180	13146	730	11200	1325
5	9763	6042	26329	0	71	156	254	2634	705	92	246	69	0	1497	3337	4068	62168	6721	473	6805	689
6	3730	2537	17804	0	41	253	122	3030	789	13	74	192	0	547	4651	4734	81590	8838	396	6963	728
7	13279	5866	49139	0	103	257	215	4313	1021	53	272	263	0	1690	5107	5267	109747	12593	526	9522	977
8	10980	0	43382	6	161	408	346	6977	1726	60	255	272	38	2677	7339	7825	177116	21105	801	14510	1580
9	10552	1971	36192	0	93	331	249	4437	1157	19	124	92	0	2466	5723	7472	114000	11551	714	11200	1130
10	91798	28759	74457	0	565	839	491	11325	2483	42	325	247	0	4447	11452	16614	301432	35008	1853	34160	3799
11	61853	0	187484	0	210	847	643	10254	2702	37	199	55	0	4678	11842	21158	252531	20513	2222	29672	2601
12	33431	13180	84839	0	232	748	419	7326	2277	48	278	388	0	3435	10767	12004	185024	16046	1106	16457	1498
13	13348	3358	49572	0	140	465	252	5795	1423	23	144	197	0	2805	6722	9243	160882	17108	890	14864	1519

APPENDIX B

Table B-2. Elemental loads of the colloids and total dissolved fraction for the baseflow and the flow events for every sampling station. Total = total filtrate $_{>750\ nm}$; Dis. = truly dissolved.

	C_{org}		P		Fe		Al		Si		Ca		Mg	
Baseflow	Total	**Dis.**	Total	**Dis.**	Total	**Dis.**	Total	**Dis.**	Total	**Dis.**	Total	**Dis.**	Total	**Dis.**
	g h^{-1}		**mg h^{-1}**											
Tile-drain 1	0	0	1	**0**	31	**30**	0	**0**	43	**15**	1065	**1048**	128	**126**
Tile-drain 2	1	1	1	**0**	67	**60**	1	**0**	63	**57**	2317	**2115**	275	**254**
Tile-drain 3	2	2	1	**0**	65	**55**	0	**0**	56	**45**	2301	**2017**	271	**244**
Tile-drain 4	4	4	3	**0**	296	**249**	2	**0**	260	**218**	10279	**8937**	1120	**1006**
Ditch 1	18	15	70	**6**	2562	**2123**	20	**0**	3124	**1766**	89585	**78254**	10867	**9609**
Ditch 2	34	31	15	**1**	1534	**1319**	11	**0**	1288	**1020**	53602	**47854**	5567	**5081**
Ditch 3	63	52	65	**6**	6555	**5622**	39	**0**	4951	**4226**	220439	**198150**	22778	**21001**
Ditch 4	176	161	228	**13**	17894	**14169**	98	**0**	12371	**9539**	615222	**539424**	63399	**57447**
Brook 1	213	196	391	**56**	6632	**5833**	106	**78**	12164	**435**	235097	**215784**	35439	**32499**
Brook 2	189	176	108	**26**	12201	**10717**	141	**16**	12366	**10316**	429932	**391385**	46421	**42828**
Brook 3	219	212	80	**10**	11172	**9903**	62	**18**	11310	**10152**	391142	**355960**	46899	**43696**
Brook 4	1636	1550	465	**47**	23639	**14933**	166	**0**	35057	**26727**	828254	**582896**	92501	**71915**
Mean														
Tile-drain	2	2	1	0	115	98	1	0	106	84	3991	3529	448	408
Ditch	73	65	94	7	7136	5808	42	0	5434	4138	244712	215921	25653	23285
Brook	564	534	261	35	13411	10347	119	28	17725	11908	471106	386506	55315	47734
Flow events														
Tile-drain														
1	1	**1**	5	**4**	37	**27**	2	**2**	46	**36**	1287	**1033**	158	**128**
2	0	**0**	3	**3**	24	**20**	1	**1**	25	**21**	853	**747**	97	**86**
3	1	**1**	10	**8**	73	**54**	3	**3**	74	**51**	2525	**2089**	273	**228**
4	2	**2**	25	**22**	131	**112**	27	**24**	106	**37**	4618	**4327**	470	**428**
5	2	**2**	12	**11**	123	**104**	13	**12**	102	**75**	4319	**3907**	450	**407**
6	2	**2**	15	**13**	130	**104**	9	**8**	114	**82**	4687	**4062**	476	**420**
7	3	**3**	28	**24**	230	**177**	36	**31**	201	**119**	8289	**7043**	818	**706**
8	4	**3**	33	**30**	238	**193**	29	**26**	192	**126**	8499	**7501**	866	**778**
9	4	**4**	7	**3**	232	**184**	3	**1**	216	**156**	8297	**7218**	951	**843**
10	12	**10**	116	**97**	589	**350**	56	**47**	762	**532**	20783	**14845**	2581	**1900**
11	5	**5**	43	**38**	313	**241**	17	**15**	330	**251**	11146	**9418**	1460	**1254**
12	8	**7**	58	**48**	574	**448**	34	**28**	551	**351**	20261	**17403**	2180	**1905**
13	5	**4**	33	**25**	440	**356**	11	**8**	412	**321**	15474	**13509**	1595	**1404**

Table B-2. (Continued)

Flow events	C_{org}		P		Fe		Al		Si		Ca		Mg	
	Total	**Dis.**	Total	**Dis.**	Total	**Dis.**	Total	**Dis.**	Total	**Dis.**	Total	**Dis.**	Total	**Dis.**
	g h^{-1}		**mg h^{-1}**											
1	70	**56**	618	**541**	4844	**3969**	360	**315**	4321	**3513**	161881	**143154**	17137	**15286**
2	40	**28**	567	**506**	4973	**4228**	310	**276**	4433	**3613**	166833	**149538**	16979	**15315**
3	102	**68**	1241	**1101**	10253	**8503**	586	**520**	8757	**7363**	353244	**311885**	36194	**32684**
4	114	**102**	1004	**898**	6571	**5313**	1524	**1364**	5044	**3343**	229283	**203687**	21500	**18902**
5	67	**58**	534	**481**	4689	**3946**	730	**657**	3529	**2835**	160959	**144725**	15154	**13674**
6	108	**89**	1268	**1098**	9613	**7832**	764	**662**	7859	**6114**	340739	**302456**	33185	**29919**
7	189	**155**	2335	**2079**	16313	**12881**	2442	**2175**	12483	**8534**	576565	**502259**	55479	**49005**
8	162	**136**	2361	**2150**	15475	**12510**	1716	**1563**	10908	**8267**	533327	**468500**	51777	**46302**
9	181	**136**	651	**430**	14482	**11590**	459	**303**	12002	**9218**	510197	**439795**	58148	**51200**
10	601	**454**	7312	**6258**	36904	**25004**	4181	**3578**	33644	**21371**	1285282	**1008208**	157369	**127837**
11	214	**164**	2784	**2407**	17566	**13497**	1686	**1458**	16452	**11819**	627883	**542953**	74151	**65268**
12	429	**316**	4844	**4122**	35218	**27389**	3657	**3112**	28212	**19197**	1205181	**1045040**	120160	**105497**
13	305	**249**	3507	**2976**	30812	**23697**	2615	**2219**	20078	**14315**	1068483	**923229**	106033	**92647**
Brook														
1	894	**690**	883	**528**	22966	**18511**	302	**180**	33039	**28657**	788148	**676822**	103979	**91817**
2	268	**252**	942	**837**	9347	**7861**	239	**212**	11466	**9916**	327054	**289713**	41019	**36926**
3	302	**279**	1370	**1192**	10729	**7750**	624	**543**	14336	**11390**	371678	**295123**	44095	**38603**
4	661	**641**	3540	**3100**	23929	**18602**	9872	**8646**	22479	**18847**	852108	**744311**	86020	**72765**
5	540	**498**	1584	**1356**	17912	**14318**	2833	**2426**	18940	**14106**	634576	**561619**	71069	**63102**
6	536	**512**	2093	**1800**	20264	**16323**	1998	**1718**	21640	**16442**	732691	**637530**	75560	**67473**
7	673	**604**	1727	**1368**	25368	**19819**	2825	**2237**	26848	**20051**	906572	**778965**	89955	**78930**
8	1073	**1019**	5890	**5315**	33550	**24501**	6022	**5434**	39092	**29037**	1211205	**1005160**	128527	**111637**
9	845	**797**	774	**349**	28884	**23041**	428	**193**	31448	**23259**	1022187	**889164**	117284	**104240**
10	1629	**1434**	6538	**5135**	41282	**26984**	2861	**2247**	52008	**36109**	1429863	**1076809**	179557	**139745**
11	2350	**2101**	6522	**5465**	60485	**46885**	1800	**1508**	76285	**59764**	2153695	**1859493**	271975	**237480**
12	1273	**1142**	4297	**3317**	48090	**38068**	3127	**2414**	48051	**33848**	1662279	**1449205**	161780	**142720**
13	1163	**1096**	3227	**2622**	34014	**26544**	1945	**1580**	38867	**29340**	1192245	**1005012**	127057	**109786**

APPENDIX B

Table B-3. Elemental stocks (kg ha^{-1}) of the three AF^4 size fractions (1st: 0.66 to 20 nm, 2nd: 20 to 100 nm, and 3rd: 100 to 450 nm) for the different soil horizons Ap, Bw, and C. (mean ± standard deviation, n = 9).

Horizons	C_{org}			P			Fe			Al			Si			Ca			Mg		
	1st	2nd	3rd	1st	2nd	3rd	1st	2nd	3rd	1st	2nd	3rd	1st	2nd	3rd	1st	2nd	3rd	1st	2nd	3rd
Ap	23	28	22	4.4	1.3	3.4	2	17	69	2	15	65	4	34	131	25	2	7	2.7	1.9	7.9
	±3	±3	±6	±1.5	±0.5	±0.6	±2	±40	±55	±1	±38	±56	±3	±86	±124	±8	±3	±5	±0.7	±4.3	±6.6
Bw	13	17	25	0.6	0.7	1.7	3	29	92	2	23	83	4	55	187	21	3	8	2.2	3.1	11.0
	±6	±6	±6	±0.8	±0.4	±0.6	±2	±47	±56	±1	±39	±50	±2	±95	±119	±6	±4	±5	±0.3	±5.1	±6.6
C	15	39	80	3.6	4.5	5.1	21	494	540	16	426	476	37	1033	1112	60	48	49	7.7	66.1	65.6
	±6	±16	±12	±2.2	±1.7	±1.4	±10	±291	±152	±8	±226	±98	±18	±582	±253	±30	±31	±16	±2.1	±42.6	±17.4

APPENDIX B

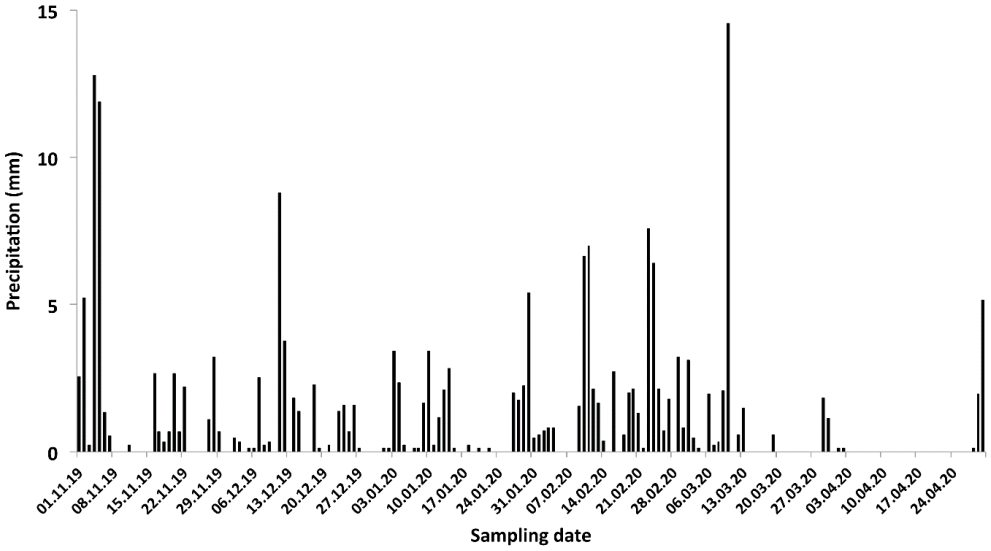

Figure B-1. Daily precipitation during the study period (2019/2020).

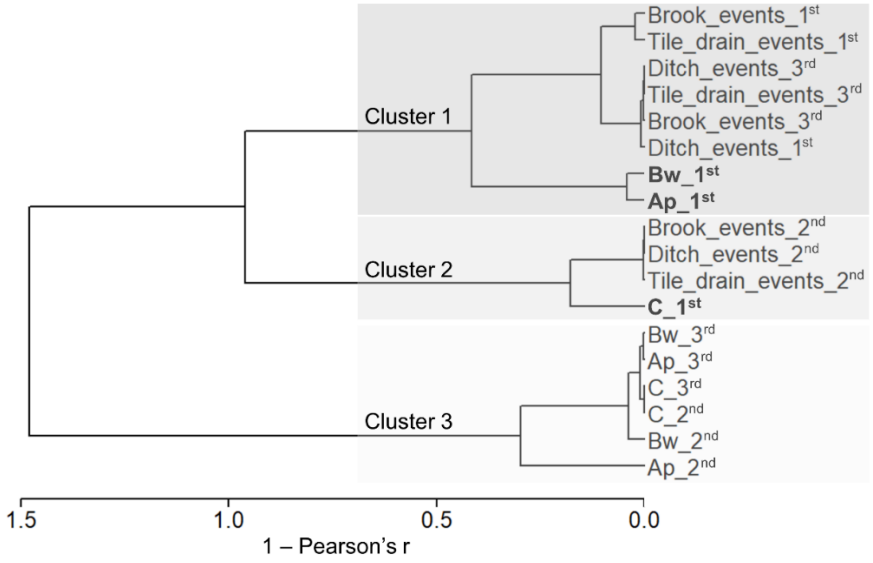

Figure B-2. Hierarchical cluster analysis of water and soil colloid samples. The last number of the sample name means the 1st, 2nd, or 3rd size fraction; TD = tile drain, DI = ditch, and BR = brook. Ap, Bw, and C denotes the soil horizons. n=13 (water samples) and n=9 (soil samples).

Appendix C

Supplementary materials for chapter 4

Uptake of essential (Cu, Zn and Fe) and non-essential (Ag, Ce and Ti) elements containing metallic nanoparticles by crops: A meta-analysis

APPENDIX C

Table C-1. Hydrodynamics diameters and dissolution behaviors of MNPs.

Types of MNPs	Main applications	TEM/SEM size (median) / nm	Hydrodynamic diameter (median) / nm	Dissolution behaviors	
				Rates	Solubilities
Ag	Electronics, biosensing, clothing, food industry	5 to 190 (23)	10 to 428 (52)	1.3×10^{-6} to 2.9×10^{-5} mol m^{-2} h^{-1} with pH from 4.5 to 7.7 (Hedberg et al., 2019)	
Ag_2S	Photocatalyst, biosensing, bioimaging	18 to 85 (37)	16 to 308 (91)		
ZnO	Biomedicine, food packaging, photocatalyst	8 to 270 (32)	20 to 1486 (248)	8.1×10^{-5} to 2.6×10^{-4} mol m^{-2} h^{-1} with pH from 6.4 to 8.6 (Hedberg et al., 2019)	
CeO_2	Catalysts, fuel/glass additives	2 to 64 (21)	2 to 2547 (184)	57.6 and 16.8 μM kg^{-1} h^{-1} for 33 nm at pH 1.6 and 4.7, respectively; 74.1 and 17.7 μM kg^{-1} h^{-1} for 77 nm at pH 1.6 and 4.7, respectively (Dahle et al., 2015)	
Fe^0	Soil and water remediation, purification	4 to 60 (32)	200 to 310 (280)		53 mg L^{-1} at pH 3 (Eljamal et al., 2018)
Fe_2O_3	Water remediation and purification	5 to 30 (10)	154 to 268 (164)		1 to 36 μmol L^{-1} for 4 nm α Fe_2O_3; 1 to 5 μmol L^{-1} for 40 nm α Fe_2O_3 (Barton et al., 2012); 3 to 10 folds higher dissolution rates of 8 nm than 40 nm α Fe_2O_3 (Lanzl et al., 2012)
Fe_3O_4	Water remediation and purification, biomedicine	10 to 75 (23)	230 to 1000 (354)		3.5×10^{-5} to 3.65×10^{-3} mol L^{-1}
Cu	Catalysts, nanofertilizer, nanopestcide, nanoherbicide, food packaging	15 to 550 (50)	91 to 2590 (244)	4.8×10^{-4} to 1.0×10^{-2} mol m^{-2} h^{-1} with pH from 6.2 to 7.0 (Tsykhanovska et al., 2019)	
CuO	Biomedicine, catalysis, electrochemistry, antifouling coatings, biocidal agents	13 to 60 (31)	40 to 1000 (280)	4.4×10^{-6} to 7.6×10^{-4} mol m^{-2} h^{-1} with pH from 5.8 to 7.7 (Hedberg et al., 2019)	
TiO_2	Photocatalyst, semiconductor, biomedicine	4 to 655 (27)			21 μmol L^{-1} at pH 1.5 (Schmidt et al., 2006)

APPENDIX C

Table C-2.1 Heterogeneity and publication bias tests for root Ag concentrations.

Group	Factors	Nr.	I^2 (%)	*P* for heterogeneity	*P* for publication bias	Group	Factors	Nr.	I^2 (%)	*P* for heterogeneity	*P* for publication bias
Overall	/	119	69.4	< 0.01	0.6660		Maize	9	33.9	0.1463	/
	1 ~ 10	28	24.5	0.1207	0.2036		Rice	16	0.00	0.7441	/
Particle size (nm)	10 ~ 30	65	72.6	< 0.01	< 0.01		Wheat	58	80.1	< 0.01	0.6287
	30 ~ 60	26	76.2	< 0.01	< 0.01	Crops	Canola	2	0.00	0.3612	/
	< -20	65	75.8	< 0.01	0.2132		Bean	7	50.0	0.0619	/
Zeta potential (mV)	> -20	29	56.9	< 0.01	0.6319		Tomato	2	0.00	0.4463	/
	Unsure	25	52.9	< 0.01	/		Other crops	25	40.3	0.0203	0.4875
	PVP	57	55.2	< 0.01	< 0.01		Soil	58	79.1	< 0.01	0.6585
	Citrate	37	82.8	< 0.01	< 0.01	Growth medium	Hydroponics	56	45.2	< 0.01	0.4299
Surface coating	Other coatings	5	37.8	0.1695	/		Other mediums	5	0.00	0.9125	/
	Bare	20	39.0	0.0390	/		< 1 d	29	69.9	< 0.01	0.3742
	< 1	19	23.1	0.1749	/	Growth period	1 d ~ 1 week	45	56.9	< 0.01	0.5099
Applied concentration	1 ~ 100	90	73.8	< 0.01	0.3287		1 week ~ 1 month	27	76.7	< 0.01	0.6129
(ppm)	100 ~ 1000	8	48.3	0.0598	/		> 1 month	18	73.3	< 0.01	0.5460
	> 1000	2	0.00	0.5425	/	MNPs type	Ag	103	68.7	< 0.01	< 0.01
							Ag_2S	16	63.7	< 0.01	0.5146

APPENDIX C

Table C-2.2 Heterogeneity and publication bias tests for shoot Ag concentrations.

Group	Factors	Nr.	I^2 (%)	*P* for heterogeneity	*P* for publication bias	Group	Factors	Nr.	I^2 (%)	*P* for heterogeneity	*P* for publication bias
Overall	/	121	76.1	< 0.01	0.9325	Crops	Maize	9	50.3	0.0412	/
Particle size (nm)	1 ~ 10	32	65.0	< 0.01	< 0.01		Rice	22	42.0	0.0207	/
	10 ~ 30	68	75.7	< 0.01	0.3972		Wheat	59	82.7	< 0.01	0.5447
	30 ~ 60	21	82.0	< 0.01	0.4164		Canola	2	0.00	0.8235	/
Zeta potential (mV)	< -20	59	82.7	< 0.01	0.3539		Bean	5	15.8	0.3137	/
	> -20	32	36.0	0.0241	< 0.01		Tomato	6	0	0.5454	/
	Unsure	30	58.1	< 0.01	< 0.01		Other crops	18	71.6	< 0.01	< 0.01
Surface coating	PVP	61	66.4	< 0.01	< 0.01	Growth medium	Soil	56	79.1	< 0.01	0.0592
	Citrate	32	82.8	< 0.01	0.3725		Hydroponics	62	53.9	< 0.01	< 0.01
	PEG+Tween20	4	33.4	0.2119	/		Other mediums	3	94.1	< 0.01	/
	PEG	2	0.00	0.5228	/	Exposure period	< 1 d	29	70.7	< 0.01	0.9674
	Other coatings	3	44.1	0.1671	/		1 d ~ 1 week	51	65.8	< 0.01	0.4610
	Bare	19	78.9	< 0.01	< 0.01		1 week ~ 1 month	21	86.8	< 0.01	0.7855
Applied concentration (ppm)	< 1	23	66.4	< 0.01	< 0.01		> 1 month	20	80.3	< 0.01	0.1604
	1 ~ 100	86	78.6	< 0.01	0.1378	MNPs type	Ag	106	74.3	< 0.01	0.0851
	100 ~ 1000	10	60.8	< 0.01	0.020		Ag_2S	15	70.7	< 0.01	0.1567
	> 1000	2	0.00	0.0151	/	Exposure way	Root	118	76.3	< 0.01	0.8732
							Foliar	3	54.3	0.1119	/

Table C-2.3 Heterogeneity and publication bias tests for leaf Ag concentrations.

Group	Factors	Nr.	I^2 (%)	*P* for heterogeneity	*P* for publication bias	Group	Factors	Nr.	I^2 (%)	*P* for heterogeneity	*P* for publication bias
Overall	/	90	70.2	< 0.01	< 0.01		Barley	2	3.70	0.3082	/
Particle size (nm)	1 ~ 10	16	73.4	< 0.01	0.6338		Bean	6	0.00	0.9130	/
	10 ~ 30	40	65.0	< 0.01	0.0305	Crops	Tomato	29	28.5	0.0784	/
	30 ~ 60	34	30.8	0.0472	/		Citrus	36	57.0	< 0.01	/
Zeta potential (mV)	< -20	46	59.3	< 0.01	0.0100		Other crops	17	48.6	0.0130	0.2291
	Unsure	44	49.8	< 0.01	0.5201	Growth medium	Soil	39	58.0	< 0.01	0.0664
Surface coating	PVP	23	49.3	< 0.01	< 0.01		Hydroponics	15	23.7	0.1910	0.6858
	Citrate	19	64.5	< 0.01	0.0866		Other mediums	36	57.7	< 0.01	/
	PEG	3	42.8	0.1739	/	Growth period	1 d ~ 1 week	77	67.4	< 0.01	< 0.01
	GA	12	63.2	< 0.01	/		1 week ~ 1 month	8	1.70	0.4160	/
	Other coatings	2	68.9	0.0731	/		> 1 month	5	62.8	0.0296	/
	Bare	31	34.9	0.0304	/	Exposure way	Root	63	73.8	< 0.01	< 0.01
Applied concentration (ppm)	< 1	10	55.5	0.0165	0.1503		Foliar	15	51.4	0.0112	0.0595
	1 ~ 100	80	67.5	< 0.01	< 0.01		Branch	12	62.6	< 0.01	/

APPENDIX C

Table C-3.1 Heterogeneity and publication bias tests for root Ce concentrations.

Group	Factors	Nr.	I^2 (%)	*P* for heterogeneity	*P* for publication bias	Group	Factors	Nr.	I^2 (%)	*P* for heterogeneity	*P* for publication bias
Overall	/	55	71.1	< 0.01	0.8542		Rice	7	47.5	0.0760	/
Particle size (nm)	1 ~ 10	29	74.4	< 0.01	< 0.01		Barley	6	73.5	< 0.01	/
	10 ~ 30	18	69.2	< 0.01	0.0445		Bean	14	52.1	0.0120	0.8665
	30 ~ 60	8	32.3	0.1702	/		Tomato	9	63.5	< 0.01	/
Zeta potential (mV)	> -20	4	21.0	0.2840	/	Crops	Cucumber	2	0.00	0.7960	/
	< 20	9	69.7	< 0.01	/		Carrot	4	46.4	0.1328	/
	> 20	12	75.8	< 0.01	0.0136		Cilantro	4	22.8	0.2739	/
	Unsure	30	65.2	< 0.01	0.0482		Grass	4	0.00	0.8037	/
Surface coating	PVP	3	37.9	0.1998	/		Other crops	5	86.7	< 0.01	/
	Citrate	4	33.9	0.2087	/	Growth medium	Soil	47	72.9	< 0.01	0.9303
	Bare	48	72.2	< 0.01	0.6144		Hydroponics	4	50.3	0.1098	/
Applied concentration (ppm)	1 ~ 100	18	63.4	< 0.01	0.3821		Other mediums	4	0.00	0.7104	/
	100 ~ 1000	36	61.4	< 0.01	0.6074	Growth period	1 d ~ 1 week	6	39.2	0.1443	/
	> 1000	1	/	/	/		1 week ~ 1 month	11	71.3	< 0.01	0.0543
Exposure way	Root	53	62.7	< 0.01	0.0720		> 1 month	38	65.3	< 0.01	< 0.01
	Foliar	2	0.00	0.9292	/	MNPs type	Ce	3	0.00	0.6281	/
							CeO_2	52	72.2	< 0.01	0.6869

APPENDIX C

Table C-3.2 Heterogeneity and publication bias tests for shoot Ce concentrations.

Group	Factors	Nr.	I^2 (%)	*P* for heterogeneity	*P* for publication bias	Group	Factors	Nr.	I^2 (%)	*P* for heterogeneity	*P* for publication bias
Overall	/	61	61.3	< 0.01	0.0474	Crops	Maize	2	0.00	0.7888	/
Particle size (nm)	1 ~ 10	44	42.2	< 0.01	0.2101		Rice	7	39.1	0.1308	/
	10 ~ 30	12	79.8	< 0.01	0.1158		Barley	6	33.3	0.1862	/
	30 ~ 60	5	58.2	< 0.01	/		Bean	15	24.3	0.1847	/
Zeta potential (mV)	> -20	16	59.0	< 0.01	0.8749		Tomato	9	19.1	0.2725	/
	< 20	6	33.3	0.1862	/		Cucumber	11	67.5	< 0.01	/
	> 20	21	74.0	< 0.01	0.1349		Cilantro	4	23.0	0.2728	/
Surface coating	Unsure	18	0.00	0.6777	0.2871		Grass	4	58.8	0.0636	/
	Citrate	4	18.5	0.2980	/		Other crops	3	80.1	< 0.01	/
	Bare	57	62.8	< 0.01	0.0538	Growth medium	Soil	32	61.6	< 0.01	0.0514
Applied concentration (ppm)	1 ~ 100	17	38.1	0.0562	0.2740		Hydroponics	25	63.1	< 0.01	0.7032
	100 ~ 1000	40	61.5	< 0.01	0.2221		Other mediums	4	22.4	0.2762	/
	> 1000	4	34.6	0.2045	/	Growth period	1 d ~ 1 week	20	46.6	0.0118	0.8398
Exposure way	Root	59	60.8	< 0.01	0.0743		1 week ~ 1 month	18	65.7	< 0.01	0.2922
	Foliar	2	58.7	0.1196	/		> 1 month	23	64.5	< 0.01	< 0.01

APPENDIX C

Table C-3.3 Heterogeneity and publication bias tests for leaf Ce concentrations.

Group	Factors	Nr.	I^2 (%)	*P* for heterogeneity	*P* for publication bias	Group	Factors	Nr.	I^2 (%)	*P* for heterogeneity	*P* for publication bias
Overall	/	58	76.7	< 0.01	0.3005		Maize	2	0.00	0.4592	/
	1 ~ 10	27	64.7	< 0.01	0.0873		Wheat	6	74.2	< 0.01	/
Particle size	10 ~ 30	20	79.0	< 0.01	0.8404		Barley	6	0.00	0.8895	/
(nm)	30 ~ 60	5	81.0	< 0.01	/		Sunflower	6	85.5	< 0.01	/
	60 ~ 100	6	70.7	< 0.01	/	Crops	Bean	12	70.9	< 0.01	0.0331
	< 20	15	85.9	< 0.01	0.1173		Tomato	8	24.4	0.2349	/
Zeta potential (mV)	> 20	18	78.5	< 0.01	0.1140		Pumpkin	6	81.7	< 0.01	/
	Unsure	25	51.3	< 0.01	0.0651		Grass	4	72.2	0.0129	/
	PVP	3	23.8	0.2692	/		Other crops	8	72.8	< 0.01	/
Surface coating	Citrate	4	30.0	0.2324	/	Growth	Soil	40	74.2	< 0.01	0.3482
	GA	9	84.1	< 0.01	/	medium	Hydroponics	18	80.1	< 0.01	/
	Bare	42	75.9	< 0.01	0.6382		1 d ~ 1 week	18	80.1	< 0.01	/
Applied concentration	1 ~ 100	28	78.4	< 0.01	0.7915	Growth period	1 week ~ 1 month	2	79.2	0.0285	/
(ppm)	100 ~ 1000	30	73.3	< 0.01	0.0330		> 1 month	38	72.9	< 0.01	0.4986
Exposure way	Root	55	76.0	< 0.01	0.4484	MNPs type	Ce	3	0.00	0.4873	/
	Foliar	3	79.2	0.0285	/		CeO_2	55	76.4	< 0.01	< 0.01

APPENDIX C

Table C-4.1 Heterogeneity and publication bias tests for root Ti concentrations.

Group	Factors	Nr.	I^2 (%)	*P* for heterogeneity	*P* for publication bias	Group	Factors	Nr.	I^2 (%)	*P* for heterogeneity	*P* for publication bias
Overall	/	41	81.8	< 0.01	0.6603	Crops	Wheat	12	87.3	< 0.01	0.6612
Particle size (nm)	1 ~ 10	8	52.3	0.0404	/		Barley	6	69.9	< 0.01	/
	10 ~ 30	28	85.5	< 0.01	0.9901		Sorghum	9	0.00	0.7493	/
	60 ~ 100	5	75.2	< 0.01	/		Tomato	6	34.6	0.1768	/
Zeta potential (mV)	> -20	5	64.4	0.0239	/		Cilantro	4	41.2	0.1643	/
	< 20	6	69.9	< 0.01	/		Other crops	4	6.6	0.3600	/
	> 20	6	34.6	0.1768	/	Growth medium	Soil	26	83.0	< 0.01	0.1827
	Unsure	24	79.9	< 0.01	0.4172		Hydroponics	15	75.9	< 0.01	< 0.01
Applied concentration (ppm)	1 ~ 100	17	70.8	< 0.01	0.9841	Growth period	1 d ~ 1 week	4	41.2	0.1643	/
	100 ~ 1000	22	85.6	< 0.01	0.0393		1 week ~ 1 month	11	78.4	< 0.01	0.0380
	> 1000	2	52.2	0.1481	/		> 1 month	26	83.0	< 0.01	0.1827

APPENDIX C

Table C-4.2 Heterogeneity and publication bias tests for shoot Ti concentrations.

Group	Factors	Nr.	I^2 (%)	*P* for heterogeneity	*P* for publication bias	Group	Factors	Nr.	I^2 (%)	*P* for heterogeneity	*P* for publication bias
Overall	/	44	71.8	< 0.01	0.1977		Wheat	9	89.8	< 0.01	/
	1 ~ 10	8	70.5	< 0.01	/		Barley	6	59.4	0.0306	/
Particle size	10 ~ 30	28	77.9	< 0.01	0.1632		Sorghum	9	0.00	0.8973	/
(nm)	60 ~ 100	5	0.00	0.5406	/	Crops	Tomato	6	12.3	0.3365	/
	> 100	3	24.1	0.2679	/		Cilantro	4	0.00	0.9188	/
	> -20	2	52.6	0.1463	/		Alfalfa	6	0.00	0.6904	/
Zeta potential	< 20	6	59.4	0.0306	/		Other crops	4	0.00	0.4213	/
(mV)	> 20	6	12.3	0.3365	/	Growth	Soil	32	70.6	< 0.01	0.1100
	Unsure	30	73.0	< 0.01	0.2261	medium	Hydroponics	12	76.2	< 0.01	0.5375
	1 ~ 100	19	70.6	< 0.01	0.4305		1 d ~ 1 week	4	0.00	0.9188	/
Applied concentration (ppm)	100 ~ 1000	23	73.1	< 0.01	0.4043	Growth period	1 week ~ 1 month	8	84.6	< 0.01	/
	> 1000	2	0.00	0.5981	/		> 1 month	32	70.6	< 0.01	0.1100

Table C-4.3 Heterogeneity and publication bias tests for leaf Ti concentrations.

Group	Factors	Nr.	I^2 (%)	*P* for heterogeneity	*P* for publication bias	Group	Factors	Nr.	I^2 (%)	*P* for heterogeneity	*P* for publication bias
Overall	/	14	45.2	0.0399	0.9235		Rice	4	44.0	0.1472	/
Particle size (nm)	1 ~ 10	4	44.0	0.1472	/	Crops	Wheat	4	54.9	0.0840	/
	10 ~ 30	9	49.0	0.0469	/		Barley	6	56.7	0.0416	/
	30 ~ 60	1	/	/	/	Growth medium	Soil	7	56.2	0.0331	/
Zeta potential (mV)	> -20	3	39.1	0.1937	/		Hydroponics	7	38.4	0.1363	/
	< 20	6	56.7	0.0416	/	Growth period	1 week ~ 1 month	7	38.4	0.1363	/
	Unsure	5	41.6	0.1441	/		> 1 month	7	56.2	0.0331	/
Applied concentration (ppm)	< 1	2	0.00	0.3414	/						
	1 ~ 100	6	53.3	0.0575	/						
	100 ~ 1000	6	56.7	0.0416	/						

APPENDIX C

Table C-5.1 Heterogeneity and publication bias tests for root Zn concentrations.

Group	Factors	Nr.	I^2 (%)	*P* for heterogeneity	*P* for publication bias	Group	Factors	Nr.	I^2 (%)	*P* for heterogeneity	*P* for publication bias
Overall	/	57	71.5	< 0.01	0.3194		Maize	8	57.1	0.0225	/
	1 ~ 10	6	20.9	0.2759	/		Rice	10	68.1	< 0.01	/
Particle size	10 ~ 30	27	68.9	< 0.01	0.1312		Wheat	14	48.3	0.0220	0.5783
(nm)	30 ~ 60	20	62.8	< 0.01	0.6316	Crops	Bean	6	20.9	0.2759	/
	60 ~ 100	4	81.3	< 0.01	/		Tomato	7	58.4	0.0254	/
	< -20	12	78.2	< 0.01	0.1456		Cucumber	5	76.7	0.0018	/
Zeta potential (mV)	> -20	6	64.0	0.0164	/		Other crops	7	80.9	< 0.01	/
	Unsure	39	65.8	< 0.01	0.2429		Soil	44	66.8	< 0.01	0.2154
Applied	1 ~ 100	40	70.7	< 0.01	0.1307	Growth medium	Hydroponics	8	71.2	< 0.01	/
concentration	100 ~ 1000	13	70.9	< 0.01	0.5329		Other mediums	5	81.8	< 0.01	/
(ppm)	> 1000	4	51.4	0.1035	/		1 d ~ 1 week	7	49.5	0.0646	/
Exposure way	Root	45	65.1	< 0.01	0.5856	Growth period	1 week ~ 1 month	16	72.7	< 0.01	0.2609
	Foliar	12	83.7	< 0.01	0.0378		> 1 month	34	72.1	< 0.01	0.0116

Table C-5.2 Heterogeneity and publication bias tests for shoot Zn concentrations.

Group	Factors	Nr.	I^2 (%)	*P* for heterogeneity	*P* for publication bias	Group	Factors	Nr.	I^2 (%)	*P* for heterogeneity	*P* for publication bias
Overall	/	59	73.1	< 0.01	0.7394	Crops	Maize	8	76.0	< 0.01	/
Particle size (nm)	1 ~ 10	6	38.8	0.1470	/		Rice	10	69.2	< 0.01	/
	10 ~ 30	23	69.0	< 0.01	0.0809		Wheat	12	69.8	< 0.01	0.6003
	30 ~ 60	24	69.6	< 0.01	0.2778		Bean	9	45.3	0.0666	/
	60 ~ 100	6	86.0	< 0.01	/		Tomato	6	28.2	0.2230	/
Zeta potential (mV)	< -20	12	75.2	< 0.01	0.1280		Cucumber	5	81.3	< 0.01	/
	> -20	6	69.3	< 0.01	/		Other crops	9	39.0	0.1079	/
	< 20	2	55.2	0.1350	/	Growth medium	Soil	40	67.8	< 0.01	0.3727
	Unsure	39	70.3	< 0.01	0.0235		Hydroponics	9	73.7	< 0.01	/
Applied concentration (ppm)	1 ~ 100	36	70.6	< 0.01	0.5041		Other mediums	10	77.1	< 0.01	/
	100 ~ 1000	19	75.5	< 0.01	0.0206	Growth period	1 d ~ 1 week	12	58.2	< 0.01	0.1409
	> 1000	4	0.00	0.3953	/		1 week ~ 1 month	17	67.1	< 0.01	0.0941
Exposure way	Root	48	72.1	< 0.01	0.0346		> 1 month	30	70.9	< 0.01	< 0.01
	Foliar	11	77.6	< 0.01	0.0701						

APPENDIX C

Table C-5.3 Heterogeneity and publication bias tests for leaf Zn concentrations.

Group	Factors	Nr.	I^2 (%)	*P* for heterogeneity	*P* for publication bias	Group	Factors	Nr.	I^2 (%)	*P* for heterogeneity	*P* for publication bias
Overall	/	34	77.6	< 0.01	< 0.01	Crops	Maize	2	0.00	0.4147	/
Particle size (nm)	1 ~ 10	8	2.70	0.4092	/		Canola	18	69.6	< 0.01	/
	10 ~ 30	3	74.6	0.0196	/		Bean	6	0.00	0.6522	/
	30 ~ 60	20	67.9	< 0.01	/		Other crops	8	79.7	< 0.01	/
	60 ~ 100	3	50.9	0.1307	/	Growth period	1 week ~ 1 month	1	/	/	/
Zeta potential (mV)	< -20	1	/	/	/		> 1 month	33	78.0	< 0.01	< 0.01
	Unsure	33	77.8	< 0.01	< 0.01	MNPs type	Zn	20	78.8	< 0.01	< 0.01
Applied concentration (ppm)	1 ~ 100	29	75.6	< 0.01	< 0.01		ZnO	14	60.4	< 0.01	0.1039
	100 ~ 1000	5	51.5	0.0828	/	Exposure way	Root	17	81.4	< 0.01	< 0.01
							Foliar	11	78.2	< 0.01	0.0850
							Seed + Foliar	6	0.00	0.8353	/

APPENDIX C

Table C-6.1 Heterogeneity and publication bias tests for root Fe concentrations.

Group	Factors	Nr.	I^2 (%)	*P* for heterogeneity	*P* for publication bias	Group	Factors	Nr.	I^2 (%)	*P* for heterogeneity	*P* for publication bias
Overall	/	68	79.7	< 0.01	0.2194		Maize	8	49.7	0.0528	/
	1 ~ 10	3	53.3	0.1177	/		Rice	9	57.3	0.0163	/
Particle size	10 ~ 30	39	82.1	< 0.01	0.2502		Wheat	14	73.0	< 0.01	0.2854
(nm)	30 ~ 60	14	30.9	0.1287	/	Crops	Cucumber	17	22.4	0.1939	/
	60 ~ 100	12	65.3	< 0.01	/		Muskmelon	6	72.1	< 0.01	/
	< -20	12	0.00	0.8145	/		Citrus	6	67.2	< 0.01	/
	> -20	13	69.0	< 0.01	/		Other crops	8	70.2	< 0.01	/
Zeta potential	< 20	2	0.00	0.4096	/		1 d ~ 1 week	6	12.8	0.3329	/
(mV)	> 20	9	57.3	0.0163	/	Growth period	1 week ~ 1 month	35	81.1	< 0.01	< 0.01
	Unsure	32	70.5	< 0.01	0.3446		> 1 month	27	72.2	< 0.01	0.8230
Applied	< 1	6	11.3	0.3434	/		Fe	9	33.5	0.1497	/
concentration	1 ~ 100	41	76.7	< 0.01	0.8703		Fe_2O_3	24	81.5	< 0.01	0.4399
(ppm)	100 ~ 1000	21	84.3	< 0.01	0.0530	MNPs type	Fe_3O_4	21	78.4	< 0.01	< 0.01
Growth	Soil	29	71.4	< 0.01	0.7592		$FePO_4$	6	0.00	0.8010	/
medium	Hydroponics	39	79.3	< 0.01	< 0.01		$CuFe_2O_4$	8	25.9	0.2220	/
Exposure way	Root	60	79.8	< 0.01	0.5814						
	Foliar	8	71.9	0.0656	/						

Table C-6.2 Heterogeneity and publication bias tests for shoot Fe concentrations.

Group	Factors	Nr.	I^2 (%)	*P* for heterogeneity	*P* for publication bias	Group	Factors	Nr.	I^2 (%)	*P* for heterogeneity	*P* for publication bias
Overall	/	73	69.4	< 0.01	0.0786	Crops	Maize	11	68.2	< 0.01	/
Particle size (nm)	1 ~ 10	8	0.00	0.5396	/		Wheat	14	63.8	< 0.01	0.8277
	10 ~ 30	36	71.3	< 0.01	0.0190		Bean	8	0.00	05396	/
	30 ~ 60	17	25.3	0.1628	/		Peanut	7	65.4	< 0.01	/
	60 ~ 100	12	67.9	< 0.01	/		Cucumber	17	61.3	< 0.01	/
Zeta potential (mV)	< -20	12	70.2	< 0.01	/		Muskmelon	6	0.00	0.9339	/
	> -20	13	64.2	< 0.01			Citrus	6	69.0	< 0.01	/
	Unsure	48					Other crops	4	55.4	0.0810	/
Applied concentration (ppm)	< 1	8	43.4	0.0893	/	Growth period	1 d ~ 1 week	7	3.90	0.3968	/
	1 ~ 100	51	69.3	< 0.01	0.0487		1 week ~ 1 month	30	66.9	< 0.01	/
	100 ~ 1000	14	76.5	< 0.01	0.2766		> 1 month	36	71.3	< 0.01	0.1422
Growth medium	Soil	40	70.3	< 0.01	0.1576	MNPs type	Fe	6	0.00	0.9277	/
	Hydroponics	33	68.2	< 0.01	/		Fe_2O_3	29	70.3	< 0.01	0.0819
	Root	59	71.2	< 0.01	0.0497		Fe_3O_4	24	71.1	< 0.01	0.3006
Exposure way	Foliar	14	52.0	0.0121	0.1257		$FePO_4$	6	65.4	0.0131	/
							$CuFe_2O_4$	8	32.9	0.1657	/

APPENDIX C

Table C-6.3 Heterogeneity and publication bias tests for leaf Fe concentrations.

Group	Factors	Nr.	I^2 (%)	*P* for heterogeneity	*P* for publication bias	Group	Factors	Nr.	I^2 (%)	*P* for heterogeneity	*P* for publication bias
Overall	/	18	90.8	< 0.01	< 0.01		Rice	9	86.9	< 0.01	/
Particle size	1 ~ 10	3	90.1	< 0.01	/	Crops	Muskmelon	6	0.00	0.4461	/
(nm)	10 ~ 30	15	90.2	< 0.01	< 0.01		Other crops	3	43.5	0.1704	/
	< 20	2	0.00	0.8595	/	Growth	Soil	8	62.3	< 0.01	/
Zeta potential	> 20	9	86.9	< 0.01	/	medium	Hydroponics	10	85.3	< 0.01	/
(mV)	Unsure	7	56.8	0.0307	/	Growth period	1 week ~ 1 month	12	90.9	< 0.01	0.0215
Applied	1 ~ 100	7	89.1	< 0.01	/		> 1 month	6	0.00	0.4461	/
concentration (ppm)	100 ~ 1000	11	92.3	< 0.01	< 0.01	MNPs type	Fe	3	90.1	< 0.01	/
							Fe_2O_3	6	91.4	< 0.01	/
							Fe_3O_4	9	90.2	< 0.01	/

APPENDIX C

Table C-7.1 Heterogeneity and publication bias tests for root Cu concentrations.

Group	Factors	Nr.	I^2 (%)	*P* for heterogeneity	*P* for publication bias	Group	Factors	Nr.	I^2 (%)	*P* for heterogeneity	*P* for publication bias
Overall	/	106	69.2	< 0.01	0.0766	Crops	Rice	36	66.7	< 0.01	0.3639
Particle size (nm)	10 ~ 30	44	67.8	< 0.01	0.5718		Wheat	2	67.1	0.0811	/
	30 ~ 60	53	67.8	< 0.01	< 0.01		Bean	6	15.3	0.3161	/
	> 100	9	70.6	< 0.01	/		Tomato	20	41.6	0.0271	/
Zeta potential (mV)	< -20	46	73.1	< 0.01	< 0.01		Cucumber	16	63.2	< 0.01	0.1728
	> -20	5	56.9	0.0544	/		Lettuce	6	60.6	0.0265	/
	Unsure	55	65.9	< 0.01	0.1696		Other crops	20	60.2	< 0.01	0.0347
Applied concentration (ppm)	< 1	10	60.1	< 0.01	/	Growth medium	Soil	62	67.1	< 0.01	0.0255
	1 ~ 100	60	70.7	< 0.01	< 0.01		Hydroponics	36	69.1	< 0.01	0.0540
	100 ~ 1000	32	62.7	< 0.01	< 0.01		Other mediums	8	0.00	0.9315	/
	> 1000	4	3.8	0.3739	/	Growth period	< 1 d	10	10.7	0.3446	/
MNPs type	Cu	12	70.6	< 0.01	0.0146		1 d ~ 1 week	11	68.8	< 0 .01	/
	CuO	76	69.8	< 0.01	0.2518		1 week ~ 1 month	49	71.1	< 0.01	0.2357
	Cu/Se	10	10.7	0.3446	/		> 1 month	36	69.0	< 0.01	< 0.01
	$CuFe_2O_4$	8	71.4	< 0.01	/						

Table C-7.2 Heterogeneity and publication bias tests for shoot Cu concentrations.

Group	Factors	Nr.	I^2 (%)	*P* for heterogeneity	*P* for publication bias	Group	Factors	Nr.	I^2 (%)	*P* for heterogeneity	*P* for publication bias
Overall	/	117	72.9	< 0.01	0.9578	Crops	Rice	36	73.6	< 0.01	0.3957
Particle size (nm)	10 ~ 30	44	74.8	< 0.01	0.6788		Wheat	4	86.6	< 0.01	/
	30 ~ 60	61	71.8	< 0.01	0.6917		Bean	13	59.9	< 0.01	/
	> 100	12	73.2	< 0.01	0.5955		Tomato	20	48.6	< 0.01	/
Zeta potential (mV)	< -20	48	72.2	< 0.01	0.7510		Cucumber	16	80.9	< 0.01	0.0549
	> -20	5	66.4	0.0182	/		Lettuce	6	78.9	< 0.01	/
	Unsure	64	73.6	< 0.01	0.6658		Alfalfa	6	72.9	< 0.01	/
Applied concentration (ppm)	< 1	10	78.6	< 0.01	< 0.01		Other crops	16	28.4	0.1389	/
	1 ~ 100	65	74.7	< 0.01	0.9251	Growth period	< 1 d	10	7.70	0.3706	/
	100 ~ 1000	38	55.5	< 0.01	0.1077		1 d ~ 1 week	20	71.3	< 0.01	0.9231
	> 1000	4	13.6	0.3245	/		1 week ~ 1 month	55	79.1	< 0.01	0.6670
Growth medium	Soil	58	69.3	< 0.01	0.8892		> 1 month	32	52.9	< 0.01	0.0790
	Hydroponics	42	77.8	< 0.01	0.9379	MNPs type	Cu	15	68.4	< 0.01	0.5153
	Other mediums	17	62.2	< 0.01	0.0138		CuO	84	73.6	< 0.01	0.9915
							Cu/Se	10	7.70	0.3706	/
							$CuFe_2O_4$	8	31.7	0.1751	/

APPENDIX C

Table C-7.3 Heterogeneity and publication bias tests for leaf Cu concentrations.

Group	Factors	Nr.	I^2 (%)	*P* for heterogeneity	*P* for publication bias	Group	Factors	Nr.	I^2 (%)	*P* for heterogeneity	*P* for publication bias
Overall	/	54	73.4	< 0.01	0.3016	Crops	Maize	5	41.0	0.1482	/
Particle size (nm)	10 ~ 30	12	82.4	< 0.01	0.0124		Rice	25	65.0	< 0.01	< 0.01
	30 ~ 60	31	53.9	< 0.01	< 0.01		Bean	6	60.4	0.0271	/
	> 100	11	72.9	< 0.01	/		Potato	6	60.4	0.0271	/
Zeta potential (mV)	< -20	21	63.5	< 0.01	< 0.01		Pepper	4	0.00	0.6606	/
	> -20	2	55.9	0.1321	/		Scallion	4	15.8	0.3128	/
	> 20	5	41.0	0.1482	/		Other crops	4	50.6	0.1079	/
	Unsure	26	73.0	< 0.01	0.0753	Growth period	1 d ~ 1 week	4	0.00	0.6160	/
Applied concentration (ppm)	< 1	9	74.1	< 0.01	/		1 week ~ 1 month	15	72.7	< 0.01	0.0214
	1 ~ 100	29	70.9	< 0.01	0.7397		> 1 month	35	73.8	< 0.01	< 0.01
	100 ~ 1000	16	69.6	< 0.01	< 0.01	MNPs type	Cu	13	82.4	< 0.01	0.0141
Exposure way	Root	45	63.7	< 0.01	0.0555		CuO	41	69.2	< 0.01	0.0340
	Foliar	9	40.5	0.0971	/						

APPENDIX C

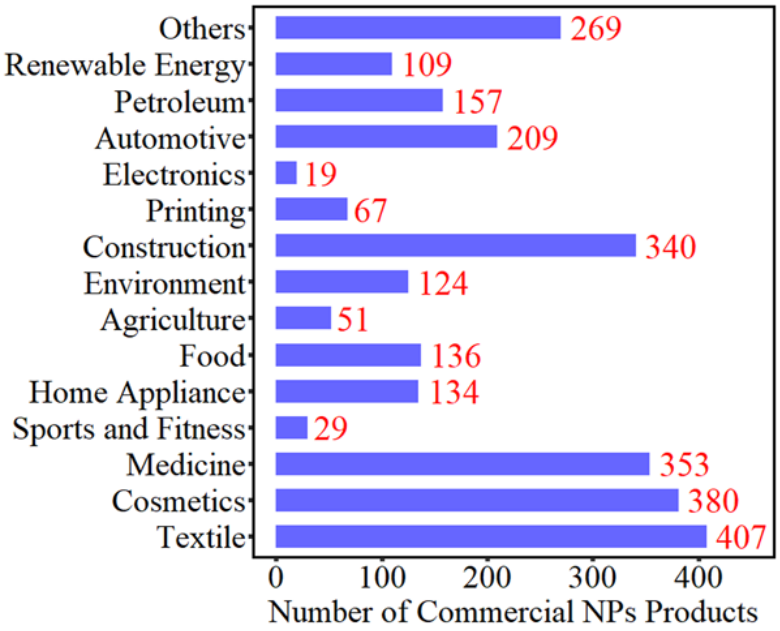

Figure C-1. Number of commercial products of nanoparticles (NPs) in various applications. Data extracted from the Nanotechnology Products Database (accessed on 2022.05.03).

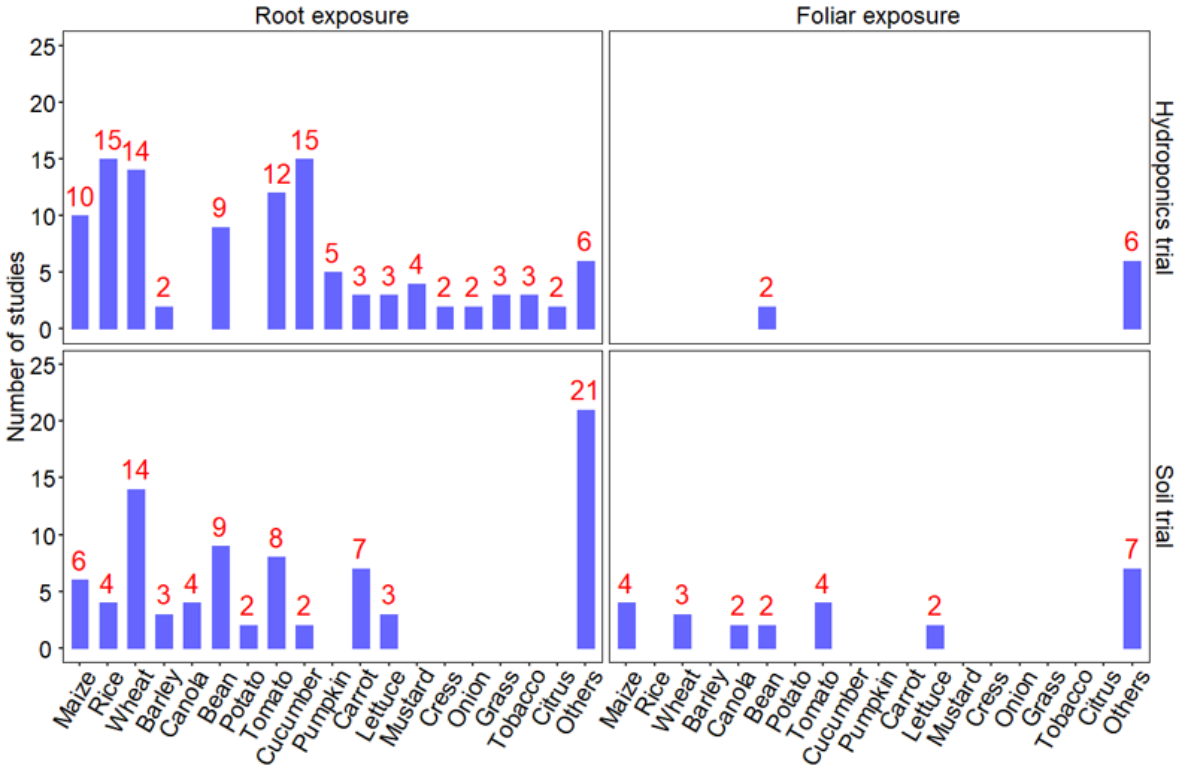

Figure C-2. Number of studies for crop plants been studied. The studies were grouped into soil and hydroponics trials firstly, and further grouped into root and foliar exposure to metallic nanoparticles for each trial type. Only crops with number of studies ≥ 2 were listed separately.

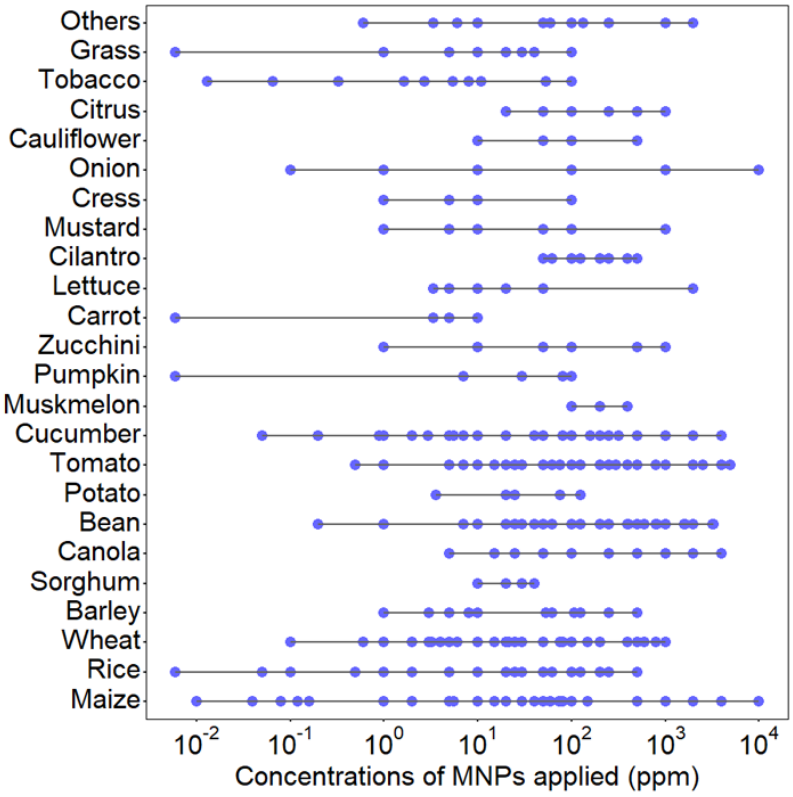

Figure C-3. The application concentrations (ppm) of metallic nanoparticles in studies with various crop plants. Please note the exponential scaled x-axis. Crops studied with ≥ 3 different applied concentration gradients were listed separately.

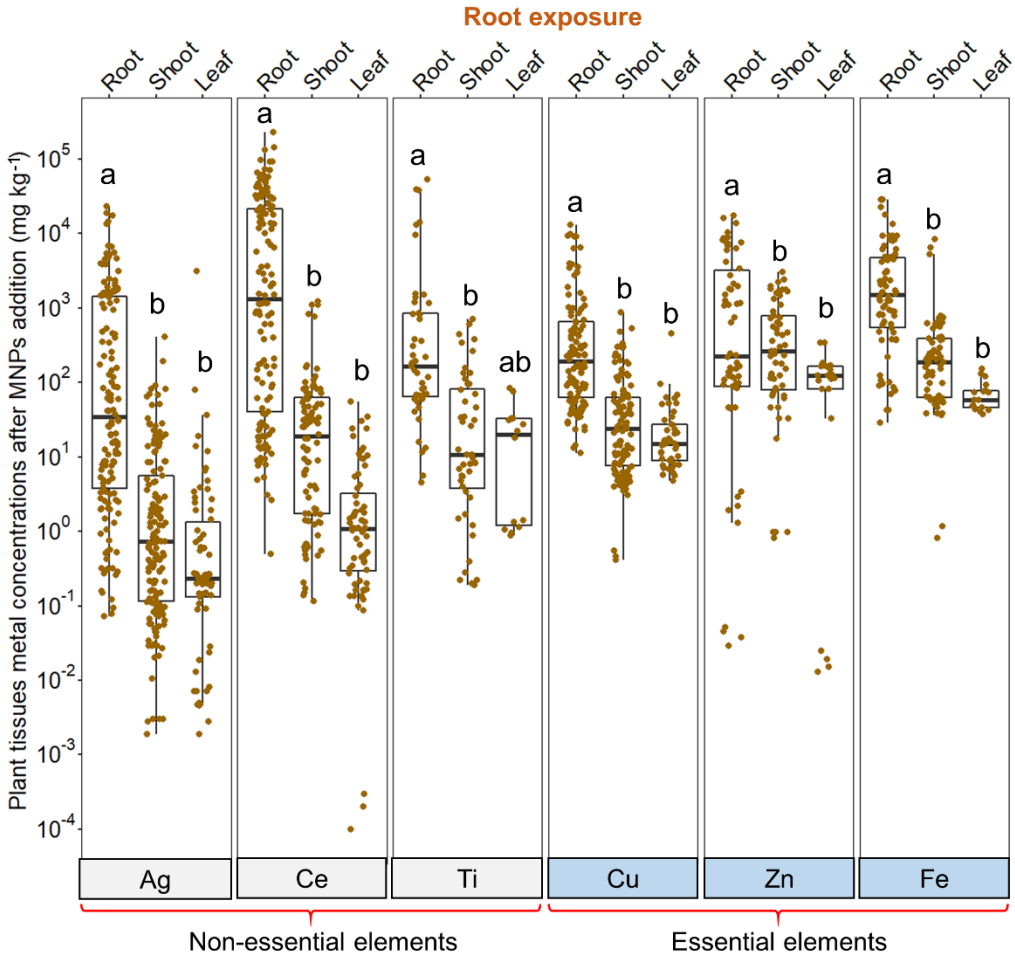

Figure C-4.1. The metal concentrations (mg kg^{-1} dry weight) (exponential-scaled y-axis) in different plant tissues after root exposure to metallic nanoparticles (MNPs). From left to right in each column, it shows metal concentration in root, shoot and leaf tissue, respectively. The left three columns are Ag, Ce and Ti which are non-essential elements, the right three ones are essential elements Cu, Zn and Fe. Significant differences between three tissues for each element were labeled with different lower-case letters. $P < 0.05$.

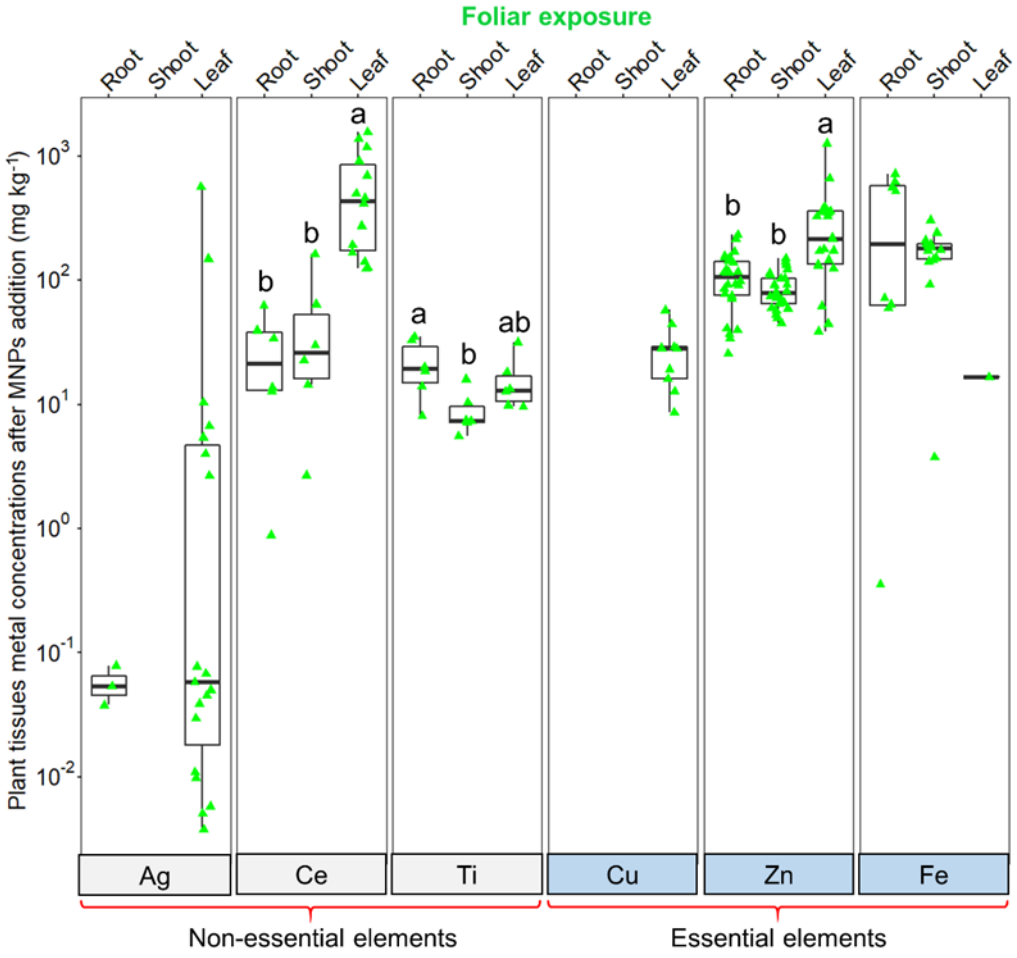

Figure C-4.2. The metal concentrations (mg kg^{-1} dry weight) (exponential-scaled y-axis) in different plant tissues after foliar exposure to metallic nanoparticles (MNPs). From left to right in each column, it shows metal concentration in root, shoot and leaf tissue, respectively. The left three columns are Ag, Ce and Ti which are non-essential elements, the right three ones are essential elements Cu, Zn and Fe. Significant differences between three tissues for each element were labeled with different lower-case letters. $P < 0.05$.

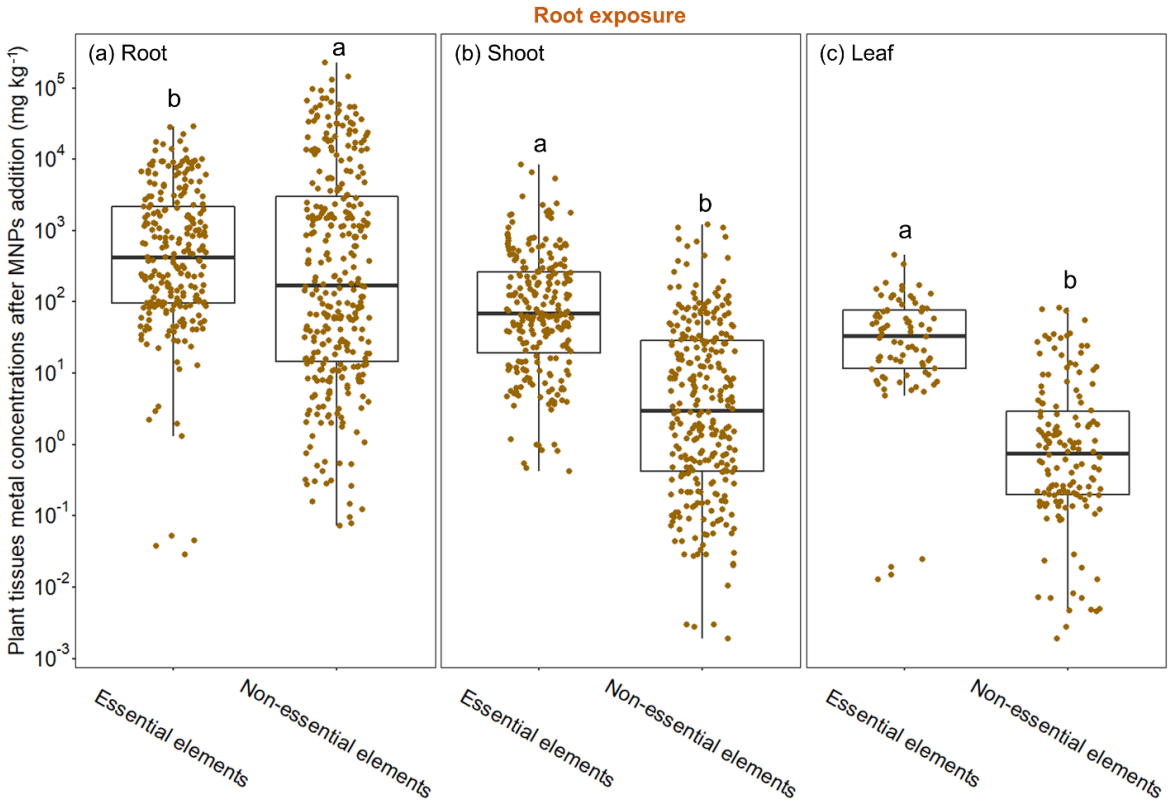

Figure C-4.3. The metal concentrations (mg kg^{-1} dry weight) (exponential-scaled y-axis) in different plant tissues after root exposure to metallic nanoparticles (MNPs). From left to right column, it shows metal concentrations in root, shoot and leaf tissue, respectively. Data of Cu, Zn, Fe is grouped together in essential elements group, and Ag, Ce, Ti is grouped into non-essential elements group. Significant differences between essential and non-essential elements were labeled with different lower-case letters. $P < 0.05$.

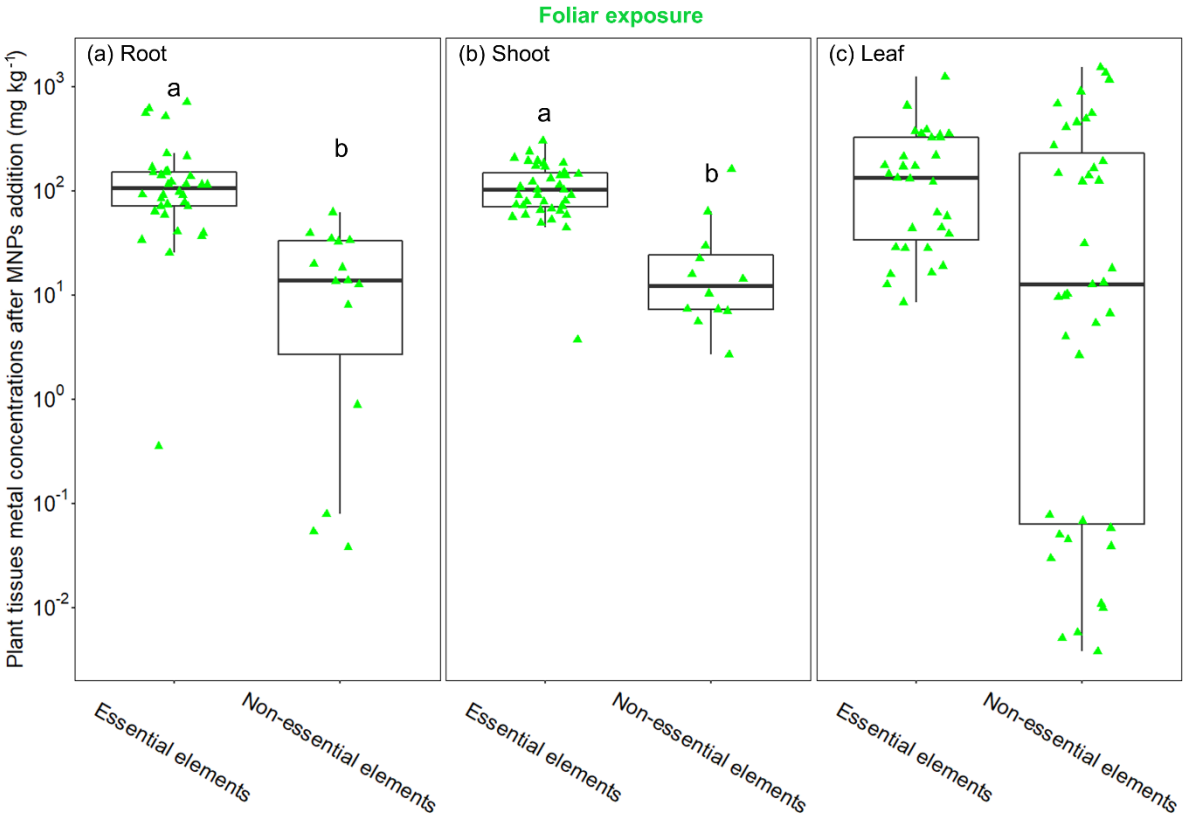

Figure C-4.4. The metal concentrations (mg kg^{-1} dry weight) (exponential-scaled y-axis) in different plant tissues after foliar exposure to metallic nanoparticles (MNPs). From left to right column, it shows metal concentrations in root, shoot and leaf tissue, respectively. Data of Cu, Zn, Fe is grouped together in essential elements group, and Ag, Ce, Ti is grouped into non-essential elements group. Significant differences between essential and non-essential elements were labeled with different lower-case letters. $P < 0.05$.

APPENDIX C

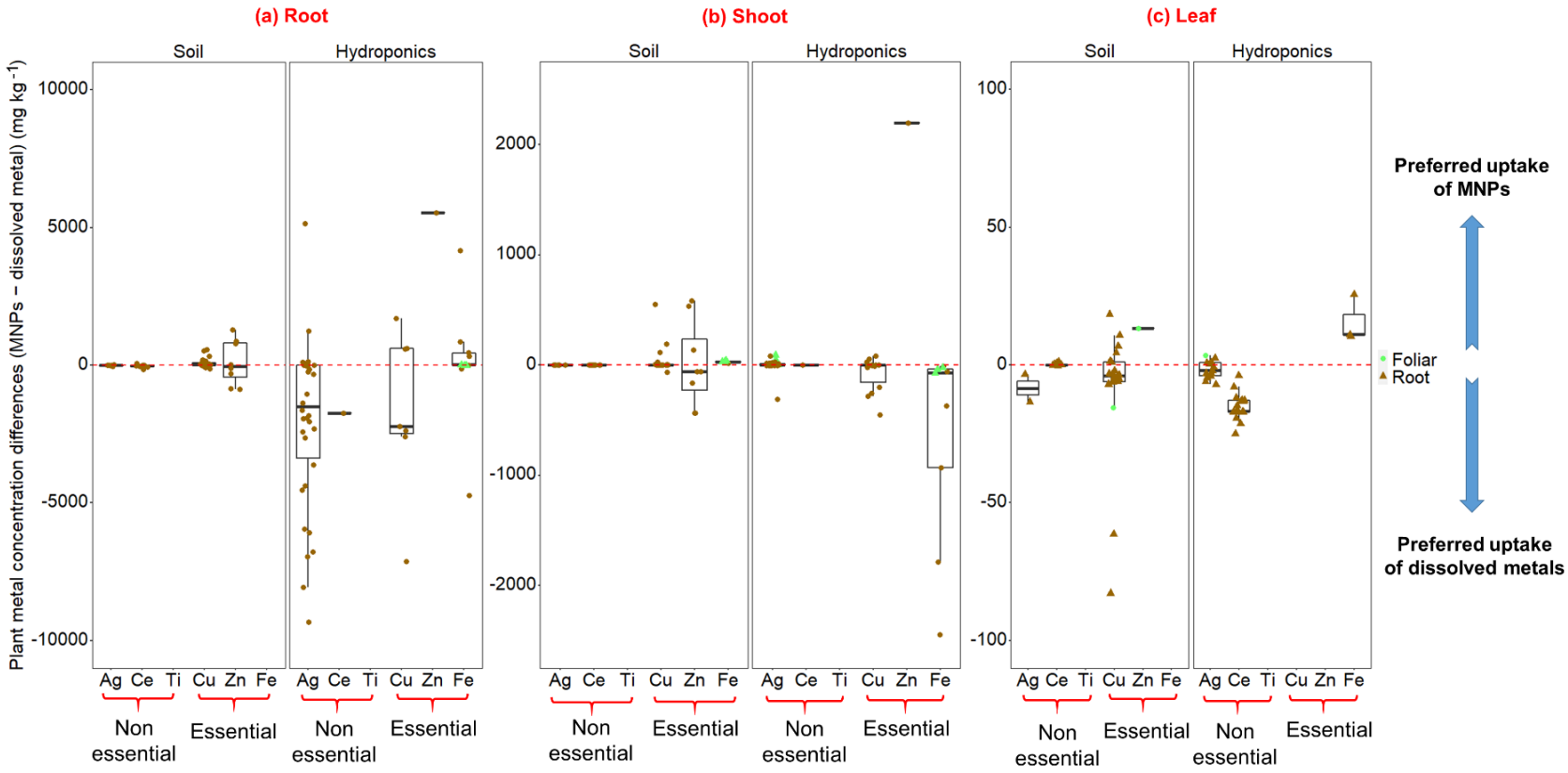

Figure C-5. Metal concentration differences (mg kg^{-1} dry weight) in various plant tissues between treated with metallic nanoparticles (MNPs) and dissolved metal salts. Data were separated by the exposure medium: soil (left) and hydroponics (right). No data for Ti as TiO_2 NPs do not dissolve. The three big columns from left to right indicate metal concentration differences in root, shoot and leaf, respectively. Note that the scales of y-axis for three tissues were different. The brown and green color represent root and foliar exposure ways, respectively. In each big column, the left three metals (Ag, Ce, Ti) and the right three ones (Cu, Zn, Fe) are plant non-essential and essential elements, respectively. If mainly data points above the zero line (red dashed horizontal line), there is preferred uptake of MNPs; otherwise, dissolved metals are more preferred by plant tissues. There were insignificant differences of concentrations of (MNPs – dissolved metals) between soil and hydroponics cultures (with chi-square test). $P < 0.05$.

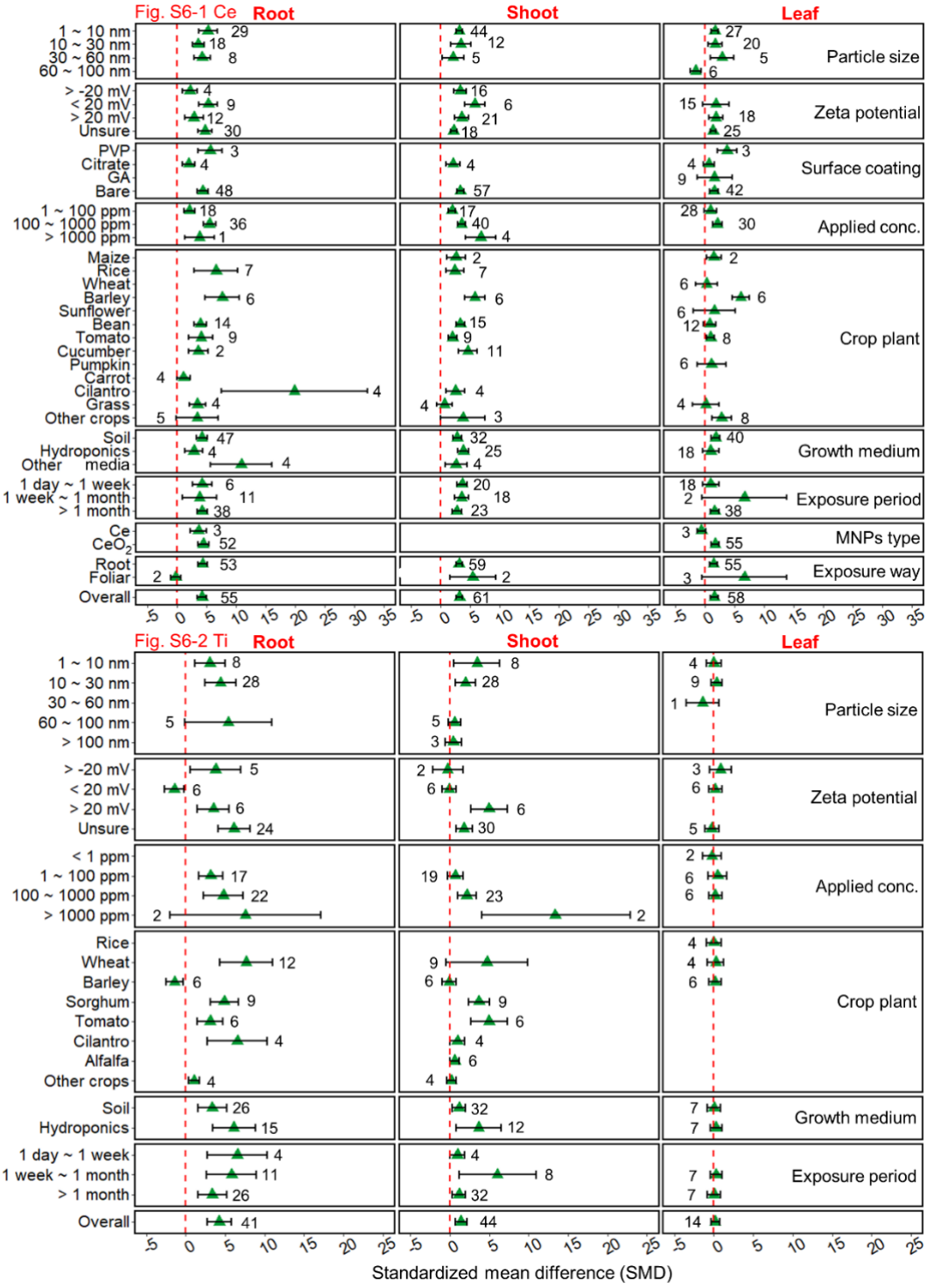

Figure C-6 (C-6.1 and C-6.2). The magnitude of effects (standardized mean difference, SMD) of Ce and Ti concentrations in root, shoot and leaf (from left to right), respectively. Note that the scales of x-axis for the two metals were different. The factors were grouped into several groups: particle size (nm), zeta potential (mV), surface coating (for Ce only), application concentration (ppm), crop plant, growth medium, exposure period, MNPs type (for Ce only) and exposure way. The error bars represent 95 % confidence intervals. There is insignificant effect if the error bar crosses the vertical red dashed line (SMD = 0). The number beside the error bars indicates the number of observations. Numbers in the right side of the error bars indicate significant positive or negative effects, while in the left side denote insignificant effects. PVP, polyvinylpyrrolidone; GA, gum Arabic; Bare indicates no surface coating.

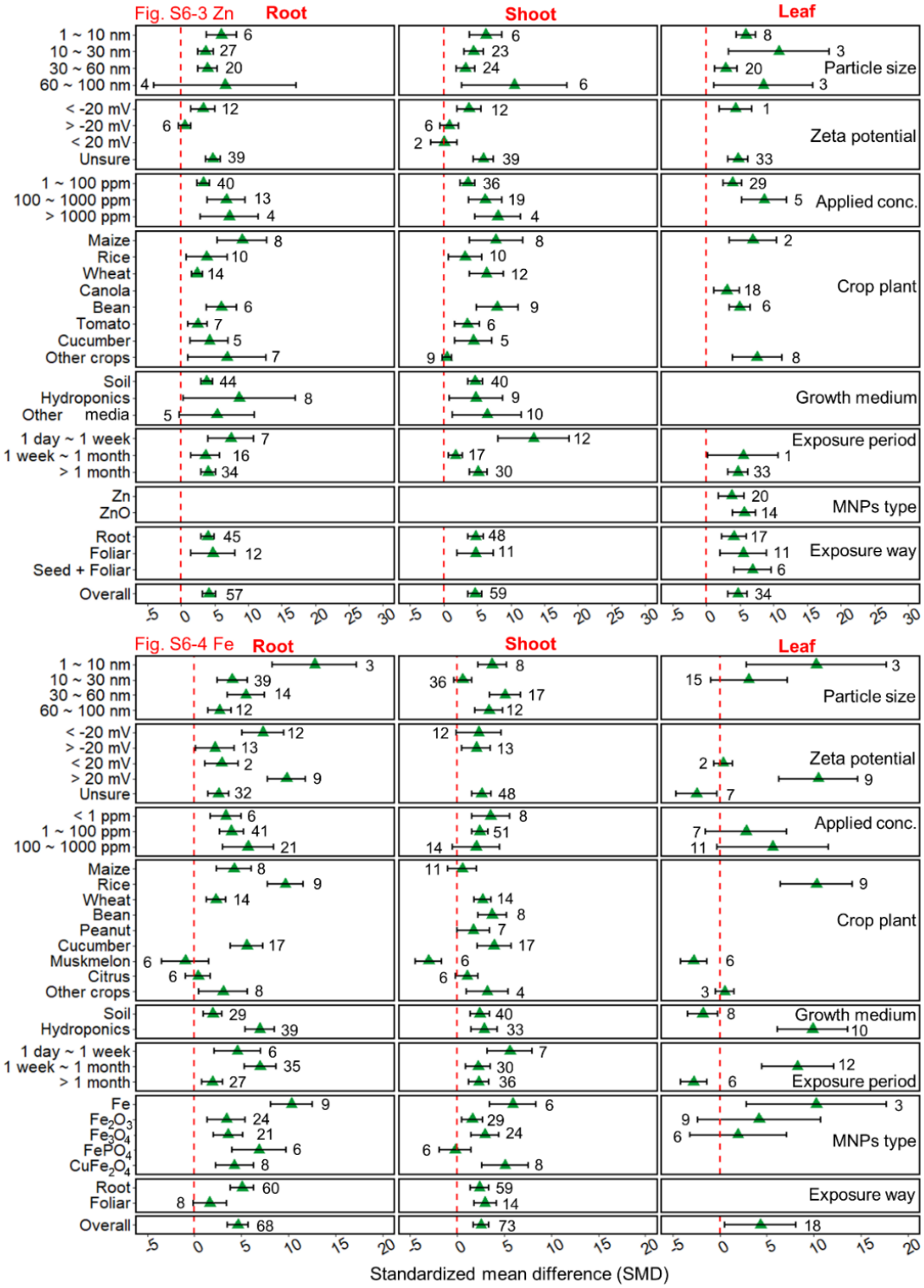

Figure C-6 (C-6.3 and C-6.4). The magnitude of effects (standardized mean difference, SMD) of Fe and Cu concentrations in root, shoot and leaf (from left to right), respectively. Note that the scales of x-axis for the two metals were different. The factors were grouped into several groups: particle size (nm), zeta potential (mV), application concentration (ppm), crop plant, growth medium, exposure period, MNPs type and exposure way. The error bars represent 95 % confidence intervals. There is insignificant effect if the error bar crosses the vertical red dashed line (SMD = 0). The number beside the error bars indicates the number of observations. Numbers in the right side of the error bars indicate significant positive or negative effects, while in the left side denote insignificant effects.

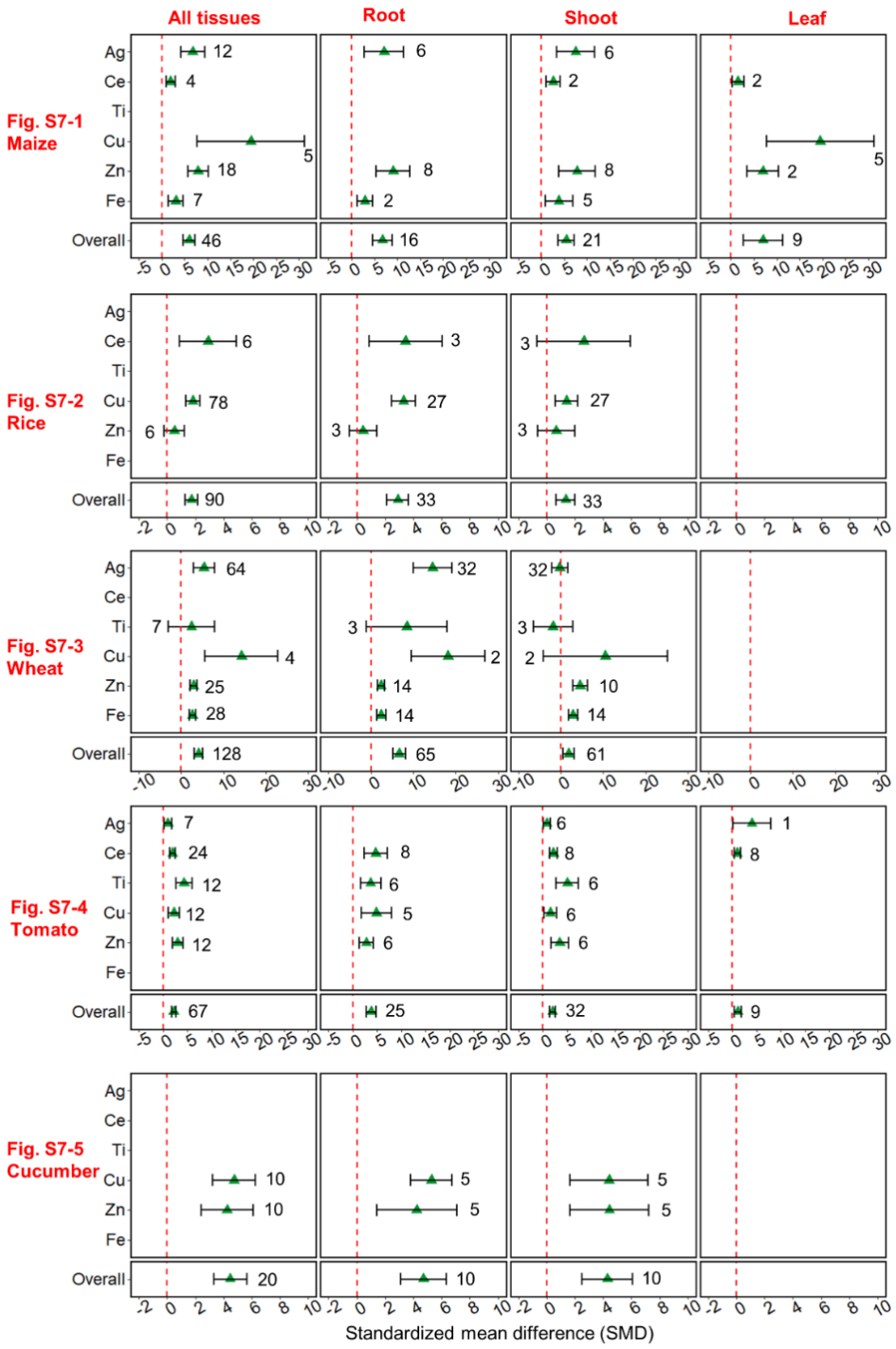

Figure C-7 (C-7.1 to C-7.5). The magnitude of effects (standardized mean difference, SMD) of essential and non-essential elements in root, shoot and leaf (from left to right) of five most studied crops under soil culture (includes both root and foliar exposures), respectively. Note that the scales of x-axis for subfigures were different. The error bars represent 95 % confidence intervals. There is insignificant effect if the error bar crosses the vertical red dashed line (SMD = 0). The number beside the error bars indicates the number of observations. Numbers in the right side of the error bars indicate significant positive or negative effects, while in the left side denote insignificant effects.

Acknowledgements

First of all, I would like to appreciate the financial support from China Scholarship Council (CSC) during my PhD.

My sincerely gratitude goes to my main doctoral supervisor Prof. Dr. Wulf Amelung. I thank Wulf for his supervision, very helpful discussions, insightful comments and bright ideas. I greatly appreciate his continuous encouragement, confidence and patience to my work.

I sincerely thank my doctoral supervisor Prof. Dr. Roland Bol, who provided me the opportunity to study in Forschungzetrum Juelich as a PhD student and work on interesting topics. I greatly appreciate his inspiring words, encouragement and all supports.

I highly thank my co-supervisors Dr. Nina Siebers and Dr. Jens Kruse, who greatly supported me in not only lab work, data analysis and writing, but also helpful advice and interesting discussions. Special thanks goes to Prof. Dr. Erwin Klumpp for his helpful supports and insightful comments on not only MNPs work, but also thesis. I would also like to thank Dr. Bei Wu and Dr. Anne Berns for supports in lab works and helpful discussions. Thanks to Dr. Volker Nischwitz, Stephan Köppchen, Claudia Walraf and Ursula Paffen for all the supports in lab work.

I would like to thank Dr. Kerstin Panten who provided long-term bone char trial samples and provided professional and scientific comments on paper writing and revising.

I would like to thank the supports and accompanies from all colleagues in our group, as well as the colleagues in IBG-3. Thanks for providing friendly and welcoming place to work here. Thanks for accompanies and funny talks daily, and attractive activities.

Last but not least, I would like to sincerely thank my parents for their unconditional love and support, my brother Yunlu Jia who always encourages and inspires me, and my lovely and beautiful girlfriend Yun Chen who always accompanies with me even if remotely.

Thank you all for your great supports and kindly understanding. I am so appreciated to have you all in my life!